High-resolution Permafrost Distribution Modelling for the Central and Southern Yukon, and Northwestern British Columbia, Canada

Philip P. Bonnaventure

Thesis submitted to the
Faculty of Graduate and Postdoctoral Studies
In partial fulfillment of the requirements
For the degree in Ph.D. Geography

Department of Geography
Faculty of Arts
University of Ottawa

Abstract

Basal Temperature of Snow (BTS) measurements were used as the primary inputs to a high resolution (30 x 30 m grid cells) empirical-statistical regional permafrost probability model for the southern and central Yukon, and northernmost British Columbia (59° - 65°N). Data from seven individual study areas distributed across the region were combined using a blended distance decay technique, with an eighth area used for validation. The model predictions are reasonably consistent with previous permafrost maps for the area with some notable differences and a much higher level of detail. The modelling gives an overall permafrost probability of 52%. North of 62°N, permafrost becomes more extensive in the lowland areas whereas farther south permafrost is typically common only above treeline.

Significant differences exist between the mountain environments of the Yukon and the Swiss Alps where the BTS method originated and as a result different modelling approaches had to be developed. This work therefore: (1) develops additional explanatory variables for permafrost probability modelling, the most notable of which is equivalent elevation, (2) confirms the use of ground truthing as a requirement for empirical-statistical modelling in the Yukon and (3) uses a combination of models for the region in order to spatially predict between study areas.

The results of this thesis will be of use to linear infrastructure route-planning, geohazard assessment and climate change adaptation strategies. Future work employing the model will allow the effects of scenario-based climate warming to be examined.

Acknowledgments

I would like to first and foremost extend my deepest gratitude and thanks to my supervisor Antoni Lewkowicz for mentoring me throughout my entire journey as a graduate student. His guidance and support, has allowed this degree to become possible and opened me to possibilities that seemed so far away at times.

To my committee members: Sharon Smith, Luke Copland and Bernard Lauriol for their help with this Ph.D. at the proposal stage and through the comprehensive exams. I am very grateful for your suggestions and encouragement throughout this process. I would also like to thank my external examiner Brian J. Moorman from the University of Calgary for his effort and comments in this process.

To all of my colleagues throughout the graduate process: Angeline Lovatt, Pauline Favero, Emily Roadhouse, Jim Coates, Amaris Page, Marian Kremer, Megan James, Jenny Throop and Christina Miceli. I am happy to have shared the world of permafrost with all of you and wish you all the very best of luck.

I am grateful for funding received from: the Canadian Foundation for Climate and Atmospheric Sciences, the Federal Government of Canada's International Polar Year Program, the Northern Scientific Training Program (Department of Indian Affairs and Northern Development) and the Faculty of Arts, University of Ottawa.

To my parents and sister: Roland, Pauline and Nicky Bonnaventure who have been with me on this journey from the very beginning. My family has seen the best and worst of my academic career, from the first report card to this thesis. They have taught me to learn from the darkest moments, remember them, and always know what you can do. I would not be the person I am today or have accomplished any of this with out their love and guidance.

Finally to my wife Patty Bonnaventure who has literally been to the Yukon and back with me. This thesis would not have been possible without your love and support, over so many years. I always know you will remember what is inside a pingo and perhaps one day I will even get a helper monkey. I love you so much Patty, and your love is what always brings me home. Let's see what's out there…

For E.N.B.

High-resolution Permafrost Distribution Modelling for the central and southern Yukon, Canada

Table of Contents

Chapter Five: Mountain Permafrost Probability Modelling in Areas Above and Below Treeline, Southern Yukon, Canada

Chapter 6: A Regional Permafrost Probability Model for the Southern Yukon and Northern British Columbia, Canada

Chapter 7: Conclusions

Appendix A:

List of Tables

List of Figures

Chapter One

Introduction

Purpose

The purpose of this thesis is to redress the lack of knowledge regarding the topographic and latitudinal distribution of mountain permafrost in extreme northern British Columbia and the southern and central Yukon (59° - 65°N). Existing permafrost maps for this region are drawn at scales of 1:1 000 000 or smaller and this greatly limits their functionality for infrastructure route planning, climate change adaptation strategies, and geohazard identification. The objective is to develop and employ methodology to spatially predict permafrost probabilities under equilibrium conditions for the entire region. The results will be of direct use to industry, government agencies and northern residents and will be high-resolution (30 x 30 m) benchmarks for an area expecting significant climatic change and anthropogenic development.

Introduction

Anthropogenically-induced climate change is expected to be enhanced in arctic and subarctic areas (IPCC 2007; ACIA, 2005) and impacts on the cryosphere are predicted to be particularly great (ACIA, 2005). Reductions in glacier and sea ice cover in and around North America are already widespread and well described (IPCC 2007; ACIA, 2005). A limited number of field studies suggest that permafrost extent has also diminished in recent decades (e.g. Kwong and Gan, 1994), but there is also potential for long-term permafrost preservation if climatic conditions remain sufficiently cold (Froese et al., 2008).

Permafrost is defined as earth materials which remain at a temperature of 0 °C or below for two or more consecutive years (ACGR, 1988; Washburn, 1979; French 2007; Williams and Smith, 1989). Permafrost is further classified into regions or zones including continuous, discontinuous, isolated patches, sub-sea and alpine or mountain permafrost (French, 2007). Mountain permafrost refers to the occurrence of cryotic conditions in mountain regions where permafrost is absent from adjacent lowlands and valleys (Harris and Corte, 1992; French, 2007; Willams and Smith, 1989). Even though permafrost is strongly related to Mean Annual Air Temperature (MAAT), the existence of mountain permafrost can be attributed to a series of complex variables (Shur and Jorgensen, 2007). Many factors, including elevation, depth of snow cover, slope, aspect, geology and vegetation can be important controls/influencing factors on the existence of permafrost in mountain environments (Lewkowicz and Ednie, 2004; Lewkowicz and Bonnaventure, 2008; Bonnaventure and Lewkowicz, 2008, Gruber and Haeberli, 2009).

The study of the distribution of mountain permafrost in the discontinuous zone is becoming increasingly important. With the effects of climate change being felt most in the arctic and sub-arctic, evaluations of these areas must be done immediately (IPCC, 2007). Warming climatic conditions in sub-arctic mountain areas will likely have a significant impact on the distribution, and potentially on the existence, of mountain permafrost (Haeberli et al., 1993).

The range of effects of climate change on permafrost include warming of surface and depth temperatures (IPCC, 2007; ACIA, 2005), increasing active layer thickness (Haeberli et al., 1993), basal melt resulting in permafrost thinning (Harris et al., 2001; Woo et al., 2008), precipitation and hydrological changes (Woo et al., 1992; Woo et al.,

2008) and the development of thermokarst features (Harris et al., 2001; Woo et al., 1992; Woo et al., 2008). Climate change will likely affect permafrost slopes, possibly generating or enhancing mass movements such as creep-related processes, rockslides, rock falls, mudslides, and active layer detachment failures (Evans & Clague, 1994; Harris et al., 2001; Lewkowicz and Harris, 2005; Dorren, 2003; Lipovsky et al., 2005; Haeberli et al., 2006). An evaluation of mountain permafrost distribution is also important for infrastructure development, such as pipelines, roads and railways. Climate change potentially threatens the structural stability of infrastructure making an accurate evaluation of mountain permafrost conditions a necessary planning aid. In order to accurately measure and map areas of mountain permafrost in North America, a reliable, cost effective and easy to implement method must be developed for use in both large and remote areas.

Background

Permafrost Detection and Modelling:

Permafrost maps for mountainous areas can be developed using direct and indirect methods of permafrost detection but ideally a combination of techniques should be used (Etzelmüller et al., 2001). Direct methods involve physically observing frozen ground, measuring the temperature of permafrost by digging, drilling, taking temperature measurements inside boreholes, or locating landforms with high concentrations of ground ice (e.g. active rock glaciers). Indirect methods include measurement of the Basal Temperature of Snow (BTS) (e.g. Gruber and Hoelzle, 2001; Lugon and Delaloye, 2001; Isaksen et al., 2002; Ishikawa and Hirakawa, 2000), predicting the Temperature at the

Top of Permafrost (TTOP) from seasonal n-factors (e.g. Smith and Riseborough, 2002), and interpretation of geophysical data (Kneisel et al., 2008; Riseborough et al., 2008).

Mapping and spatially modelling the distribution of permafrost in mountain regions can be accomplished using a combination of these techniques. Models, which are the essential elements of a problem expressed in physical or mathematical terms and examined within the framework of a system (Inkpen, 2005; Riseborough et al., 2008), attempt to predict permafrost conditions from a series of factors. Often models involve explicit assumptions about, or simplifications of, the system, making validation a necessary element. Ultimately the value of any model depends on its usefulness for a given purpose and not its sophistication (Riseborough et al., 2008). Models are a key resource in permafrost mapping as they can be used in hypothesis testing as well as to potentially predict the results of "what if" scenarios (Riseborough et al., 2008). Models predicting mountain permafrost are classified based on the number and type of inputs measured. Common types include empirical-statistical and process-oriented models (Etzelmüller et al., 2001; Riseborough et al., 2008).

Empirical-Statistical Models:

Empirical-statistical models do not directly estimate the energy exchange that takes place between the ground and the atmosphere. Instead, they use representative terrain or climate variables as proxies for these fluxes. They make use of indirect influences on permafrost, including slope, aspect, elevation, snow cover, Potential Incoming Solar Radiation (PISR), substrate characteristics and land cover. Empirical-statistical models have used freezing and thawing indices (Nelson & Outcalt, 1987; Smith

and Riseborough, 2002), PISR (Hoelzle, 1992) as well as MAAT (Etzelmüller et al., 1998; Etzelmüller et al, 2006; Etzelmüller et al., 2007) as inputs.

Empirical-statistical models view complex energy exchanges at the surface and in the upper portion of the active layer as a grey box. From this vantage point, factors that influence permafrost presence and or distribution can be selected based on order of importance with the aid of field observations or satellite imagery (Hoelzle, et al., 2001; Kneisel et al., 2007). The advantage of these types of models is that they do not necessarily require climate data in order to complete the analysis; thus, remote locations with little or no climate recording infrastructure can still be modeled (e.g. Etzelmüller et al., 2007).

Empirical-statistical models use regression functions based on attributes that affect permafrost distribution such as elevation and PISR, to predict the probability of permafrost in each grid cell of a Digital Elevation Model (DEM). The models generate a surface of values such as Basal Temperature of Snow (BTS), which can then be validated by collecting actual BTS measurements. One advantage of this type of method is that the calculated stochastic surface can easily be altered to predict the effects of climate change (Lugon & Delaloye, 2001; Lewkowicz & Ednie, 2004; Bonnaventure and Lewkowicz, 2008, 2010).

Process-Oriented and Semi-empirical Models:

Process-oriented models examine exchanges between the surface and the atmosphere in detail. These models usually use a combination of an energy balance approach and a thermal offset approach (Hoelzle et. al., 2001). In an energy balance model the presence of permafrost or ground temperature is an outcome of exchanges

between the atmosphere and the surface of short-wave and long-wave radiation, sensible and latent heat fluxes. Energy balance models require an extensive set of input parameters which are often difficult to collect, especially in mountainous terrain and to date have not been successful in predicting the turbulent energy exchange accurately (e.g. Stocker-Mittaz et al., 2002).

A continuous surface of modeled ground temperatures can be used in a thermal offset model. Offset models are essentially empirical models but are often used in conjunction with process-oriented models to initiate the modelling procedure (e.g. Duchesne et al., 2008). The values from this surface can then be used to examine and predict values of the mean annual ground surface temperature (MAGST) and mean annual temperature at the permafrost table (MAPT or TTOP) (Burn & Smith, 1988; Smith & Riseborough, 2002). A thermal offset model works on the assumption that the relationship between the ground surface temperature and the top of the permafrost is mainly determined by conductive heat flow (Smith & Riseborough, 2002). Common thermal offset models include TTOP (Smith & Riseborough, 1996), and the finite-element one dimensional conduction model T-ONE (Wright et al., 2003; Ednie at al., 2008; Duchesne et al., 2008). Thermal offset models can be used to examine the transient impact of climate change on permafrost distribution (e.g. Smith & Riseborough, 1993, 2002), but are limited in usefulness in mountain regions by the high degree of microclimatic variability (Hoelzle et al., 2001).

Permafrost Sampling Techniques:

Various techniques exist to detect and/or infer the presence of mountain permafrost, including probing using a metallic rod in late summer, DC resistivity

profiling, Ground Penetrating Radar (GPR), seismic techniques, radiometry, transient electromagnetic methods and BTS (Vonder Mühill et al., 2000; Putkonen, 2003; Kneisel et al., 2008). Although all of these techniques have been verified, it is important to note that only the BTS method and probing can be used on more than a local scale.

The Basal Temperature of Snow (BTS) Method:

The BTS method was first devised by Haeberli (1973) for the detection of alpine permafrost in the Swiss Alps. It has since been refined and verified in many locations, including central Europe (e.g. Gruber & Hoelzle, 2001; Lugon & Delaloye, 2001; Gardaz, 1997; Hoelzle et al., 1999; Imhof et al., 2000; Hoelzle, 1992; King, 1992; Dobinski, 1998), Scandinavia (e.g. Isaksen et al., 2002; Jeckel, 1988; Ødegard et al., 1996), Japan (e.g. Ishikawa & Hirakawa, 2000), and, most recently, in North America (Lewkowicz & Ednie, 2004; Bonnaventure and Lewkowicz, 2008; Lewkowicz and Bonnaventure, 2008; Bonnaventure and Lewkowicz, 2010). The BTS method relies on the low heat transfer capacity of deep snow cover (> 0.8 m) that insulates the ground from diurnal and other short-term surface energy balance changes (Hoelzle et al., 1993). As a result, equilibrium temperatures that develop at the snow-ground interface in mid to late-winter reflect thermal conditions within the ground. During the fall, as the ground and its porewater begin to freeze, latent heat is released, sometimes over several months, resulting in a zero curtain (Williams and Smith, 1989; French, 2007). In permafrost areas the active layer freezes progressively until the freezing front reaches the top of permafrost. Since this layer is already frozen, the release of latent heat to the surface is limited to slow freezing of the unfrozen moisture in the cryotic soil. Many factors including substrate properties, moisture content and snow depth can affect the rate of

surface freeze up, and thus the transfer of energy to the surface. In particular these factors can influence the variability of freezing N-factors (Throop, 2010) in heterogeneous areas making the BTS measurements sensitive to inter-annual variations. Temperatures at the base of snow in late winter in permafrost areas fall to <-3°C due to the termination or reduction in latent heat release. In areas where permafrost does not exist, the seasonal frost line continues to advance throughout the winter, continuously releasing latent heat and thus maintaining warmer temperatures at the ground snow interface (e.g. BTS ≈ 0°C) (Figure 1.1).

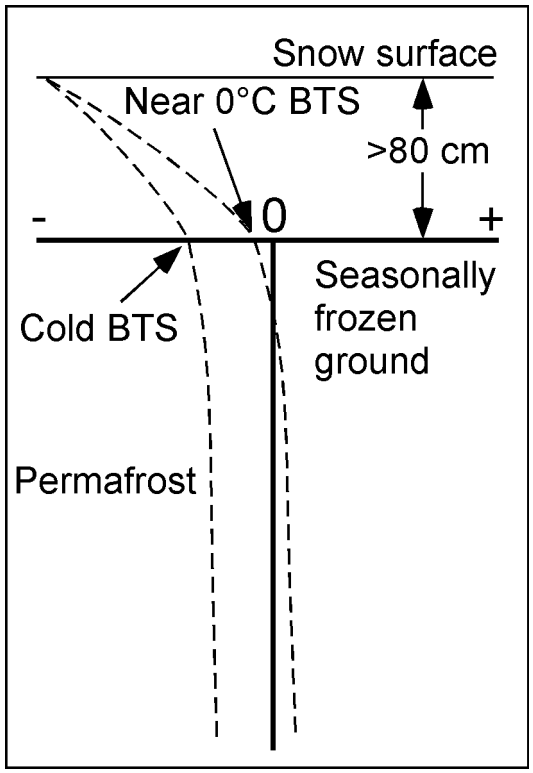

Figure 1.1: Diagram illustrating the principle behind the BTS method for areas with and without permafrost. Temperature profiles are shown for late winter.

BTS measurements must be taken in mid to late-winter to ensure that the snow-ground interface is in thermal equilibrium (Imhof et al., 2000; Brenning et al., 2005).

BTS measurements have generally been classified into categories based on 'rules-of-thumb': values < -3 °C indicate probable permafrost, values of -2 °C to -3 °C indicate possible permafrost and values > -2 °C indicate that permafrost is improbable (Hoelzle, 1992). These 'rules of thumb' serve as indicators of permafrost but do not reflect 100% likelihood for the probable category or 0% for the improbable category (Lewkowicz and Ednie, 2004). In addition, the 'rules of thumb' were developed in the Swiss Alps and do not appear to be correct for the mountains of North America (Lewkowicz and Ednie, 2004; Bonnaventure and Lewkowicz, 2008).

BTS measurements provide point indications of permafrost likelihood that can be related statistically with factors such as elevation, slope, aspect and PISR. When incorporated into a Geographic Information System (GIS), the BTS method requires limited inputs and provides a predictive model that is easily applied and cost effective (Hoelzle et al. 2001). Other advantages of the BTS method include the fact that models generated in a GIS can be locally calibrated using the same methodology for different alpine locations (e.g. Dobinski, 1998; Ishikawa & Hirakawa, 2000; Jeckel, 1988; Lewkowicz & Ednie, 2004; Lewkowicz and Bonnaventure, 2008).

A major potential limitation of the BTS method is that it requires a snow depth of at least 80 cm in order to achieve equilibrium temperatures at the snow-ground interface. Due to the uneven nature of surfaces in mountain areas, snow accumulates at certain sites and is wind-scoured in others. Uneven snow packs result in BTS measurements that can only be taken in deep-snow locations, which are likely to be the warmest parts of the landscape. Another drawback is that the location and depth of snow can vary inter-annually causing different readings from year to year. Inter-annual variations can also be

caused by the timing of snow cover development in autumn and early winter. If the snow cover is established early, heat loss to the atmosphere is reduced while ground temperatures are still at relatively high values. If snow cover is established later, ground temperatures are considerably colder (Imhof et al., 2000; Vonder Muhll et al., 1998; Brenning et al., 2005, Keller & Grubler, 1993). Finally, there is a general problem of spatial autocorrelation in the BTS measurements (e.g. Lewkowicz & Ednie, 2004). If this occurs, the assumed independence of each point is compromised (Sokal & Oden, 1978). It is usually possible to avoid these effects by locating BTS sampling points at least 150 m apart (Brenning et al., 2005).

Objectives

This thesis is written in article format and the chapters are designed to address individual objectives within the broader goal of increasing knowledge on mountain permafrost in northern Canada.

Objective 1: Examine the sensitivity of mountain permafrost to potential climatic change

The objective of Chapter two is to use three study areas to explore the equilibrium effects on mountain permafrost under scenario-based changes in (1) MAAT of -2K to +5K, (2) cloud cover, through altering the partitioning of direct beam and diffuse radiation (±5% to ±10%), and (3) the two changes acting together. Due to the nature of discontinuous permafrost in mountain areas the distribution of permafrost is particularly complex. Given the variety of micro-sites within such mountainous environments, it can be assumed that terrain will be present that has mean annual air and ground surface

temperatures close to 0°C. If seasonally frozen, such sites may become permafrost during sustained atmospheric cooling or periods of reduced snowfall, or if permafrost, they may thaw during sustained warming or long-term increases in snowfall. Consequently it is evident that mountain permafrost areas should be spatially sensitive to climatic change. The objective of the paper is to identify the locations most sensitive to climatic change and to estimate the extent and impact of potential changes on permafrost extent.

Objective 2: Explore the viability of interchanging local permafrost models within a large region

The objective of Chapter three is to examine the possibility of interchanging permafrost models between study areas located 200-250 km apart, and varying in terms of terrain and climate. This paper serves as a step towards examining the utility of empirical-statistical models outside the area in which they are generated. This is important because it would not be possible to undertake intense data collection across the entire northwestern cordillera. It was hypothesised that areas with similar climatic conditions would provide the highest degree of interchangeability. The objective addresses the feasibly of generating high-resolution permafrost probability models for areas where intense sampling is not possible.

Objective 3: Develop a permafrost predictive variable capable of incorporating the effects of variable surface lapse rates

The objective of Chapter four is to present *equivalent elevation*, a new permafrost predictive variable for mountain permafrost, this variable incorporates variable surface lapse rates and can be derived for large areas. The BTS method was developed in the

Swiss Alps where mountain permafrost is highly correlated with elevation, but where permafrost is located almost exclusively above treeline. In the mountains of the Yukon extensive permafrost can be present below treeline in major topographic hollows and valleys but a simple use of elevation cannot respond to this. This difference is caused by the interfingering of mountain and latitudinal permafrost, and is influenced by the presence of gentle or inverted surface lapse rates through the forests. As a result, the relationship between BTS and elevation is non-linear and a new variable is required to reflect this.

Objective 4: Model permafrost probability above and below treeline and examine the potential use of additional explanatory variables

The objective of Chapter five is to model and map permafrost probability above and below treeline for five different areas located within the southern and central Yukon. This paper is the first to incorporate the equivalent elevation variable, which is required because local surface lapse rates are an important controlling factor on permafrost distribution. The paper addresses a key issue for modelling mountain permafrost in northwest North America where a lower elevation limit for permafrost cannot be defined due to interfingering of latitudinal and mountain permafrost. A secondary objective includes exploring the potential use of additional explanatory variables in the BTS modelling procedure. These include PISR, Topographic Position Index (TPI), slope and Normalized Difference Vegetation Index (NDVI). In addition the paper discusses a potential mechanism for expanding the modeled area using alternatives to simple interchangeability or extension throughout climatic zones.

Overall Objective: Model permafrost probability at high-resolution for the Yukon between 59° - 65°N

The overall objective of this thesis, and the topic of Chapter six, is the high-resolution modelling of permafrost probability for the entire discontinuous mountain permafrost zone in the Yukon and extreme northern B.C. (59° - 65°N). The goal is to develop a regional permafrost model based on individual empirical-statistical BTS-based permafrost probability models created for seven different areas within the study region. Secondary objectives include validation of the results of the model using data from rock glaciers and borehole locations, to examine the inaccuracies in the model and compare the results to previous permafrost maps for the area. The overall objective of this paper is to serve as a benchmark of current permafrost conditions before the onset of additional climatic change and to be of direct use for infrastructure route planning, geohazards assessment, northern development.

Thesis Organization (contribution to each chapter)

The five main chapters constituting the thesis have been written up as individual manuscripts for peer-reviewed journals. I am primary author on three of the chapters with my supervisor as second author, and he is the primary author on two with me as second author. Marian Kremer is a third author on chapter six as she aided in the GIS modelling to produce the regional permafrost model. All research and analyses in each paper were created with original ideas from my supervisor and me and in the case of the published chapters, they incorporate suggestions from the anonymous reviewers. The order of authorship is based on the relative contribution to the intellectual property. The data

collection for all papers with the exception of the BTS and ground truthing data for Wolf Creek was conducted by me with the aid of field assistants. Analyses, including all data analyses, empirical-statistical modelling, geomatic analyses, the production of all figures and thesis writing was completed by me with the aid and editing of my supervisor on a weekly basis throughout the thesis process.

Chapter Two

Bonnaventure P.P and Lewkowicz A.G. 2010. Modelling Climate Change Effects on the Spatial Distribution of Mountain Permafrost at Three Sites in Northwest Canada. *Climatic Change.* **105** (1-2, 293-312). DOI 10.1007/s10584-010-9818-5.

This work uses data collected for my M.Sc. thesis but the analyses do not appear in that document as they were carried out during the Ph.D. Field data for Wolf Creek was collected by A.G. Lewkowicz, M. Phillips and M. Ednie in 2001-02. I collected the data in 2005-06 for the Ruby Range and Haines Summit. All data analysis and modelling was undertaken by me in collaboration with my supervisor.

Chapter Three

Lewkowicz A.G. and **Bonnaventure P.P.** (2008). Interchangeability of Mountain Permafrost Probability Models, Northwest Canada, *Permafrost and Periglacial Processes,* **19**: 49-62. DOI 10.1002/ppp.612

This work uses data collected for my M.Sc. thesis but the analyses do not appear in that document as they were carried out during the Ph.D. Field data for Wolf Creek was collected by A.G. Lewkowicz, M. Phillips and M. Ednie in 2001-02. I collected the data in 2005-06 for the Ruby Range and Haines Summit. All data analysis and modelling was undertaken by me in collaboration with my supervisor. The latter conceived of the ideas regarding the relative importance of elevation and solar radiation which are discussed in this paper.

Chapter Four

Lewkowicz A.G. and **Bonnaventure P.P.** 2011. Equivalent Elevation: a New Method to Incorporate Variable Surface Lapse Rates Into Mountain Permafrost Modelling. *Permafrost and Periglacial Processes.* DOI 10.1002/ppp.720

The idea for this paper was conceived by A.G. Lewkowicz to address difficulties in the BTS methodology for the Yukon. All data collection, analysis and paper write-up was completed by myself with edits and consultation from my supervisor.

Chapter Five

Bonnaventure P.P. and Lewkowicz A.G. *In Review*. Mountain Permafrost Probability Modelling in Areas Above and Below Treeline, Southern Yukon, Canada. *Canadian Journal of Earth Sciences.* Submitted November, 2010.

All ideas, analysis, modelling and manuscript writing for this paper were completed by myself with input, edits and collaboration from my supervisor during regular weekly meetings.

Chapter Six

Bonnaventure P.P., Lewkowicz A.G. and Kremer M. *In Review.* A Regional Permafrost Probability model for the Southern Yukon and Northern British Columbia, Canada. *Permafrost and Periglacial Processes.* Submitted January 2011.

All ideas, analysis, modelling and manuscript writing for this paper were completed by myself with input, edits and collaboration from my supervisor during regular weekly meetings.

References

Arctic Climate Impact Assessment. 2005. http://www.acia.uaf..edu.

ACGR 1988. *Glossary of Permafrost and Related Ground-Ice Terms.* National Research of Canada, Technical Memorandum No. 142. pp.64.

Bonnaventure P.P. and Lewkowicz A.G. 2008. Mountain Permafrost Probability Mapping Using the BTS Method in two Climatically Dissimilar Locations, Northwest Canada. *Canadian Journal of Earth Sciences,* **45**: 443-455.

Bonnaventure P.P. and Lewkowicz A.G. 2010. Modelling climate change effects on the spatial distribution of mountain permafrost at three sites in northwest Canada. *Climatic Change*. DOI 10.1007/s10584-010-9818-5.

Brenning A., Gruber S., & Hoelzle M., 2005. Sampling and Statistical Analyses of BTS Measurements. *Permafrost and Periglacial Processes***. 16** 1 – 11.

Burn, C.R. and Smith, C.A.S. 1988. Observations of the "thermal offset" in near-surface mean annual ground temperatures at several sites near Mayo, Yukon Territory, Canada. *Arctic*, **41**(2): 99-104.

Dobinski, W. 1998. Permafrost occurrences in the alpine zone of the Tatra Mountains, Poland. *In* A.G. Lewkowicz and M. Allard, (eds.) *Proceedings, Seventh International Conference on Permafrost, Yellowknife, June 23-27, 1998.* Nordicana, Centre d'Etudes Nordiques, Quebec City. 231- 237.

Dorren L.K.A. 2003. A Review of Rockfall Mechanics and Modelling Approaches. *Progress in Physical Geography.* **27(1)**: 69-87.

Duchesne C., Wright J.F., and Ednie M. 2008. High Resolution numerical modelling of climate change impacts to permafrost in the vicinities of Inuvik, Norman Wells, and Fort Simpson , NWT, Canada. *Proceedings of the Ninth International Permafrost Conference, Fairbanks, Alaska.*

Ednie M., Wright J.F., and Duchesne C. 2008. Establishing initial conditions for transient ground thermal modelling in the Mackenzie Valley: a paleo-climatic reconstruction approach. *Proceedings of the Ninth International Permafrost Conference, Fairbanks, Alaska.*

Etzelmüller B, Ødegard RS, Berthling I, Sollid JL. 2001. Terrain parameters and remote sensing data in the analysis of permafrost distribution and periglacial processes: principles and examples from southern Norway. Permafrost and Periglacial Processes **12**: 79–92.

Etzelmüller, B., Berthling, I., and Ludvig Sollid, J. 1998. The distribution of permafrost in southern Norway- a GIS approach. *In* A.G. Lewkowicz and M. Allard, (eds.) *Proceedings, Seventh International Conference on Permafrost, Yellowknife, June 23-27, 1998.* Nordicana, Centre d'Etudes Nordiques, Quebec City. 251- 256.

Etzelmüller, B., Heggem, E.S.F., Sharkhuu, N., Frauenfelder, R., Kääb, A. and Goulden, C. 2006. Mountain permafrost distribution modelling using a multi-criteria approach in the Hövsgöl area, northern Mongolia. *Permafrost and Periglacial Processes*, **17**: 91-104.

Etzelmüller, B., Farbrot, H., Guomundsson, A., Humlum, O., 2007. The regional distribution of mountain permafrost in Iceland. *Permafrost and Periglacial Processes*, **18**: 185-199.

Evans, S.G. and Clague, J.J. 1994. Recent climatic change and catastrophic geomorphic processes in mountain environments. *Geomorphology*, **10** 107-128.

French, H.M. 2007. *The Periglacial Environment third edition*. John Wiley and Sons Inc., 111 River Street, Hoboken, NJ 07030, USA.

Froese, D.G., Westgate, J.A., Reyes, A.V., Enkin, R.J., Preece, S.J. 2008. "Ancient permafrost and a future, warmer arctic." *Science* **321**(5896): 1648.

Gardaz J.M. 1997. Distribution of Mountain Permafrost, Fontanesses Basin, Valaisian Alps, Switzerland. *Permafrost and Periglacial Processes* **8** 101-105.

Gruber, S. and Hoelzle, M. 2001. Statistical modeling of mountain permafrost distribution: Local calibration and incorporation of remotely sensed data. *Permafrost and Periglacial Processes*, **12** 69-77.

Gruber, S. & Haeberli, W. 2009: Mountain permafrost. In: *Permafrost Soils,* edited by: Margesin, R., Biology Series Vol. 16, Springer, 33–44, doi: 10.1007/978-3-540-69371-0_3. <http://www.geo.unizh.ch/~stgruber/pubs/gruber_2009_pf-soils.pdf >
Haeberli W. 1973. Die Basis-Temperatur der winterlichen Schneedecke als möglicher Indikator für die Verbreitung von Permafrost in den Alpen. *Zeitschrift für Gletscherkünde und Glazialgeologie* **1-2**: 221-227.

Haeberli, W., Guodong, C., Gorbunov, A.P. and Harris, S.A. 1993. Mountain permafrost and climatic change. *Permafrost and Periglacial Processes*, **4** 165-174.

Haeberli W., Hallet B., Arenson L., Elconin R., Humlum O., Kaab A., Kaufmann V., Ladanyi B., Matsuoka N., Springman S., Vonder Muhll D. 2006. *Permafrost and Periglacial Processes.* Permafrost Creek and Rock Glacier Dynamics. **17**: 189-214.

Harris S.A. 1987. Altitude Trends in Permafrost Active Layer Thickness, Kluane Lake, Yukon Territory. *Arctic*, **40** 179-185.

Harris, C., Davies, M.C.R. and Etzelmüller, B. 2001. The assessment of potential geotechnical hazards associated with mountain permafrost in a warming global climate. *Permafrost and Periglacial Processes*, **12** 145-156.

Harris, S.A. and Corte, A.E. 1992. Interactions and relations between mountain permafrost, glaciers, snow and water. *Permafrost and Periglacial Processes*, **3** 103-110.

Hoelzle, M., 1992. Permafrost occurrence from BTS measurements and climatic parameters in the Eastern Swiss Alps. *Permafrost and Periglacial Processes*, **3** 143-147.

Hoelzle M. Wegmann M. Krummenacher B. 1999. Miniature Temperature Dataloggers for Mapping and Monitoring of Permafrost in High Mountain Areas: First Experiences from the Swiss Alps. *Permafrost and Periglacial Processes*, **10** 113-124.

Hoelzle, M., Mittaz, C., Etzelmüller, B. and Haeberli, W. 2001. Surface energy fluxes and distribution models of permafrost in European Mountain areas: an overview of current developments. *Permafrost and Periglacial Processes*, **12** 53-68.

Huscroft C.A., Lipovsky P.S. and Bond J.D. 2004b. Permafrost and Landslide Activity: Case Studies from Southwestern Yukon Territory. In: Yukon Exploration and Geology 2003, D.S. Emond and L.L. Lewis (eds.) Yukon Geological Survey. p. 107-199.

Imhof, M., Pierrehumert, G., Haeberlie, W. and Kienholz, H. 2000. Permafrost investigation in the Schilthorn Massif, Bernese Alps, Switzerland. *Permafrost and Periglacial Processes*, **11** 189-206.

Inkpen, R. 2005: *Science, Philosophy and Physical Geography*. Routledge, 2 Park Square, Milton Park, Abingdon, Oxon. New York.

IPCC. 2007. http://www.ipcc.ch/ipccreports/assessments-reports.htm.

Ishikawa, M.and Hirakawa., 2002. Mountain permafrost distribution based on BTS measurements and DC resistivity soundings in the Daisetu Moutains, Hokkaido, Japan. *Permafrost and Periglacial Processes*, **11** 109-123.

Isaksen K, Hauck C, Gudevang E, Ødegård RS, Sollid JL. 2002. Mountain permafrost distribution in Dovrefjell and Jotunheimen, southern Norway, based on BTS and DC resistivity tomography data. Norsk Geografisk Tidsskrift 56: 122–136.

Jeckel, P.P. 1988. Permafrost and its altitudinal zonation in N. Lapland. In *Proceedings of the Fifth International Conference on Permafrost, Trondheim*. Tapir, Trondheim. Vol.**1** 332-337.

Keller, F. and Gubler, H. 1993. Interaction between snow cover and alpine permafrost, Murtle Corvatsch. Swiss Alps. In *Proceedings of the Sixth International Conference on Permafrost, Beijing*. South China University of Technology, Beijing. Vol. 1: 332-337.

King, L. 1992. Prospecting and mapping of mountain permafrost and associated phenomenon. *Permafrost and Periglacial Processes*, **3** 73-81.

Kneisel C., Rothenbühler C., Keller F., Haeberli W. 2007. Hazard assessment of potential periglacial debris flows based on GIS-based spatial modelling and geophysical field surveys: a case study in the Swiss Alps. *Permafrost and Periglacial Processes*. **18**: 259-268.

Kneisel C., Hauck C., Fortier R., and Moorman B. 2008. Advances in Geophysical Methods for Permafrost Investigation. *Permafrost and Periglacial Processes*. **19**: 157-178.

Kwong, Y. T. and Gan, T.Y. 1994. Northward migration of permafrost along the Mackenzie Highway and climatic warming. *Climatic Change* **26**(4): 399-419.

Lewkowicz A.G. and Bonnaventure P.P. 2008. Interchangeability of Mountain Permafrost Probability Models, Northwest Canada, *Permafrost and Periglacial Processes,* **19**: 49-62.

Lewkowicz, A.G. and Ednie, M. 2004. Probability mapping of mountain permafrost using the BTS method, Wolf Creek, Yukon Territory, Canada. *Permafrost Periglacial. Processes.,* **15** 67-80.

Lewkowicz A.G. and Harris C. 2005. Frequency and Magnitude of active-layer detachment failures in discontinuous and continuous permafrost, northern Canada. *Permafrost and Periglacial Processes.* **16**: 115-130.

Lipovsky P.S., Coates J., Lewkowicz A.G. and Trochim E. 2005. Active-layer Detachments Following the Summer 2004 Forest Fires Near Dawson City, Yukon. In: Yukon Exploration and Geology 2005, D.S. Emond, L.H. Weston, G.D. Bradshaw and L.L. Lewis (eds.), Yukon Geological Survey.

Lugon R. & Delaloye R. 2001. Modeling alpine permafrost distribution , Val de Rechy, Valais Alps (Switzerland) *Norsk geogr. Tidsskr.* **55** 224-229.

Nelson, F.E. and Outcalt, S.I. 1987. A computational method for predicting and rationalization of permafrost. *Arctic and Alpine Research,* **3** 279-288.

Ødegard R. S., Isaksen K., Mastervik M., Billdal L., Engler M., & Sollid J. L. 1996. Comparison of BTS and Landsat TM data from Jotunheimen, southern Norway. *Norsk geogr. Tidsskr.* **53** 226 – 233.

Putkonen J. 2003. Determination of Frozen Soil Thermal Properties by Heated Needle Probe. *Permafrost and Periglacial Processes*, **14** 343-347.

Riseborough D., Shiklomanov N., Etzelmuller B., Gruber S. and Mrchenko S. 2008. Recent Advance in Permafrost Modelling. (2008). *Permafrost and Periglacial Processes* **19**: 137-156

Shur Y. and Jorgenson M.T. 2007. Patterns of Permafrost Formation and Degradation in Relation to Climate and Ecosystems. *Permafrost and Periglacial Processes* **18**: 7-19

Smith, M.W. and Riseborough, D.W. 1996. Permafrost monitoring and detection of climate change. *Permafrost and Periglacial Processes*, **7** 301-309.

Smith, M.W. and Riseborough, D.W. 2002. Climate and limits of permafrost: A zonal analysis. *Permafrost and Periglacial Processes*, **13** 1-15.Sokal & Oden, 1978

Stocker-Mittaz, C., Hoelzle, M., Haeberli, W. 2002. Modelling alpine permafrost distribution based on energy-balance: a first step. *Permafrost and Periglacial Processes* **13**: 271–282.

Sokal, R. and Oden, N. 1978: Spatial autocorrelation in biology 1. Methodology. *Biological Journal of the Linnean Society*, **10** 199-228.

Throop J. 2010. Spatial and temporal variability in permafrost conditions, northern Canada. M.Sc. Thesis, Department of Geography, University of Ottawa.

Vonder Mühll, D., Stucki, T. and Haeberli, W. 1998. Borehole temperatures in alpine permafrost: A ten year study. *In* A.G. Lewkowicz and M. Allard, (eds.) *Proceedings, Seventh International Conference on Permafrost, Yellowknife, June 23-27, 1998.* Nordicana, Centre d'Etudes Nordiques, Quebec City. 1089-1095.

Washburn, A.L. 1979. *Geocryology.* Edward Arnold, London. 406pp.

Williams P.J. and Smith M.W. 1989. The Frozen Earth: Fundamentals of Geocryology Cambridge University Press. The Edinbrugh Building, Shaftsbury Road, Cambridge CB2 2RU.

Woo M.K., Lewkowicz A.G., Rouse W.R. 1992. Response of the Canadian Permafrost Environment to Climate Change. *Physical Geography:* **13** 287 – 317.

Woo M., Kane D.L., Carey S.K., and Yang D. 2008. Progress in Permafrost Hydrology in the New Millennium. *Permafrost and Periglacial Processes*. **19**: 237-254.

Wright J.F., Duchesne C. & Cote M.M. 2003. Regional-scale permafrost mapping using the TTOP ground temperature model. *Proceedings, eighth International Conference on permafrost, Zurich, Switzerland, July 21-25, 2003* (pp. 1241-1246).

Chapter Two

Modelling climate change effects on the spatial distribution of mountain permafrost at three sites in northwest Canada

Abstract

Spatial models of present-day mountain permafrost probability were perturbed to examine potential climate change impacts. Mean annual air temperature (MAAT) changes were simulated by adjusting elevation in the models, and cloud cover changes were examined by altering the partitioning of direct beam and diffuse radiation within the calculation for potential incoming solar radiation (PISR). The effects of changes in MAAT on equilibrium permafrost distribution proved to be more important than those due to cloud cover. Under a -2 K scenario (approximating Little Ice Age conditions), permafrost expanded into an additional 22-43% of the study areas as zonal boundaries descended by 155-290 m K^{-1}. Under warming scenarios, permafrost probabilities progressively declined and zonal boundaries rose in elevation. A MAAT change of +5 K, caused two of the areas to become essentially permafrost-free. The absolute values of these predictions were affected up to ±10% when lapse rates were altered by ±1.5 K km^{-1} but patterns and trends were maintained. A higher proportion of diffuse radiation (greater cloud cover) produced increases in permafrost extent of only 2-4% while decreases in the diffuse radiation fraction had an equal but opposite effect. Notwithstanding the small change in overall extent, permafrost probabilities on steep south-facing slopes were significantly impacted by the altered partitioning. Combined temperature and PISR partitioning scenarios produced essentially additive results, but the impact of changes in the latter declined as MAAT increased. The modelling illustrated that mountain

permafrost in the discontinuous zone is sensitive spatially to long-term climate change and identified those areas where changes may already be underway following recent atmospheric warming.

Key Words

Mountain permafrost, Cryosphere, Climate change, Spatial Modelling, Cloud cover.

Introduction

Anthropogenically-induced climate warming is expected to be enhanced in arctic and subarctic areas (IPCC, 2007) and impacts on the cryosphere are predicted to be particularly great (ACIA, 2004). Impacts on glacier and sea ice cover in North America are already widespread and well-described. Limited numbers of studies have been undertaken to examine changes in permafrost extent but they suggest that permafrost has also diminished in recent decades (e.g. Kwong and Gan, 1994). However, there is also potential for long-term permafrost preservation if climatic conditions remain sufficiently cold (Froese et al., 2008).

Loss of permafrost can be difficult to detect directly, and predictions of future change are hampered by the paucity of knowledge concerning the current spatial distribution of permafrost at a local scale. The latter is illustrated by available maps of permafrost zones for the circum-Arctic (Brown et al., 1997) or Canada (Heginbottom et al., 1995) in which vast areas are classified according to the percentage of terrain underlain by permafrost: continuous (>90%), discontinuous (10-90%; often further divided into sporadic (10-50%) and widespread (50-90%)), and isolated patches (<10% extent). Mountain permafrost, a final category which is usually left undivided because of its complexity, refers to the occurrence of permafrost in mountains in regions where it is absent from adjacent lowlands and valleys (Harris and Corte, 1992). The dominant characteristic of mountain permafrost is its extreme spatial variability with respect to nearly all surface and near-surface characteristics and properties (Gruber and Haeberli, 2009). In the North American Cordillera, the delineation of mountain and latitudinal permafrost is difficult because many major valleys are at elevations of several hundred

metres above sea-level (asl). Here we use the term loosely to describe perennially frozen ground throughout this mountainous region.

The distribution of permafrost in mountainous areas is particularly complex because changes in air temperature, precipitation and vegetation cover that influence permafrost conditions and develop progressively across hundreds of kilometres in lowlands, can be generated by differences in elevation of a few hundred metres. Consequently, mountainous areas located in permafrost zones classified as discontinuous may locally span the entire range of permafrost conditions, from isolated patches at low elevations on north-facing slopes to continuous permafrost on mountain plateaus and summits (Lewkowicz and Ednie, 2004). Given the variety of micro-sites within such mountainous environments, it can be assumed that terrain will be present that has mean annual air and ground surface temperatures close to 0°C. If seasonally frozen, such sites may become permafrost during sustained atmospheric cooling or periods of reduced snowfall, or if permafrost, they may thaw during sustained warming or long-term increases in snowfall. Consequently it is evident that mountain permafrost areas should be spatially sensitive to climatic change.

Publications that explore climate change impacts on mountain permafrost are quite limited in number. They include Hoelzle and Haeberli (1995), who examined changes on permafrost and glaciers in the Swiss Alps, Janke (2005) who studied the Colorado Front Range, USA and Salzmann et al. (2007) who examined changes to ground surface temperatures in high mountain areas. Research has been limited by the paucity of high-resolution permafrost maps, especially for North America. We have recently developed such maps based on fieldwork and modelling for three locations in

extreme northwest British Columbia and southern Yukon, Canada (Lewkowicz and Ednie, 2004; Bonnaventure and Lewkowicz, 2008; Lewkowicz and Bonnaventure, 2008). The goal of this paper is to use these sites to explore the equilibrium effects on mountain permafrost of changes in (1) Mean Annual Air Temperature (MAAT) of -2K to +5K, (2) cloud cover, through altering the partitioning of direct beam and diffuse radiation (±5% to ±10%), and (3) the two changes acting together.

Study Areas

The three study areas of the Wolf Creek Basin, Ruby Range, and Haines Summit are located in the mountains of northwest Canada between 59° and 61°N (Figure 2.1).

Wolf Creek (60°30' N, 135°10' W) is situated 20-30 km south of Whitehorse and is a 190 km^2 watershed with elevations of 715-2080 m a.s.l. It is located within the sporadic discontinuous permafrost zone according to the Permafrost Map of Canada (Heginbottom et al., 1995) with 38-43% of the terrain underlain by permafrost (Lewkowicz and Ednie, 2004; Lewkowicz and Bonnaventure, 2008). The climate is continental with dry, cold conditions (Wahl et al., 1987). The closest climatological station is Whitehorse Airport (60° 42'N, 135° 4' W) at an elevation of 706 m a.s.l. where the MAAT is -0.7°C and the mean annual precipitation is 270 mm, 35% of which falls as snow (Environment Canada, 2007). MAAT measured in a valley within the central part of the basin at 1250 m a.s.l. is -3.0°C (07/2001-06/2008) while on Mount Granger, the highest point in the basin, it is -7.0°C (07/2006-06/2008). Mean annual precipitation in Wolf Creek is slightly greater than at Whitehorse, varying from 300-400 mm with 40% falling as snow (Janowicz, 1999). Basin vegetation comprises boreal forest, with sub-

alpine forest, shrubs, and an alpine tundra zone at progressively higher elevations (Francis, 1997).

The Ruby Range (61°12' N, 138°19' W) is located east of Kluane Lake in the precipitation shadow of the St. Elias Mountains and has a similar regional climate to Wolf Creek (Wahl et al., 1987). The area studied is approximately 425 km^2 in extent with elevations ranging from 760 to 2350 m a.s.l. Permafrost has been mapped as continuous for the high-elevation parts of the Ruby Range (Heginbottom and Radburn, 1992) but on the Permafrost Map of Canada the area is bisected by the boundary between the zones of sporadic and extensive discontinuous permafrost (Heginbottom et al., 1995). Our modelling gives an overall permafrost extent of 69% (Bonnaventure and Lewkowicz, 2008). Vegetation consists of coniferous forest including spruce and balsam fir at lower elevations. Willow and birch shrubs and krummholz forms as well as alpine tundra replace the trees as elevations increase (Harris 1987). Burwash Landing, the closest climatological station to the Ruby Range, is located 40 km to the northwest at an elevation of 805 m a.s.l. Its MAAT is -3.8°C (1971–2000), and annual precipitation is 280 mm, 40% of which falls as snow (Environment Canada, 2005). Our measurements at 1400 m a.s.l. in a valley in the middle of the study area, however, gave a MAAT of -1.7°C (07/2004–06/2006), 0.6°C *warmer* than at Burwash for the same two-year period which itself was 1.5°C warmer than the long-term mean.

The Haines Summit area (59° 37' N, 136° 27' W) in northwestern British Columbia has a maritime climate as a result of being located only 75 km from the Pacific Ocean. The area studied is 535 km^2 in extent with elevations ranging from 600 to 2210 m a.s.l. and it is mapped as being within the zone of isolated patches of permafrost

(Heginbottom et al., 1995). Our modelling, however, suggests that this classification represents an under-prediction at the local scale and that permafrost underlies 44% of the non-glacier-covered terrain (Bonnaventure and Lewkowicz, 2008). Vegetation consists of a dense shrub willow and birch zone at lower elevations and alpine tundra or bare fractured rock surfaces on higher terrain. Pleasant Camp, the closest climatological station, is located approximately 35 km to the south at 274 m a.s.l. and has a MAAT of 2.7°C (1971–2000; Environment Canada, 2005). Measurements within the study area at an elevation of 1230 m a.s.l. from 2003-2008 (with some data gaps) give a MAAT of -2.1°C. Annual precipitation recorded at Pleasant Camp averages about 1400 mm (Environment Canada 2005), with 52% falling as snow. Typical snow depths within the study area in late winter are around 2 m, several times those present at the other two study sites (Lewkowicz, 2008).

Methods

Permafrost Mapping and Modelling

Empirical-statistical models of permafrost distribution in the three study areas were developed from basal temperature of snow (BTS) measurements made at numerous sites in late winter in each area following the sampling recommendations outlined by Brenning et al. (2005). BTS values, measured beneath at least 80 cm of snow, are indicators of the presence or absence of permafrost (e.g., Haeberli, 1973; Hoelzle, 1992; Gruber & Hoelzle, 2001). The ground is sufficiently insulated from air temperature variations (Hoelzle et al., 1993) that BTS values are close to 0°C for seasonally frozen

sites, reflecting the presence of a freezing front at shallow depths. BTS values are lower at permafrost sites because the active layer is completely frozen in late-winter.

To move from the point measurements to a spatial model, the geo-referenced BTS values were related to elevation and potential incoming solar radiation (PISR), both derived from a 30 m digital elevation model (DEM) (Table 2.1). As in our previous publications (Bonnaventure and Lewkowicz, 2008; Lewkowicz and Bonnaventure 2008), the PISR field includes both direct beam and diffuse radiation. At the Haines Summit site, the relation between PISR and BTS proved to be statistically non-significant, probably due to persistent cloud cover and fog in this maritime study area (Bonnaventure and Lewkowicz, 2008). Observations using pits and ground temperature profiles in late summer of the presence of frozen ground (permafrost) or its absence (seasonal frost) were linked through logistic regression (Table 2.2) to the modeled BTS. Additional details on the field and statistical methods used are given in previous publications (Lewkowicz and Ednie, 2004; Bonnaventure and Lewkowicz, 2008). The analyses result in maps of present-day permafrost probability for 30 x 30 m grid cells. We assume that permafrost probability can be equated over many grid cells to calculate permafrost extent (Lewkowicz and Ednie, 2004).

Climate Change Scenario Modelling

Future increases in air temperature due to higher atmospheric concentrations of greenhouse gases are widely discussed, for example in the latest IPCC reports (IPCC 2007) and the Arctic Climate Impact Assessment (ACIA, 2004). We investigated a range of warming values up to +5 K based on IPCC and ACIA predictions for the upcoming

century. Scenario temperature changes in this paper are indicated in degrees Kelvin (K) rather than degrees Celsius (°C) in order to indicate change and avoid confusion with MAATs which are recorded in Celsius. We chose this approach rather than using Global or Regional Climate Model predictions because of the problem of adequately representing the topography in the western Cordillera where our sites are located (see Burn, 1994). We also investigated permafrost conditions under a cooler climate (-1 K and -2 K) which may have existed during the Little Ice Age (Farnell et al., 2004). This choice of changes in temperature is poorly constrained because the earliest air temperature records in northwest Canada start at the very end of the 19th Century, and isotopic analyses from ice cores and lakes in the region are linked to water source rather than past temperatures (Anderson et al., 2005; Fisher et al., 2004, 2008). Dendrochronological results for the region show that maximum temperatures during summers from 1684-1850 AD were generally 0-1 K colder than in the 1961-1990 reference period (Youngblut and Luckman, 2008) but summer temperatures may exhibit less variability than annual values. Consequently, we emphasize that we are exploring the impacts of scenarios of past cooling or future warming in this paper, rather than indicating that such changes took place or will take place.

Changes in MAAT were simulated in the spatial model by uniformly increasing the elevations in the DEM for cooling scenarios and decreasing them for warming scenarios (Janke, 2005) and then running the model to produce an altered BTS surface. This in turn affects the predicted permafrost probabilities which are calibrated with the non-linear logistic regression coefficients determined for the base (present-day) case (Table 2.2). We used an elevation change of 154 m K^{-1} which is equivalent to the

standard environmental lapse rate of 6.5 K km^{-1}. This method has the benefit of preserving all elements of the spatial model such as aspect and shading, as well as the relationships that exist between changes in BTS values and elevation, which vary from site to site. This rate is less than the BTS lapse rate of 8.2 K km^{-1} in Wolf Creek, but more than those observed in Ruby Range (5.0 K km^{-1}) and Haines Summit (3.2 K km^{-1}) (Lewkowicz and Bonnaventure, 2008). In order to explore the model's sensitivity to the choice of lapse rate, we varied it by ±1.5 K km^{-1}, increasing it to 8 K km^{-1} and decreasing it to 5 K km^{-1}. However, actual air temperature lapse rates in the study areas differ from the values chosen and may vary within the areas as well, so the results are regarded as a first attempt to examine the patterns and scale of change rather than as precise predictions.

Future changes in the partitioning of solar radiation induced by cloud cover are not well prescribed within climate models (IPCC, 2007) so we again used a scenario-type approach. The permafrost probability models employ modeled grids of PISR created within an ArcGIS 9.3 environment by the area solar radiation tool in Spatial Analyst. PISR was calculated for the snow-free period (May 15 - October 15) for each site using a diffuse radiation proportion (relating to cloud cover) based on observations of average cloud cover for the same period from Whitehorse (60%) and Burwash (65%) (Environment Canada, 2005) for Wolf Creek and Ruby Range respectively. PISR, calculated by comparing site observations of air and ground temperature, proved to be not statistically significant for Haines Summit (Table 2.1; Bonnaventure and Lewkowicz, 2008) so it was not possible to examine changes in this variable for this site. To simulate potential changes in cloud cover, the diffuse fraction for the other two areas was altered

over a range from -10% to +10%. During this procedure, an error was discovered in the software used to calculate PISR: increases in the proportion of diffuse radiation were accomplished by increasing the total incoming radiation while leaving direct beam unchanged. We corrected this problem by multiplying the predictions from the model by (1- diffuse proportion). Following correction, average PISR values changed slowly with the partitioning, with a decrease of about 1% as the proportion of diffuse radiation increased by 10% (Table 2.3). Once the adjusted PISR grids were computed the models were re-run using the original multiple linear regression and logistic regression equations.

Results

Temperature change scenarios

The impact of even a small degree of atmospheric warming or cooling on permafrost extent in the three study areas is considerable. An increase or decrease in MAAT of 1 K allows permafrost to form or degrade over time in about 20% of the Wolf Creek and Haines Summit study areas, while the change is about 14% for the Ruby Range (Figure 2.2). If MAATs during the LIA were 2 K colder, the models predict that 75-90% of the study areas would have been underlain by permafrost under equilibrium conditions. If MAATs increase by 5 K, Wolf Creek and Haines Summit will effectively lose all permafrost (<1% remaining) while the extent in the Ruby Range will be reduced to slightly more than 10% (Figure 2.2). The model predictions are for equilibrium states and do not account for lag times associated with permafrost formation and degradation. Given these lag effects, the outputs are best thought of as referring to the upper few metres of permafrost only.

The impacts of changes in MAAT on the spatial pattern of permafrost probabilities are broadly similar for the three study areas (Figures 2.3-2.5). Reducing the MAAT to represent possible conditions during the LIA increases the probability of permafrost, especially at lower elevations. Increasing the MAAT reduces the probability of permafrost in general, but high-elevation and shaded sites are almost unaffected when MAAT increases are small. The cells most sensitive to changes in air temperature are located in zones where base-case probabilities are intermediate. For example, in Wolf Creek, average permafrost probability for elevations around 1200 m asl increases from 0.17 to 0.46 for a reduction in MAAT of 1 K, and to 0.78 for a further 1 K drop (Figure 2.6). An increase of MAAT by 1 K for elevations at 1400 m asl in the same study area reduces the mean permafrost probability from 0.5 to 0.2 and a further 1 K increase reduces it to 0.06. In the field, sites such as these have ground temperatures close to 0°C: a reduction in MAAT allows permafrost probabilities to increase substantially (i.e. permafrost forms in an increasing percentage of the cells) while an increase makes permafrost unsustainable in most cells in the long-term. In contrast, elevation bands with cells that already exhibit high permafrost probabilities under the base case can change little during cooling, while those with very low probabilities at low elevations are only slightly affected during warming.

Permafrost zonal boundaries are represented by the critical mean probabilities of 0.1 (between isolated patches and sporadic discontinuous), 0.5 (between sporadic and widespread discontinuous) and 0.9 (between discontinuous and continuous) in Figure 2.6. Raising the MAAT causes these boundaries to ascend and lowering the MAAT does the reverse. The probability boundaries generally shift by 165-185 m K^{-1} at Wolf Creek, by

165-290 m K^{-1} at Ruby Range and virtually uniformly by 155 m K^{-1} at Haines Summit. For the +5 K scenario, the probabilities for both Wolf Creek and Ruby Range become less similar to the other curves and the degree of boundary shift is greater.

The permafrost probability vs. elevation curves are smooth for Haines Summit, slightly irregular for Wolf Creek and still more irregular for Ruby Range (Figure 2.6). These differences relate to the relative importance of PISR in each BTS model, from its exclusion at Haines Summit to its greatest strength at Ruby Range (Table 2.1). The strength of PISR affects the variability of permafrost probabilities within an individual elevation band in relation to aspect, slope and shading. Since this depends on the landscape morphometry which is not constant with elevation, irregular patterns can result. The impact is particularly evident at the highest elevations in Ruby Range where mean probabilities actually decrease with increasing elevation under +2 K and +5 K scenarios. Exposed summits in the area receive more radiation on average than the elevation bands immediately below them, and because of the strength of the PISR coefficient in the model, this is enough to reverse the general tendency for more permafrost at higher elevations.

Sensitivity analysis of lapse rate selection

The choice of lapse rate used in the model affected the absolute values of the predictions (Figure 2.7). A weakened lapse rate of 5 K km^{-1} resulted in a lower rate of spatial change per degree K of warming or cooling while a strengthened lapse rate (8 K km^{-1}) had the opposite effect. The trends are non-linear and differ from the base case by up to 10% within the range of MAAT changes tested. At +5 K, the results for Wolf Creek

and Haines Summit show virtually no permafrost remaining irrespective of the lapse rate used. These sensitivity runs indicate that the lapse rate in the field may affect the spatial pattern and the degree of change relating to atmospheric warming or cooling, but that the trends remain unaffected.

Solar radiation partitioning change scenarios

The impact of changing the proportion of total incoming radiation arriving as diffuse radiation on permafrost extent is virtually linear and quite limited overall for both Wolf Creek and the Ruby Range (Figure 2.8). A greater proportion of diffuse radiation within the modeled PISR increases the percentage of permafrost in part because the average PISR decreases (Table 2.3), but also because of the impact of non-linearity in the logistic regression curve. A 10% increase in the diffuse fraction at the Ruby Range results in permafrost extent increasing by 4% and a similar change at Wolf Creek produces a change of less than 2% (Figure 2.8). The reverse happens when the proportion of diffuse radiation is decreased. The slightly greater effect at Ruby Range is related to the greater strength of its PISR variable (as expressed by the standardized β-coefficient – see Table 2.1).

Notwithstanding the small change overall, the spatial impacts of the changes in PISR are quite noticeable, though more so at Ruby Range than Wolf Creek. The most sensitive cells are on south-facing slopes at mid-elevations (Figure 2.9). As the proportion of diffuse radiation is increased, these cells receive less direct beam radiation and the probability of permafrost increases significantly (Figure 2.9). There is virtually no change elsewhere in the landscape: equivalent north-facing slopes are almost

unaffected because sun angles are low so that the total incoming radiation to be partitioned is much smaller. The end result of the changes in the diffuse to direct beam partitioning is not only a small general reduction in permafrost extent but a spatial redistribution that almost exclusively affects the most irradiated sites.

Combination climate change scenarios

The combined effects of changing MAAT and the partitioning of solar radiation for Wolf Creek and the Ruby Range are shown in Figure 2.10. The changed partitioning results are quasi-parallel to those of the PISR base case for alterations in MAAT of -1 to +2 K, but predictions converge as MAAT changes become more extreme and predicted permafrost extents approach 0 or 100%.

An examination of spatial differences in the permafrost probabilities (not shown) demonstrated that areas where major changes take place between the base PISR case and the altered diffuse proportion cases, migrate as the MAAT changes. The south-facing slopes affected significantly in model runs with lower MAATs are located at lower elevations than those in runs with higher MAATs. The explanation is that the limited elevation band of sensitive mid-probability cells (where the logistic regression curve between modeled BTS temperatures and permafrost probability is steepest) itself relocates to lower or higher elevations.

Discussion

The scenario-type models presented above are best regarded as conceptual analyses for a number of reasons. First, they predict equilibrium, not transient permafrost

probability conditions. Since the models are empirically-statistically based, they cannot take into account lag times associated with permafrost formation and degradation. Potential changes in permafrost distribution are subject to varying lag times with depth (e.g. Burn and Nelson, 2006; Lawrence et al., 2008), and ice-rich permafrost in colder parts of the discontinuous permafrost zone may be quite resilient to thaw (Froese et al., 2008). On the other hand, mountain permafrost is usually less ice-rich than lowland permafrost, has a thinner organic mat, lower organic content, the surficial sediments are often coarse and the substrate may be bedrock. All of these characteristics would tend to promote a more rapid thermal response than in ice-rich lowland permafrost due to a combination of higher thermal conductivity and especially a lower latent heat content (e.g. Smith and Riseborough, 1983). Second, changes of MAAT to the extent we have modeled would also impact other environmental factors that in turn promote or militate against permafrost, notably vegetation and snow cover (Riseborough and Smith, 2002). Finally, field data show that the three study areas are affected to varying degrees by air temperature inversions in both winter and summer. These likely affect ground temperatures and hence permafrost probability distributions (Lewkowicz and Ednie 2004). The distribution models presented here do not yet incorporate these impacts, nor do we know the extent to which the pattern of inversions may be maintained as the regional MAAT changes.

In terms of sensitivity to atmospheric warming, it is clear that changes in MAAT in the order of those that have occurred over the past few centuries and that according to the IPCC (2007) and ACIA (2004) are likely in the upcoming century can substantially affect mountain permafrost probabilities in the three study sites described here. Given

current MAAT values of about 0 to -7°C over the elevational range in the area, it is not surprising that an increase of 5 K would be enough to eliminate most permafrost from these mountains in the long term, but the modelling shows that a much smaller degree of change can also have a substantial impact in critical elevation bands. This supports the hypothesis that mountain permafrost areas with discontinuous permafrost at present are sensitive to almost any type of climate change because the variety of ground temperature conditions present in a relatively small area is great. The modelling also identifies the elevations and aspects where changes might be expected as a result of recent and future atmospheric warming.

Trends in permafrost extent as a response to MAAT change are non-linear. The analyses show that permafrost probability zones migrate upwards as MAAT values decline and downwards as they rise. The actual amount of movement is impacted by the strength of the lapse rate used in the model. The interaction of these changes with the hypsometry of the study areas affects the percentage predictions. Hence loss of permafrost from the small peak areas will have a lesser apparent impact on overall permafrost extent than loss from mid-elevation valleys which may occupy much larger parts of the study area.

The validity of the adjustments to the partitioning of the PISR is much harder to assess and it should be noted that the probability model cannot incorporate potential accompanying changes in the long-wave balance. Alterations to the partitioning of PISR alone, and the combined model runs with MAAT changes, suggest that only minor changes in total extent are likely. However, there are significant impacts locally on south-facing slopes with intermediate permafrost probabilities. The level of irradiation is

high so that a small percentage change in partitioning affects the total PISR, which in turn alters the predicted BTS temperature. If the predicted BTS values fall on the steep part of the logistic regression curve, this is enough to alter the permafrost probability significantly. The group of cells with these characteristics also migrates spatially in relation to MAAT so that cells at lower elevations are impacted by the changed proportion of diffuse radiation when MAAT is reduced, and higher elevation cells are affected at increased MAATs.

Conclusions

We conclude the following:

1) Empirical-statistical permafrost distribution models can be used to explore the potential effects of higher or lower mean annual air temperatures, changes in the partitioning of incoming solar radiation, or a combination of the two. Our scenario-type modelling is for equilibrium states and does not account for lag times associated with permafrost formation and degradation. Given these lag effects, the outputs are best thought of as referring to only the upper few metres of permafrost in the near-term.

2) It is predicted that changes in MAAT have significant impacts on permafrost extent and spatial distribution. A reduction in MAAT of 2 K, which may be representative of LIA conditions, roughly doubles the extent of permafrost in the Wolf Creek and Haines Summit study areas. The change in the Ruby Range is limited to an increase of about one-third because this area has close to 70% permafrost extent under the base case (present-day). An increase in

MAAT of 2 K causes loss of more than two-thirds of the extant permafrost in Wolf Creek and Haines Summit, while extent in the Ruby Range declines by about one-third. The absolute values alter by up to ±10% relative to the base case if the lapse rate is perturbed by ±1.5 K km^{-1}.

3) Changes in the partitioning of PISR between diffuse and direct beam radiation have a smaller impact on permafrost extent in the study areas. However, non-uniform spatial changes develop, concentrated on steep south-facing slopes. The elevation band of most-affected cells in the models itself alters in relation to the air temperature scenario used.

4) The results support the concept that areas of discontinuous mountain permafrost are sensitive to climate change because micro-sites exist which are close to 0°C. Seasonally-frozen locations can become permafrost with a slight reduction in mean annual surface temperature. Conversely, locations with permafrost near 0°C may thaw during relatively slight warming. It is very likely that changes in permafrost conditions in these sensitive zones, which are identified by our modelling, have occurred during the past few decades, with concomitant impacts on other environmental variables, such as vegetation type, runoff generation and short-term landscape evolution. Use of the methodology to identify areas of potential future permafrost change should be helpful for hazard mapping and infrastructure development in mountainous parts of northwest North America.

Acknowledgments

This project was supported financially by the Canadian Foundation for Climate and Atmospheric Sciences, the Natural Sciences and Engineering Research Council of Canada, the Northern Scientific Training Program (Department of Indian Affairs and Northern Development), the Yukon Geological Survey, the Geological Survey of Canada, and the Faculty of Arts, University of Ottawa. Logistical support was provided by the Yukon Department of the Environment, courtesy of Rick Janowicz. Jim Coates, Marcia Phillips, and Andje Lewkowicz-Lalonde helped carry out the BTS surveys, and Mark Ednie, Reid Van Brabant and Emily Schultz provided assistance with the pits. The authors are also grateful for the reviews of Professor Wilfried Haeberli and Dr. Stephan Gruber.

References

Arctic Climate Impact Assessment. 2004 http://www.acia.uaf..edu.

Anderson, L., Abbott, M.B., Finney, B.P. and Burns, S.J. 2005. Regional atmospheric circulation change in the North Pacific during the Holocene inferred from lacustrine carbonate oxygen isotopes, Yukon Territory, Canada. *Quaternary Research* **64**: 21–35.

Bonnaventure P.P., and Lewkowicz A.G. 2008. Mountain Permafrost Probability Mapping Using the BTS Method in two Climatically Dissimilar Locations, Northwest Canada. *Canadian Journal of Earth Sciences,* **45**: 443-455.

Brenning, A., Gruber, S. & Hoelzle, M. 2005: Sampling and statistical analyses of BTS measurements. *Permafrost and Periglacial Processes*, **16(4)**, 383–393.

Brown, J., O.J. Ferrians, Jr., J.A. Heginbottom, and E.S. Melnikov, eds. 1997. Circum-Arctic map of permafrost and ground-ice conditions. Washington, DC: U.S. Geological Survey in Cooperation with the Circum-Pacific Council for Energy and Mineral Resources. Circum-Pacific Map Series CP-45, scale 1:10,000,000.

Burn, C. R. 1994. "Permafrost, tectonics, and past and future regional climate change, Yukon and adjacent Northwest Territories." *Canadian Journal of Earth Sciences* **31**: 182-191.

Burn, C. R. and F. E. Nelson 2006. "Comment on "A projection of severe near-surface permafrost degradation during the 21st century" by David M. Lawrence and Andrew G. Slater." *Geophysical Research Letters* **33**(21): L21503.

Croke M. S. Cess R. D. and Hameed S. 1999. Regional Cloud Cover Change Associated with Global Climate Change: Case Studies for three Regions of the United States. *Journal of Climate* **12:** 2128-2134.

Environment Canada. 2005. http://climate.weatheroffice.ec.gc.ca/climate_normals [Accessed May 17, 2005].

Environment Canada. 2007. http://www.climate.weatheroffice.ec.gc.ca/climateData/canada_e.html [Accessed June 5, 2007].

Farnell R., Hare P. G., Blake E., Bowyer V., Schweger C., Greer S., and Gotthardt R. 2004. Multidisciplinary Investigations of Alpine Ice Patches in Southwest Yukon, Canada. *Arctic* **57:** 247-259.

Fisher D., Osterberg E., Dyke A., Dahl-Jensen D., Demuth M., Zdanowicz C., Bourgeois J., Koerner, R.M., Mayewski P., Wake C., Kreutz K., Steig E., Zheng J., Yalcin K., Goto-Azuma K., Luckman B. and Rupper S. 2008: The Mt. Logan Holocene-late Wisconsinan Isotope Record: Tropical Pacific-Yukon Connections. *Holocene*. **18(5)**: 667-677.

Francis S. 1997. *Data Integration and Ecological Stratification of Wolf Creek Watershed, South-Central Yukon.* Report prepared for Indian and Northern Affairs Canada and Agriculture Canada. Applied Ecosystem Management Ltd.: Whitehorse. 23 pp.

Froese, D.G., Westgate, J.A., Reyes, A.V., Enkin, R.J., Preece, S.J. (2008). "Ancient permafrost and a future, warmer arctic." *Science* **321**(5896): 1648.

Gruber, S. and Hoelzle, M. 2001: Statistical modelling of mountain permafrost distribution: Local calibration and incorporation of remotely sensed data. *Permafrost and Periglacial Processes*, **12** 69-77.

Gruber, S. & Haeberli, W. 2009: Mountain permafrost. In: *Permafrost Soils,* edited by: Margesin, R., Biology Series Vol. 16, Springer, 33–44, doi: 10.1007/978-3-540-69371-0_3. http://www.geo.unizh.ch/~stgruber/pubs/gruber_2009_pf-soils.pdf

Haeberli W. 1973. Die Basis-Temperatur der winterlichen Schneedecke als möglicher Indikator für die Verbreitung von Permafrost in den Alpen. *Zeitschrift für Gletscherkünde und Glazialgeologie* **1-2**: 221-227.

Haeberli, W., Guodong, C., Gorbunov, A.P. and Harris, S.A. 1993: Mountain permafrost and climatic change. *Permafrost and Periglacial Processes*, **4** 165-174.

Harris S.A. 1987: Altitude Trends in Permafrost Active Layer Thickness, Kluane Lake, Yukon Territory. *Arctic*, **40** 179-185.

Harris, S.A. and Corte, A.E. 1992. Interactions and relations between mountain permafrost, glaciers, snow and water. *Permafrost and Periglacial Processes*, **3** 103-110.

Heginbottom JR, Dubreuil MA and Haker PT. 1995. Canada Permafrost. (1:7,500,000 scale). In *The National Atlas of Canada*, 5th Edition, sheet MCR 4177. Ottawa: National Resources Canada.

Heginbottom JA and Radburn LK. 1992. Permafrost and ground ice conditions of northwestern Canada; (Scale 1:1,000,000). *Geological Survey of Canada Map* 1691A.

Hilbich C. Hauck C. Hoelzle M. Scherler M. Schudel L. Völksch I. Vonder Mühll D. and Mäusbacher R. 2008. Monitoring mountain permafrost evolution using electrical resistivity tomography: A 7-year study of seasonal, annual, and long-term variations at Schilthorn, Swiss Alps. *Journal of Geophysical Research* 113**:** FO1S90.

Hoelzle M. 1992. Permafrost occurrence from BTS measurements and climatic parameters in the Eastern Swiss Alps. *Permafrost and Periglacial Processes* **3:** 143-147.

Hoelzle, M., Haeberli, W., Keller, F. 1993. Application of BTS measurements for modelling mountain permafrost distribution. In *Proceedings of the Sixth International Conference on Permafrost, Beijing*. South China University of Technology, Beijing. Vol.1: 272-277.

Hoelzle, M., and W. Haeberli 1995: Simulating the effects of mean annual air temperature changes on permafrost distribution and glacier size. An example from the Upper Engadin, Swiss Alps, *Ann. Glaciol*., 21, 400–405.

IPCC. 2007. http://www.ipcc.ch/ipccreports/assessments-reports.htm

Janke, J.R. 2005. Modelling past and future alpine permafrost distribution in the Colorado front range. Earth Surface Processes and Landforms, **30:** 1495-1508.

Janowicz JR. 1999. Wolf Creek Research Basin - Overview. Wolf Creek Research Basin: Hydrology, Ecology, Environment. *In* Pomeroy, J.W., Granger, R.J (eds.) *Wolf Creek Research Basin: Hydrology, Ecology, Environment*. Saskatoon: National Water Research Institute. 125-134.

Kwong, Y. T. and Gan, T.Y. (1994). "Northward migration of permafrost along the Mackenzie Highway and climatic warming." *Climatic Change* **26**(4): 399-419.

Lawrence D. M. Slater A. G. Romanovsky V. E. and Nicolsky D. J. 2008. Sensitivity of a model projection of near-surface permafrost degradation to soil column and representation of soil organic matter. *Journal of Geophysical Research* **113:** F02011.

Lewkowicz, A.G. 2008. Evaluation of Miniature Temperature-loggers to Monitor Snowpack Evolution at Mountain Permafrost Sites, Northwestern Canada. *Permafrost Periglacial Processes.,* **19:** 323-331.

Lewkowicz, A.G. and Ednie, M. 2004 Probability mapping of mountain permafrost using the BTS method, Wolf Creek, Yukon Territory, Canada. *Permafrost Periglacial. Processes.,* **15** 67-80.

Lewkowicz A.G. and Bonnaventure P.P. (2008). Interchangeability of Mountain Permafrost Probability Models, Northwest Canada, *Permafrost and Periglacial Processes,* **19**: 49-62.

Salzmann, N., J. Noetzli, C. Hauck, S. Gruber, M. Hoelzle, and W. Haeberli 2007: Ground surface temperature scenarios in complex high-mountain topography based on regional climate model results, *Journal of Geophysical Research.*, 112, F02S12, doi:10.1029/2006JF000527.

Smith, M.W. and D.W. Riseborough (1983). Permafrost sensitivity to climate change. *Permafrost, Procedeedings of the fouth International Confrence.* Washington D.C., National Acadeny Press. **1:** 1178-1183.

Wahl HE, Fraser DB, Harvey RC and Maxwell JB. 1987. *Climate of Yukon.* Canadian Government Publishing Centre.

Youngblut, D.K. and Luckman, B.H. 2008: Maximum June–July temperatures in the southwest Yukon over the last 300 years reconstructed from tree-rings. *Dendrochronologia* 25, 153–66.

Table 2.1: Linear regression coefficients used to predict BTS values in the three study areas (after Lewkowicz and Bonnaventure, 2008)

Study area and year		Elevation (m)	PISR[a] (MJ/m^2)	Intercept	Standardized β-coefficient ratio	n	r^2
Wolf Creek Basin (2001 and 2002)	Coefficient	-0.0082	0.0055	Non-significant	2.60	317	0.31
	P-value	0.0000	0.0000	-			
	Standard Error	0.0007	0.0005	-			
Ruby Range (2006)	Coefficient	-0.0050	0.011	-13.91	0.94	29	0.29
	P-value	0.007	0.004	0.003			
	Standard Error	0.0017	0.0036	4.37			
Haines Summit (2005 and 2006)	Coefficient	-0.0032	Non-significant	1.87	∞	77	0.36
	P-value	0.000	-	0.003			
	Standard Error	0.0005	-	0.608			

[a]Note: coefficients differ from those in Lewkowicz and Bonnaventure (2008) because values in the PISR field are corrected from those generated before the error in the Solar Analyst software was discovered (see text).

Table 2.2: Logistic regression statistics for permafrost probability models (Lewkowicz and Bonnaventure, 2008)

Study area	n	BTS coefficient	Std. Error	Significance level	Constant	Std. Error	Significance level
Wolf Creek	145	-1.15	0.22	<0.01	-3.91	0.85	<0.01
Ruby Range	85	-1.56	0.32	<0.01	-6.66	1.49	<0.01
Haines Summit	95	-5.8	1.17	<0.01	-12.2	2.38	<0.01

Table 2.3: Effect of change in proportion of diffuse radiation on PISR in model runs

Study area	Mean PISR in study area (MJ/m^2) associated with indicated change in diffuse proportion				
	-10%	-5%	Base case	+5%	+10%
Wolf Creek	1464	1456	1448	1440	1432
Ruby Range	1415	1408	1402	1396	1389

List of Figures

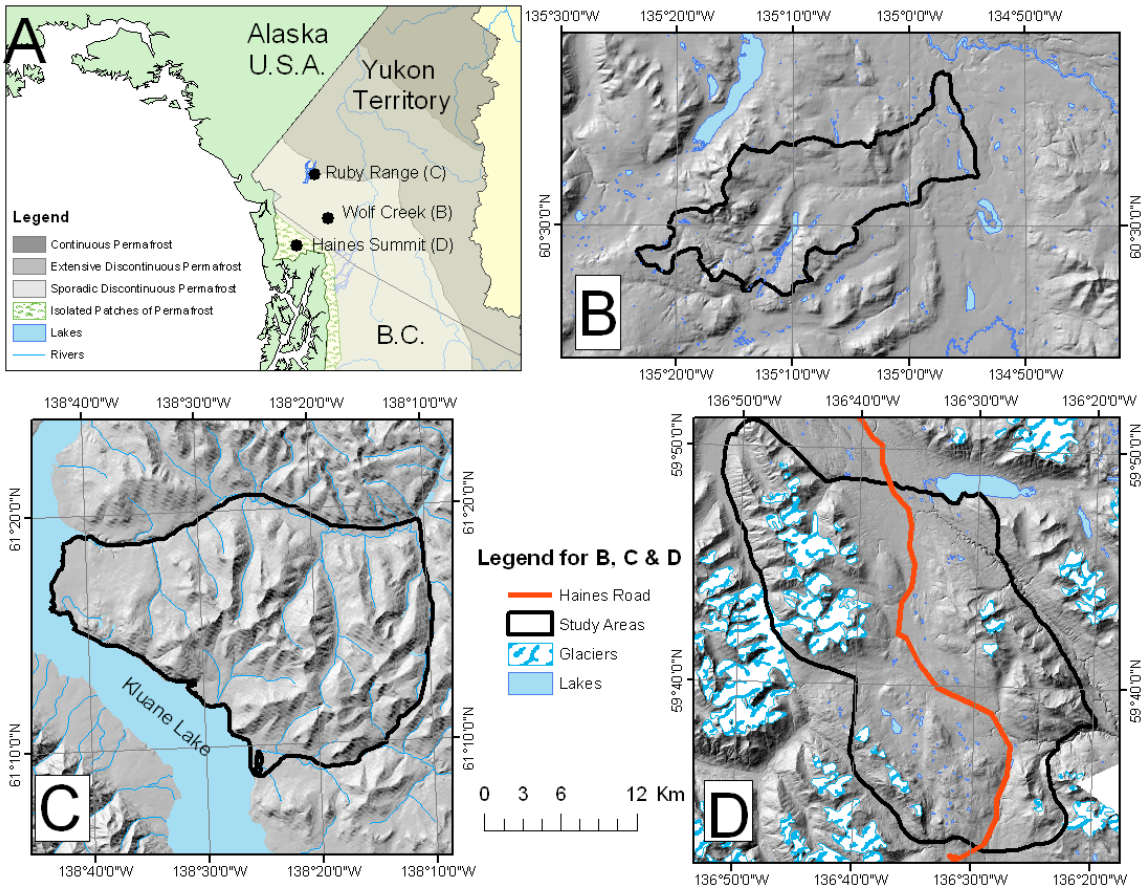

Figure 2.1: (A) Location of the three study areas in relation to permafrost zones (after Heginbottom et al., 1995) in northwest Canada; (B) Wolf Creek; (C) Ruby Range; (D) Haines Summit.

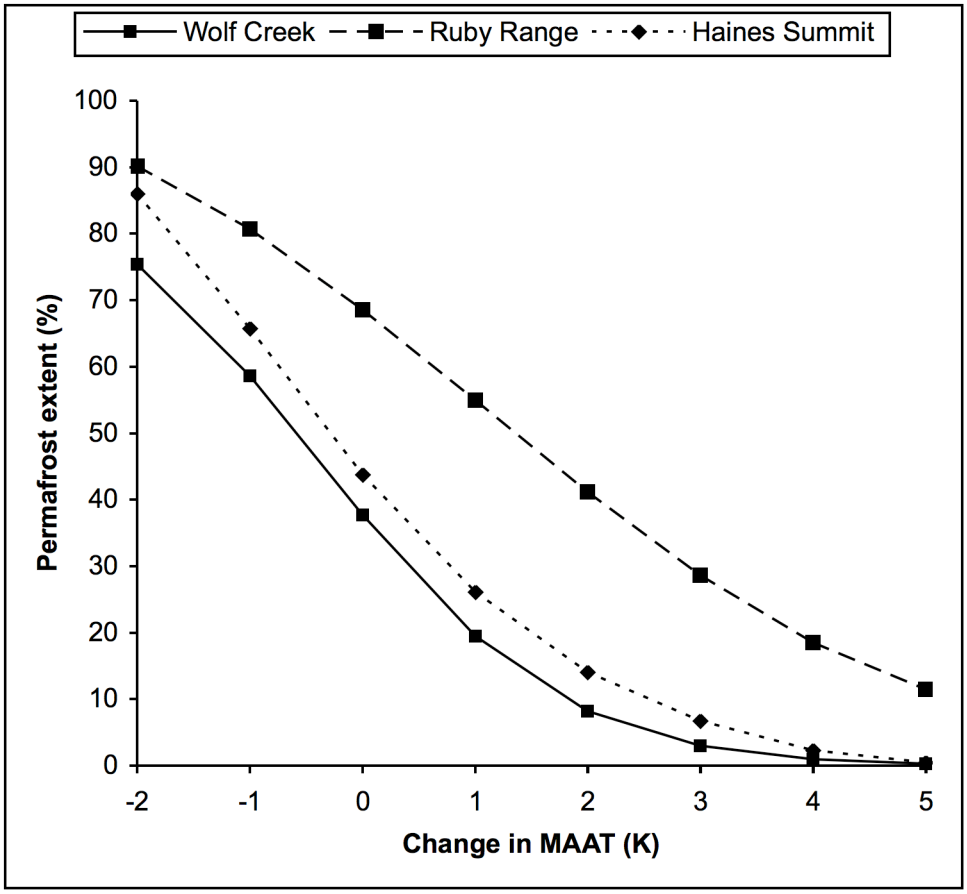

Figure 2.2: Predicted percentage of terrain underlain by permafrost in the three study areas for MAAT changes from -2 K to +5 K. Note: glacier-covered areas in Haines Summit were excluded from the percentage calculations as permafrost conditions beneath the ice are unknown.

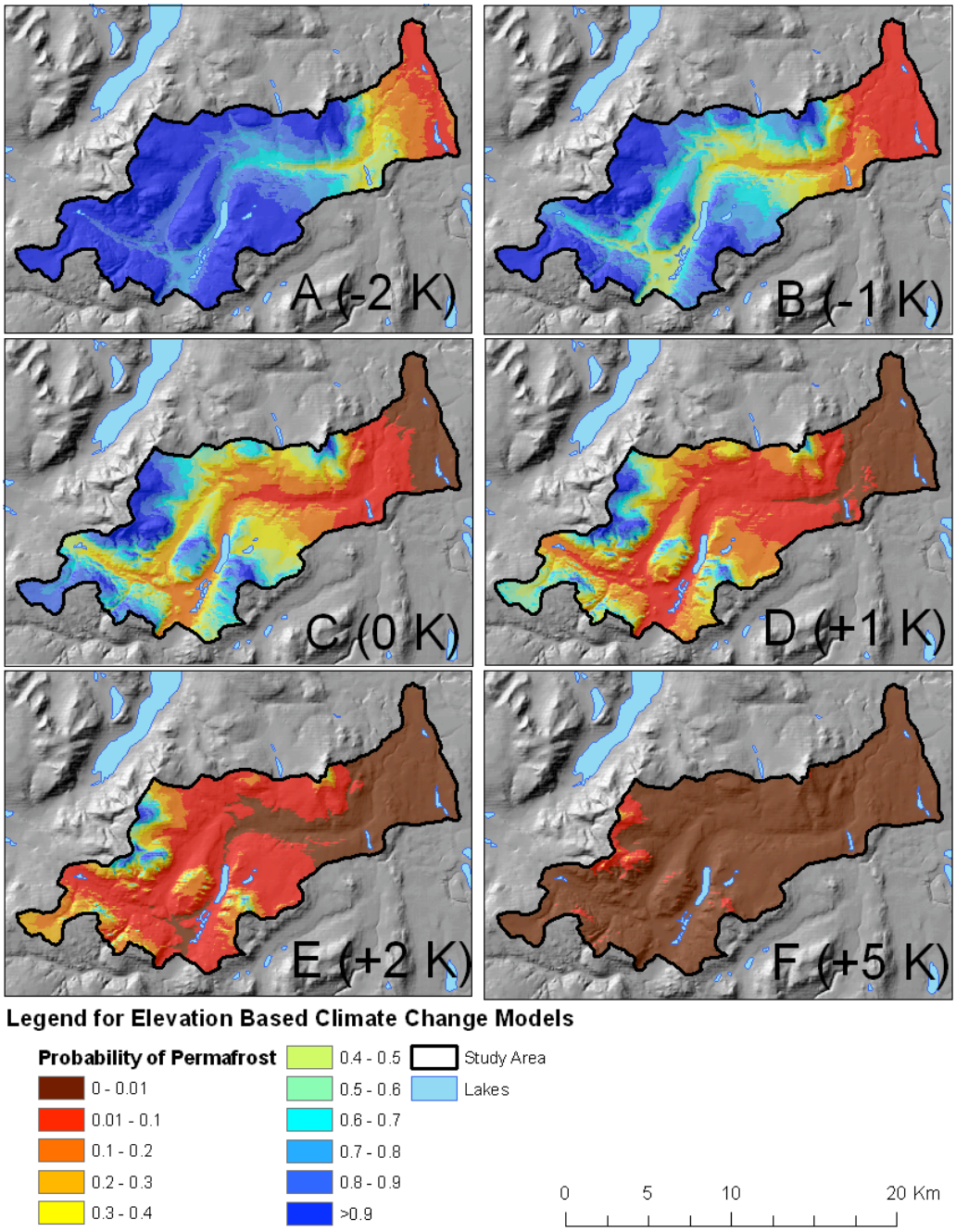

Figure 2.3: Modelled permafrost probability in Wolf Creek for the base case (present-day) and equilibrium conditions under climatic change scenarios of ± 1 K, ± 2 K and +5 K. Note that the model does not account for lag times associated with permafrost formation and degradation. Given these lag effects, the model outputs are best thought of as referring to the upper few metres of permafrost only.

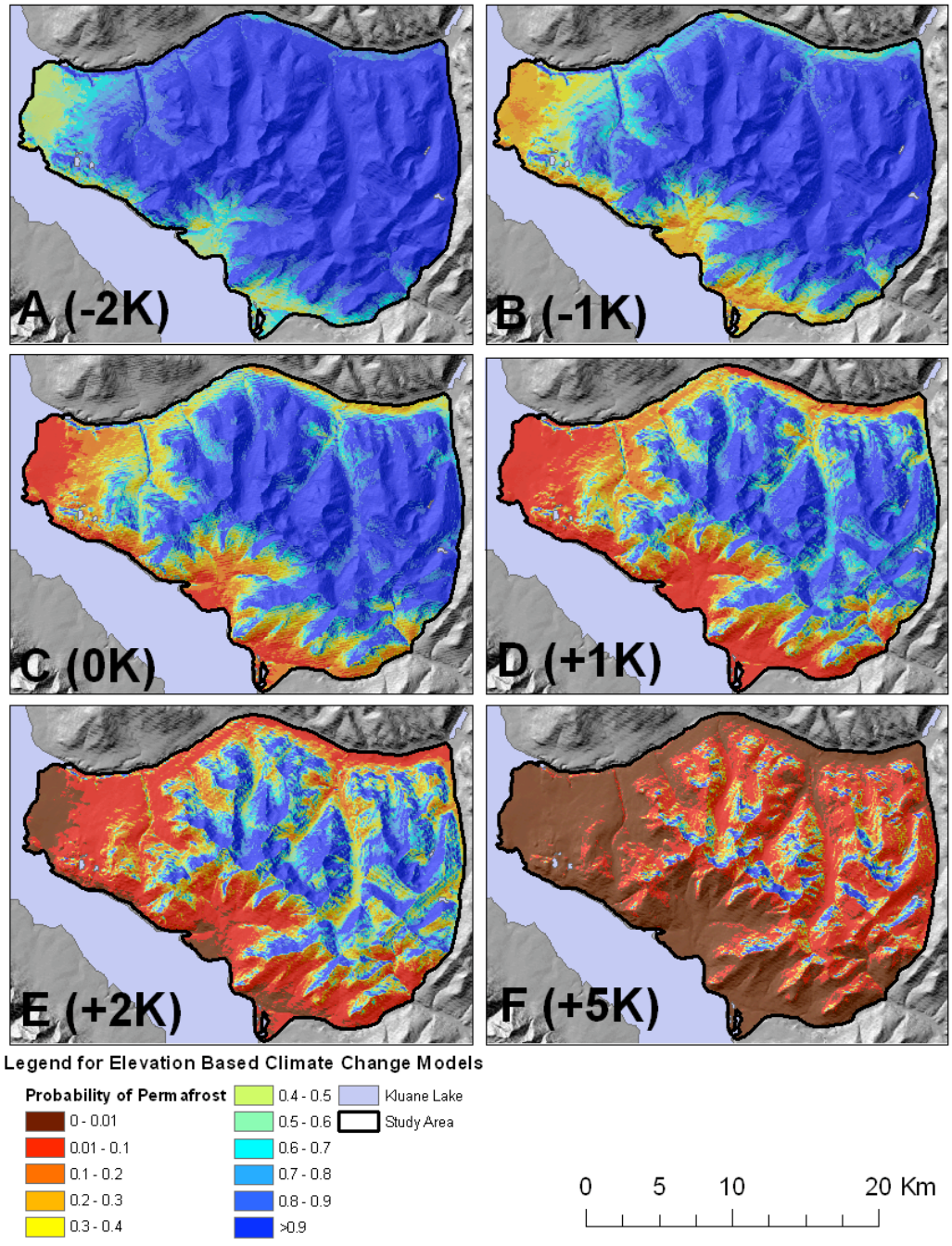

Figure 2.4: Modelled permafrost probability in Ruby Range for the base case (present-day) and equilibrium conditions under climatic change scenarios of ± 1 K, ± 2 K and +5 K. Note that the model does not account for lag times associated with permafrost formation and degradation. Given these lag effects, the model outputs are best thought of as referring to the upper few metres of permafrost only.

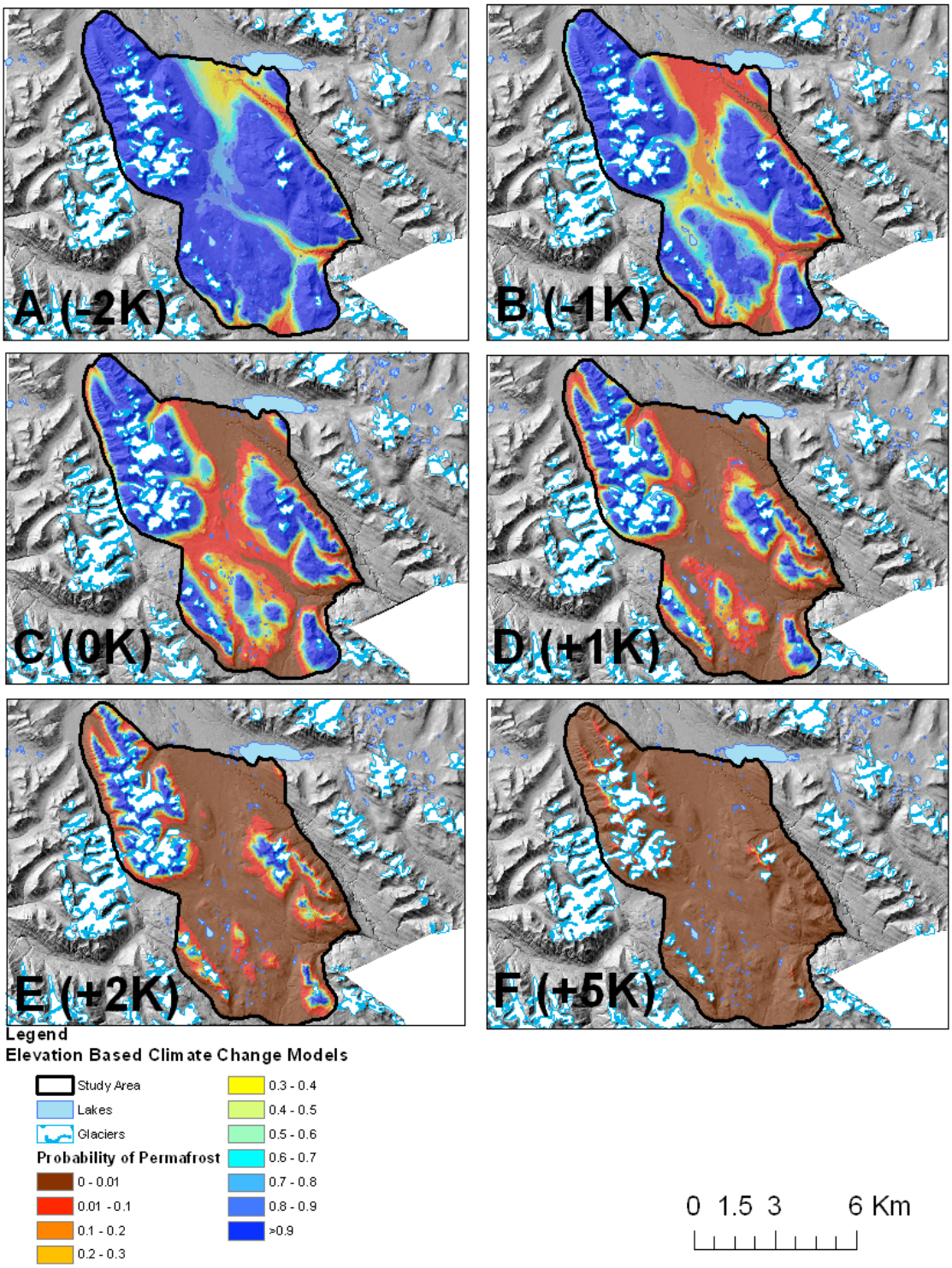

Figure 2.5: Modelled permafrost probability in Haines Summit for the base case (present-day) and equilibrium conditions under climatic change scenarios of ± 1 K, ± 2 K and +5 K. Note that the model does not account for lag times associated with permafrost formation and degradation. Given these lag effects, the model outputs are best thought of as referring to the upper few metres of permafrost only.

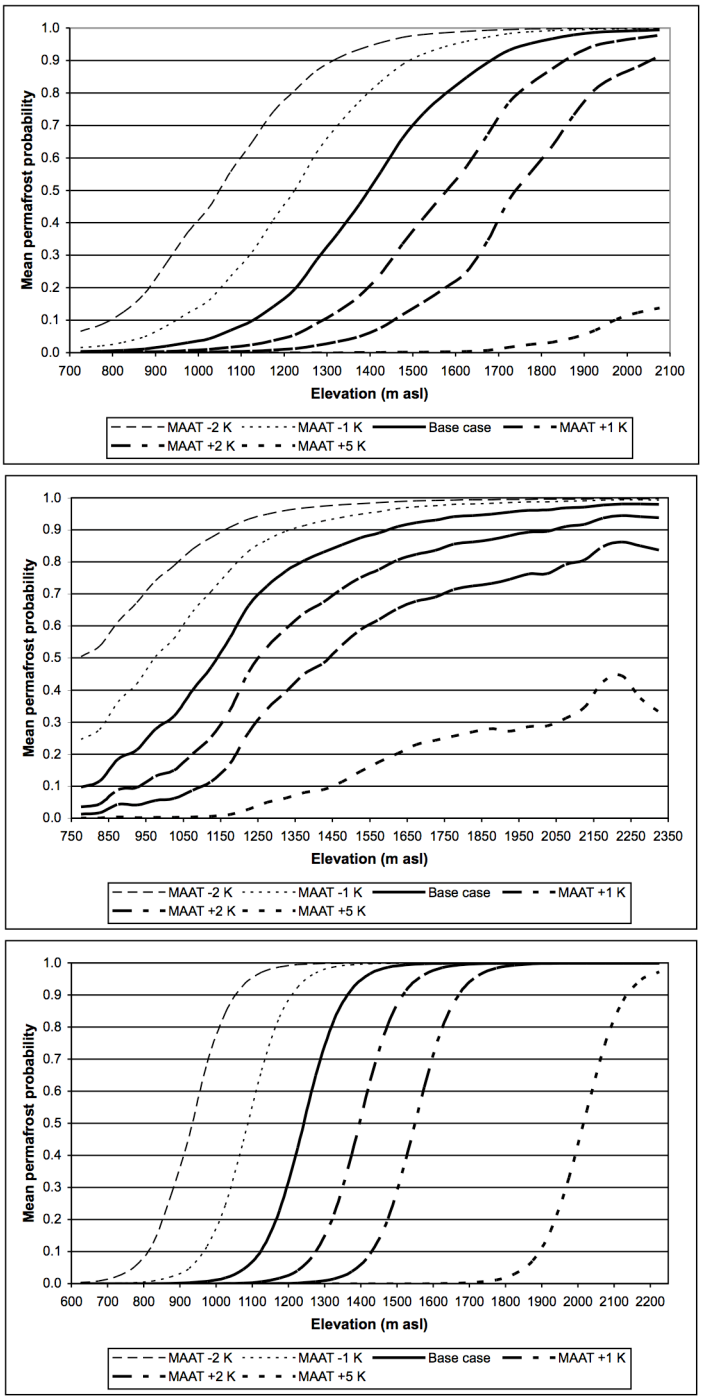

Figure 2.6: Mean permafrost probabilities vs. elevation under the base case (present-day) and reductions and increases in MAAT. Upper graph: Wolf Creek; middle graph: Ruby Range; lower graph: Haines Summit. Probability levels of 0.1, 0.5 and 0.9 respectively represent the lower boundaries of the sporadic discontinuous, widespread discontinuous and continuous permafrost zones.

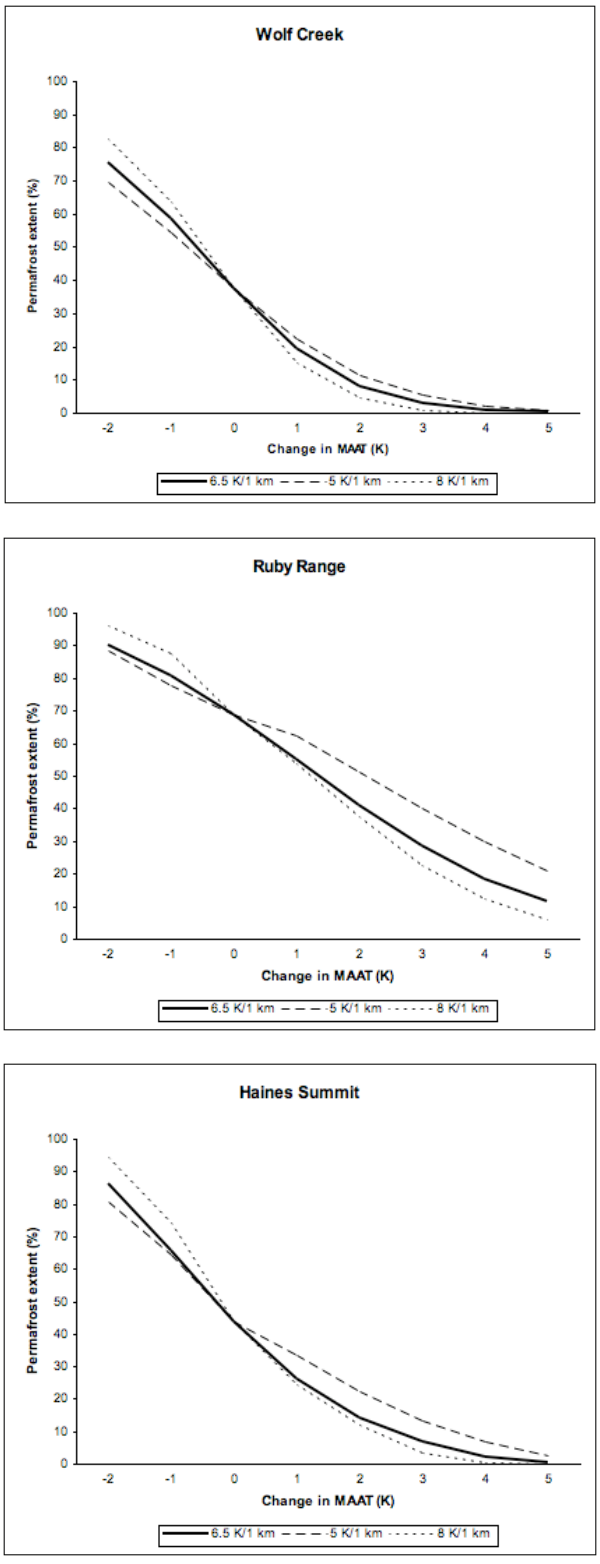

Figure 2.7: Sensitivity of predicted area underlain by permafrost to changes in MAAT with weakened (5 K km^{-1}) or strengthened (8 K km^{-1}) lapse rates, for Wolf Creek, Ruby Range and Haines Summit.

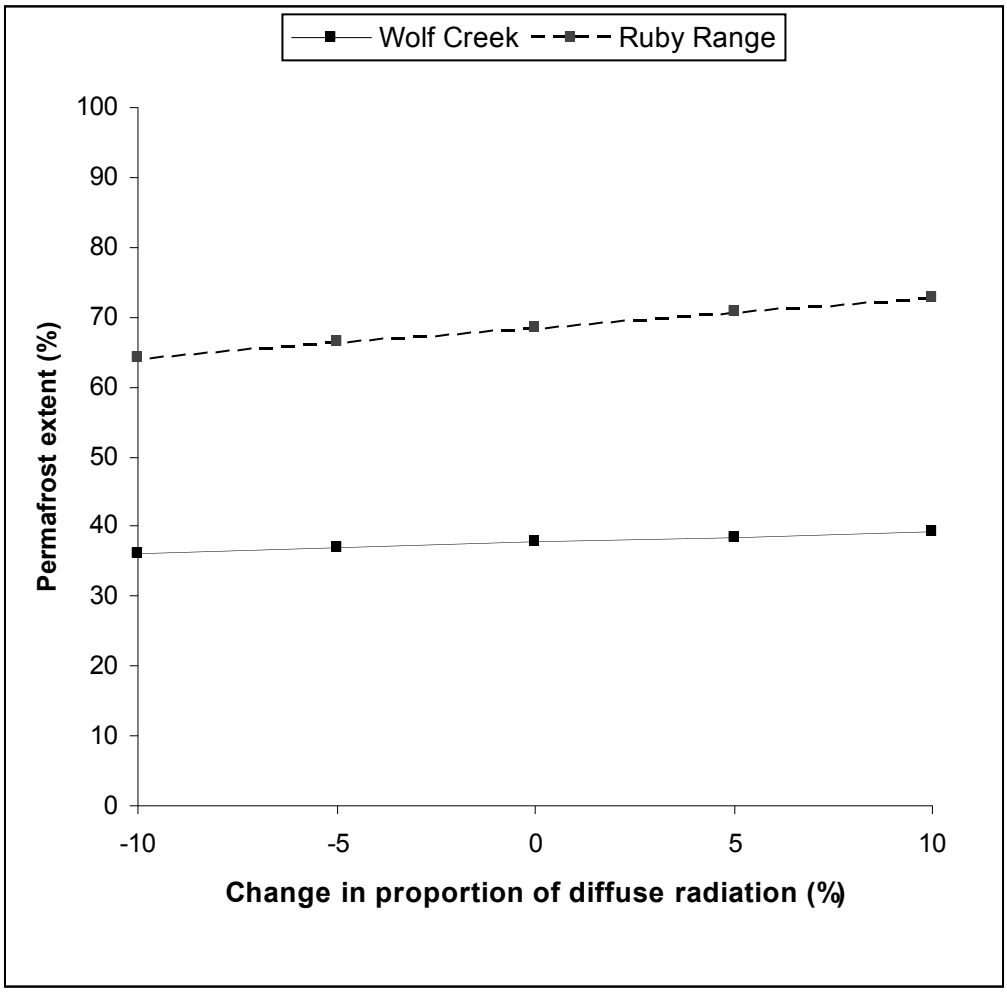

Figure 2.8: Predicted percentage of terrain underlain by permafrost at Wolf Creek and Ruby Range for base case MAAT with changes in the partitioning of diffuse radiation in the PISR calculation.

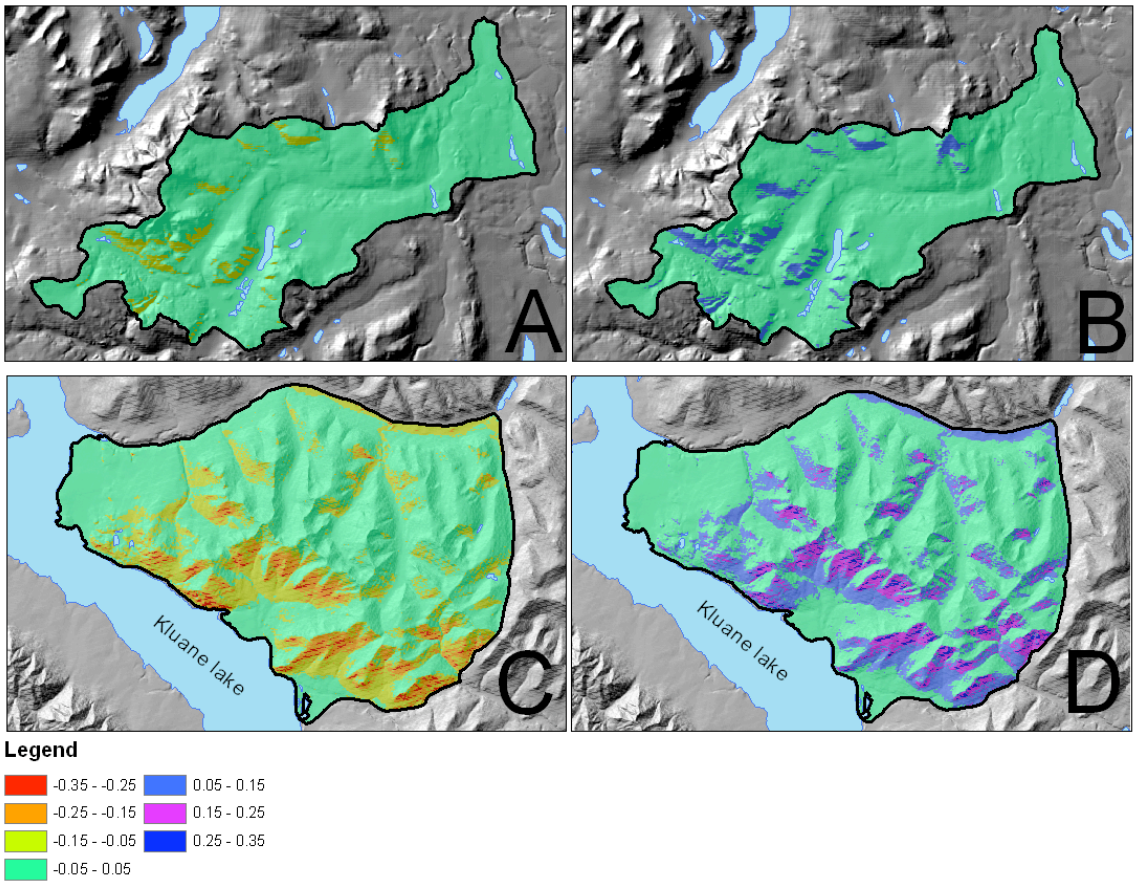

Figure 2.9: Probability difference maps vs. the base case with current MAAT for (A) Wolf Creek -10% diffuse, (B) Wolf Creek +10% diffuse, (C) Ruby Range -10% diffuse, (D) Ruby Range +10% diffuse. Model predictions are for equilibrium states and do not account for lag times associated with permafrost formation and degradation. Given these lag effects, the model outputs are best thought of as referring to the upper few metres of permafrost only.

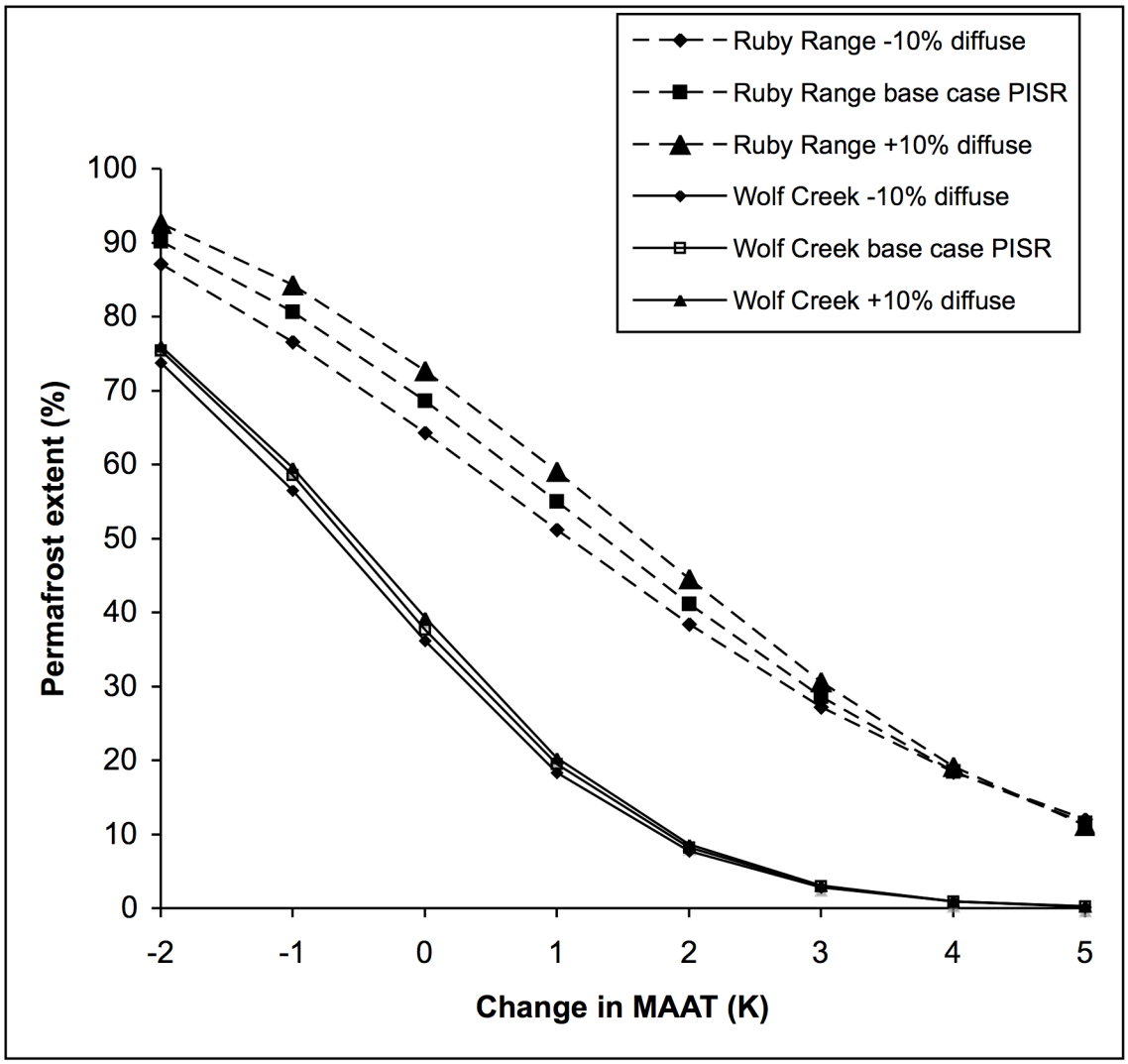

Figure 2.10: Predicted percentage of terrain underlain by permafrost at Wolf Creek and Ruby Range for changes in MAAT and in the partitioning of diffuse radiation in the PISR calculation relative to the base case.

Chapter Three

Interchangeability of mountain permafrost probability models, northwest Canada

Abstract

Spatial models of mountain permafrost probability based on measurements of the Basal Temperature of Snow (BTS) and ground-truthing were developed for three study areas located >200 km apart. The interchangeability of these locally-derived empirical-statistical models was examined by predicting BTS values from the equations developed at the other two sites, and using logistic regression to relate these modelled values to the local ground-truthed data. Equations for two of the areas were effectively interchangeable, producing permafrost extent predictions within 2% of each other, and permafrost probabilities within ±0.1 for more than 85% of the cells. Predictions were much less similar when their equations were applied to the third area and when its equation was applied to them. Model interchangeability appears to depend on where a site lies on a continuum from elevation-controlled (infinite ratio of the standardized coefficient of elevation to that of potential incoming solar radiation in the BTS equation), to radiation-dominated (ratio much less than unity of the same variables). Extensive ground-truthing is essential, helping to constrain the logistic regression and hence the overall permafrost percentage. Additional investigations are needed to relate these ratios to regional climate in order to allow the spatial interpolation of permafrost probability models across the North American Cordillera.

Key words: Mountain permafrost; BTS; modeling; logistic regression.

Introduction

Mapping the occurrence and extent of permafrost at a scale meaningful to infrastructure and natural hazard planning is a significant challenge in mountainous environments. Mean substrate temperatures exhibit high spatial variability produced by factors such as elevation, gradient, aspect, and snow depths. This complexity, together with the logistical difficulties of operating in steep, high elevation areas, has led to the development of numerous predictive models (e.g. Etzelmüller et al., 2001, 2007; Gruber and Hoelzle, 2001; Heggem et al., 2006). A few of these employ a process-oriented approach, such as the Temperature at the Top of Permafrost model (Juliussen and Humlum, 2007), but most use an empirical-statistical approach that relates the occurrence of permafrost to specified variables, most commonly to the Basal Temperature of Snow (BTS) (e.g. Haeberli, 1973; Hoelzle, 1992; Ishikawa and Hirakawa, 2000; Isaksen et al., 2002; Julián and Chueca, 2007).

The BTS approach has the advantage that field measurements from a relatively limited number of sample localities can be used to generate spatial models for much larger areas because the major explanatory variables, typically elevation and potential incoming solar radiation (PISR) can be derived from digital elevation models (DEMs). However, to our knowledge, there has been no attempt to explore the limits of applicability of model equations generated in one area to distant sites, as might be required in North America where mountain permafrost extends thousands of kilometres along the western Cordillera (Harris and Brown, 1982; Harris, 1983, 1987; Heginbottom et al., 1995). The overall utility of the method over extensive areas, therefore, is unknown.

Most studies using the BTS technique have assumed a relationship between modelled BTS values and a three-fold qualitative classification of permafrost presence (the BTS 'rules-of-thumb') as probable, possible, or improbable (e.g. Hoelzle, 1992; Julián and Chueca, 2007), or have tested this classification with a small number of ground-truthing points derived from rock glacier distributions (e.g. Janke, 2004, 2005) or geophysical soundings (e.g. Gardaz, 1997; Ishikawa and Hirakawa, 2000; Tanarro et al., 2001). In contrast, extensive physical validation of permafrost conducted in late summer allowed Lewkowicz and Ednie (2004) to use logistic regression to develop quantitative probability maps of mountain permafrost for the Wolf Creek basin near Whitehorse. This technique has now been applied successfully to two other areas in northwest Canada (Bonnaventure and Lewkowicz, 2008) located between 59° and 61°N (Figure 3.1 and Table 3.1). To date, BTS and ground-truthing relationships have been developed independently in the three study sites and applied over areas of 200-500 km^2. However, discontinuous permafrost zones encompass more than 500,000 km^2 in the mountains of northwest Canada and it is clear that modelling at a scale suitable for infrastructure development or hazard mapping cannot feasibly be based on detailed sampling throughout this vast area.

As a step towards developing interpolation methods, this paper examines the interchangeability of predictive equations generated at the three study areas located 200-250 km apart and varying in terms of terrain and climate. The results provide a basis for future efforts to generate detailed mountain permafrost probability predictions over large areas of northwestern North America and across significant climatic gradients.

Study Areas

Wolf Creek, Yukon Territory

Wolf Creek is situated 20-30 km south of Whitehorse where the mean annual air temperature (MAAT) at an elevation of 706 m a.s.l. is -0.7°C and the mean annual precipitation is 270 mm, 35% of which falls as snow (Environment Canada, 2007). Our measurement of MAAT in a valley within the central part of the basin is -3.0°C (08/2001-07/2007) at an elevation of 1250 m a.s.l.. Mean annual precipitation in Wolf Creek is slightly higher than at Whitehorse, varying from 300-400 mm with 40% falling as snow (Janowicz, 1999).

Wolf Creek is located within the sporadic discontinuous permafrost zone according to the Permafrost Map of Canada (Heginbottom et al., 1995). Basin vegetation comprises boreal forest, sub-alpine forest, a shrub zone dominated by willows up to 3 m high, and an alpine tundra zone at progressively higher elevations (Francis, 1997).

Ruby Range, Yukon Territory

The Ruby Range is located east of Kluane Lake in the precipitation shadow of the St. Elias Mountains. The closest climate station is Burwash Landing (61° 22’ N, 139° 3’ W), 40 km to the northwest at an elevation of 805 m a.s.l. The MAAT there is -3.8°C (1971–2000), with approximately 280 mm of precipitation, 40% of which falls as snow (Environment Canada, 2005). Our measurements at 1400 m a.s.l. in the valley of Swanson Creek in the middle of the study area, however, give a MAAT of -1.7°C

(07/2004–06/2006), 0.6°C *warmer* than at Burwash for the same two-year period which itself was 1.5°C warmer than the 30-year mean.

The high-elevation part of the Ruby Range mapped by Heginbottom and Radburn (1992) at a scale of 1:1,000,000 is shown as continuous permafrost, while on Heginbottom et al. (1995) at a scale of 1:7,500,000 the area is bisected by the boundary between the zones of sporadic (10-50%) and extensive discontinuous permafrost (50-90%). Vegetation consists of coniferous forest including spruce and balsam fir at lower elevations. Willow and birch shrubs and krummholtz forms as well as alpine tundra replace the trees as elevations increase (Harris, 1987).

Haines Summit, British Columbia

The Haines Summit area in northwestern British Columbia straddles the Haines Road close to the border with the Alaskan panhandle and has a maritime climate due to the influence of the Pacific Ocean only 75 km to the southwest. The closest climatological station, Pleasant Camp, approximately 35 km south of Haines Summit at 274 m a.s.l., has a MAAT of 2.7°C (1971–2000; Environment Canada 2005). Our measurements from 2003-2006 (with some data gaps) on Three Guardsmen Mountain at the southern end of the study area give a MAAT of -1.5°C at an elevation of 1230 m a.s.l. Annual precipitation recorded at Pleasant Camp averages about 1400 mm (Environment Canada, 2005), with 52% falling as snow. Mean precipitation is unknown for the study site but is likely to be still higher and the percentage of snow is likely to be greater because of the elevation difference. Typical snow depths on the ground in the late winter are 2–3 m, several times greater than at the other two sites.

The area chosen for study falls within the zone of isolated patches of permafrost indicating that less than 10% of the terrain is expected to be underlain by perennially frozen ground (Heginbottom et al. 1995). Vegetation consists of a dense shrub willow and birch zone at lower elevations and alpine tundra or bare fractured rock surfaces on higher terrain.

Methods and Results

Generation of Local Permafrost Probability Maps

Permafrost predictive equations were first generated for Wolf Creek with field data collected in 2001 and 2002 (Lewkowicz and Ednie, 2004) and subsequently for Haines Summit and the Ruby Range with fieldwork in 2005 and 2006 (Bonnaventure and Lewkowicz, 2008). Field procedures involved deployment of surface temperature loggers to check on the timing of BTS measurements, geo-referenced measurement of BTS in two successive years, and late-summer ground-truthing for the presence or absence of permafrost using numerous pits and near-surface temperature profiles. Spatial modeling of the BTS temperature field was then undertaken using linear regression and predicted grid cell values were related through logistic regression to the ground-truthed data (Lewkowicz and Ednie, 2004). The logistic regression procedure is essential to calibrate the BTS measurements which must be taken where snow depths exceed 80 cm and therefore in the northwest Cordillera typically represent sites with relatively warm ground temperatures (Lewkowicz and Ednie, 2004).

Linear regression in Wolf Creek employed the independent variables of elevation and PISR to predict BTS values. Elevation was extracted from a 30-m digital elevation

model (Geobase, 2005) and PISR was calculated for the snow-free period in ESRI ArcView 3.2 using the Solar Analyst extension (Fu and Rich, 1999). Cloud cover was set to 60% based on mean cloud cover information for Whitehorse (Environment Canada, 2005). Initially, BTS predictions in the lowest part of the basin exceeded 0°C, and the elevation variable was cubed before regression to avoid this problem (Lewkowicz and Ednie, 2004). Equations generated for the other two sites, however, used a linear relationship with elevation, as is common in the literature (e.g. Gardaz, 1997; Imhof et al., 2000; Lugon and Delaloye, 2001; Isaksen et al., 2002; Gruber and Hoelzle, 2001; Tanarro et al., 2001). For the current study, to allow the transfer of the equations between the sites, the Wolf Creek data were re-analysed and a new linear predictive equation was produced. Since the intercept in the new regression equation was not significant, it was omitted when modeling the BTS field (Table 3.2).

As in the original analysis, a modeled BTS value was generated for each of the 145 ground-truthing points where permafrost presence or absence had been recorded. Logistic regression was used to relate modeled BTS values to the probability of permafrost presence and the resultant model was used to generate a map for the basin which exhibited only slight differences from that previously published (Lewkowicz and Ednie, 2004).

Equivalent procedures were followed for the Ruby Range and Haines Summit areas. The only differences were: (1) four temperature measurements were made within a radius of 5 m to characterise each BTS sampling point, in order to minimize the nugget effect. The nugget effect is defined as the degree to which BTS measurements differ from each other within the same general area (Brenning et al., 2005); (2) measurement sites

were spaced sufficiently (>150 m) to avoid significant spatial autocorrelation; (3) surface wetness index was included as an additional independent variable but did not significantly improve BTS predictions and so was omitted for the analyses presented in this paper; (4) cloud cover percentages were set to 65% for the Ruby Range based on records from Burwash Landing and to 70% for Haines Summit based on an analysis of air and surface ground temperature records (Bonnaventure and Lewkowicz, in review); (5) in the Ruby Range, BTS data were obtained in a single winter because low snow conditions prevented access in 2005. The last point resulted in the number of sampling sites being relatively low (29) but their distribution through a range of elevations and orientations meant that there was a good fit between observed and predicted probabilities (Figure 3.2). Permafrost probability maps for all three study areas are shown in Figures 3.3A, 3.4A and 3.5A.

Model Transfer

Each of the empirically-derived equations (Table 3.2) was used to predict BTS values for the other two study sites. Logistic regression was then performed by comparing the newly modeled BTS values with the study area's ground-truthing results (Table 3.3). Maps of predicted permafrost probability were generated with the transferred models (Figures 3.3B and 3.3C, 3.4B and 3.4C, 3.5B and 3.5C). In addition, probability differences were mapped to display spatial differences in the model predictions (Figures 3.3D and 3.3E, 3.4D and 3.4E, 3.5D and 3.5E). Differences are shown as positive if the transferred model increased the permafrost probability of a grid cell compared to the site-specific model, and negative if it reduced it. Histograms of the probability differences are shown in Figure 3.6.

Although the maps show permafrost probability, because the 30 x 30 m grid cells are very numerous (>200 x 10^3 in each of the areas), it can be assumed that the overall percentage of permafrost in the areas is calculable from an average of the grid cell probabilities (Lewkowicz and Ednie, 2004).

Wolf Creek

The site-specific model (WC) predicts that 38% of the basin is underlain by permafrost (Figure 3.3A), 5% less than that estimated using a cubed relationship with elevation (Lewkowicz and Ednie, 2004). The transferred equations from the Ruby Range (WC-rr) and Haines Summit (WC-hs) give predicted permafrost extents of 50% and 36% respectively and the broad spatial patterns generated by the three models appear quite similar (Figures 3.3A-3.3C). In detail, however, probabilities predicted using the WC-rr model are greater than the WC model in the lower part of the basin and are not as high on the peaks, with the former outweighing the latter (Figure 3D). The WC-hs model provides a much better fit with the WC model in both average permafrost probability and in distribution. Nevertheless, some steep north- and south-facing slopes , particularly in the upper part of the basin, exhibit differences because the Haines Summit equation does not include PISR as a predictor variable. The difference histogram shows that WC-rr in general produces results that differ from the WC model: only 27% of the grid cells predicted using the former are within ±0.1 of the probability of the latter (Figure 3.6). In contrast, the WC-hs, produces probabilities within ±0.1 of the WC model for 87% of the grid cells (Table 3.4).

Ruby Range

The site-specific model (RR) gives a permafrost areal extent of 66% whereas the model transferred from Wolf Creek (RR-wc) yields 69%, and that from Haines Summit (RR-hs) predicts 71%. The permafrost probability maps again show broadly similar patterns, but there are significant differences in particular locations (Figure 3.4A-3.4C). The biggest differences are concentrated on upper elevation south-facing slopes where the transferred models over-predict permafrost probability compared to the site-specific model, and on lower elevation north-facing slopes where the transferred models under-predict probability. The Wolf Creek equation more closely mimics the site-specific probabilities, producing values within ±0.1 for 72% of the cells, while the Haines Summit equation achieves this for only 62% (Figure 3.6).

Haines Summit

The site-specific model (HS) predicts that 44% of the area is underlain by permafrost. The transferred models from Wolf Creek (HS-wc) and the Ruby Range (HS-rr) predict 44% and 41% respectively. The difference map with the HS-wc model shows predicted probability differences exceeding ±0.1 only in the small transition zones between permafrost and non-permafrost terrain especially on south-facing slopes (Figure 3.5D). The HS-rr model, in spite of its similar overall permafrost percentage, generates major differences through virtually the entire area, but especially on steep, south-facing slopes. The histograms of probability difference show that only 18% of the cells have probabilities within ±0.1 of the site-specific case, and that nearly 16% have differences <-

0.5 or >+0.5 (Figure 3.6). The HS-wc model, however, produces results that are within ±0.1 of the site-specific model for 87% of the grid cells.

Discussion

When the BTS equations are applied to other sites, the resultant temperatures often differ significantly from the originally modelled values. If we had used the 'rules-of-thumb' (Haeberli, 1973) to convert these temperatures to qualitative permafrost probability, the extent of permafrost in the resultant maps would have changed considerably. The results of the transfer modelling using the ground-truthing, however, are all within 12% of the original site-specific models, an outcome that we attribute to the ground-truthing points constraining the logistic regression. This demonstrates the critical importance of ground-truthing to the modelling procedure.

The relationships derived for Wolf Creek and Haines Summit can be used to accurately predict the permafrost percentage at the other site, producing estimates within 2% of the site-specific predictions (Table 3.4). Moreover, the spatial pattern is quite similar, with more than 85% of the grid cells in both transferred models having a permafrost probability within ±0.1 of those from the site-specific case. When these models are applied to the Ruby Range, however, the results are less coherent. Predicted permafrost percentages are similar for the RR-wc and RR models, but only 72% of the grid cells are within ±0.1 (Table 4). RR-hs differs more from RR in permafrost percentage and there is a lower level of spatial accord between the predicted probabilities.

The biggest differences arise when the Ruby Range equations are used at the other two sites. The WC-rr model predicts 12% more permafrost than the WC model and

only 27% of the cells are within ±0.1. Results for HS-rr are closer in terms of permafrost percentage (-3% compared to HS) but the concordance in the spatial pattern is lower, with only 18% of the cells within ±0.1 and many more of the cells showing extreme differences (Figure 3.6).

The most important influence on interchangeability appears to be the relative importance of elevation and PISR in the prediction of BTS (Table 3.2). The elevation coefficient controls the vertical change in modelled BTS temperatures through the terrain while the PISR strength influences the degree of variability in BTS values within an elevation band, brought about by aspect and slope. The relative importance of the variables can be assessed using ratios of the standardized β-coefficients (Bring, 1994). The absolute values of these ratios vary from infinity for Haines Summit, to 2.6 for Wolf Creek, to unity for the Ruby Range (Table 3.2). These values indicate that the pattern of permafrost probability is elevation-controlled at Haines Summit (Figure 3.5A), elevation-dominated at Wolf Creek (Figure 3.3A) and equally elevation- and radiation- influenced in the Ruby Range (Figure 3.4A). Along the potential continuum from elevation-controlled to radiation-controlled, Wolf Creek and Haines Summit appear to be quite close, with the result that differences between their predictions emerge only on steep north-facing and south-facing slopes within critical elevation bands where a change in modelled BTS values substantially impacts permafrost probability (e.g. Figures 3.3E and 3.5D). Wolf Creek and Ruby Range are apparently further apart on the continuum and when the former's equation are applied to the latter only 72% of the grid cells have probability differences within ±0.1 (Table 3.4). As would be expected, a still lower proportion (62%) fall into this group when the Haines Summit transfer equations are

applied. Differences are greater when the Ruby Range equations are applied to the other two sites. The percentage of grid cell probabilities within ±0.1 of those for the site-specific model is slightly higher for Wolf Creek than Haines Summit (27% vs. 18%), and the percentages of very different probability predictions (<-0.5 or >0.5) are much greater at the latter site (Figure 3.6).

A second factor that appears to affect the similitude of transferred models compared to the site-specific models is the hypsometry of the study areas. This works in tandem with the BTS predictor coefficient ratios and is thought to be the reason for the lower applicability of the Ruby Range equations to the other two sites. Wolf Creek has extensive valley floors and slopes between 1300 and 1600 m a.s.l. that constitute almost 50% of the basin (Figure 3.7). These areas, which field sampling and the site-specific modelling both indicate are transitional in terms of permafrost probability, have much higher probabilities predicted by the WC-rr model than by the WC model. The result is that differences in the transferred equation are amplified by the weighting of the area and permafrost for the basin as a whole is over-predicted. In addition, many parts of these extensive areas exhibit probabilities that are not within ±0.1 of the site-specific model so that the overall percentage in this category is low. Over-prediction is not the same at Haines Summit because the areally dominant elevation bands are below 1400 m a.s.l. (Figure 3.7) which in this warmer, maritime environment is low enough that none of the models predicts substantial permafrost within them. The hypsometry, therefore, impacts the actual percentage of permafrost predicted for the study areas and the apparent goodness-of-fit.

We have found only one other study in the literature which provides data suitable for comparison with our standardized β-coefficients. Julián and Chueca (2007) predicted permafrost distribution for a small area of the Spanish Pyrenees using elevation and May PISR. The ratio of their β-coefficients is 0.18 indicating that this area is radiation-dominated, as suggested by the critical influence of shading on permafrost distribution. This very low ratio may well represent the extreme opposing end of the continuum from elevation-controlled areas.

Conclusions and Future Work

This study has shown for the first time that it is possible to use permafrost probability equations developed at one site to provide a reasonable prediction of the extent and spatial distribution of mountain permafrost for a location more than 200 km distant. Successful interchangeability of the models appears to depend on where the source and target sites lie on a continuum between elevation-controlled to radiation-dominated. This can be assessed by examining the ratio of the standardized coefficients for elevation and PISR in the BTS equations. Success is also influenced by the hypsometry of the areas within critical elevation ranges where permafrost probabilities change rapidly. In all cases, extensive ground-truthing is vital to maintaining an accurate prediction of the percentage of permafrost during model transfer.

Further investigations are underway to assess whether the three sites studied to date encompass the variability in the ratios of coefficients in northwestern Canada and to examine relationships between the ratios and standard climatic variables. Extrapolation between regions will require an assessment of how the BTS coefficients vary through

space as well as the testing of predictions at intermediate ground-truthing points. This information will be needed to allow accurate permafrost probability modelling across the vast North American Cordillera.

Acknowledgments

This project was supported financially by the Canadian Foundation for Climate and Atmospheric Sciences, the Natural Sciences and Engineering Research Council of Canada, the Northern Scientific Training Program (Department of Indian Affairs and Northern Development), the Yukon Geological Survey, the Geological Survey of Canada, and the Faculty of Arts, University of Ottawa. Logistical support was provided by the Yukon Department of the Environment, courtesy of Rick Janowicz. Jim Coates, Marcia Phillips, and Andje Lewkowicz-Lalonde helped carry out the BTS surveys, and Mark Ednie, Reid Van Brabant and Emily Schultz provided assistance with the pits. The comments of the two anonymous referees are appreciated, as is the assistance of Professor Charles Harris, Associate Editor, who handled the review process.

References

Bonnaventure PP and Lewkowicz AG. (2008). Mountain permafrost probability mapping using the BTS method in two climatically dissimilar locations, northwest Canada. *Canadian Journal of Earth Science,* **45**: 443-455.

Brenning A, Gruber S, and Hoelzle M. 2005. Sampling and statistical analyses of BTS Measurements. *Permafrost and Periglacial Processes***. 16**: 383-393.

Bring J. 1994. How to standardize regression coefficients. *The American Statistician* **48**: 209-213.

Environment Canada. 2005. http://climate.weatheroffice.ec.gc.ca/climate_normals [Accessed May 17, 2005].

Environment Canada. 2007. http://www.climate.weatheroffice.ec.gc.ca/climateData/canada_e.html [Accessed June 5, 2007].

Etzelmüller B, Hoelzle M, Heggem ESF, Isaksen K, Mittaz C, Vonder Mühll D, Ødegård RS, Haeberli W, and Sollid JL. 2001. Mapping and modelling the occurrence and distribution of mountain permafrost. *Norwegian Journal of Geography* **55**: 186-194.

Etzelmüller B, Farbrot H, Gudmundsson A, Humlum O, Tveito OE, and Björnsson H. 2007. The regional distribution of mountain permafrost in Iceland. *Permafrost and Periglacial Processes* **18**: 185-199.

Francis S. 1997. *Data Integration and Ecological Stratification of Wolf Creek Watershed, South-Central Yukon.* Report prepared for Indian and Northern Affairs Canada and Agriculture Canada. Applied Ecosystem Management Ltd.: Whitehorse. 23 pp.

Fu, P. and Rich, P.M. 1999: Design and implementation of the Solar Analyst: an Arcview extension for modeling solar radiation at landscape scales. http://www.esri.com/library/userconf/proc99/proceed/papers/pap867/p867.htm [Accessed May 21, 2005].

Gardaz, JM. 1997. Distribution of mountain permafrost, Fontanesses Basin, Valaisian Alps Switzerland. *Permafrost and Periglacial Processes* **8:** 101-105.

Geobase NTS 105D, 115G, 114P, 30 m resolution DEMs. http://www.geobase.ca [Accessed May 25, 2005].

Gruber S and Hoelzle M. 2001. Statistical modeling of mountain permafrost distribution: local calibration and incorporation of remotely sensed data. *Permafrost and Periglacial Processes* **12:** 69-77.

Haeberli W. 1973. Die basis-temperatur der winterlichen schneedecke als moglicher indikator fur die verbeitung von permafrost in den alpen. *Zeitschrift für Gletscherkünde und Glazialgeologie* **1-2**: 221-227.

Harris SA. and Brown RJE. 1982. Permafrost distribution along Rocky Mountains in Alberta. *In* French, HM (ed.) *The Roger J.E. Brown Memorial Volume, Proceedings of the Fourth Canadian Permafrost Conference, Calgary, Alberta, March 2-6, 1981*. National Research Council: Ottawa, pp. 59-67.

Harris SA. 1983. Comparison of the climatic and geomorphic methods of predicting permafrost distribution in western Yukon Territory. In *Permafrost: Fourth International Conference, Proceedings, Fairbanks, Alaska, July 17-22, 1983*. National Academy Press: Washington, DC, pp. 450-455.

Harris SA. 1987. Altitude trends in permafrost active layer thickness, Kluane Lake, Yukon Territory. *Arctic* **40:** 179-185.

Heggem ESF, Etzelmüller B, Anarmaa S, Sharkhuu N, Goulden CE, Nandinsetseg B. 2006. Spatial distribution of ground surface temperatures and active layer depths in the Hövsgöl area, northern Mongolia. *Permafrost and Periglacial Processes* **17**: 357-369.

Heginbottom JR, Dubreuil MA and Haker PT. 1995. Canada Permafrost. (1:7,500,000 scale). In *The National Atlas of Canada*, 5th Edition, sheet MCR 4177. Ottawa: National Resources Canada.

Heginbottom JA and Radburn LK. 1992. Permafrost and ground ice conditions of northwestern Canada; (Scale 1:1,000,000). *Geological Survey of Canada Map* 1691A.

Hoelzle M. 1992. Permafrost occurrence from BTS measurements and climatic parameters in the Eastern Swiss Alps. *Permafrost and Periglacial Processes* **3:** 143-147.

Imhof M, Pierrehumert G, Haeberli W and Kienholz H. 2000. Permafrost investigation in the Schilthorn Massif, Bernese Alps, Switzerland. *Permafrost and Periglacial Processes* **11**: 189-206.

Isaksen K., Hauck C, Gudevang E, Ødegård RS and Sollid JL. 2002. Mountain permafrost distribution in Dovrefjell and Jotunheimen, southern Norway, based on BTS and DC resistivity tomography data. *Norsk Geografisk Tidsskrift* **56:** 122-136.

Ishikawa M and Hirakawa K. 2000. Mountain permafrost distribution based on BTS measurements and DC resistivity soundings in the Daisetu Moutains, Hokkaido, Japan. *Permafrost and Periglacial Processes* **11:** 109-123.

Janke JR. 2004. The occurrence of alpine permafrost in the Front Range of Colorado. *Geomorphology* **67**: 375-389.

Janke JR. 2005. Modeling past and future alpine permafrost distribution in the Colorado Front Range. *Earth Surface Processes and Landforms* **30:** 1495-1508.

Janowicz JR. 1999. Wolf Creek Research Basin - Overview. Wolf Creek Research Basin: Hydrology, Ecology, Environment. *In* Pomeroy, JW, Granger, RJ (eds.) *Wolf Creek Research Basin: Hydrology, Ecology, Environment*. Saskatoon: National Water Research Institute. 125-134.

Julián A and Chueca J. 2007. Permafrost distribution from BTS measurements (Sierra de Telera, Central Pyrenees Spain): assessing the importance of solar radiation in a mid-elevation shaded mountainous area. *Permafrost and Periglacial Processes* **18:** 137-149.

Juliussen H and Humlum O. 2007. Towards a TTOP Ground Temperature Model For Mountainous Terrain in Central-Eastern Norway. *Permafrost and Periglacial Processes* **18**: 161-184.

Lewkowicz AG and Ednie M. 2004. Probability mapping of mountain permafrost using the BTS method, Wolf Creek, Yukon Territory, Canada. *Permafrost and Periglacial Processes* **15:** 67-80.

Lugon R and Delaloye R. 2001. Modeling alpine permafrost distribution, Val de Rechy, Valais Alps (Switzerland). *Norsk Geografisk Tidsskrift* **55**: 224-229.

Tanarro LM, Hoelzle M, Garcia A, Ramos M, Gruber S, Gomez A, Piqueer M, and Palacios D. 2001. Permafrost distribution modelling in the mountains of the Mediterranean: Corral del Veleta, Sierra Nevada, Spain. *Norsk Geografisk Tidsskrift* **55**: 253 – 260.

Wahl HE, Fraser DB, Harvey RC and Maxwell JB. 1987. *Climate of Yukon.* Canadian Government Publishing Centre.

Table 3.1: Characteristics of the three study areas

Study area	Latitude and Longitude	Area (km^2)	Elevation range (m a.s.l.)	Permafrost zone[a]	Climatic type and region[b]	Sampling years[c]
Wolf Creek	60°30'N, 135°10'W	190	660-2080	Sporadic discontinuous	Continental: Upper Yukon-Stikine Basin	BTS: 2001 & 2002; GT: 2002
Ruby Range	61°12'N, 138°19'W	425	750-2300	Sporadic/Widespread discontinuous	Continental: Upper Yukon-Stikine Basin	BTS: 2006; GT: 2005
Haines Summit	59°37'N, 136°27'W	535	850-2200	Isolated patches	Maritime: St. Elias-Coast Range	BTS: 2005 & 2006; GT: 2005

[a] Based on Heginbottom *et al.* (1995)

[b] Based on Wahl *et al.* (1987)

[c] BTS: years of Basal Temperature of Snow sampling; GT: years of summer ground-truthing.

Table 3.2: Linear regression coefficients to predict BTS values in the three study areas

Study area		Elevation (m)	PISR (MJ/m^2)	Intercept	Standardized β-coefficient ratio[b]	n	r^2
Wolf Creek Basin	Coefficient	-0.0082	0.0022	NS[a]	2.60	317	0.31
	P-value	0.0000	0.0000	-			
	Standard Error	0.0007	0.0005	-			
Ruby Range	Coefficient	-0.0052	0.0043	-9.39	0.99	29	0.29
	P-value	0.008	0.008	0.01			
	Standard Error	0.0019	0.0015	3.39			
Haines Summit	Coefficient	-0.0032	NS[a]	1.87	∞	77	0.36
	P-value	0.000	-	0.003			
	Standard Error	0.0005	-	0.608			

[a] NS: Omitted because non-significant

[b] Absolute ratio of standardized coefficient of elevation to PISR

Table 3.3: Logistic regression statistics for original and transferred models of permafrost probability.

Model[a]	N	BTS coefficient	Standard Error	Constant	Standard Error
WC	145	-1.15	0.22	-3.91	0.85
WC-hs	145	-2.37	0.46	-6.31	1.33
WC-rr	145	-1.08	0.31	-5.73	1.82
RR	85	-1.17	0.25	-4.84	1.19
RR-wc	85	-1.05	0.21	-3.99	0.95
RR-hs	85	-2.59	0.52	-4.68	1.05
HS	95	-5.8	1.17	-12.2	2.38
HS-wc	95	-4.0	1.07	-19.37	5.15
HS-rr	95	-0.75	0.25	-4.65	1.26

[a] Model designation is XX (modeled field area),–xx (source area for BTS equations). WC – Wolf Creek; RR – Ruby Range; HS – Haines Summit. Note: the coefficient and constant in each of the equations are significant at $p < 0.01$.

Table 3.4: Summary of average permafrost probability and percent grid cell probability differences within ±0.1 between site-specific and transferred models

Area	Model Used					
	Wolf Creek		Ruby Range		Haines Summit	
	Average	% within ±0.1	Average	% within ±0.1	Average	% within ±0.1
Wolf Creek	38	N.A.	50	27	36	87
Ruby Range	69	72	66	N.A.	71	62
Haines Summit	44	87	41	18	44	N.A.

List of Figures

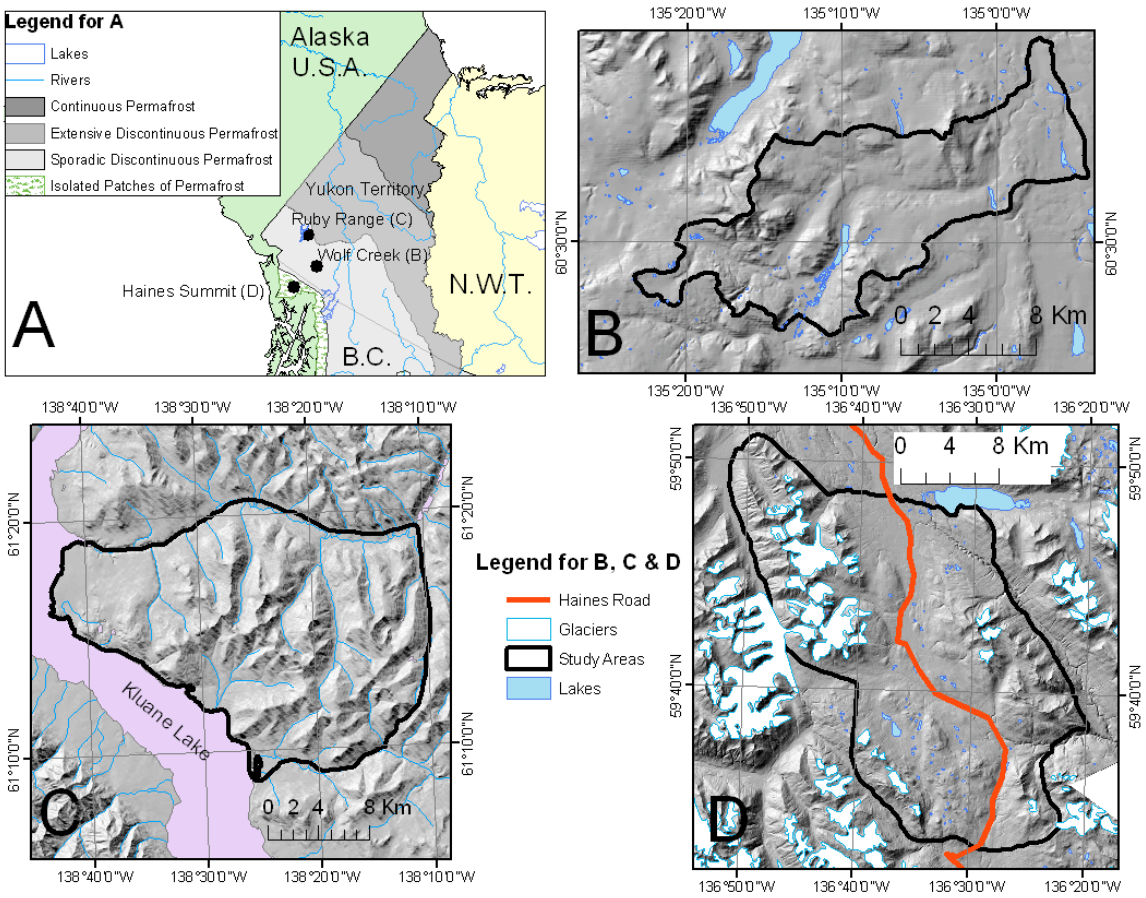

Figure 3.1: Study area maps. A: Location of Wolf Creek Basin, Ruby Range and Haines Summit relative to permafrost zones within the Yukon Territory and northern British Columbia (after Heginbottom et al. 1995); B: Wolf Creek Basin; C: Ruby Range area; D: Haines Summit area. Source data for B, C and D: Geobase (2005) NTS maps 105 D, 115G and 114P respectively.

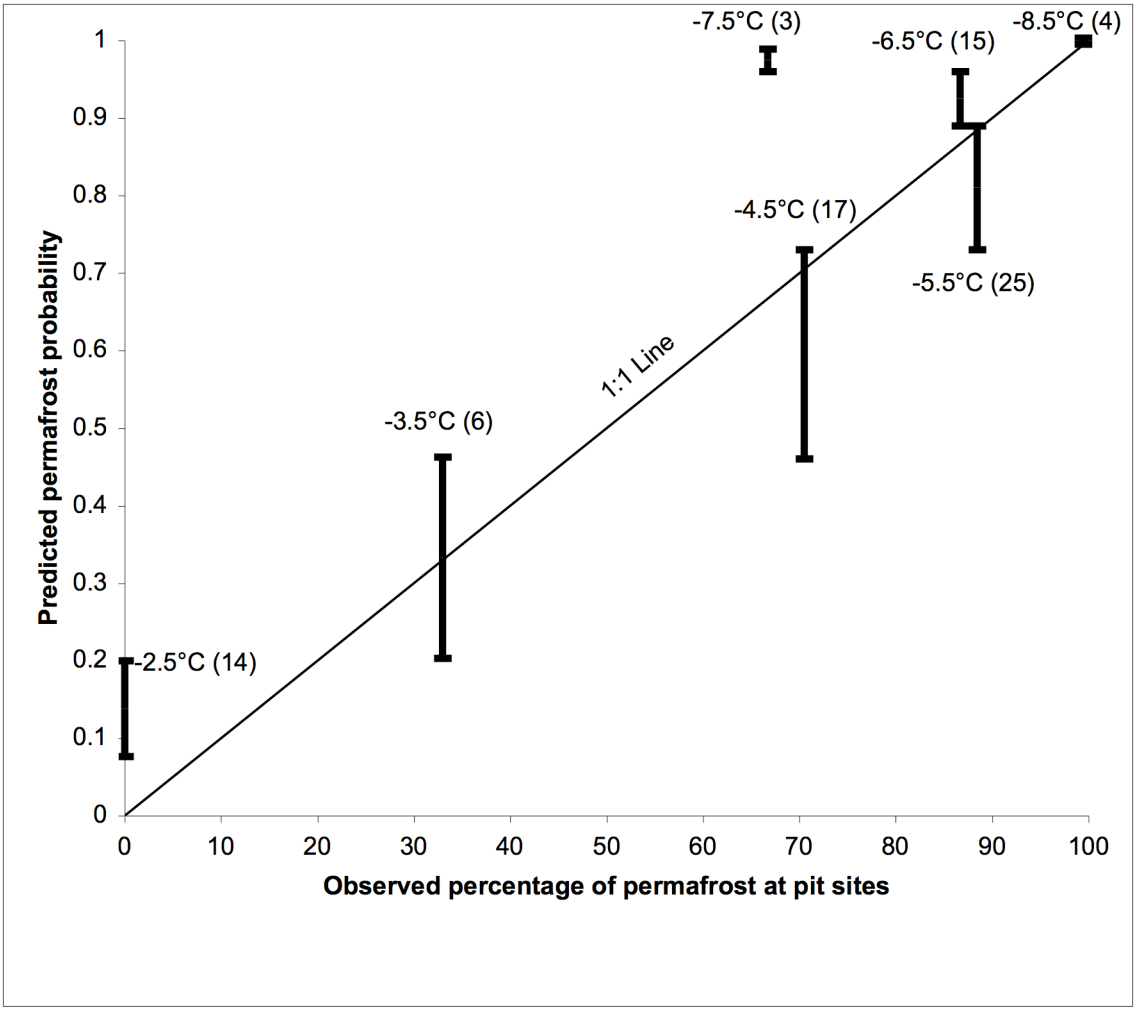

Figure 3.2: Comparison of observed permafrost percentage at the pit sites in Ruby Range grouped according to ranges of modeled BTS with predicted probability percentages according to the RR model. The bars represent the range of predicted probability for a 1°C range of modeled BTS values centred on the temperature shown. The number of pits within each range of modeled BTS temperatures is shown in parentheses.

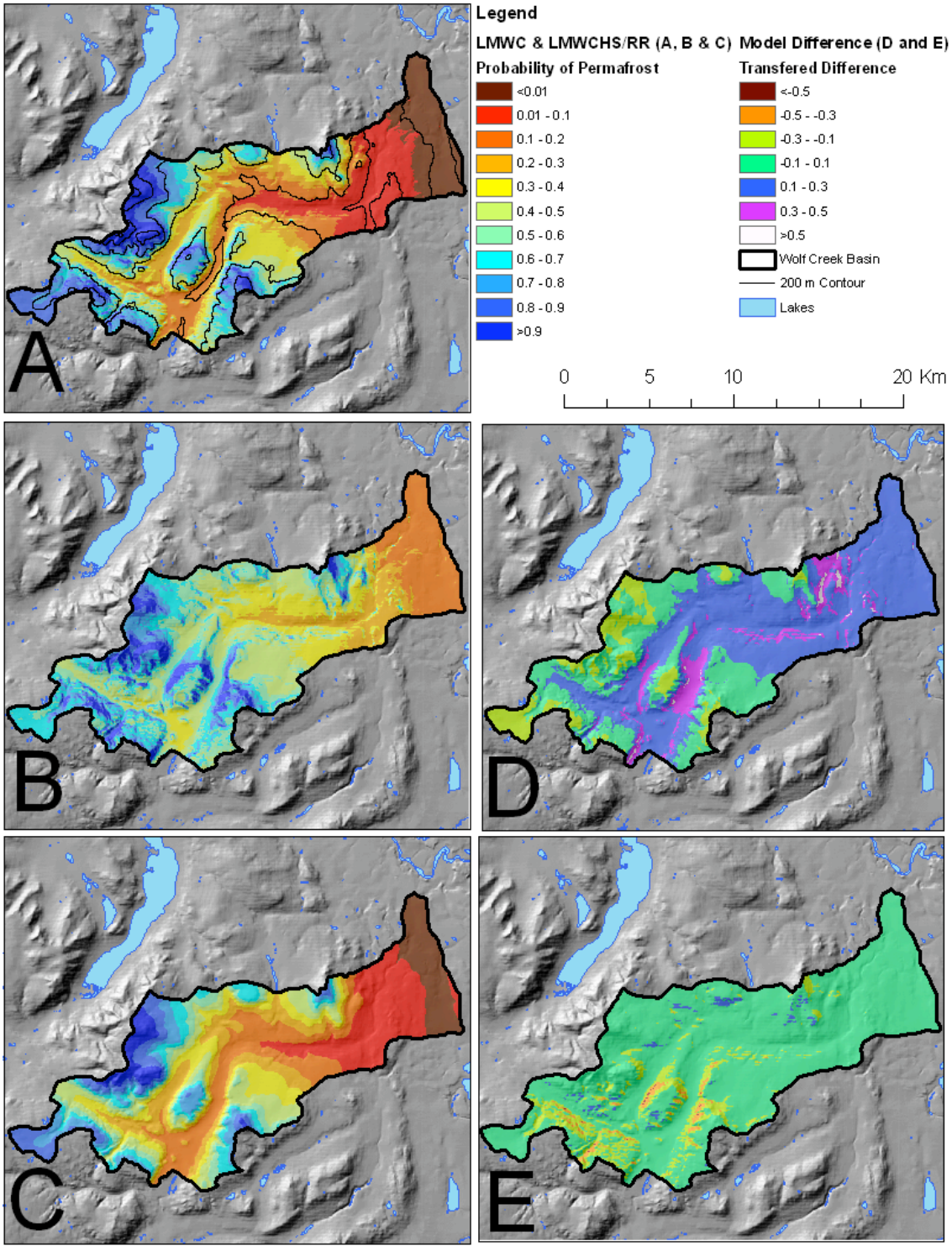

Figure 3.3: Probability of permafrost maps for Wolf Creek basin using (A) the site specific linear model, (B) the transferred model from Ruby Range (WC-rr) and (C) the transferred model from Haines Summit (WC-hs). Maps (D) and (E) show the difference

in probabilities predicted by subtracting the site-specific model from the adjacent transferred model predictions.

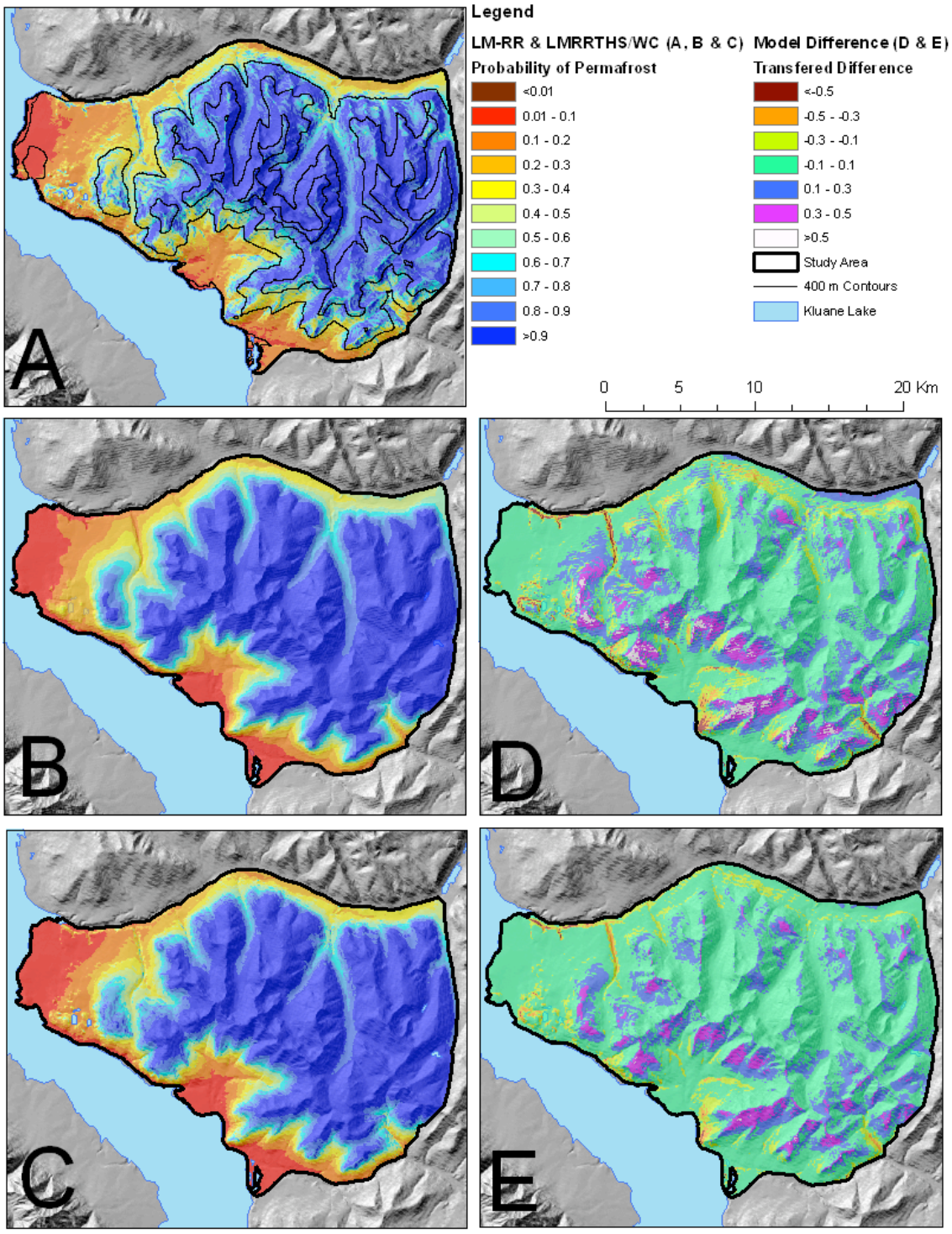

Figure 3.4: Probability of permafrost maps for Ruby Range using (A) the site specific linear model, (B) the transferred model from Wolf Creek (RR-wc) and (C) the transferred model from Haines Summit (RR-hs). Maps (D) and (E) show the difference in probabilities predicted by subtracting the site-specific model from the adjacent transferred model predictions.

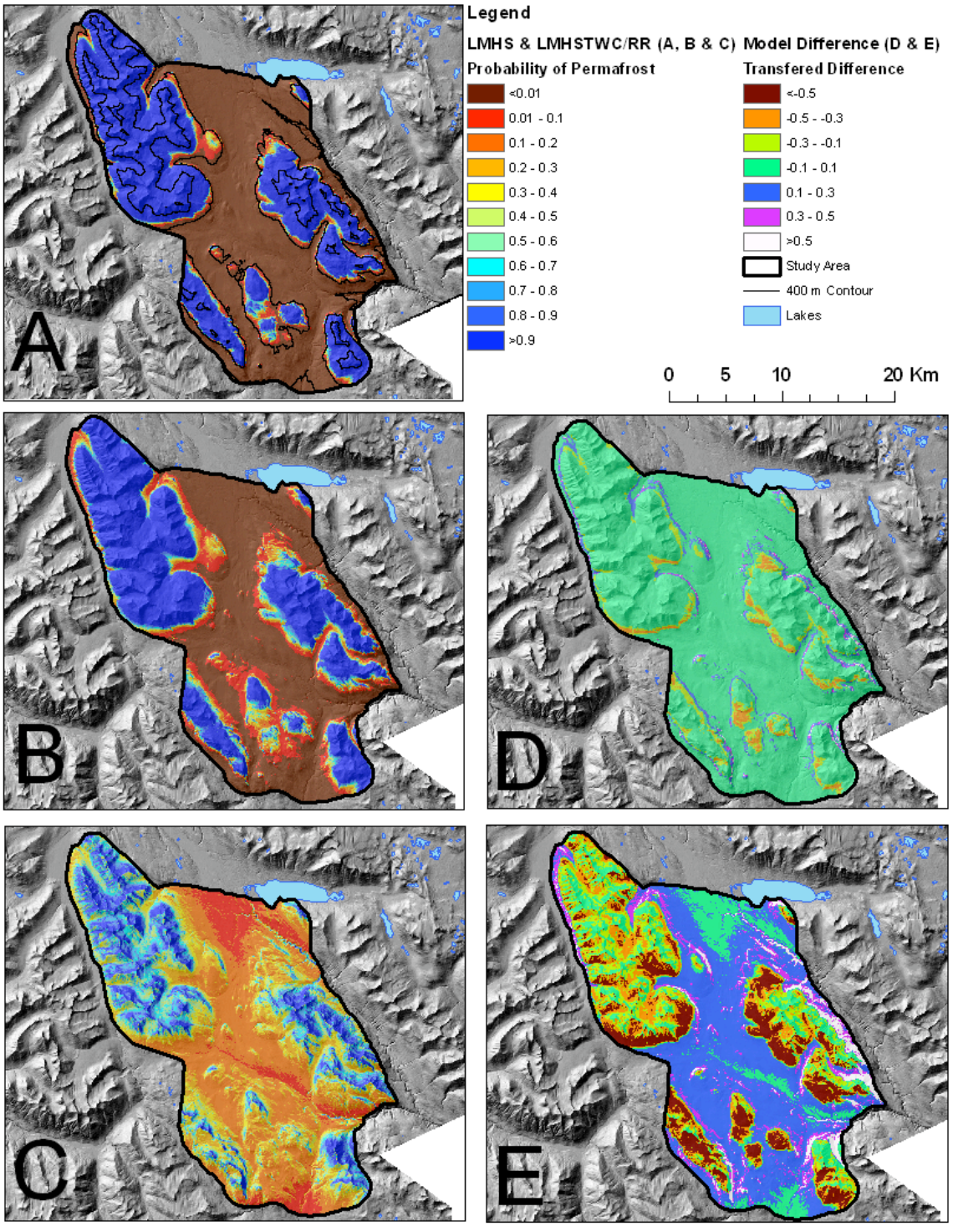

Figure 3.5: Probability of permafrost maps for Haines Summit using (A) the site specific linear model, (B) the transferred model from Wolf Creek (HS-wc) and (C) the transferred model from Ruby Range (HS-rr). Maps (D) and (E) show the difference in probabilities predicted by subtracting the site-specific model from the adjacent transferred model predictions.

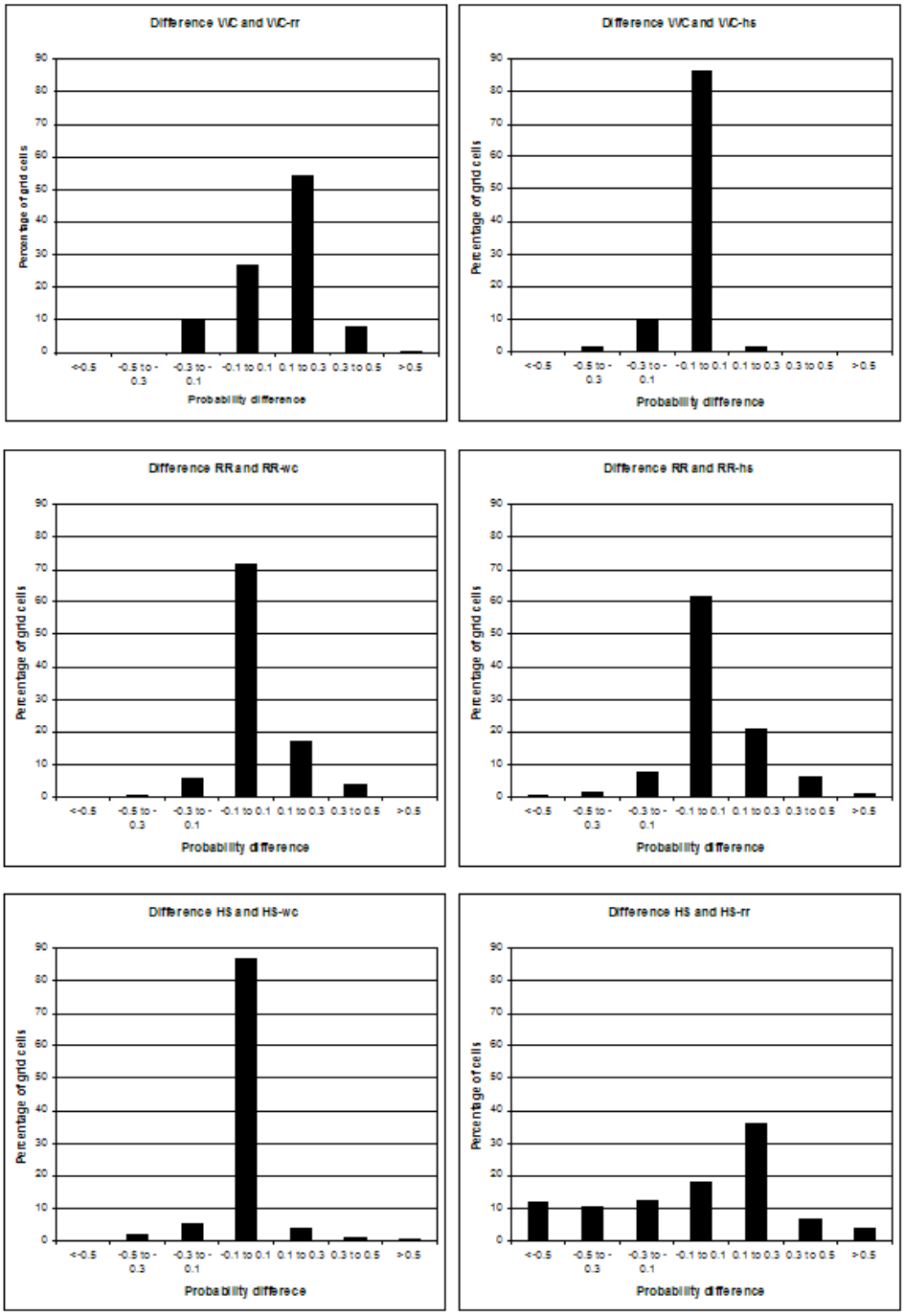

Figure 3.6: Histograms of probability differences shown in parts D and E of Figures 3.3-3.5.

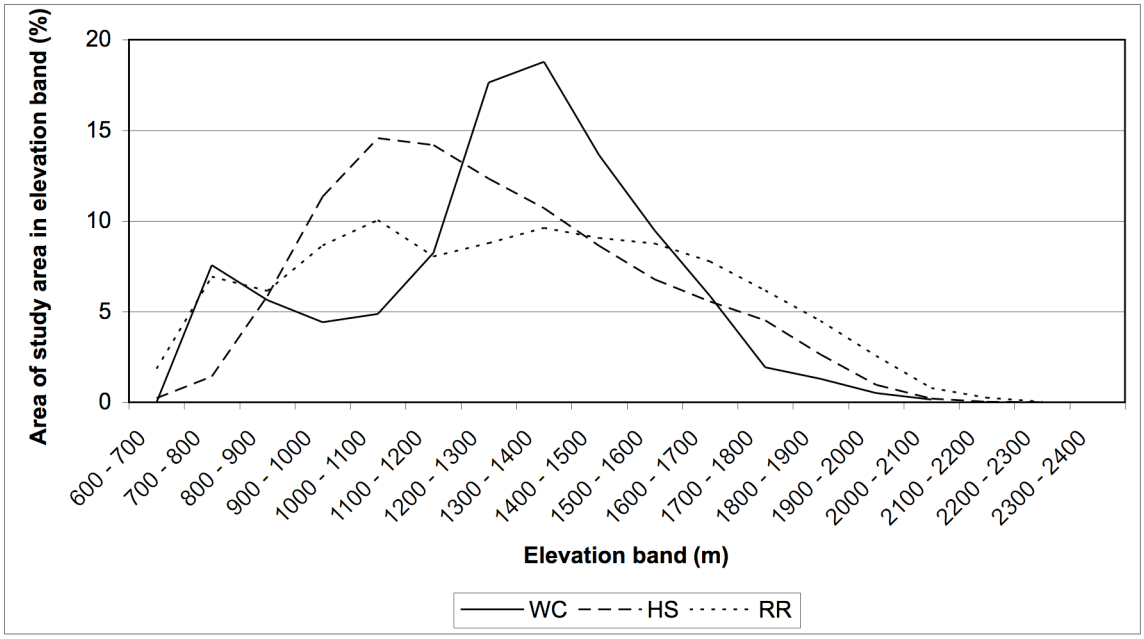

Figure 3.7: Hypsometric curves for the three study areas.

Chapter Four

Equivalent Elevation: a New Method to Incorporate Variable Surface Lapse Rates Into Mountain Permafrost Modelling

Abstract

Permafrost is present at multiple elevations with no defined lower limit in the southern Yukon Territory, Canada. Empirical-statistical modelling of permafrost probability in the region required the development of *equivalent elevation*, a new variable that reflects measured differences between surface air temperature lapse rates below and above treeline. In areas where surface lapse rates are negative (normal) but gentle up to the altitudinal treeline, equivalent elevation results in a compressed elevational range. Where surface lapse rates are positive (inverted) in the forest due to the strength of winter inversions, equivalent elevations calculated for valley floors are higher than those at treeline. There is a strong relationship between the magnitude and sign of surface lapse rates below treeline and the annual amplitude of monthly air temperatures at nearby climate stations, which permits prediction of equivalent elevation for the entire region. Permafrost probability modelling using equivalent elevation produced statistically significant results in several study areas whereas actual elevation values did not. The concept is of particular use where forested areas are underlain by permafrost, and may be transferable to areas with similar terrain and climate such as those in the Canadian Northwest Territories, Alaska and Mongolia.

Key Words: Equivalent Elevation, Mountain Permafrost, Permafrost Modelling, Surface Lapse Rates, Air Temperature Inversions

Introduction

Mountain permafrost represents the occurrence of permafrost in mountains in regions where it is absent from adjacent lowlands and valleys (ACGR, 1988; Harris and Corte, 1992). Latitudinal permafrost, on the other hand, occurs independently of elevation. In the northern parts of the Western Cordillera in North America, the distinction between these two types becomes blurred: the valley floors are located at 300 m asl or higher and permafrost may be present beneath them (i.e. there is no actual lower elevation limit), but on the other hand, permafrost would likely be absent at sea level. Most parts of this sub-Arctic region have continental climates, with long cold winters and shorter warm summers (Wahl et al., 1987), but there are few climatic data sets outside the main valley floors where standard meteorological stations are located and hence the overall distribution of permafrost is uncertain. Predicting how air and ground temperatures change over horizontal and vertical distances is particularly difficult because of the complexity of mountain environments with respect to nearly all surface and near-surface characteristics and properties (Gruber and Haeberli, 2009). Given plans for future infrastructure development in the region and links between permafrost degradation and natural hazards, a better understanding of the current distribution of permafrost in the region is essential.

Previous work on mountain permafrost spatial modelling in the Yukon (Lewkowicz and Ednie, 2004; Bonnaventure and Lewkowicz, 2008; Lewkowicz and Bonnaventure, 2008; Bonnaventure and Lewkowicz, 2010) showed that it was possible to obtain reasonable results using the Basal Temperature of Snow (BTS) technique when analyzed in relation to variables employed elsewhere, such as elevation and Potential

Incoming Solar Radiation (PISR) (Gruber and Hoelzle, 2001; Etzelmüller et al., 2001, 2007; Ishikawa and Hirakawa, 2000). However, almost all BTS sample points in these studies were collected from areas above treeline because snow deep enough for the technique may be absent at lower elevations. Trends established above treeline were simply extrapolated down to the main valley floors and little was known about the actual distribution of permafrost through the forested zone.

In our latest studies in five new areas of the Yukon (Figure 4.1), particular efforts were made to sample below treeline for both BTS and other analytical methods (Bonnaventure and Lewkowicz, *In Review*; Kremer et al., 2011). In addition, air and ground temperatures were measured from the main valley floors through the forested zone to above treeline. These new data sets led us to the conclusion that the use of elevation as a proxy for temperature was incorrect for this region.

The purpose of this paper is to introduce a new variable, *equivalent elevation*, which was developed in order to establish statistically significant relationships for the newly acquired BTS data but which can be used in any type of permafrost spatial modelling (e.g. Kremer et al., 2011). While equivalent elevation proved necessary for the southern half of the Yukon, we believe that it may also improve permafrost modelling in other areas such as the adjacent Northwest Territories and Alaska, as well as Mongolia, where mountain permafrost extends below treeline.

Study Areas

The five new study areas range from 60 – 65° N and from 129 – 140° W (Figure 4.1). In addition, we provide data from Wolf Creek and Haines Summit, which were

previously analyzed based on BTS points collected above treeline (Lewkowicz and Ednie, 2004; Bonnaventure and Lewkowicz, 2008). All of these areas have dense boreal forest at lower elevations, relatively sharp treelines at 1100 -1400 m (800 m at Haines Summit) and shrub tundra, alpine tundra or bare ground at higher elevations. According to the permafrost map of Canada (Heginbottom et al., 1995), one area (Haines Summit) is within the isolated patches permafrost zone (<10% underlain by permafrost), three of the areas are classified as being in the sporadic discontinuous permafrost zone (Wolf Creek, Johnson's Crossing and the Sa Dena Hes mine site; 10-50% underlain by permafrost), one is on the boundary between sporadic and extensive discontinuous permafrost (Faro) and two are in the latter zone (Dawson and Keno; 50-90% underlain by permafrost) (Figure 4.1). Actual permafrost distribution within the five new areas, however, is unknown.

Methods

Field Data Collection

We collected BTS values from below to above treeline over all vegetation types in all of the study areas, in winters 2007 and 2008, except Faro in the latter year only, in Wolf Creek in winters 2001 and 2002, and in Haines Summit in winters 2005 and 2006. Up to 90 points, each representing an average of three individual measurements, were collected at each of the new sites, and data-sets from the two years were combined after adjustments of up to 1°C to account for different patterns of winter temperatures and snowpack accumulation (e.g. Lewkowicz and Ednie, 2004; Bonnaventure and Lewkowicz, 2008; Ishikawa and Hirakawa, 2000). This adjustment was achieved by

lowering the BTS values in the warmer year relative to the colder year in order to avoid temporal autocorrelation in the regression residuals.

The effects of elevation and topography on air temperatures were examined using data-logger networks established during the spring of 2006 in the Johnson's Crossing, Sa Dena Hes, Faro and Keno areas, in Dawson in August 2007, in Wolf Creek largely in spring 2004 and in Haines Summit in summer 2003. Each network consisted of multiple stations at various elevations recording hourly shielded air temperature at a height of 1.6 m above the surface (3.2 m in Haines Summit due to high winter snowfalls) using an Onset Hobo Pro logger with an external thermistor with accuracy of ± 0.2°C and a precision of 0.02°C calibrated in an ice bath at 0°C (Table 4.1).

Monitoring stations were located in each study area to sample locations with differing aspects, elevations and landform types. The goal was to see if topographic attributes played a role in the development of air temperature inversions. The selection process to determine logger location was undertaken using the ArcView add-in program Topographic Position Index (TPI) and a 30-m DEM. The TPI is positive if a grid cell's elevation is higher than the average of surrounding cells within a fixed radius, or negative if the reverse is true. Based on the magnitude of the TPI, and in some cases incorporating slope, the grid cell is assigned to a landform class, such as mountain tops, mid-slopes, U-shaped valleys and plains (Jenness, 2006). Previous analyses have shown that the presence of U-shaped valleys promotes the development of air temperature inversions (Lewkowicz and Ednie, 2004) which in turn may influence the spatial distribution of permafrost.

Results

Problems of BTS Analysis

Initial regression analysis attempted to use elevation and PISR as variables to model BTS. However, statistically significant trends with respect to elevation were not present. Given that previous modelling (Lewkowicz and Ednie, 2004; Bonnaventure and Lewkowicz, 2008) had successfully linked BTS values to elevation, the absence of a strong relationship was attributed to the extensive sampling below treeline. The new results led us to reconsider an underlying assumption of the previous BTS studies, that air temperatures decrease uniformly with elevation.

Air Temperature Trends

The network of temperature loggers allowed an examination of the pattern of air temperatures in the individual study areas. In Wolf Creek, for example, the annual surface lapse rate (SLR) measured in the forest from 870 m asl to 1290 m asl (at treeline) was -2.2 °C km^{-1}, whereas at sites from treeline up to 2070 m asl the SLR averaged -6.1 °C km^{-1} (Figure 4.2). In addition, the monthly SLRs above treeline (Figure 4.2A) were consistently negative throughout the year (although gentler in winter) whereas those below treeline were positive (i.e. inverted) through most of the winter and negative in the summer, resulting in the gentle negative annual SLR (Figure 4.2B). Similar patterns of air temperatures were present below treeline at the other sites, but sampling above treeline was limited in some of them, because the terrain extended only 100-200 m higher. The air temperature data from all of the study areas showed that SLRs varied by month during the year (Figure 4.3). Surface lapse rates are highly inverted in the winter months (usually

October – March) while they are normal and negative in the summer months (April – September). Haines Summit is an exception as inversions are present only between December and April and are less pronounced, likely because of its more maritime location.

The summer and winter SLR trends below treeline act to counteract each other over the year as a whole. Depending on their relative strength, some areas have gentle normal SLRs on an annual basis (e.g. Wolf Creek), while others have nonexistent or inverted SLRs from the valley floor to treeline (e.g. Keno, Figure 4.3). The inversions in winter are attributed to the effects of cold-air pooling at lower elevations under the typical Arctic High present over the region in this season (Wahl et al., 1987).

Development of a Synthetic Year

We sought to minimize the potential effects of inter-annual variation in our short-term air temperature data by forming a synthetic year, because permafrost is influenced by long-term climate. The monthly records of the closest official climate station to each area were examined for the years of our field measurements and for each month, the year with the average closest to the normal (1971-2000) was identified (Table 4.2). The synthetic years for the climate stations themselves averaged ±0.3°C of their respective normals, with the maximum difference being 0.7°C (Table 4.2). The SLR for each month contributing to the synthetic year was determined by linear best-fit using our field data, and an average SLR for the year was calculated. Because we wanted generalized SLRs through the forest (Figure 4.4), some logger sites that showed evidence of frequent localized cold-air pooling (mostly U-shaped valley locations) were excluded from the

analysis, as were loggers located above treeline. Annual SLRs for the synthetic year varied for the seven regions from -6.4°C km^{-1} to +0.7°C km^{-1} (Table 4.3).

Equivalent Elevation

Equivalent elevation is conceptualized as a way to incorporate the pattern of mean annual air temperatures (MAATs) in an area so that a given increase in equivalent elevation represents a uniform decrease in MAAT. To do this, the numerical elevations in a DEM of grid cells below treeline are adjusted to take into account the weakened or reverse SLRs in the forest compared to the strong normal negative SLRs above. Thus grid cells that are well below treeline may be increased significantly in elevation, areas close to treeline are changed very little and areas above treeline remain unchanged. Equivalent elevation is evaluated from:

$$Z'_x = Z_t - (Z_t - Z_x) \times \frac{L_1}{L_2} \qquad (4.1)$$

Where Z'_x is equivalent elevation (m asl), Z_t is the elevation of treeline (1400 m asl in Johnson's Crossing, Sa Dena Hes, Faro and Keno, 1150 m asl in Dawson, 1300 m in Wolf Creek and 800 m in Haines Summit), Z_x is actual grid cell elevation (m asl), L_1 is the measured SLR below treeline (°C km^{-1}) (See Table 4.3) and L_2 is the SLR above treeline (assumed to be -6.5°C km^{-1}). Equation (4.1) is applied only to grid cells at nominal elevations below local treeline, while actual elevations are used for the remainder of the grid. Using equation (4.1) within a spatial context alters the topography of the terrain in relation to air temperature variation, compressing elevations below

treeline if gentle normal SLRs are present, or inverting the topography with minimum elevations at treeline if the forest SLRs are inverted (Figure 4.5).

The utility of the concept of equivalent elevation is revealed by regressing measured BTS values against grid cell values calculated with equation (4.1). Using the example of Dawson, the variation in true elevation of the BTS points from 900 to 1250 m asl (Figure 4.6A) is transformed into equivalent elevation from 1150 to 1260 m asl and the lowest sites are now amongst the highest (Figure 4.6B). However, Figure 4.6B is not a mirror image of Figure 4.6A because the elevations of all sites above treeline at 1150 m asl are unchanged. A best-fit line through the data produces a statistically significant relationship. Linear relationships were used, as is typical in BTS modelling, because curvilinear relationships can produce spurious results outside the range of measured variables.

Discussion

The pattern of the of SLRs in Table 4.3 was explored by comparing them to the amplitude of average monthly temperatures over a year (i.e. mean July minus mean January temperatures) at the closest standard weather station to the study areas (Figure 4.7). The statistically significant correlation obtained was used with long-term climate data from throughout the Yukon, northern British Columbia and extreme southwest Northwest Territories to predict local SLRs (Figure 4.8A). Measured and predicted negative (normal) SLRs become weaker northwards and eastwards, and ultimately become inverted, a pattern attributed to increasing continentality with latitude and with distance from the influence of the Pacific Ocean. This spatial pattern could be reproduced

using a third order polynomial trend surface (Figure 4.8A). To ensure that trend surface values near the margins of the region do not become unrealistic, maximum and minimum SLR values were set at +1 °C km^{-1} and -6.5 °C km^{-1} respectively. The maximum difference between the point values shown in Figure 4.8A and the trend surface predictions is about 1°C km^{-1} (Figure 4.8B). The trend surface, together with treeline elevations, can be used to determine equivalent elevation over the region, and represents a necessary precursor to modelling mountain permafrost distribution.

A question that has not yet been answered is why air temperature trends change at treeline, an observation that was also made by Taylor et al. (1998). Figures 4.2 and 4.3 show that the magnitude of this change on an annual basis, actually relates to differences in SLRs in the winter and parts of the fall and spring. It appears that colder air pools in the main valleys up to treeline, at least near the ground surface where we are measuring. The propensity for inversions below treeline may relate to reduced mixing within the forest allowing colder air to remain in contact with the ground. Above treeline, the absence of trees means that mixing is more likely if even slight air movements occur.

Our set of air temperature and permafrost observations in the Yukon is unique, but similar frozen ground and climate conditions should exist across the border in Alaska north of the influence of the Gulf of Alaska. Modelling for Alaska (e.g. Jorgenson et al., 2008) has not yet taken inversions into account or has focused only on valley-bottoms (Panda et al., 2010). In Mongolia, modelling of the likelihood of permafrost linked its presence in valley bottoms to drainage conditions (Etzelmüller et al., 2006; Heggem et al., 2006). Given the continentality of this region, however, it may also be due to persistent air temperature inversions. In both areas, therefore, the concept of equivalent

elevation could prove useful to mountain permafrost modelling. Evidence of this possibility also comes from the Norman Wells region of the Northwest Territories where the annual SLR below treeline is about +5°C km^{-1} (Taylor et al., 1998). This value is much higher than in the adjacent parts of the Yukon and has a significant impact on ground temperatures, possibly eliminating permafrost at mid-elevations despite cold annual temperatures at the valley-bottom climate station.

Conclusions

The following conclusions can be drawn as a result of this research:

1) Inversions are frequent in the forested environments of the Yukon Territory especially in winter, resulting in gentle, nonexistent or inverted SLRs up to treeline on an annual basis.

2) The strength and sign of the SLRs through the forest is strongly related to continentality expressed as the difference between January and July mean temperatures, with the highest amplitudes relating to inverted SLRs on an annual basis. This relationship can be used to model the spatial pattern of SLRs across the region.

3) The non-uniform SLR precluded successful use of elevation as an independent variable in empirical statistical permafrost modelling based on BTS measurements. Previous use of elevation in the region was successful because all BTS measurements were made above treeline where SLRs are normal (i.e. negative) and trends were extrapolated to the remainder of the terrain.

4) Equivalent elevation takes variable SLRs into account, producing a flattened or inverted surface that adjusts low elevation areas while leaving areas above treeline unchanged. The relationship between continentality and SLRs, and hence equivalent elevation, provides a means for modelling mountain permafrost probability across the entire region in the future.

5) Equivalent elevation, as a variable, is of direct use for empirical statistical permafrost modelling in the Yukon Territory and may be useful in areas with similar terrain such as the Northwest Territories, Alaska and Mongolia.

Acknowledgments

This project was supported financially by the Canadian Foundation for Climate and Atmospheric Sciences, the Natural Sciences and Engineering Research Council of Canada, The Federal Government of Canada International Polar Year Program, The Northern Scientific Training Program (Department of Indian Affairs and Northern Development), the Yukon Geological Survey, the Geological Survey of Canada, and the Faculty of Arts, University of Ottawa. We would also like to acknowledge all of the field assistants involved in this project for their hard work, including Chris Andrews, Patty Bonnaventure, Roland Bonnaventure, Jim Coates, Bernd Etzelmüller, Marian Kremer, Dan Odell, Emily Schultz (Roadhouse), Jason Skucas, and Andrea Sitler. We thank Philippe Gingras for assistance in assembling the logger data. The comments of two anonymous referees helped improve an earlier version of the paper. Associate Editor Julian Murton kindly handled the review process.

References

ACGR 1988: *Glossary of Permafrost and Related Ground-Ice Terms.* National Research of Canada, Technical Memorandum No. 142. pp.64.

Bonnaventure PP, and Lewkowicz AG. 2008. Mountain Permafrost Probability Mapping Using the BTS Method in two Climatically Dissimilar Locations, Northwest Canada. *Canadian Journal of Earth Sciences,* **45**: 443-455.

Bonnaventure PP, and Lewkowicz AG. 2010. Modelling climate change effects on the spatial distribution of mountain permafrost at three sites in northwest Canada. *Climatic Change*. Accepted February 11, 2010.

Bonnaventure PP and Lewkowicz AG. *In Review*. Mountain Permafrost Probability Modelling in Areas Above and Below Treeline, Southern Yukon, Canada. *Canadian Journal of Earth Sciences.* Submitted November, 2010.

Etzelmüller B, Heggem ESF, Sharkhuu N, Frauenfelder R, Kääb A, and Goulden C. 2006. Mountain permafrost distribution modelling using a multi-criteria approach in the Hövsgöl area, northern Mongolia. *Permafrost and Periglacial Processes*, **17**: 91-104.

Etzelmüller B, Ødegard RS, Berthling I, Sollid JL. 2001. Terrain parameters and remote sensing data in the analysis of permafrost distribution and periglacial processes: principles and examples from southern Norway. *Permafrost and Periglacial Processes* **12**: 79–92.

Etzelmüller B, Farbrot H, Guomundsson A, Humlum O. 2007. The regional distribution of mountain permafrost in Iceland. *Permafrost and Periglacial Processes*, **18**: 185-199.

Gruber S, and Hoelzle M. 2001. Statistical modeling of mountain permafrost distribution: Local calibration and incorporation of remotely sensed data. *Permafrost and Periglacial Processes*, **12** 69-77.

Gruber S. and Haeberli W. 2009: Mountain permafrost. In: *Permafrost Soils,* edited by: Margesin, R., Biology Series Vol. 16, Springer, 33–44, doi: 10.1007/978-3-540-69371-0_3. <http://www.geo.unizh.ch/~stgruber/pubs/gruber_2009_pf-soils.pdf >

Harris SA, and Corte AE. 1992: Interactions and relations between mountain permafrost, glaciers, snow and water. *Permafrost and Periglacial Processes*, **3** 103-110.

Heggem ESF, Etzelmüller B, Anarmaa S, Sharkhuu N, Goulden CE, and Nandinsetseg B. 2006. Spatial distribution of ground surface temperatures and active layer depths in the Hovsgol area Mongolia. *Permafrost and Periglacial Processes* **17**, 357-369.

Heginbottom, J.A., Dubreuil, M.A., and Haker, P.T. 1995. Canada Permafrost. (1:7,500,000 scale). In *The National Atlas of Canada*, 5th Edition, sheet MCR 4177. Ottawa: National Resources Canada.

Ishikawa M, and Hirakawa. 2000. Mountain permafrost distribution based on BTS measurements and DC resistivity soundings in the Daisetu Moutains, Hokkaido, Japan. *Permafrost and Periglacial Processes*, **11** 109-123.

Jenness J. 2006. Topographic Position Index (TPI) v. 1.2. Online manual, Jenness Enterprises, 3020 N. Schevene Blvd. Flagstaff, AZ, 86004, USA.

Jorgenson T, Yoshikawa K, Kanevskiy M, and Shur Y. 2008. Permafrost Characteristics of Alaska, *Conference proceedings from the ninth international conference on permafrost*, June 29 - July 3, 2008. Fairbanks, Alaska, USA.

Kremer, M., Lewkowicz, A.G., Bonnaventure, P.P. and Sawada, M.C. 2011. Utility of classification and regression tree analyses and vegetation in mountain permafrost models, Yukon Territory, Canada. *Permafrost and Periglacial Processes.*DOI 10.1002/ppp.719

Lewkowicz AG, and Ednie M. 2004. Probability mapping of mountain permafrost using the BTS method, Wolf Creek, Yukon Territory, Canada. *Permafrost Periglacial. Processes.* **15** 67-80.

Lewkowicz AG, and Bonnaventure PP. 2008. Interchangeability of Mountain Permafrost Probability Models, Northwest Canada, *Permafrost and Periglacial Processes,* **19**: 49-62.

Panda SK, Prakash A, Solie DN, Romanovsky VE, Jorgenson MT. 2010. Remote sensing and field-based mapping of permafrost distribution along the Alaska Highway corridor, interior Alaska. *Permafrost and Periglacial Processes*, **21**, in press.

Taylor A, Nixon M, Eley J, Burgess M, and Egginton P. 1998. Effects of atmospheric temperature inversions on ground surface temperatures and discontinuous permafrost, Norman Wells, Mackenzie Valley, Canada. *Conference Proceedings of the seventh international conference on permafrost.* June 23-27, Yellowknife, Canada. Pages 1043-1047.

Wahl HE, Fraser DB, Harvey RC, Maxwell JB. 1987. *Climate of Yukon.* Canadian Government Publishing Centre.

Table 4.1: Air and ground temperature monitoring networks in the Yukon study areas.

Study area	**Number of logger sites**	**Climate zone and closest Environment Canada station (km)**	**Data period**
Johnson's Crossing	13	Pelly-Cassiar Mountains (Teslin Airport 50 km)	May-June 2006 – Sept 2009; 10 operating to present
Sa Dena Hes	13	Liard Basin (Watson Lake Airport 45 km)	May-June 2006 – Sept 2009
Faro	13	Central Yukon Basin (Faro Airport 0 km)	May-June 2006 – Sept 2009
Keno	12	Ogilvie-Mackenzie Mountains (Mayo Airport 50 km)	May-June 2006 – present
Dawson	13	Central Yukon Basin (Dawson Airport 3 km)	August 2007 – present
Wolf Creek	23	Upper Yukon Stikine Basin (Whitehorse Airport 15 km)	June 2004 – Sept 2009; 13 operating to present
Haines Summit	5	St. Elias Coast Mountains (Pleasant Camp 15 km)	July 2003 – present

Table 4.2: Month and year used to create the synthetic year for each of the study areas.

Area[a]	Month												Synthetic year mean[b] (°C)	Climate station normal[b] (°C)
	J	F	M	A	M	J	J	A	S	O	N	D		
JC	2009	2008	2008	2008	2007	2006	2006	2009	2006	2008	2007	2007	-1.3	-1.2
SDH	2009	2007	2008	2007	2007	2009	2007	2008	2007	2007	2007	2007	-2.8	-2.9
F	2009	2009	2008	2008	2007	2008	2006	2009	2008	2008	2008	2007	-2.6	-2.2
K	2008	2008	2008	2008	2009	2008	2006	2009	2007	2007	2008	2008	-2.9	-3.1
D	2008	2009	2008	2008	2009	2008	2009	2009	2008	2007	2007	2007	-3.7	-4.4
WC	2009	2009	2009	2007	2006	2006	2005	2009	2008	2004	2008	2008	-0.6	-0.7
HS	2006	2006	2008	2009	2006	2007	2006	2009	2008	2005	2005	2008	3.0	2.7

[a] JC: Johnson's Crossing; SDH: Sa Dena Hes; F: Faro; K: Keno; D: Dawson; WC: Wolf Creek; HS: Haines Summit

[b] For closest climate stations, see Table 1; normals are for 1971-2000

Table 4.3: Annual surface lapse rates for the synthetic year calculated within the forest up to treeline for each of the study areas.

Area[a]	Treeline elevation (m)	Surface lapse rate below treeline (°C km^{-1})
JC	1400	-2.4
SDH	1400	-0.7
F	1400	-2.3
K	1400	+0.3
D	1150	+0.7
WC	1300	-2.2
HS	800	-6.4

[a] JC: Johnson's Crossing; SDH: Sa Dena Hes; F: Faro; K: Keno; D: Dawson; WC: Wolf Creek; HS: Haines Summit

Figures:

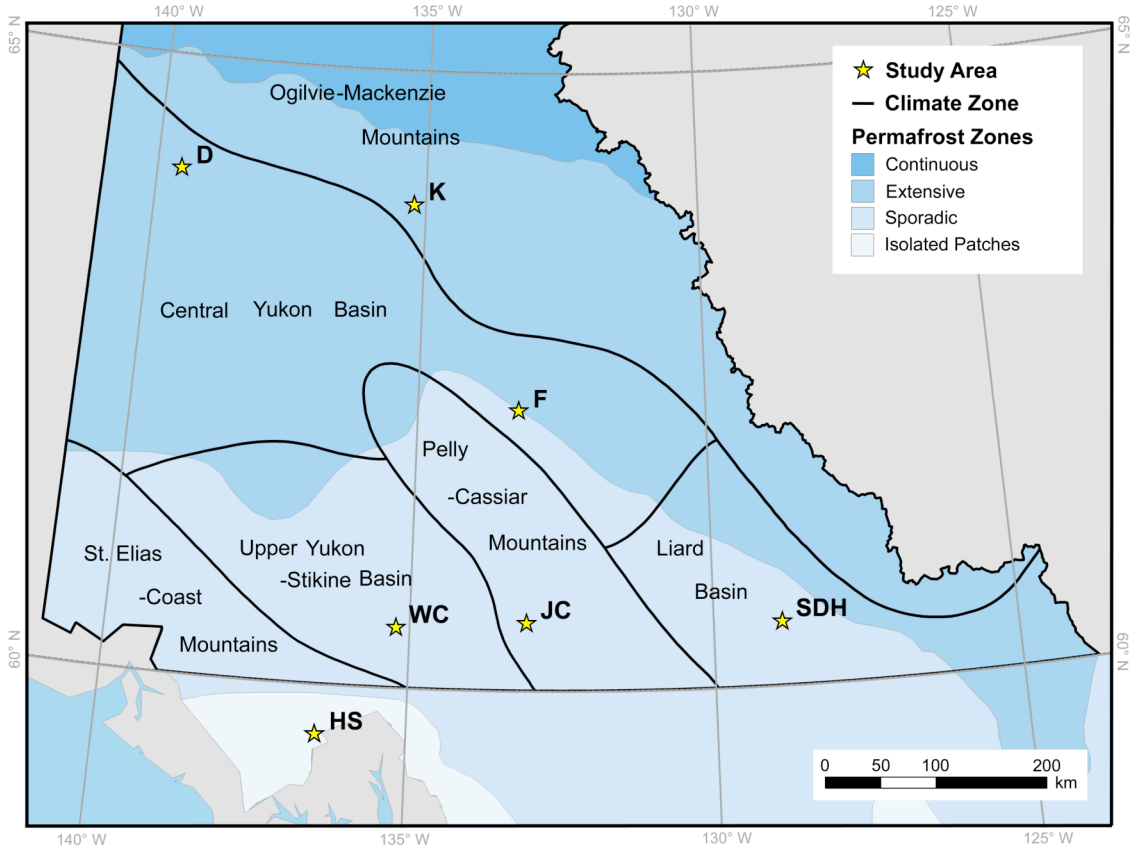

Figure 4.1: Location of study areas in the Yukon and northern British Columbia in relation to permafrost zones (Heginbottom et al. 1995) and climatic regions (Wahl et al., 1987). D – Dawson; K – Keno; F – Faro; WC – Wolf Creek; JC – Johnson's Crossing; SDH – Sa Dena Hes mine site; HS – Haines Summit, B.C.

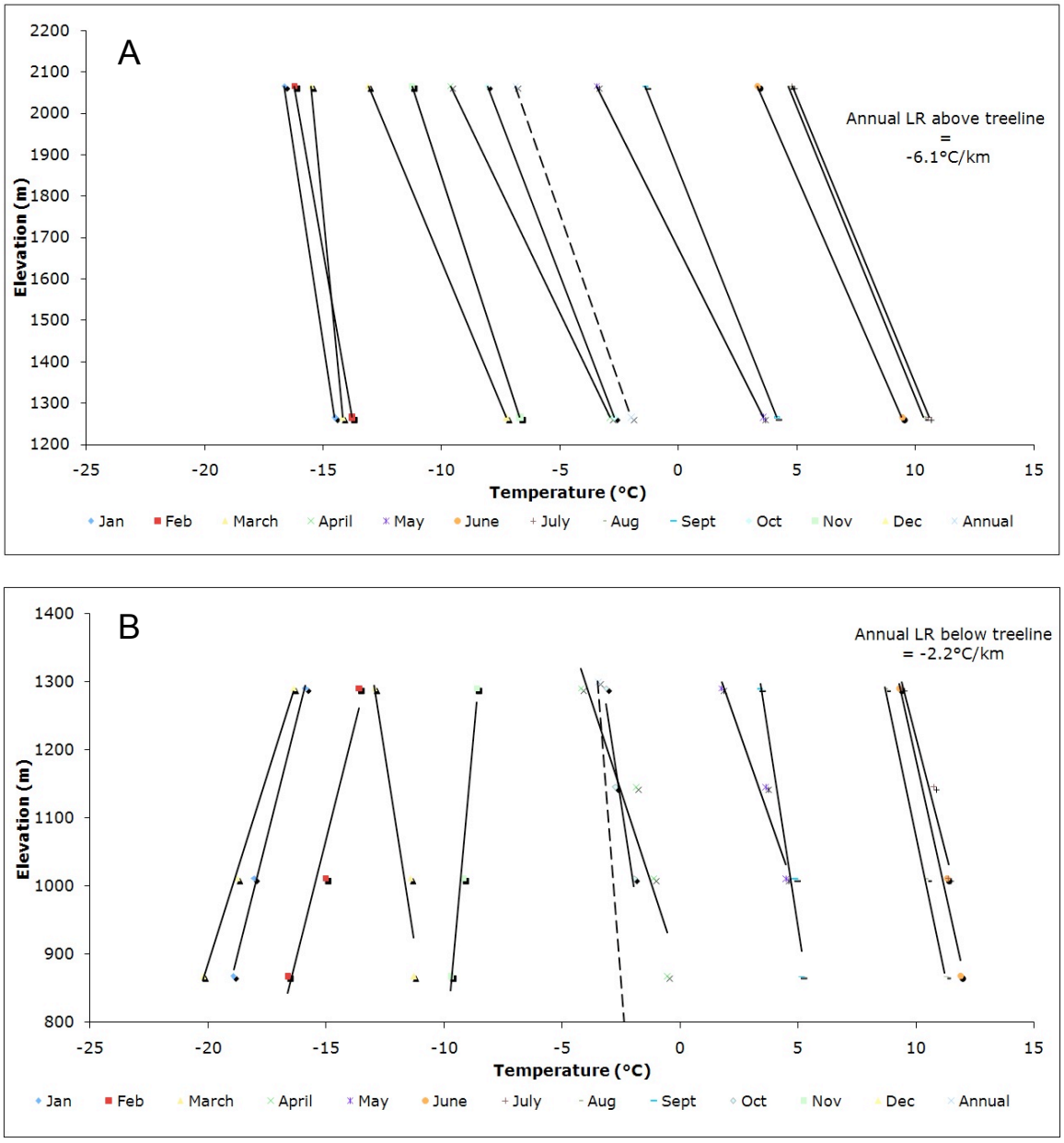

Figure 4.2: Changes in temperature with elevation at Wolf Creek for a synthetic year (see text): (A) From treeline to the top of Mt. Granger (2070 m asl); (B) Along a forest transect up to treeline. Dashed lines are annual surface lapse rates. Note: the uppermost logger in the forest transect is not the same as the lower one in (A).

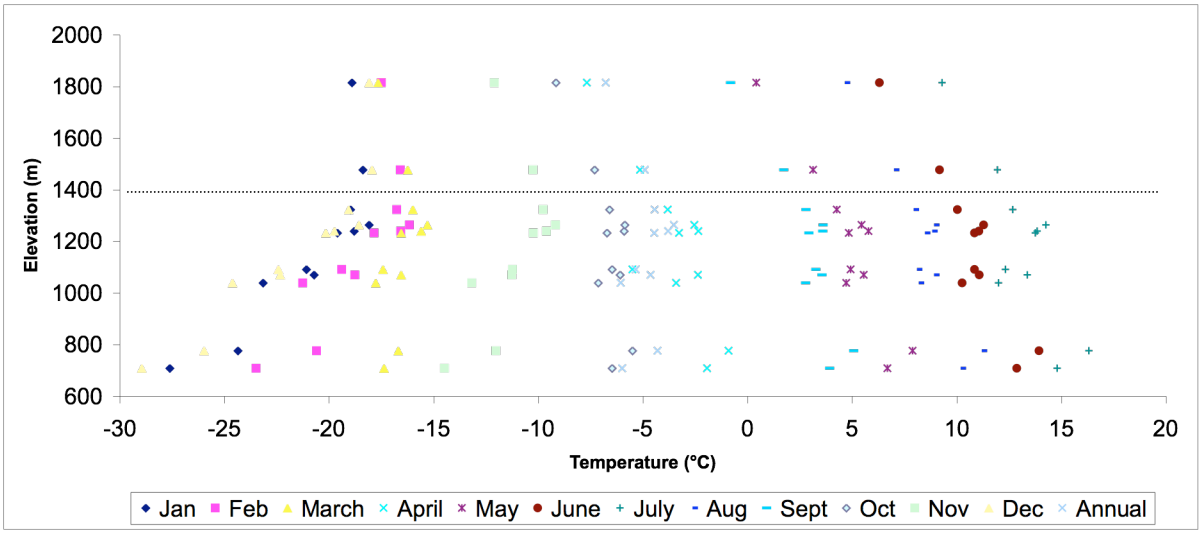

Figure 4.3: Monthly air temperatures vs. elevation for 2008-2009 at Keno. Note the change in slope across treeline (1400 m asl, indicated with a dashed line) in all but the warmest months.

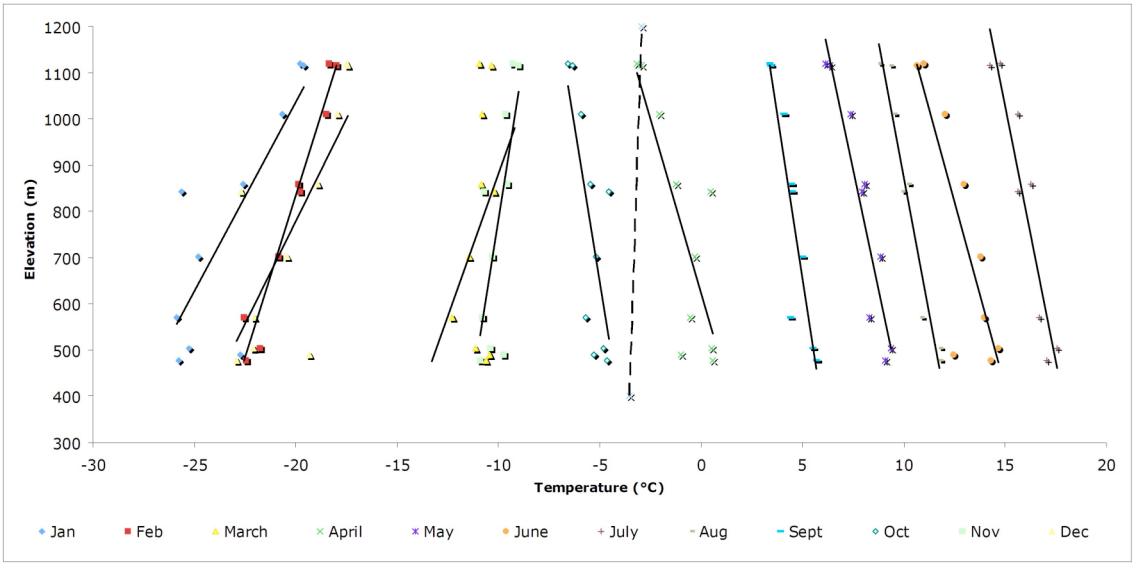

Figure 4.4: Monthly air temperature below treeline vs. elevation for Dawson generated for a synthetic year. Measurements in areas known to experience cold-air pooling or areas above treeline (1150 m asl for Dawson) were excluded from analysis. The annual surface lapse rate in this area (dashed line) is positive (+0.7°C km^{-1}).

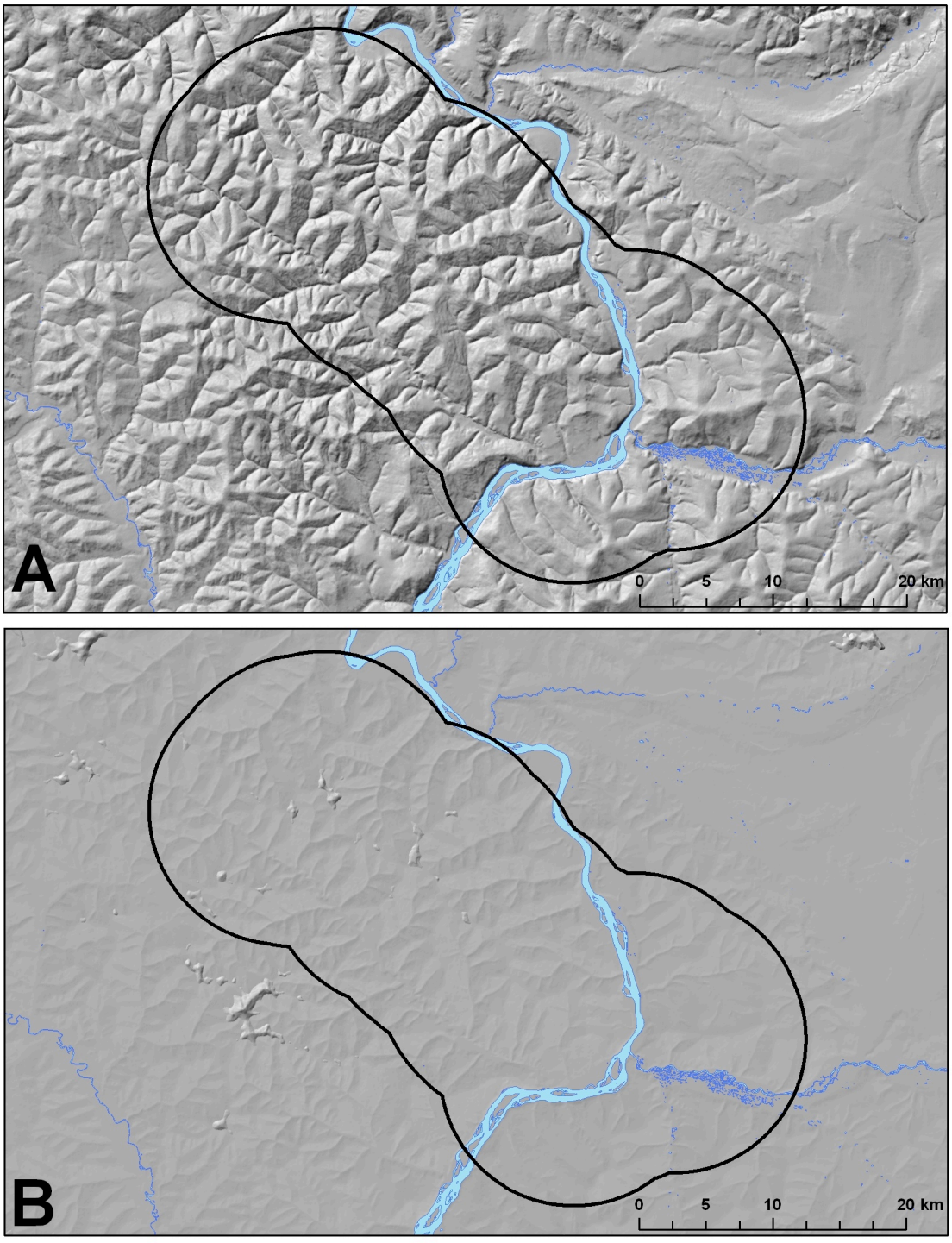

Figure 4.5: Dawson study area map: (A) shades relief of elevations from DEM; (B) equivalent elevation surface. In (B), the valley floors are at equivalent elevations slightly above treeline due to the annually inverted surface lapse rate through the forest. Source of the DEM is Geobase (2009). Black outline shows the study area extent.

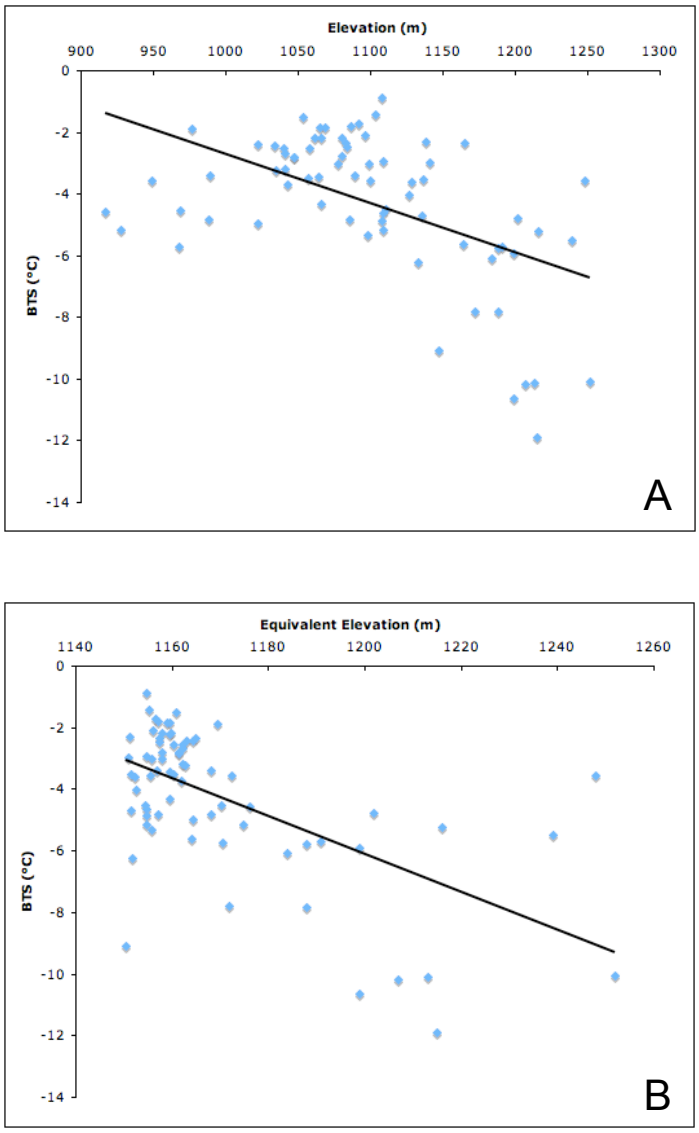

Figure 4.6: (A) Relationship between true elevation and BTS for the Dawson area. Treeline is at 1150 m asl. The best-fit line has an r^2 value of 0.26 and is not statistically significant at the $p = 0.05$ level. A second order polynomial fitted to the same data would produce unrealistically low predictions (<-60°C) for the main valley floor at 300 m asl. (B) Relationship between equivalent elevation and BTS for the Dawson area. The best-fit line has an r^2 value of 0.35 and is statistically significant at $p = 0.05$.

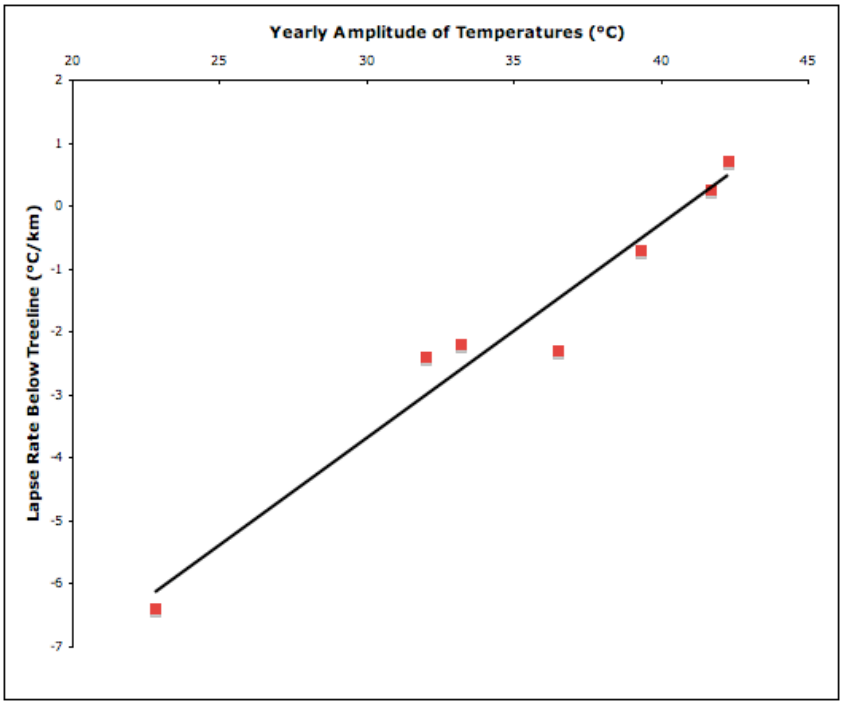

Figure 4.7: Correlation of surface lapse rates through the forest at the study sites with yearly amplitude of monthly temperatures (i.e. mean July minus mean January temperature) at nearby valley floor weather stations ($r^2 = 0.96$; $n = 7$). Climate normal data are from 1971-2000 (Environment Canada, 2010).

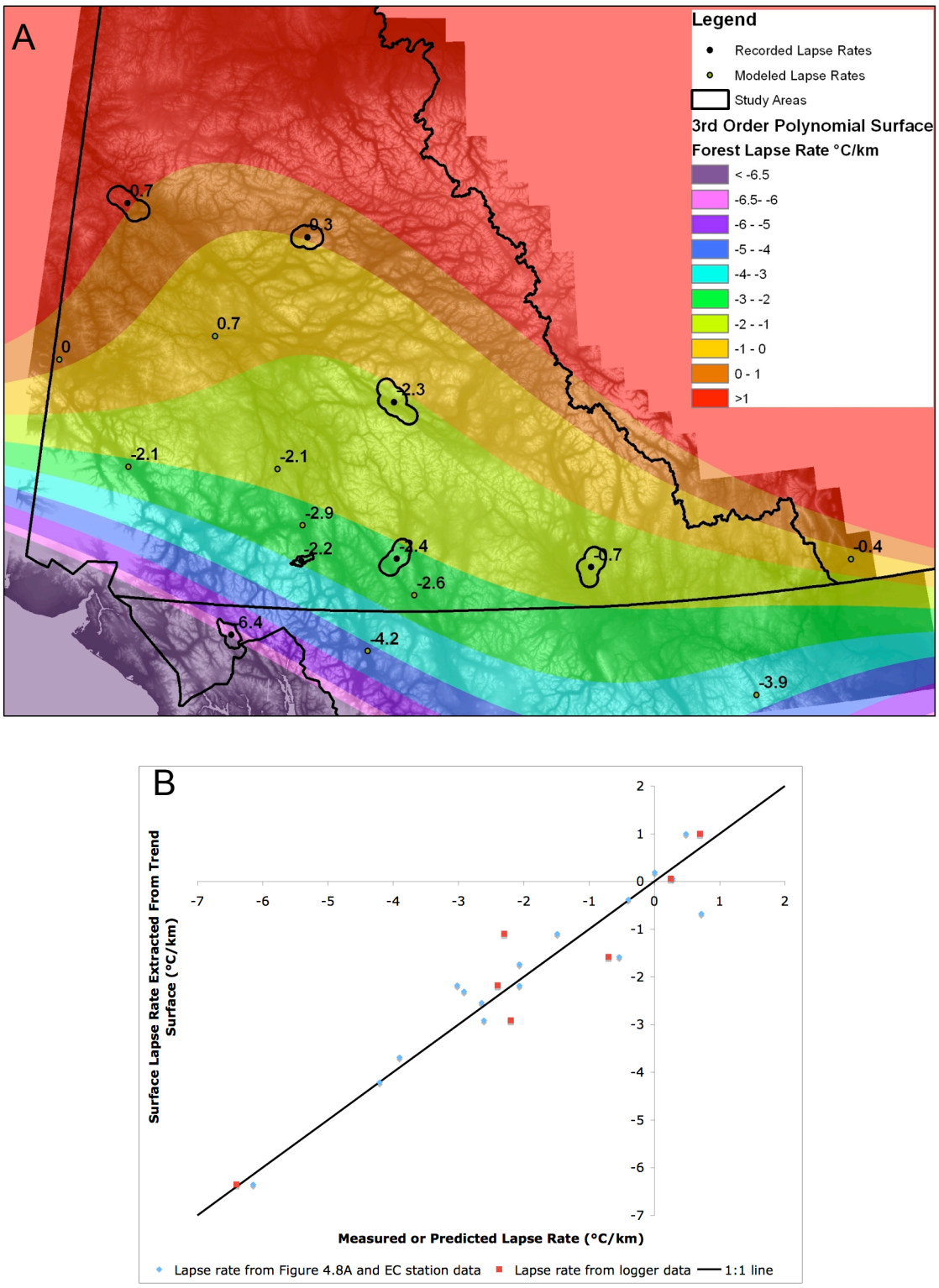

Figure 4.8: (A) Third order polynomial trend surface for surface lapse rates through the forest zone across the southern Yukon and northern British Columbia based on measured values at the study areas and predicted values for valley-bottom weather stations from the relationship in Figure 4.7. The trend surface predicts values <-6.5 °C km^{-1} and > +1°C

km^{-1} near the margins of the study region but there are no field data to support such extremes. Consequently, the legend has been truncated at these levels. (B) Measured surface lapse rates (from our measurement sites) and predicted surface lapse rates from Figure 4.7 (for Environment Canada stations) compared to values extracted from the trend surface in (A).

Chapter Five

Mountain Permafrost Probability Modelling in Areas Above and Below Treeline, Southern Yukon, Canada

Abstract

Empirical-statistical methods were used to model mountain permafrost probability above and below treeline for five areas distributed across the southern half of the Yukon (60° - 64°N). The modelling addressed a key issue by incorporating the effects of inverted or weak surface lapse rates below treeline. The variables used to predict the Basal Temperature of Snow (BTS) by linear regression included equivalent elevation, Potential Incoming Solar Radiation (PISR), slope and Normalized Difference Vegetation Index (NDVI). Topographic Position Index (TPI) was also examined as an explanatory variable but was not statistically significant in any of the areas. Predicted BTS temperatures were compared using logistic regression to late-summer physical verification of permafrost presence or absence. The resulting models indicate that permafrost underlies 19-24% of the Johnson's Crossing area, 30% of the Sa Dena Hes area, 63% of the Faro and Dawson study areas and 79% of the Keno area. In the most northerly study locations where surface lapse rates are inverted, they predict high permafrost probabilities within valleys, and decreasing probabilities up to treeline. The results represent a step towards developing empirical-statistical permafrost probability models for the entire region, but suggest that blended combination modelling may be needed to make predictions outside the individual study areas.

Key Words: Permafrost Modelling, Mountain Permafrost, BTS, Equivalent Elevation, Interchangeability, Yukon.

Introduction

The Basal Temperature of Snow (BTS) method, first devised by Haeberli (1973) for the detection of alpine permafrost in the Swiss Alps, has been applied in numerous mountain permafrost areas. These have included central Europe (e.g. Gruber & Hoelzle, 2001; Lugon & Delaloye, 2001; Gardaz,1997; Hoelzle et al., 1999; Imhof et al., 2000; Hoelzle, 1992; King, 1992; Dobinski, 1998), Scandinavia (e.g. Isaksen et al., 2002; Jeckel, 1988; Ødegard et al., 1996), Japan (e.g. Ishikawa & Hirakawa, 2000), and, most recently, North America (Lewkowicz & Ednie, 2004; Janke, 2005ab; Bonnaventure and Lewkowicz, 2008; Lewkowicz and Bonnaventure, 2008; Bonnaventure and Lewkowicz, 2010). The advantages of this form of empirical statistical modelling are that it is relatively inexpensive to apply, the limited inputs required are available even for isolated locations, and many of the modelling inputs can be generated within a GIS allowing predictions to be mapped.

BTS-based modelling to date has been concentrated on terrain above treeline in mountainous areas similar in physiography to the Swiss Alps. Most of these models rely on relations between elevation, Potential Incoming Solar Radiation (PISR) and measured BTS values to generate predicted BTS surfaces. These are then classified into categories of permafrost likelihood based on 'rules-of-thumb' (Haeberli, 1973): modeled BTS values < -3 °C indicate probable permafrost, values of -2 °C to -3 °C indicate possible permafrost, and values > -2 °C indicate that permafrost is improbable (Hoelzle, 1992). The 'rules of thumb' serve as indicators of permafrost and do not reflect 100% likelihood for the probable category or 0% for the improbable category (Lewkowicz and Ednie,

2004). In addition, they do not appear to be entirely appropriate for the mountains of North America (Lewkowicz and Ednie, 2004; Bonnaventure and Lewkowicz, 2008).

A fundamental characteristic of permafrost in the mountains of the Yukon and Alaska is its extensive presence below treeline, because latitudinal and mountain permafrost begin to interfinger in this subarctic region (e.g. Williams and Burn, 1996). Similar conditions exist in Mongolia (Etzelmüller et al., 2006). Several factors contribute to the existence of permafrost within the forest even where its distribution is discontinuous: (1) strong continentality that maintains Mean Annual Air Temperatures (MAAT) below 0°C in spite of summers that are warm enough to promote forest growth; (2) shallow snowpacks which reduce but do not eliminate ground to atmosphere heat losses through the winter; (3) topography which promotes cold-air pooling and inverted surface lapse rates (SLR) (such as in U-shaped valleys); and (4) specific vegetation assemblages which maintain colder temperatures through thick organic mats (Lewkowicz and Ednie, 2004; Shur and Jorgenson, 2007; Fukui et al., 2008). The result is that permafrost distribution may not increase linearly with elevation as it tends to within the European Alps where the BTS method originated.

This paper examines and models permafrost probability for five areas within four different climatic zones in the Yukon (Wahl et al., 1987) (Figure 5.1). The presence of permafrost beneath forested terrain, as well as above treeline required the introduction of additional explanatory variables. In addition to producing analyses for the individual areas, this study is a step towards modelling permafrost probability over the entire southern Yukon using empirical-statistical blending and distance decay techniques.

Study Areas

Five areas located from 60° to 64°N were selected for study: Johnson's Crossing, Sa Dena Hes, Faro, Keno and Dawson (Figure 5.1; Table 5.1). Each study area was demarcated by drawing a 10 km buffer around all sampled points and dissolving the boundaries in ArcGIS. Minimum elevations in the study areas were about 600 m above sea level (asl) except for Dawson where the Yukon River is at 270 m asl. Maximum elevations ranged from 1250 m asl at Dawson to 2050 m asl at Faro and Keno. All areas except Dawson were glaciated during the Wisconsinan (Ward et al., 2007; Duk-Rodkin, 1996). These areas are part of the Cordilleran orogen geological grouping, comprising large mountain belts of deformed and metamorphosed sedimentary and volcanic rocks mainly of Phanerozoic and Proterozoic ages (DEMR, 1974; Wahl et al., 1987; Eyles and Miall, 2007)

Climatic gradients across the region are relatively gentle. The entire area is in the Boreal Cordillera ecozone, which is characterized physiographically by mountain ranges with numerous high peaks and extensive plateaus, and climatically by long, cold winters and short, warm summers, varying with altitude and mountainside orientation (Natural Resources Canada, 2010). MAATs measured at the standard weather stations in the major valleys range from -1.2 °C to -4.4 °C and decrease from south to north (Table 5.1). Continentality increases in the same direction but also from west to east, with the greatest range of monthly temperatures at Dawson (Table 5.1). Annual precipitation ranges between about 300 and 400 mm with the highest amounts in the Liard Basin climatic region. Our measurements of MAAT over two years cover a much larger elevation range

than the standard weather stations. The lowest recorded MAAT was -6.8°C at 1815 m asl in the Keno study region.

All of the study areas experience wintertime inversions in SLR through forested terrain (Lewkowicz and Bonnaventure, *Submitted*). In Johnson's Crossing, Sa Dena Hes and Faro, this results in gentle SLRs below treeline on an annual basis (-2.4, -0.7 and -2.3 °C km^{-1}, respectively). In the more continental locations of Keno and Dawson, annual inverted SLRs are present (0.3 and 0.7 °C km^{-1}, respectively).

Vegetation in all areas comprises boreal forest with coniferous trees and some boreal broadleaf trees in lowland areas, while sub-alpine forest, shrubs, alpine tundra, barren patches, and exposed rock occur progressively at higher elevations (Wahl et al., 1987). The Keno area is the only exception as it is very close to a ecosystem boundary where vegetation begins to transition to full-scale tundra with alpine sedges, grasses and shrubs present above treeline (Wahl et al., 1987).

Methods

Data Logger Network

Networks of 12-13 monitoring sites were established in all areas in May-June 2006, except for Dawson where the logger network was established in August 2007. Each site was equipped with loggers recording hourly air temperature (Onset Hobo Pro series with accuracy of ± 0.2°C) at a height of 1.6 m above the surface, ground surface temperature (2-5cm below the surface), temperature at or close to the top of permafrost (TTOP) (30-100 cm depth) and snow depths using iButtons (accuracy ± 1°C) (see Lewkowicz, 2008).

BTS Measurements

The BTS methodology for this study was adapted from Bonnaventure and Lewkowicz (2008) and incorporated recommendations from Brenning et al. (2005). BTS values were measured in mid-March 2007 and 2008 in all of the locations except for Faro where readings were only taken in the latter year due to a lack of snow in 2007. Approximately 80 BTS points were collected in each location over the two seasons with about 55 measurements made in Faro during 2008.

BTS measurements require snow depths >80 cm since this is the minimum needed to insulate the ground from diurnal air temperature fluctuations (Haeberli, 1973). BTS sampling was conducted in all study areas on all major slope aspects, as well as in valley bottoms, and across vegetation zones from forest to tundra. In order to avoid spatial autocorrelation, the minimum distance between any pair of sampling locations was aimed to be at least 150 m horizontal meters (Brenning et al., 2005). Brenning et al. (2005) also recommend that in order to minimize the chances of an outlier, four BTS measurements should be taken within a 10 m radius. Four BTS measurements were taken in a previous study (Bonnaventure and Lewkowicz, 2008) but analysis of these data indicated that at more than 90% of the sites, the maximum difference between using three or four points changed the average by <± 0.5°C. The only cases when the difference exceeded ±1°C occurred where the average BTS temperature was <-5°C which indicates that permafrost probability was already high. The decision to use three measurements reduced the number of personnel needed in the field to conduct measurements to three. A full description of all other field procedures relating to the BTS measurements is given in Bonnaventure and Lewkowicz (2008).

Physical Validation of Permafrost Presence

Physical validation allows quantitative permafrost probability modelling using the BTS method. This step also removes the sampling bias associated with taking BTS measurements only at sites where snow depths exceed 80 cm, which typically have relatively warm ground temperatures (Lewkowicz and Ednie, 2004).

Field verification of the presence or absence of permafrost was performed by probing and/or excavating pits in the study areas during August 2007 and 2008. Approximately 90 sites were investigated in each of the study areas over a range of elevations, aspects, slopes and vegetation types. The temperature monitoring sites provided an additional set of ground truthing locations. The procedures and methods for permafrost verification were the same as those used in previous work and are outlined in Bonnaventure and Lewkowicz (2008).

Analytical Methods

For each of the five areas, a combination of variables was used to predict BTS. The full set of variables comprised equivalent elevation (Lewkowicz and Bonnaventure, 2011), Topographic Position Index (TPI), Potential Incoming Solar Radiation (PISR), slope and Normalized Difference Vegetation Index (NDVI).

Equivalent elevation was calculated using a 30 x 30 m DEM supplied by the Yukon Geological Survey and Geobase (2009), and air temperatures measured within and above the forested zone in each area. Equivalent elevation reflects air temperature trends in a region by manipulating the numerical elevations of grid cells below treeline to take

into account the weakened or reversed SLR in the forest compared to the normal negative SLR above treeline. Grid cells that are well below treeline may be increased significantly in elevation, areas close to treeline are changed very little and elevations above treeline remain unaltered (Lewkowicz and Bonnaventure, *Submitted*).

TPI was included in order to examine localized topographic effects of cold-air pooling and snow cover accumulation patterns on BTS. It was calculated using the DEM and the ArcView add-in program Topographic Position Index (TPI). The algorithm compares the elevation of each grid cell in a DEM to the average elevation of the surrounding cells within a defined radius. TPI values for this study were generated using radii of 1000 m. The comparison of pixel elevations results in a positive or negative TPI value (Jenness, 2006).

PISR was calculated using the ArcGIS Spatial Analyst program Area Solar Radiation. A model was created for each area using inputs for snow-free periods and cloud cover. The start of the snow-free period was determined from the date that measured ground surface temperatures first rose above 0°C. The end of the snow-free period was set as the date that ground surface temperatures stopped exhibiting diurnal fluctuations above 0°C and the iButton data indicated snow on the ground (Lewkowicz, 2008). Cloud cover values were selected following examination of day-time cloud cover percentages from any nearby Environment Canada climate station, as well as from diurnal fluctuations in air and ground surface temperatures which can be used to interpolate cloud cover conditions (Bonnaventure and Lewkowicz, 2008; Lewkowicz and Bonnaventure, 2008).

Slope in degrees was calculated from the DEM in ArcGIS. Slope affects PISR but it also potentially impacts permafrost through snow depths. Steeper slopes may not be able to accumulate as much snow as gentle slopes due to redistribution by wind or avalanche.

NDVI was calculated for each area using Landsat TM 5 or 7 imagery within a PCI Geomatica environment (Table 5.2) (Kremer et al., 2011). NDVI measures the greenness of vegetation and classifies it between -1 and 1, where values approaching -1 indicate water, values close to 0 show barren land and values approaching 1 show lush forest (Rouse *et al*., 1974). NDVI was processed for an area about 10 km larger on all sides than the study area itself to avoid any topographic shadowing or edge effects. The imagery was corrected for topographic effects on brightness values using methods similar to that of a cosine correction (Meyer et al., 1993; Teillet et al., 1982; Jensen, 2005).

Results

BTS Regression

Multiple regression analysis using measured BTS values as the dependent variable were performed for each area using the independent variables described in the methods section above. Before these could be undertaken for areas with more than one year of BTS data (all except Faro), the values were checked to see if adjustment was required to take inter-annual differences into account (Lewkowicz and Ednie, 2004; Bonnaventure and Lewkowicz, 2008; Ishikawa, 2003). Data from the logger network showed that conditions leading into the fall and winter of 2006-2007 were considerably colder than that in the following year, and in much of the region were the coldest in 20

years (Environment Canada, 2010). The former was what Brenning et al. (2005) describe as an R2 winter, when the ground surface is exposed to very cold air temperatures before the onset of a continuous snow cover. To allow the data sets to be merged, BTS temperatures for 2007-2008 were adjusted by subtracting a constant value. For Johnson's Crossing and Dawson a -1°C subtraction was applied while a subtraction of -0.5°C was used for Keno. These adjustments were completed to account for different patterns of winter temperatures and snowpack accumulation (e.g. Lewkowicz and Ednie, 2004; Bonnaventure and Lewkowicz, 2008; Ishikawa and Hirakawa, 2000). The BTS data for Sa Dena Hes did not require any adjustment as the area received large amounts of snow early in the season in both years, insulating the ground. The adjusted distribution of BTS points was tested for normality using a Kolmogorov-Smirnov test. In each of the areas initial regression analysis began by including all BTS predictor variables in the multiple regression and then eliminating non-statistically significant variables from the analysis to obtain the best statistically significant fit.

The results of the multiple regression analyses are given in Table 5.3, and modeled BTS (MBTS) are plotted against measured BTS in Figure 5.2. JC_WC* is a model created for Johnson's Crossing using BTS equations for the Wolf Creek Basin 150 km to the west (Lewkowicz and Bonnaventure, 2008). The multiple regression analyses generated models with r^2 values ranging from a low of 0.21 for Sa Dena Hes to a high of 0.48 for Faro. These values are similar to those obtained in other BTS models developed for the Yukon and the Alps (e.g. 0.39, Gruber and Hoelzle, 2001; 0.4, Lewkowicz and Ednie, 2004; 0.29 and 0.36, Bonnaventure and Lewkowicz, 2008). There is a roughly

even distribution of points above and below the 1:1 line in the BTS versus MBTS plots (Figure 5.2).

Equivalent elevation was statistically significant in all areas except Sa Dena Hes, where BTS was best explained by NDVI and slope. It appears however, that equivalent elevation is the most useful variable for predicting BTS over multiple areas that are separated by hundreds of kilometers. This variable may combine multiple factors that promote the occurrence of permafrost including thick organic mats and cold-air pooling in low-lying valley bottoms. The slope variable was statistically significant in three of the five areas (F, JC and SDH). Steeper slopes were linked to colder BTS temperatures in the model, possibly because snow cover is intermittently removed from steep slopes by wind action or avalanche so that these locations only just maintain a cover >80 cm and thus have colder BTS. PISR was significant only in the Keno area. PISR has been widely employed in previous BTS modelling within high mountain areas but the results suggest that it is less important in forested areas.

Logistic Regression Modelling

The probability of permafrost for each of the five study areas was calculated using logistic regression (Hosmer and Lemeshow, 1989) based on the relationship between modeled BTS values and observed presence or absence of late-summer frozen ground at the ground-truthing sites (e.g. Lewkowicz and Ednie, 2004; Bonnaventure and Lewkowicz, 2008). The logistic regression coefficients are given in Table 5.4, and the logistic regression curves for each area are shown in Figure 5.3.

The results of the logistic modelling show that except for Keno and Sa Dena Hes the numerical values of modeled BTS have different meanings among the areas. The differences in the remaining curves indicate the importance of combining BTS with ground-truthing. This is especially true for Faro where the model appears reversed and warmer BTS temperatures indicate higher probabilities of permafrost. It is likely that the curve reversal is the result of snow distribution: sites at higher elevation but below the treeline in this area generally have greater snow depths, which therefore raise the temperature at the base of snowpack in areas underlain by permafrost. However, the range of probabilities produced by the model for Faro is smaller than in any of the other areas so that permafrost is probable at almost any modeled BTS temperature. This results in the controlling factor on BTS temperature being snow depth at many sample locations, and since depth increases with elevation within the forest, the curve is reversed.

Permafrost Probability Mapping

The equations generated from the logistic regression analysis for each area were applied to the BTS surfaces to generate maps of permafrost probability.

Johnson's Crossing

The probability of permafrost modelling predicted that approximately 24% of the Johnson's Crossing area is underlain by permafrost (Figure 5.4). The lowest probability areas (1 – 10%) are mostly low-lying open valleys where significant topographic relief and slope do not surround the site. Maximum probabilities (80 - 99% likelihood) are predicted for the steepest slopes, but these areas are very limited in extent. Mountain summits above treeline show similar probabilities as mid- and low-elevation areas. Much

of the study area has low to intermediate permafrost probabilities (20 – 30%), which increase slowly with elevation due to the slow change in equivalent elevation within the forest.

We believe that the probability of permafrost model created for Johnson's Crossing may not be the best representation of this area's permafrost distribution because of problems sampling above treeline. Snow was generally thinner with increasing elevation above treeline so that BTS samples in this zone are limited. Ground truthing was also difficult as much of the terrain above treeline has near-surface bedrock or clast-rich soils making digging or probing to the frost table impossible. As an alternative, the BTS model created for the Wolf Creek Basin (Lewkowicz and Ednie, 2004; Lewkowicz and Bonnaventure, 2008; Bonnaventure and Lewkowicz, 2010) (150 km west of JC) was utilized to create a BTS surface and validated using the ground truthing collected for Johnson's Crossing (Figure 5.5). The use of this model can be justified by the similarity in forest SLRs (WC -2.2 °C km^{-1}, JC -2.4 °C km^{-1}), similar mean annual temperatures for climate stations (Whitehorse A -0.7 °C at 706 m asl; Teslin A -1.2 °C at 705 m asl) and treeline (1300 m and 1350 m asl respectively). This model indicates that about 19% of the area may be underlain by permafrost, less than using the original model, but the distribution appears to be more realistic as low-lying areas have low probabilities (0-10%) and mountain peaks have the highest permafrost probabilities (90-99%) as is known from the logger network results. This model also incorporates PISR into the BTS predictions, resulting in higher probabilities for permafrost on north-facing slopes.

Sa Dena Hes

Permafrost probabilities in the Sa Dena Hes area are relatively homogeneous with almost the entire terrain being classified as within the 20 – 30% probability range (Figure 5.6). According to the modelling, approximately 30% of the area is underlain by permafrost with a maximum probilities of 90% occurring on very small areas of upper elevation steep and sparsely vegetated slopes. The lowest probability areas (around 15%) are in areas of thick tree cover and low relief close to the main highway. The homogeneity of the surface is caused by the very limited areas above treeline, while below treeline SLRs are very small (-0.7 °C km^{-1}) (Lewkowicz and Bonnaventure, *Submitted*). With the exception of the steepest areas, which are often associated with high elevations, the probability of encountering permafrost at almost all elevations within the study area varies very little.

Faro

The Faro area also exhibits fairly homogeneous permafrost probabilities, but the average value is much higher than at the more southerly sites (Figure 5.7). The model predicts that about 63% of the area is underlain by permafrost. The highest values (85%) exist on the highest and steepest mountain peaks while relatively high values (45 – 55%) also exist at the lowest elevations within U-shaped valleys and along the Pelly River. Low permafrost probabilities are not predicted, likely due to the occurrence of significant cold-air pooling in the area and the generally colder climate. In addition, low-lying poorly drained areas, which are covered by very thick organic mats, dominate the valley bottoms. Vegetation of this type has been shown to promote the formation and

preservation of permafrost (Williams and Burn, 1996; Shur and Jorgenson, 2007; Fukui et al., 2008).

Keno

The Keno area has the greatest range of elevations and shows the highest probabilities of permafrost (about 79% overall) of the five areas (Figure 5.8). Permafrost in this area is strongly influenced by aspect due to the strength of the PISR variable, with the effects of inverted SLR within the forest also being evident. The highest probabilities (90 – 99%) exist on steep upper elevation north-facing slopes far above treeline, as well as at the bottom of the main valleys where vegetation types and organic mats similar to those at Faro are present. The lowest probabilities (25 – 30%) exist on areas that receive high PISR including upper elevation south-facing slopes.

Dawson

The model for the Dawson area is controlled strictly by equivalent elevation and predicts approximately 63% of the area to be underlain by permafrost (Figure 5.9). The maximum probabilities (70 – 80%) are predicted for low-lying areas, especially the Yukon and Klondike River Valleys, which experience poor drainage and colder temperatures in winter resulting in an inverted annual SLR (0.7°C km^{-1}) (Lewkowicz and Bonnaventure, *Submitted*). The lowest probabilities (40 – 50%) are predicted for the terrain just below treeline and probabilities then increase on the highest ridges.

Probability of Permafrost Model Validation

The results of the permafrost probability models for each of the study sites were compared to the actual presence of permafrost observed at the late-summer ground

truthing sites and ground temperature measurement sites (Figure 5.10). The results show an acceptable relationship between observed and predicted permafrost probabilities for Dawson, Keno and Sa Dena Hes. However, the Faro results show that the warmer BTS values correspond to higher permafrost probabilities, producing the counter-intuitive logistic regression curve (Figure 5.3).

For Johnson's Crossing, it is evident that the model using the BTS relations from Wolf Creek performs better than the original. In the original model the highest probabilities are predicted for pit locations that do not contain permafrost, whereas when the combination model is used, the relation is substantially improved as seen by the proximity of points to the 1:1 line (Figure 5.10).

Discussion

Model Results

Permafrost distribution in the five study areas has, until now, been understood in only the most general terms (see Figure 5.1). Our predictions give high-resolution permafrost probabilities and match the zonal classification on the permafrost map of Canada (Heginbottom et al., 1995) except for Faro. Our modelling there gives an areal coverage of 63% indicating that it should be considered part of the extensive discontinuous permafrost zone, whereas it is shown as sporadic discontinuous on the permafrost map of Canada (Heginbottom at al., 1995). This is likely the result of relatively high probabilities in low-elevation valley areas, which also occur in the other northerly study areas (Keno and Dawson) as a result of mountain permafrost interfingering with latitudinal permafrost.

This modelling differs from that done previously in the Yukon (Lewkowicz and Ednie, 2004; Bonnaventure and Lewkowicz, 2008) because of the extensive fieldwork within the forest and the integration of SLRs into the models. Earlier models were primarily elevation-controlled whereas these results indicate that permafrost probability can be highest in the lowest valley areas. Above treeline, however, permafrost probability follows a similar pattern to that obtained previously as a result of a normal negative SLR (Lewkowicz and Bonnaventure, *Submitted*).

Errors and Inaccuracies

The spatial modelling undertaken has a number of challenges that may have affected the results. In areas where treeline was close to the summits, it proved difficult to obtain BTS samples because ridge tops were largely blown clear. These differences in snow cover dynamics among the areas may explain why modeled BTS values represent such different probabilities in each study area (Figure 5.3). This reinforces earlier indication that BTS values themselves are not necessarily transferable between areas, and that the ground truthing is a vital part of their use in North America.

Ground truthing of the presence or absence of permafrost was also problematic where the substrate was coarse or composed of solid rock. Since these conditions were typically encountered at high elevation sites, they were under-represented in the sample and this could have affected the predictions of permafrost probabilities on peaks in some of the study areas. This is most evident in the Johnson's Crossing area where the combination model, derived from sampling above treeline in Wolf Creek, is likely more accurate than the original. Although the final representations of permafrost distribution in the Dawson and Keno areas appear reasonable, logistical challenges also occurred there.

Dawson had only a small elevational range above treeline while in Keno, lower elevation sites were unintentionally favoured due to logistics. Both may have introduced a bias in the resultant models. In order to improve the modelling, the use of other ground-truthing methods, such as DC resistivity, boreholes and additional ground temperature loggers should be explored (e.g. Ishikawa and Hirakawa, 2000; Hauck and Kneisel, 2006; Tanarro et al., 2001; Isaksen at al., 2002). However, all of these take much more time and/or are more costly to undertake so that the numbers of sites examined would be quite limited.

Permafrost explanatory variables

Most BTS-based models have used only elevation and PISR as explanatory variables. Attempts have been made in the Alps to include vegetation using Soil Adjusted Vegetation Index (SAVI) but this led only to a very minor improvement (Gruber and Hoelzle, 2001). Given that this study examined a continental forested mountain environment, we tested additional variables.

TPI was included to examine localized cold-air pooling which is known to occur in some mountain valleys and appears to influence permafrost probabilities (Lewkowicz and Ednie, 2004). However, this variable did not emerge as statistically significant in any area. It may be that localized cold-air pooling in topographic hollows, where TPI values are negative is offset by greater snow depths, which actually result in net warming effects. This explanation is supported by negative but non-significant coefficients that emerged for some study areas.

Vegetation cover was introduced as an explanatory variable as the presence of certain vegetation types can promote the existence of permafrost (Shur and Jorgenson,

2007). This variable was added because in the field the "look" of a site with respect to vegetation can often tell an experienced permafrost researcher if permafrost is present or not (Kremer et al., 2011). A complete Classification and Regression Tree (CART) analysis showed that vegetation types which are commonly associated with permafrost included stunted spruce trees in the presence of developed spruce forests, and thick organic mats of moist moss (Kremer at al., 2011).

In our modelling, NDVI was used as the primary vegetation variable as it can be calculated for the entirety of each study area. NDVI was statistically significant in Sa Dena Hes where higher values were linked to warmer BTS temperatures and hence to an absence of permafrost. This is likely because many of the areas containing permafrost in Sa Dena Hes were above treeline with NDVI values close to 0. At the other sites however, NDVI did not emerge as a significant variable, possibly because NDVI is not sensitive enough to detect changes in vegetation within the forest, such as the presence or absence of thick surface organic mats, that impact ground temperatures.

It was particularly surprising that PISR was statistically significant only for the Keno area where it had a standardised ß-coefficient twice that of equivalent elevation. PISR has been shown to be statistically significant in many areas in the Alps (e.g. Gruber and Hoelzle, 2001; Julián and Chueca, 2007) and Scandinavia (e.g. Hauck et al., 2004; Juliussen and Humlum, 2007) as well as in Wolf Creek and Ruby Range in the Yukon (Lewkowicz and Ednie, 2004; Bonnaventure and Lewkowicz, 2008). However, all of the areas had the majority or all of their sampling carried out above treeline whereas that was not the case in the present study. Keno may have appeared as an exception because it has the maximum elevation range of any study area and has the greatest proportion above

treeline. These results lead us to believe that PISR does affect permafrost distribution in the forest, as has been described in studies going back many decades (e.g. Brown, 1966; 1970) but it is simply not strong enough to show up in the models at the scale chosen.

Spatial Extension of the Models

At the start of this research, we hypothesized that climatic regions (Figure 5.1) would provide a way to infer permafrost conditions outside the individual study areas. However, the results show that the study areas differ from one another in terms of explanatory variables (Table 5.3) and logistic regression curves (Figure 5.3). The results for areas in the same climate region (e.g. Faro and Dawson, and in previous studies Wolf Creek and Ruby Range (Lewkowicz and Bonnaventure, 2008) also differ. It is therefore clear that being within a given climatic zone does not provide a good measure of interchangeability between areas.

In order to expand the modeled area using empirical-statistical techniques, an alternative to simple interchangeability (Lewkowicz and Bonnaventure, 2008) or extension throughout a climatic zone will be needed. One option may be to use a combination of all models outside any given study area, blending the results based on a distance-decay function. The result of such modelling would provide an initial overview of permafrost conditions in the Yukon that could be used for infrastructure route planning, climate change adaptation strategies, and geohazard identification.

Summary and Conclusions

This research showed:

1) BTS-based models based on a combination of variables including equivalent elevation, slope, PISR and NDVI can be used to predict permafrost probability in the Johnson's Crossing, Sa Dena Hes, Faro, Keno and Dawson areas. Topographic Position Index was also examined as a possible explanatory variable but was not statistically significant in any area. The ground truthing step in the modelling was shown to be an essential part of the methodology.
2) Based on the probability modelling, the percent of each area predicted to be underlain by permafrost varied from 19-24% for Johnson's Crossing to 79% for Keno. Four of the five areas fall within the appropriate zone of permafrost according to the permafrost map of Canada. Faro, which is on the boundary between the sporadic and extensive zones, should be considered a part of the latter according to the model results.
3) Study areas with inverted surface lapse rates (Dawson and Keno) have high probabilities of permafrost in low-lying forested terrain as well as on summit areas above treeline. In areas where surface lapse rates are normal but gentle, higher probabilities are seen on mountaintops while valley bottoms exhibit low to moderate probabilities.
4) These models have addressed a key issue for modelling mountain permafrost in northwest North America where a lower elevation limit for permafrost cannot be defined due to interfingering of latitudinal and mountain

permafrost. The equivalent elevation responds to these particularities, incorporating site-specific SLRs for areas below treeline.

5) The interchangeability of these models is relatively poor and there appears to be no relation between climatic region and permafrost explanatory variables. Thus any attempt to model permafrost outside the study areas would require the use of a blended combination of all models, potentially weighted using a distance decay function.

Acknowledgments

This project was supported financially by the Canadian Foundation for Climate and Atmospheric Sciences, the Federal Government of Canada's International Polar Year Program, the Natural Sciences and Engineering Research Council of Canada, the Northern Scientific Training Program (Department of Indian Affairs and Northern Development), the Yukon Geological Survey, the Geological Survey of Canada, and the Faculty of Arts, University of Ottawa. Field assistance for BTS was carried out by Julie Cossett, Paul Pearson, Katherine Henry and Chris Andrews while summer assistance with the pits was carried out by Dan Odell, Patty Bonnaventure, Jason Skucas, Andrea Sitler and Marian Kremer. Support with data processing and GIS analysis was given by Philippe Gingras and Marian Kremer.

References

Bonnaventure, P.P., and Lewkowicz, A.G. 2008. Mountain permafrost probability mapping using the BTS method in two climatically dissimilar locations, Northwest Canada. *Canadian Journal of Earth Sciences,* **45**: 443-455.

Bonnaventure, P.P., and Lewkowicz, A.G. 2010. Modelling climate change effects on the spatial distribution of mountain permafrost at three sites in northwest Canada. *Climatic Change*. DOI 10.1007/s10584-010-9818-5.

Brenning, A., Gruber, S., and Hoelzle, M. 2005. Sampling and Statistical Analyses of BTS Measurements. *Permafrost and Periglacial Processes***. 16**: 1 – 11.

Brown, R.J.E. 1966. Influence of vegetation on permafrost, Proceedings, 1st International Permafrost Conference, Purdue University, 1963. National Academy of Sciences-National Research Council Publication 1287, pp. 20-25.

Brown, R.J.E. 1970. Permafrost in Canada-its influence on northern development. University of Toronto Press, Toronto, 234 pp.

Department of Energy Mines and Resources, Canada. 1974. Physiographic regions of Yukon and surrounding Canadian territory. Published in *Climate of Yukon.* Canadian Government Publishing Centre.

Dobinski, W. 1998. Permafrost occurrences in the alpine zone of the Tatra Mountains, Poland. *In* A.G. Lewkowicz and M. Allard, (eds.) *Proceedings, Seventh International Conference on Permafrost, Yellowknife, June 23-27, 1998.* Nordicana, Centre d'Etudes Nordiques, Quebec City. 231- 237.

Duk-Rodkin, A. 1996. Surficial geology, Dawson, Yukon Territory. Geological Survey of Canada, open file 3288, 1:250 000 scale.

Etzelmüller, B., Heggem, E.S.F., Sharkhuu, N., Frauenfelder, R., Kääb, A. and Goulden, C. 2006. Mountain permafrost distribution modelling using a multi-criteria approach in the Hövsgöl area, northern Mongolia. *Permafrost and Periglacial Processes*, **17**: 91-104.

Eyles, N. and Miall, A. 2007. Canada Rocks, The Geologic Journey. Fitzhenry and Whiteside limited. Markham Ontario.

Fukui, K. Sone, T., Yamagata, K., Otsuki, Y., Sawada, Y., Vetrova, V. and Vyatkina, M. 2008. Relationships between permafrost distribution and surface organic layers near Esso, central Kamchatka, Russian Far East. *Permafrost and Periglacial Processes.* **19**: 85-92.

Gardaz, J.M. 1997. Distribution of Mountain Permafrost, Fontanesses Basin, Valaisian Alps, Switzerland. *Permafrost and Periglacial Processes* **8**: 101-105.

Geobase (http://www.geobase.ca/) [Acceded May 2009].

Geomatics Yukon. 2006. 30 Meter Yukon Digital Elevation Model [data file]. Whitehorse,
Yukon. Available download: ftp://ftp.geomaticsyukon.ca/DEMs/30m [compiled in 2007].

Gruber, S., and Hoelzle, M. 2001. Statistical modeling of mountain permafrost distribution: Local calibration and incorporation of remotely sensed data. *Permafrost and Periglacial Processes*, **12**: 69-77.

Haeberli, W. 1973. Die Basistemperatur der winterlichen Schnee decke als möglicher Indikator für die Verbreitung von Perma rost in den Alpen. Zeitschrift für Gletscherkunde und Glazialgeologie, **1–2**: 221–227.

Hauck, C., and Kneisel, C. 2006. Application of Capacitively-coupled and DC Electrical Resistivity Imaging for Mountain Permafrost Studies. *Permafrost and Periglacial Processes.* **17**: 169–177.

Hauck, C., Isaksen, K., Vonder Mühll, D., and Sollid, J.L. 2004. Geophysical Surveys Designed to Delineate the Altitudinal Limit of Mountain Permafrost: an Example from Jotunheimen, Norway. *Permafrost and Periglacial Processes.* **15**: 191–205.

Heginbottom, J.A., Dubreuil, M.A., and Haker, P.T. 1995. Canada Permafrost. (1:7,500,000 scale). In *The National Atlas of Canada*, 5th Edition, sheet MCR 4177. Ottawa: National Resources Canada.

Hoelzle, M. 1992. Permafrost occurrence from BTS measurements and climatic parameters in the Eastern Swiss Alps. *Permafrost and Periglacial Processes*, **3**: 143-147.

Hoelzle, M., Wegmann, M., Krummenacher, B. 1999. Miniature Temperature Dataloggers for Mapping and Monitoring of Permafrost in High Mountain Areas: First Experiences from the Swiss Alps. *Permafrost and Periglacial Processes*, **10**: 113-124.

Hosmer, D.W., and Lemeshow, S. 1989. *Applied logistic regression*. John Willey & Sons, New York, U.S.A. 16-17.

Imhof, M., Pierrehumert, G., Haeberlie, W., and Kienholz, H. 2000. Permafrost investigation in the Schilthorn Massif, Bernese Alps, Switzerland. *Permafrost and Periglacial Processes*, **11**: 189-206.

Isaksen, K., Hauck, C., Gudevang, E., Ødegård, R.S., and Sollid, J.L. 2002. Mountain permafrost distribution in Dovrefjell and Jotunheimen, southern Norway, based on BTS and DC resistivity tomography data. Norsk Geografisk Tidsskrift. Norwegian Journal of Geography, **56**: 122–136. doi:10.1080/00291950 2760056459.

Ishikawa, M., and Hirakawa, N. 2000. Mountain permafrost distribution based on BTS measurements and DC resistivity soundings in the Daisetu Moutains, Hokkaido, Japan. *Permafrost and Periglacial Processes*, **11** 109-123.

Ishikawa, M. 2003. Thermal regimes at the snow-ground interface and their implications for permafrost investigation. *Geomorphology.* **52**:105-120.

Janke, J.R. 2005a. The Occurrence of Alpine Permafrost in the Front Range of Colorado.

Geomorphology. **67**: 375-389.

Janke, J.R. 2005b. Modeling past and future alpine permafrost distribution in the Colorado Front Range. *Earth Surface Processes and Landforms* **30**: 1495-1508. DOI: 10.1002/esp.1205.

Jeckel, P.P. 1988. Permafrost and its altitudinal zonation in N. Lapland. In *Proceedings of the Fifth International Conference on Permafrost, Trondheim*. Tapir, Trondheim. **1** 332-337.

Jenness, J. 2006. Topographic Position Index (TPI) v. 1.2. Online manual, Jenness Enterprises, 3020 N. Schevene Blvd. Flagstaff, AZ, 86004, USA.

Jensen, J.R. 2005. *Introductory Digital Image Processing*. Toronto: Pearson Education Inc.

Julián, A., and Chueca, J. 2007. Permafrost distribution from BTS measurements (Sierra de Telera, Central Pyrenees Spain): Assessing the importance of solar radiation in a mid-elevation shaded mountainous area. Permafrost and Periglacial Processes, **18**: 137–149. doi:10.1002/ppp.576.

Juliussen, H., and Humlum, O. 2007. Towards a TTOP Ground Temperature Model for Mountainous Terrain in Central-Eastern Norway. *Permafrost and Periglacial Processes*. **18**: 161-184.

King, L. 1992. Prospecting and mapping of mountain permafrost and associated phenomenon. *Permafrost and Periglacial Processes*, **3**: 73-81.

Kremer, M., Lewkowicz, A.G., Bonnaventure, P.P. and Sawada, M.C. 2011Utility of classification and regression tree analyses and vegetation in mountain permafrost models, Yukon Territory, Canada. *Permafrost and Periglacial Processes.* DOI 10.1002/ppp.719

Lewkowicz, A.G. 2008. Evaluation of miniature temperature-loggers to monitor snowpack evolution at mountain permafrost sites, northwestern Canada. *Permafrost and Periglacial Processes.* **19**: 323-331.

Lewkowicz, A.G. and Bonnaventure, P.P. 2008. Interchangeability of Mountain Permafrost Probability Models, Northwest Canada, *Permafrost and Periglacial Processes,* **19**: 49-62.

Lewkowicz, A.G. and Bonnaventure, P.P. 2011. Equivalent Elevation: a New Method to Incorporate Variable Lapse Rates Into Mountain Permafrost Modelling. *Permafrost and Periglacial Processes.* DOI 10.1002/ppp.720

Lewkowicz, A.G. and Ednie, M. 2004. Probability mapping of mountain permafrost using the BTS method, Wolf Creek, Yukon Territory, Canada. *Permafrost Periglacial. Processes.* **15** 67-80.

Lugon, R., and Delaloye, R. 2001. Modeling alpine permafrost distribution , Val de Rechy, Valais Alps (Switzerland) *Norsk geogr. Tidsskr.* **55**: 224-229.

Meyer, P., Itten, K.I., Kellenberger, T., Sandmeier, S., and Sandmeier, R. 1993. Radiometric
corrections of topographically induced effects on Landsat TM data in an alpine environment. *Journal of Photogrammetry and Remote Sensing* **48**: 17-28.

Natural Resources Canada. 2010. Forest ecosystems of Canada http://ecosys.cfl.scf.rncan.gc.ca/classification/classif08-eng.asp [Accessed June, 2010].

Ødegard, R.S., Isaksen, K., Mastervik, M., Billdal, L., Engler, M. and Sollid, J.L. 1996. Comparison of BTS and Landsat TM data from Jotunheimen, southern Norway. *Norsk geogr. Tidsskr.* **53**: 226 – 233.

Rouse, J.W. Jr., Hass, R.W., Schell, J.A., Deering, D.W., and Harlan, J.C. 1974. Monitoring the vernal advancement and retrogradation (Greenwave effect) of natural vegetation. NASA/GSFCT Type III Final Report, Greenbolt, MD, USA.

Shur, Y., and Jorgenson, M.T. 2007. Patterns of Permafrost Formation and Degradation in Relation to Climate and Ecosystems. *Permafrost and Periglacial Processes* **18**: 7-19

Tanarro, L.M., Hoelzle, M., Garcia, A., Ramos, M., Gruber, S., Gomez, A., Piqueer, M., and Palacios, D. 2001. Permafrost distribution modelling in the mountains of the Mediterranean: Corral del Veleta, Sierra Nevada, Spain. Norsk Geografisk Tidsskrift **55**: 253– 260.

Teillet, P.M., Guindon, B., and Goodenough, D.G. 1982. On the slope-aspect correction of
multispectral scanner data. *Canadian Journal of Remote Sensing* **8**: 84-106.

Wahl, H.E., Fraser, D.B., Harvey, R.C., Maxwell, J.B. 1987. *Climate of Yukon.* Canadian Government Publishing Centre.

Ward, B.C., Bond, J.D., and Gosse, J.C. 2007. Evidence for a 55–50 ka (early Wisconsin) glaciation of the Cordilleran ice sheet, Yukon Territory, Canada. *Quaternary Research.* **68**: 141-150.

Williams, D.J., and Burn, C.R. 1996. Surficial characteristics associated with the occurrence of permafrost near Mayo, Central Yukon Territory, Canada. *Permafrost and Periglacial Processes.* **7**: pg. 193-206.

Tables

Table 5.1: Study area physiography and climate.

Study Area	Area Modeled (km^2)	Coordinates of Centre	Elevation Range (m asl)	Permafrost Zone[a]	Climate Zone[b]	Closest Meteorological Station and climate normals (1971-2000)[c]			MAAT 08/2007 – 08/2009 (°C)[d]	
Johnson's Crossing	955	60° 34' N, 133° 9' W	670-1860	Sporadic discontinuous	Pelly-Cassiar Mountains	Teslin Airport (705 m asl)			Low (896 m asl)	High (1512 m asl)
						MAAT (°C)	Precipitation (mm)	Monthly Temperature Range (°C)[e]		
						-1.2	343	32.0	-2.2	-3.9
Sa Dena Hes	1050	60° 25'N, 128° 58' W	630-1565	Sporadic discontinuous	Liard Basin	Watson Lake Airport (705 m asl)			Low (821 m asl)	High (1506 m asl)
						MAAT (°C)	Precipitation (mm)	Monthly Temperature Range (°C)[e]		
						-2.9	404	39.3	-2.9	-3.9
Faro	1415	62° 13'N, 133° 8' W	600-2045	Sporadic discontinuous / Extensive discontinuous	Central Yukon Basin	Faro Lake Airport (717 m asl)			Low (644 m asl)	High 1538 m asl)
						MAAT (°C)	Precipitation (mm)	Monthly Temperature Range (°C)[e]		
						-2.2	316	36.5	-3.4	-3.8

Keno	820	63° 55'N, 135° 20' W	610-2050	Extensive discontinuous	Ogilvie-Mackenzie Mountains	Mayo Airport (504 m asl)			Low (777 m asl)	High (1815 m asl)
						MAAT (°C)	Precipitation (mm)	Monthly Temperature Range (°C)[e]		
						-3.1	313	41.7	-3.7	-6.8
Dawson	1130	64° 7'N, 139° 41' W	270-1255	Extensive discontinuous	Central Yukon Basin	Dawson Airport (370 m asl)			Low (331 m asl)	High (1223 m asl)
						MAAT (°C)	Precipitation (mm)	Monthly Temperature Range (°C)[e]		
						-4.4	324	42.3	-5.2	-4.4

[a] From Heginbottom et al. (1995)

[b] From Wahl et al. (1987)

[c] Environment Canada (2010)

[d] Results from lowest and highest monitoring site in each study area.

[e] July mean temperature minus January mean temperature.

Table 5.2: Remotely sensed images used for each study area to develop NDVI.

Study Area	Sensor	Path	Row	Acquisition Date
Dawson	Landsat 5	064	015	July 3, 2008
Faro*	Landsat 7	058	017	August 15, 2001
	Landsat 7	059	016	August 1, 1999
Keno	Landsat 5	061	015	August 31, 2008
Johnson's Crossing	Landsat 7	057	018	August 3, 1999
Sa Dena Hes	Landsat 5	055	018	August 5, 2008

**Two images selected because area is located at the edge of both images*

Table 5.3: BTS multiple linear regression statistics (only statistically significant variables are shown).

Area	Statistic	Equivalent elevation	PISR	Slope	NDVI	Intercept	*n*	r^2
JC	Coefficient	0.0056	NA	-0.14	NA	-9.3	79	0.29
	P-value	0.04	NA	<0.001	NA	0.01		
	Standard Error	0.0021	NA	0.03	NA	3.5		
JC_WC*	Coefficient	-0.0082	0.0055	NA	NA	NA	317	0.31
	P-value	<0.001	<0.001	NA	NA	NA		
	Standard Error	0.0007	0.0005	NA	NA	NA		
SDH	Coefficient	NA	NA	-0.06	2.05	-2.6	92	0.21
	P-value	NA	NA	<0.001	0.02	<0.001		
	Standard Error	NA	NA	0.01	0.92	0.6		
F	Coefficient	0.015	NA	-0.09	NA	-20.6	52	0.46
	P-value	<0.001	NA	<0.001	NA	<0.001		
	Standard Error	0.003	NA	0.02	NA	5.0		
K	Coefficient	-0.013	0.02	NA	NA	-10.3	71	0.48
	P-value	<0.001	<0.001	NA	NA	0.03		
	Standard Error	0.003	0.002	NA	NA	4.8		
D	Coefficient	-0.061	NA	NA	NA	67.2	72	0.35
	P-value	<0.001	NA	NA	NA	<0.001		
	Standard Error	0.012	NA	NA	NA	11.7		

*Statistics taken for the Wolf Creek Basin and used to model Johnson's Crossing area (Lewkowicz and Bonnaventure 2008; Bonnaventure and Lewkowicz 2010).

Table 5.4: Permafrost probability logistic regression statistics.

Area	Statistics	Modeled BTS	Constant
JC	Coefficient[a]	-0.48	-2.7
	P value	<0.01	<0.01
	Standard error	0.4	1.2
JC_WC*	Coefficient[a]	-2.6	-9.4
	P value	<0.01	<0.01
	Standard error	0.9	2.8
SDH	Coefficient[a]	-0.78	-2.1
	P value	<0.01	<0.01
	Standard error	0.47	0.98
F	Coefficient[a]	0.1	0.7
	P value	<0.01	<0.01
	Standard error	0.05	0.4
K	Coefficient[a]	-0.73	-2.31
	P value	<0.01	<0.01
	Standard error	0.21	0.97
D	Coefficient[a]	-0.26	-1.1
	P value	<0.01	<0.01
	Standard error	0.12	0.66

[a]Coefficient used to predict Y in the equation P = 1 / (1 + Exp (-Y)) where P is the probability of permafrost ranging from 0 – 1 and Y is a constant developed from the independent variable in the regression (modeled BTS).* Relationship computed using BTS equations for Wolf Creek (Bonnaventure and Lewkowicz 2010) with ground truthing collected at Johnson's Crossing.

Figures

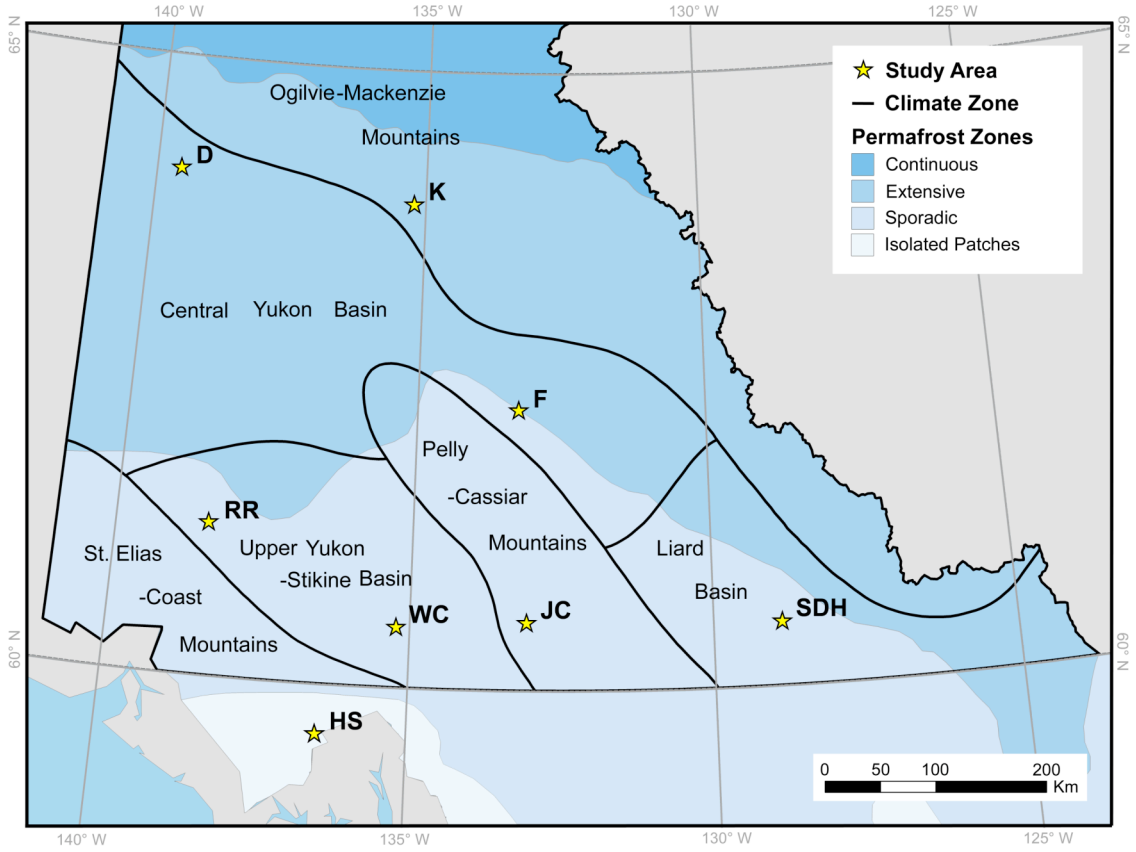

Figure 5.1: Map of the study region showing the locations of the Johnson's Crossing (JC), Sa Dena Hes (SDH), Faro (F), Keno (K) and Dawson (D) study areas in relation to permafrost zones (Heginbottom et al. 1995) and climatic regions (Wahl et al. 1987). Permafrost probability modelling was previously undertaken for the Ruby Range (RR), Haines Summit (HS) and Wolf Creek (WC) areas (Bonnaventure and Lewkowicz 2008; Lewkowicz and Ednie 2004).

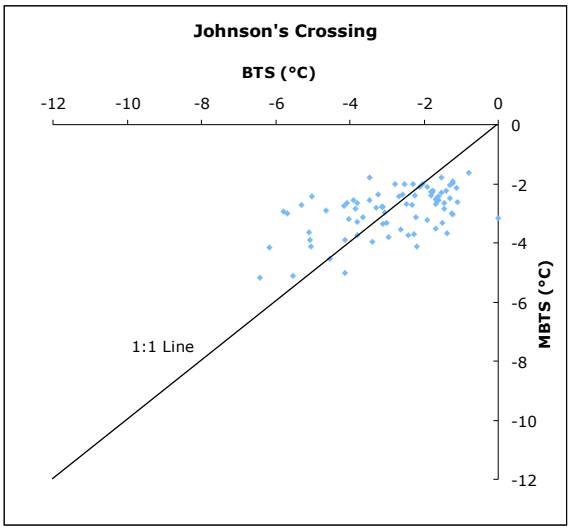
Johnson's Crossing
BTS (°C)
-12 -10 -8 -6 -4 -2 0
0 -2 -4 -6 -8 -10 -12
MBTS (°C)
1:1 Line

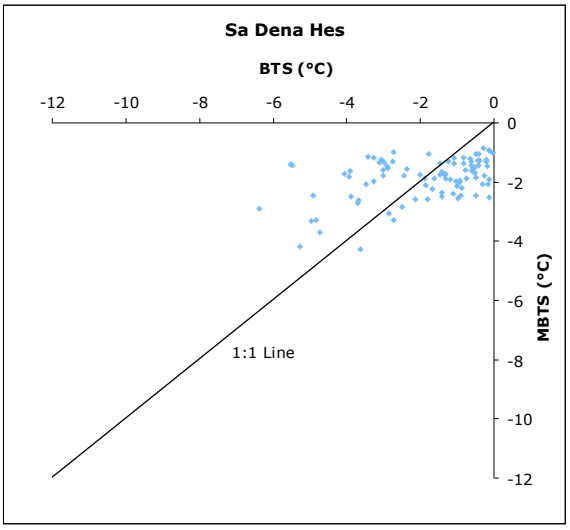
Sa Dena Hes
BTS (°C)
-12 -10 -8 -6 -4 -2 0
0 -2 -4 -6 -8 -10 -12
MBTS (°C)
1:1 Line

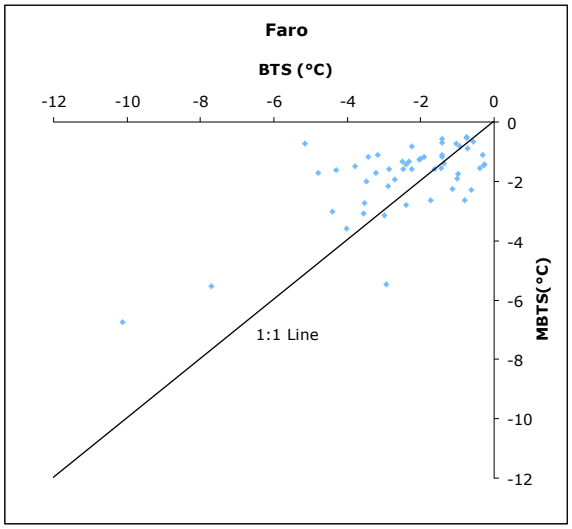
Faro
BTS (°C)
-12 -10 -8 -6 -4 -2 0
0 -2 -4 -6 -8 -10 -12
MBTS(°C)
1:1 Line

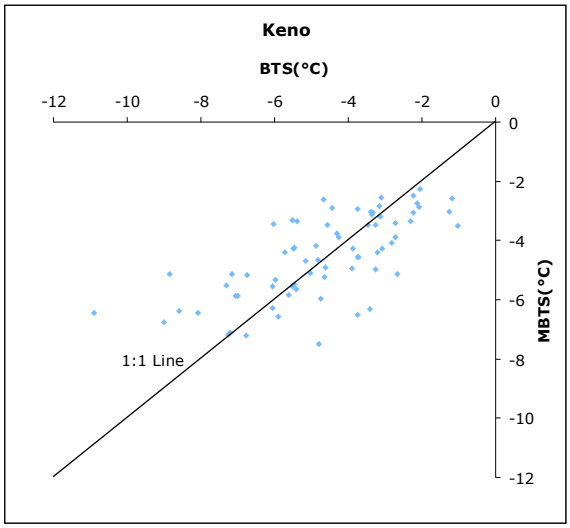
Keno
BTS(°C)
-12 -10 -8 -6 -4 -2 0
0 -2 -4 -6 -8 -10 -12
MBTS(°C)
1:1 Line

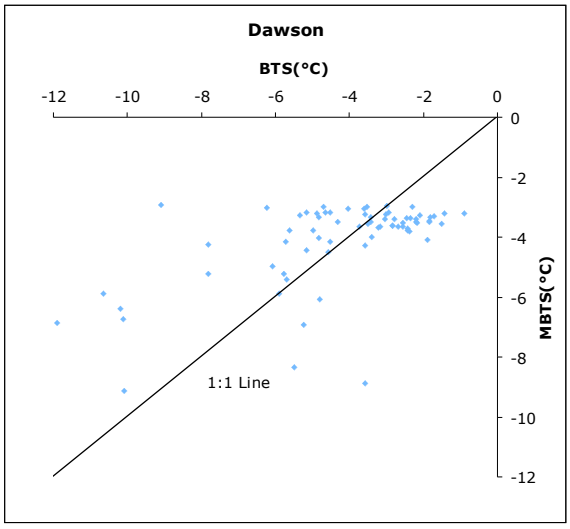
Dawson
BTS(°C)
-12 -10 -8 -6 -4 -2 0
0 -2 -4 -6 -8 -10 -12
MBTS(°C)
1:1 Line

Figure 5.2: Scatter plots of measured BTS versus modeled BTS (MBTS) for all five study areas.

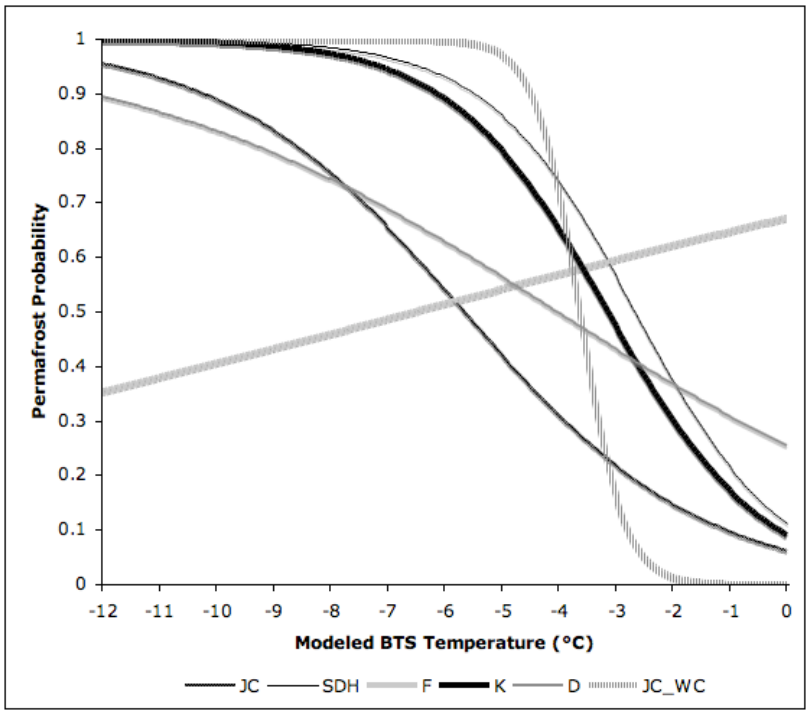

Figure 5.3: Permafrost probability curves for all five study areas.

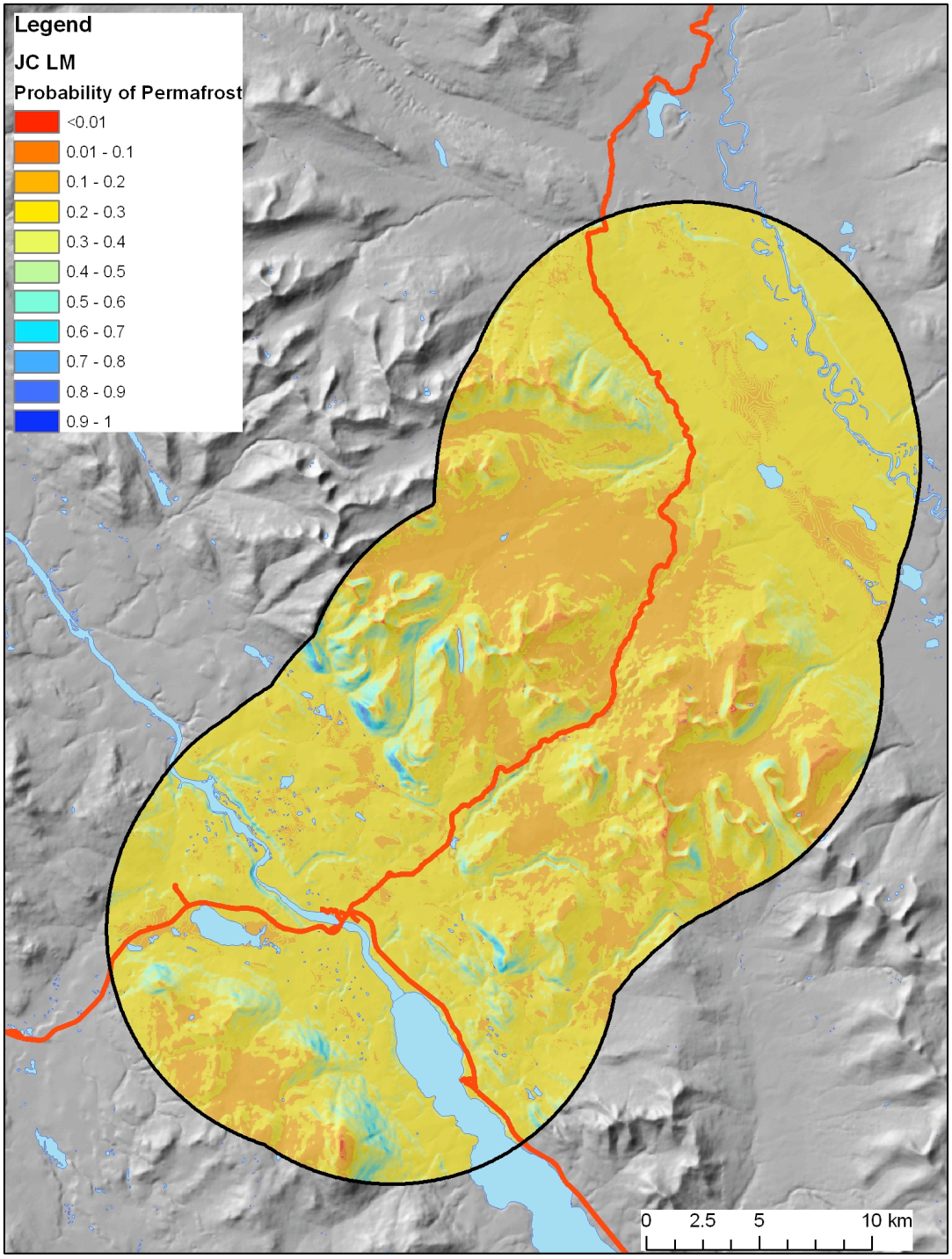

Figure 5.4: Map of permafrost probability for Johnson's Crossing based on BTS relationships with equivalent elevation and slope, and logistic regression based on ground truthing points. Roads are indicated in red.

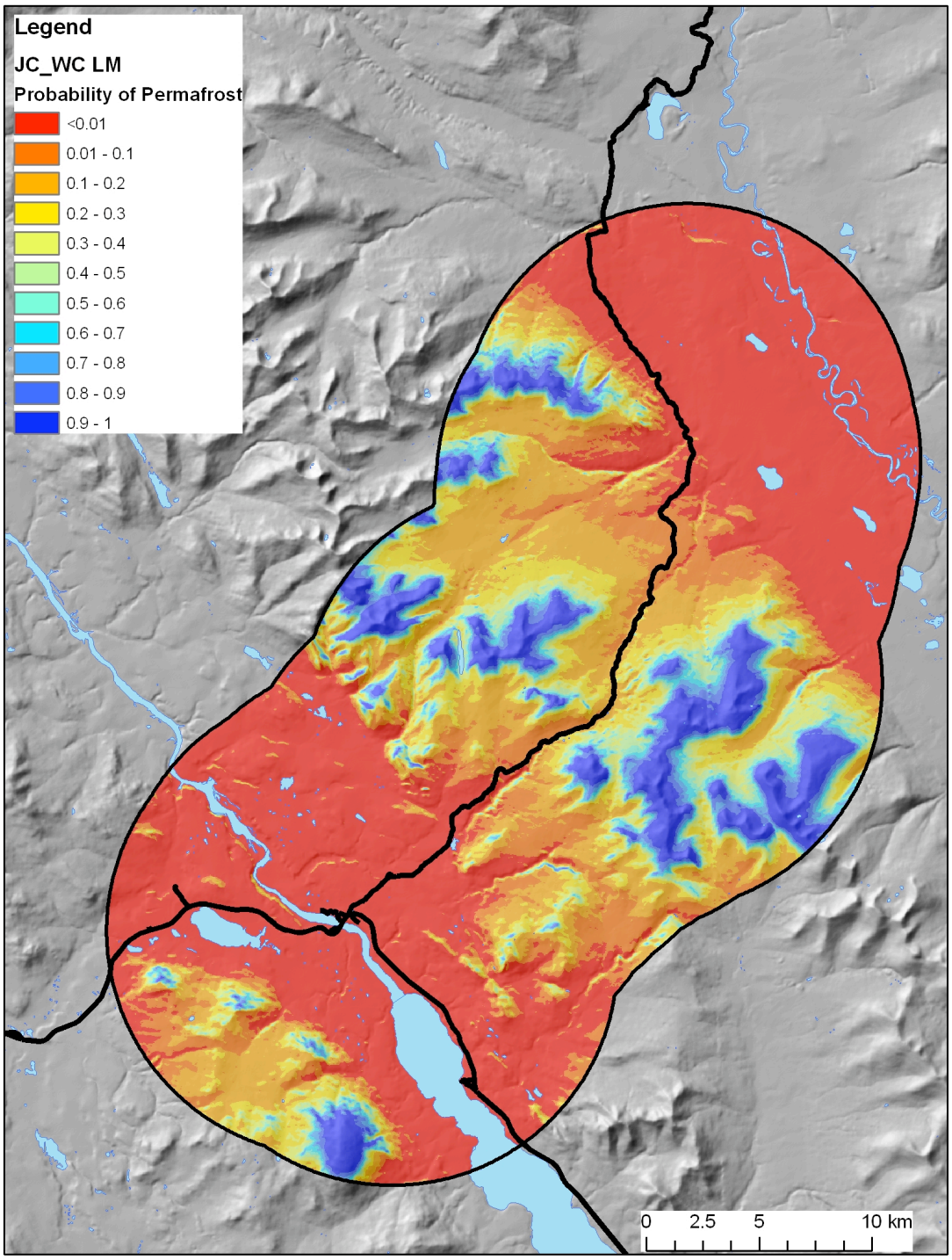

Figure 5.5: Permafrost probability map for Johnson's Crossing based on BTS relationships with equivalent elevation and PISR from BTS measurements in Wolf Creek, and logistic regression based on ground truthing points collected in Johnson's Crossing. Roads are indicated in black.

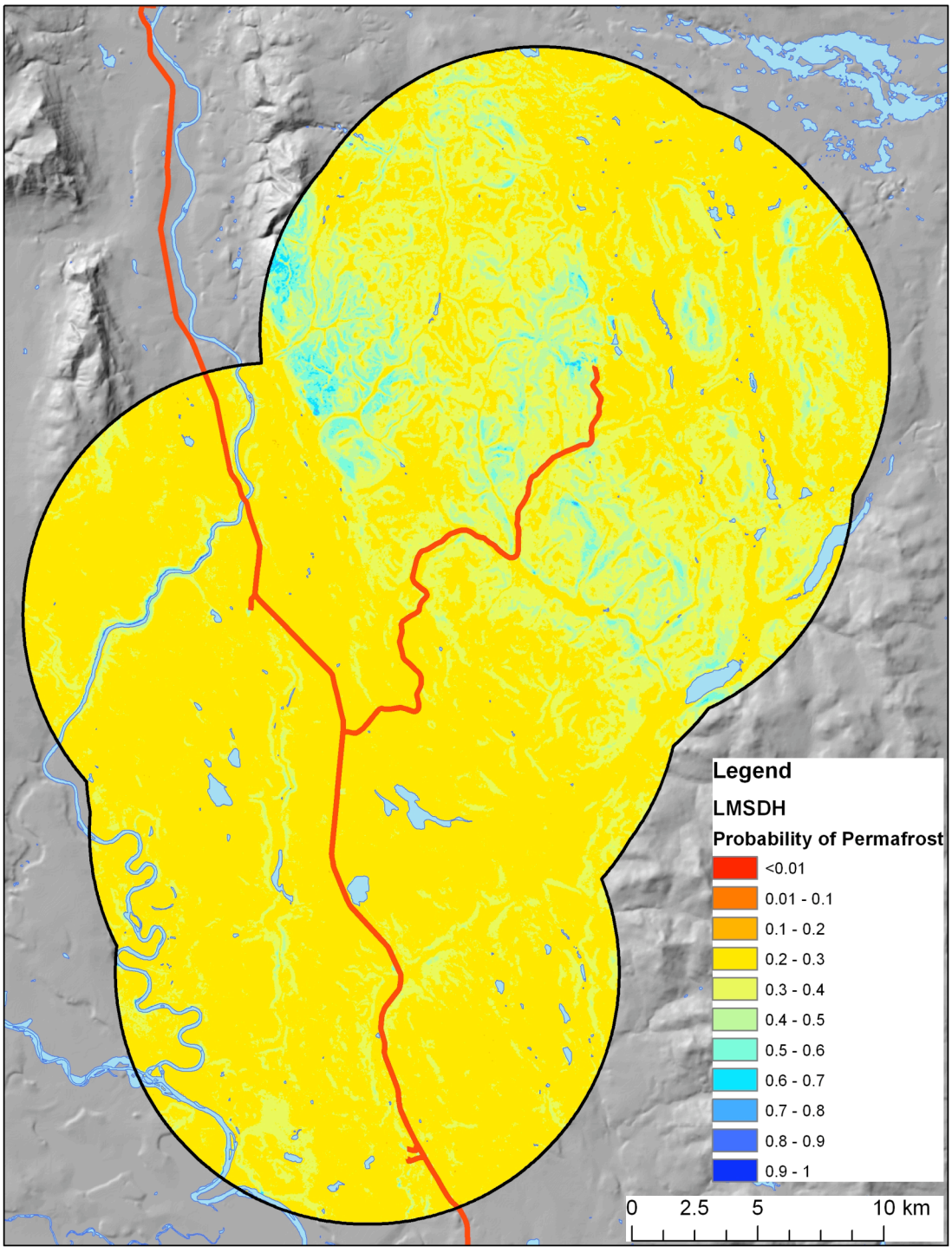

Figure 5.6: Permafrost probability map for Sa Dena Hes based on BTS relationships with NDVI and slope, and logistic regression based on ground truthing points. Roads are indicated in red.

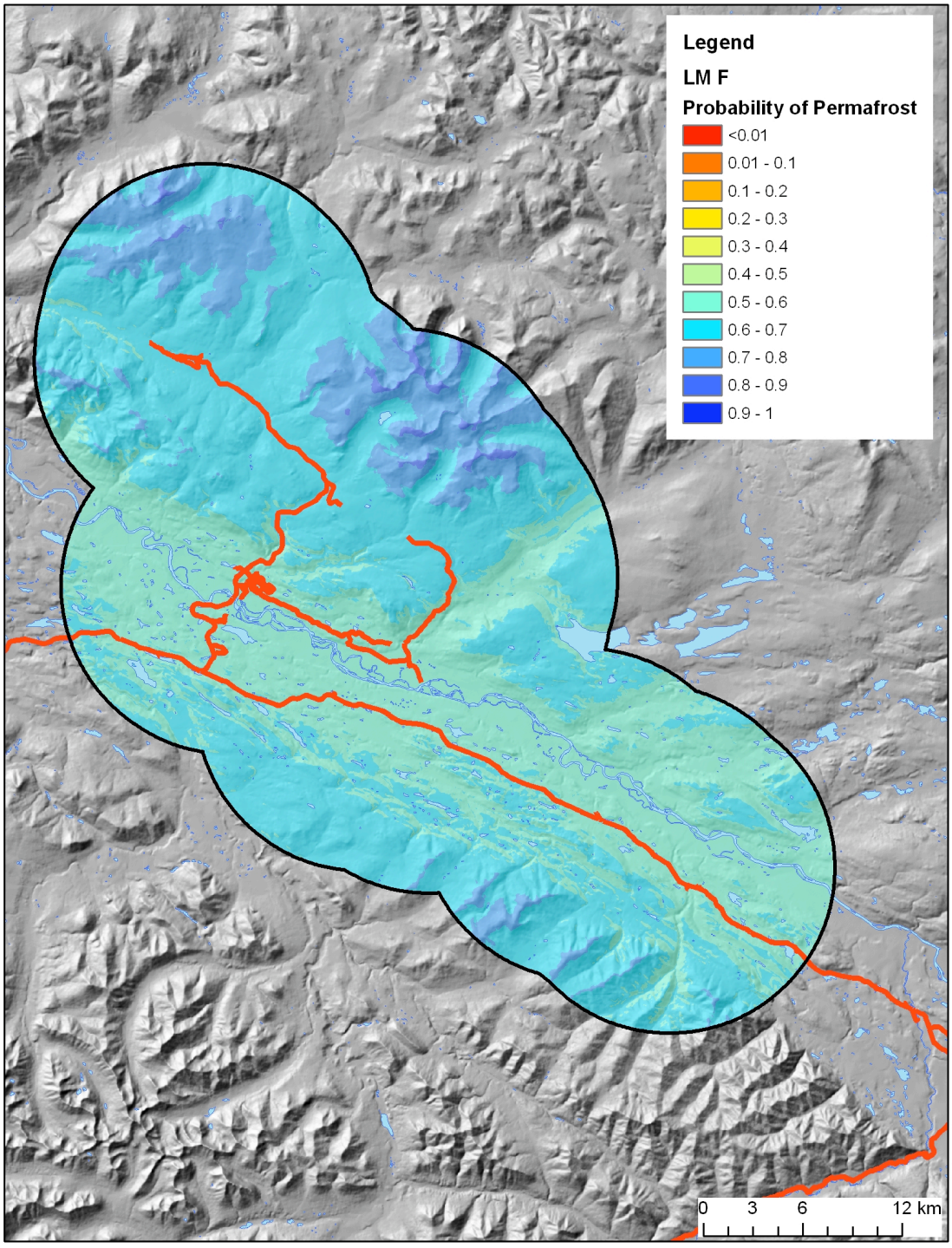

Figure 5.7: Permafrost probability map for Faro based on BTS relationships with equivalent elevation and slope, and logistic regression based on ground truthing points. Roads are indicated in red.

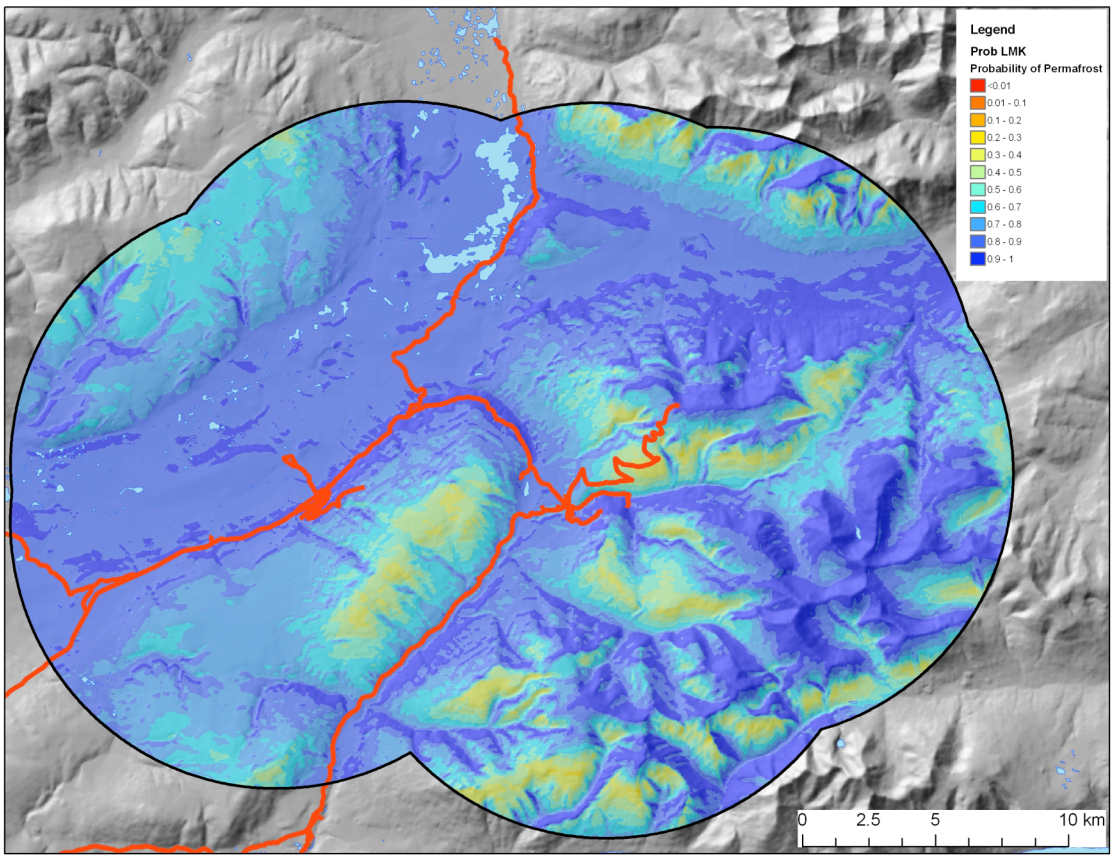

Figure 5.8: Permafrost probability map for Keno based on BTS relationships with equivalent elevation and PISR, and logistic regression based on ground truthing points. Roads are indicated in red.

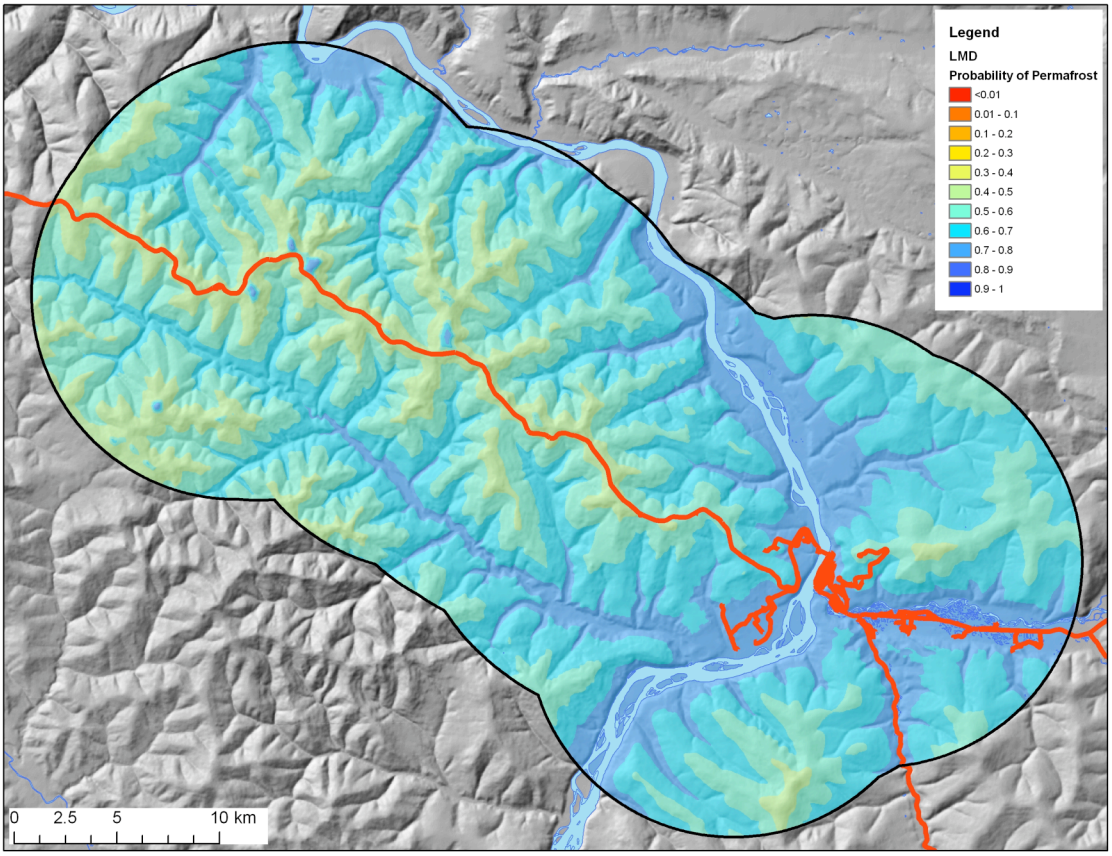

Figure 5.9: Permafrost probability map for Dawson based on BTS relationships with equivalent elevation and logistic regression based on ground truthing points. Roads are indicated in red.

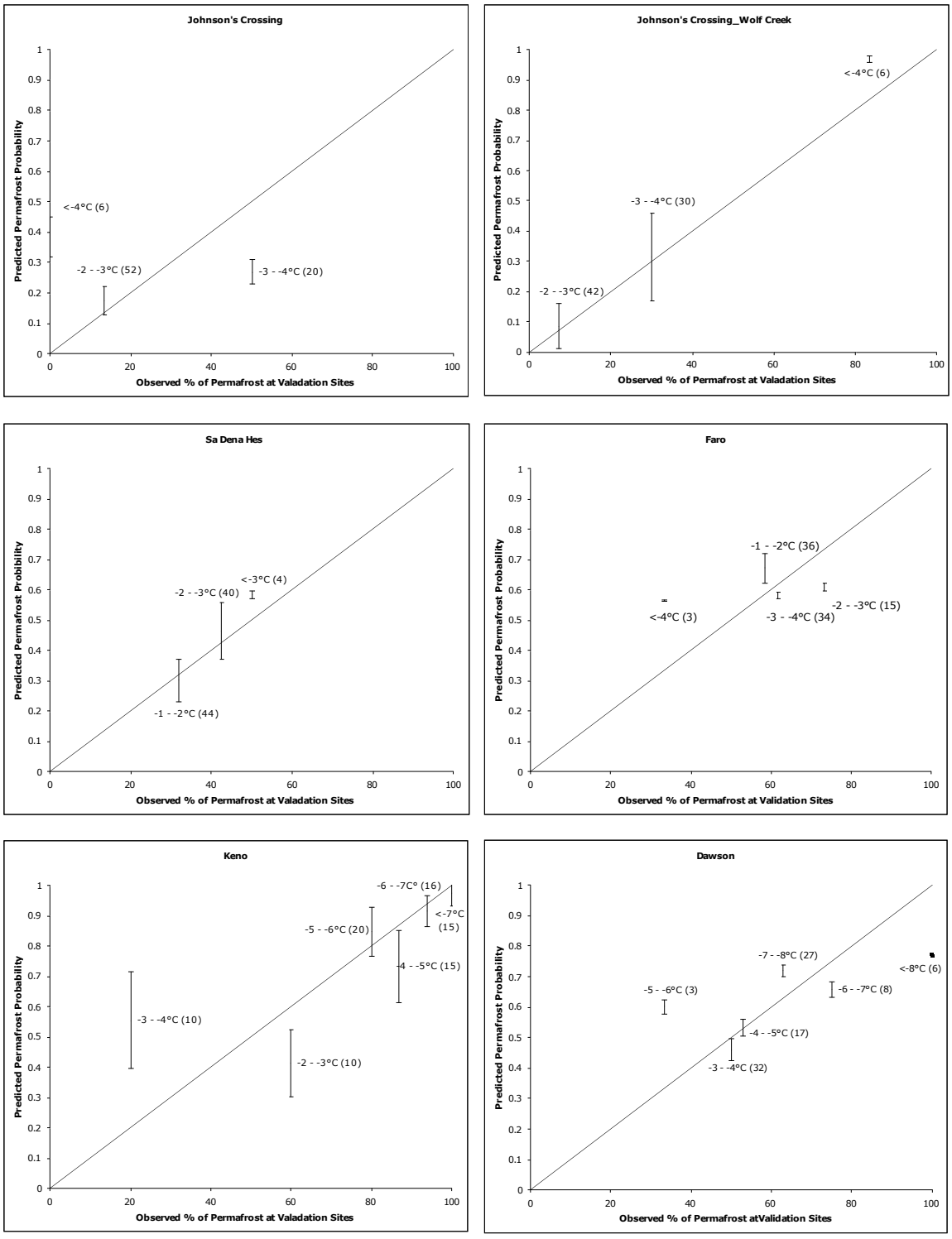

Figure 5.10: Observed permafrost percentages at pit and ground temperature monitoring sites grouped according to ranges of modeled BTS values compared to predicted permafrost probability percentages for Johnson's Crossing, Johnson's Crossing using Wolf Creek BTS, Sa Dena Hes, Faro, Keno and Dawson. The bars represent the predicted probabilities for the range of temperatures centered on the temperature shown. The number of pits for each range is shown in parentheses.

Chapter Six

A Regional Permafrost Probability model for the Southern Yukon and Northern British Columbia, Canada

Abstract

Permafrost maps are needed for infrastructure planning, climatic change adaptations strategies and northern development but often lack sufficient detail to be useful. The high-resolution probability model presented in this paper (Regional Model) uses a combination of seven empirical-statistical models. The models are blended using a distance decay powers approach to map permafrost probability for the southern Yukon and northern British Columbia (between 59 – 65°N). The results are similar to those seen in previous permafrost maps of the area, but include certain notable differences. The main variable used in these models is equivalent elevation, which incorporates the effects of gentle or inverted surface lapse rates (common in the Yukon) into permafrost probability. The regional model predicts an overall permafrost probability of 52% for the area. In the regional model only the southwestern area shows similar permafrost distributions to that of the Swiss Alps where the BTS technique was developed. The rest of the region shows permafrost distribution patters that are non-linear, resembling more continental areas such as Mongolia. The most significant uncertainties associated with the regional model are from the use of the trend surfaces used to calculate the equivalent elevation variable. Inaccuracies in this calculation can lead to the over- or under-prediction of permafrost and are most significant in areas of high relief.

Key Words: Mountain Permafrost Modelling, BTS, Equivalent Elevation, Surface Lapse Rate, Yukon, British Columbia.

Introduction

High resolution empirical-statistical permafrost modelling has been used in mountain areas in many locations, including central Europe (e.g. Gruber & Hoelzle, 2001; Lugon & Delaloye, 2001; Gardaz, 1997; Hoelzle et al., 1999; Imhof et al., 2000; Hoelzle, 1992; King, 1992; Dobinski, 1998), Scandinavia (e.g. Isaksen et al., 2002; Jeckel, 1988; Ødegard et al., 1996), Japan (e.g. Ishikawa & Hirakawa, 2000), and, most recently, in North America (Lewkowicz & Ednie, 2004; Bonnaventure and Lewkowicz, 2008; Lewkowicz and Bonnaventure, 2008; Bonnaventure and Lewkowicz, 2010). These types of models have been used to generate maps with unprecedented fine resolution, but they have almost exclusively been used to make predictions for relatively small areas within a single mountain range.

High-resolution permafrost distribution maps for large areas are needed in order to establish current conditions before the onset of increasing climatic warming. Sub-arctic areas within the Yukon and northern British Columbia located in the discontinuous permafrost zone could be strongly affected by climatic change (AICA, 2004; IPCC, 2007). Increased air temperatures or greater winter precipitation can disturb discontinuous permafrost which is generally relatively warm (close to 0°C) and potentially thin (Lewkowicz et al., *In Press*). This in turn means that, at any given time, sensitive areas that could thaw with only slight increases in temperature exist within the discontinuous zone. This thawing could have potentially problematic consequences with respect to infrastructure, geohazards, northern development as well as potential greenhouse gas release, including methane (Brouchkov and Fukuda, 2002; Kneisel et al., 2007).

In the Yukon Territory empirical-statistical permafrost probability models have been generated using the Basal Temperature of Snow (BTS) method from differing variables for several areas over a range of climatic zones (Lewkowicz and Ednie, 2004; Lewkowicz and Bonnaventure, 2008; Bonnaventure and Lewkowicz, *Submitted*). The objective of this paper is to model permafrost probability at high-resolution for the entire southern half of the Yukon and northernmost British Columbia between 59°N and 65°N. This model was created using BTS and ground truthing techniques described in previous publications (e.g. Lewkowicz and Ednie, 2004; Bonnaventure and Lewkowicz, 2008) and linked together for multiple areas using a combination of all models in a blended distance decay powers model (Regional Model).

Permafrost Modelling Techniques

A review of empirical-statistical mountain permafrost modelling techniques including the BTS method can be found in previous publications (Lewkowicz and Ednie, 2004; Bonnaventure and Lewkowicz, 2008; Bonnaventure and Lewkowicz, *Submitted*). In addition, an extensive review of all permafrost modelling methods for mountain and lowland areas including process-orientated and finite element models is given in Riseborough et al. (2008).

Study Area

The study area for this project covers 59°N to 65°N and 141°W to as far as 123° 5'W, representing an area of about 490 000 km^2 (Figure 6.1). This area is considered part of the Cordilleran orogen geological grouping, comprising large mountain belts of deformed and metamorphosed sedimentary and volcanic rocks, mainly of the

Phanerozoic and Proterozoic ages (DEMR 1974; Wahl et al. 1987; Eyles and Miall 2007). During the Wisconsinan glacial maximum, the study area in the southern to central portions were covered by the thick ice masses of the Cordilleran ice sheet whereas the northwestern portion around the Dawson area was mostly unglaciated (Duk-Rodkin, 1996).

The elevation range is considerable, from a low point of 250 m asl in the Yukon River Valley to greater than 3000 m asl in the St. Elias Mountains. The area includes all permafrost zones (except subsea), from isolated patches in the southwest to continuous in the most northerly areas. Climatic gradients across the region are relatively gentle except in the southwest where there is a strong precipitation gradient from 1415 mm at Pleasant Camp B.C. to 270 mm at Whitehorse Y.T. over a distance of 150 km. The entire area is in the Boreal Cordillera ecozone, which is characterized by mountain ranges with numerous lofty peaks and extensive plateaus with long, cold winters and short, warm summers, varying with altitude and mountainside orientation (Natural Resources Canada, 2010). Continentality increases northward and eastward. Annual precipitation (outside the St. Elias) ranges between about 300 and 400 mm with the highest amounts in the Liard Basin climatic region (Wahl et al., 1987). The entire study region experiences wintertime inversions in surface lapse rates (SLR) through the forested zone (Lewkowicz and Bonnaventure, 2011). The results of inverted SLRs on an annual basis are increased permafrost probabilities in valley bottoms in areas of high continentality while in more maritime environments, SLRs are gentle, but normal, so that permafrost is less common at low elevations.

Vegetation in the region comprises boreal forest with coniferous trees and some boreal broadleaf trees in lowland areas, while sub-alpine forest, shrubs, alpine tundra, barren patches, and exposed rock occur progressively at higher elevations (Wahl et al. 1987). The northernmost portion of the study area is very close to an ecosystem boundary where vegetation begins to transition to full-scale tundra with alpine sedges, grasses and shrubs dominating (Wahl et al. 1987).

Climatic boundaries in individual study areas are shown in Figure 6.1 and are described more fully in previous publications (Lewkowicz and Ednie, 2004; Lewkowicz and Bonnaventure, 2008; Bonnaventure and Lewkowicz, *Submitted*).

Methods

The methodology to compile the regional model involved map algebra using ArcGIS 9.3 with multiple steps completed in Raster Calculator. This section explains each of these steps and addresses important data issues in model development, including the derivation of variables used in the modelling techniques.

Digital Elevation Model

The Yukon portion of the DEM for the regional model analysis was provided by the Yukon Geological Survey (Geomatics Yukon, 2006). The DEM has a resolution of 30 x 30 m and is larger than the study area itself, including sections for the borders of British Columbia to the south, the Northwest Territories to the east (provided by Geobase, 2010) and Alaska to the west (provided by the United States Geological Survey, 2010). These outer DEM sections were included to eliminate errors associated with edge effects during analysis and were incorporated into the main DEM using the Mosaic tool in ArcGIS.

Solar Radiation Modelling

The creation of a Potential Incoming Solar Radiation (PISR) model for the entire study area that took into account specific latitude represented a considerable challenge. Due to software restrictions in the ArcGIS Area Solar Radiation tool, relatively small sections of the PISR model had to be run individually. The total area was thus divided into 34 sections of the DEM that were 0.5° in latitude, and varied in longitude from about 0.5° to about 2°. These sections were also overlapped by 0.125° in both latitude and longitude to reduce the error associated with edge effects. The specific climatic inputs needed to run the Area Solar Radiation tool were derived from both air and ground temperatures, light logger data from our logger network (Lewkowicz and Bonnaventure, 2011) and cloud cover data from nearby Environment Canada Stations. The amount of cloud cover (diffusivity) was set to one of three values based on the results of the analysis (65%, 70% or 75%) for each of the 34 DEM sections. The snow-free period was established by examining logger data from all of the study areas to determine the average date when snow covered the surface (Fall) and when ground temperature rose above 0°C (Spring). The snow-free period varies within the region and is partially controlled by elevation. For the purpose of this model, however, it was set from May 15 to Sept 30. Modeled PISR is in MJ/m^2 with the highest values being observed on south-facing, high elevation slopes, and the lowest values on steep, low elevation, north-facing slopes. The specifications of the solar modelling process conform to those used in Bonnaventure and Lewkowicz (2008, 2010). Once all 34 PISR models had been created, they were assembled into one grid using the mosaic tool in ArcGIS.

Equivalent Elevation

Empirical-statistical spatial mountain permafrost models were initially created for the European Alps where permafrost distribution is highly dependent on elevation (Gruber & Hoelzle, 2001; Lugon & Delaloye, 2001). In the Yukon, the relationship between permafrost distribution and elevation is more complex and valley bottoms are also at relatively high elevations (300 – 700 m asl) with permafrost perhaps being present. The concept of equivalent elevation (Lewkowicz and Bonnaventure, 2011) was developed to deal with these complexities. True elevations in a DEM are manipulated to reflect mean annual air temperatures based on local SLRs. The numerical elevations of grid cells below treeline are adjusted to take into account weakened or reversed SLRs in the forest compared to the strong normal negative SLRs above treeline. Thus grid cells that are well below treeline may be increased significantly in elevation, areas close to treeline are changed very little and areas above treeline remain unchanged. Equivalent elevation is evaluated from:

$$Z_x^{'} = Z_t - (Z_t - Z_x) \times \frac{L_1}{L_2} \qquad (6.1)$$

Where $Z^{'}_x$ is equivalent elevation (m asl), Z_t is the elevation of treeline (m asl), Z_x is actual grid cell elevation (m asl), L_1 is the measured or predicted SLR below treeline (°C km^{-1}) and L_2 is the SLR above treeline (assumed to be -6.5°C km^{-1}).

The derivation of equivalent elevation for the study area involved trend surfaces to represent the treeline and SLR inputs (Lewkowicz and Bonnaventure, 2011). The polynomial order of the trend surfaces was selected based on goodness of fit relative to the source data, as well as visual inspection, especially near the edges of the study area.

To predict treeline, a fourth order polynomial trend surface was created in ArcGIS using a series of 43 points where treeline had been inspected. Treeline analysis was completed by examining the average value of treeline from the National Topographic System (NTS) maps for each of the map tiles in the study area. These values were checked by extensive visual inspection of Google Earth Images. A third order polynomial was used for SLR. SLRs in the Yukon are highly related to the annual amplitude of monthly air temperatures (i.e. July mean minus January mean). Larger amplitudes produce SLRs that are inverted or close to 0°C km^{-1}, whereas smaller amplitude sites have normal negative SLRs (Lewkowicz and Bonnaventure, 2011). Using these correlations, measured SLRs at 7 sites and calculated values for a further 10 locations, were used to create this trend surface. Equation 6.1 was used with the trend surfaces and the DEM to calculate equivalent elevation for the entire study area (Lewkowicz and Bonnaventure 2011).

Regional Permafrost Probability Model

The regional permafrost probability model was developed from the seven individual empirical statistical permafrost probability models, themselves based on the BTS modelling approach. The regional model uses a distance decay function to weight the contribution of each of the individual models and then assigns a permafrost probability value based on a sum of scores (Figure 6.2).

The decay grid for each model was calculated using the Euclidian Distance tool in ArcGIS. The grid originated from the outline of each set of study area boundaries, which were created by generating a 10 km buffer around all of the field sample points and dissolving the buffers together. It was decided based on the spacing of the sample areas

that each model would have 100% of its influence within its own study area and then decay at a rate defined by:

$$Y = e^{-0.01x} \qquad (6.2)$$

where x is measured in kilometers. This produced an individual decay grid in which a model's influence was diminished by about half at a distance of approximately 100 km.

The distance decay grids for each area were summed to obtain a sum of powers grid. This was used as a denominator for each individual grid in order to obtain a percent power grid for each model. The prediction for the region as a whole for each permafrost probability model was multiplied by its corresponding percent power. These seven grids were added together to produce the final values for the regional model which was fitted by a series of masks that enabled blending outside the specific study areas while maintaining 100% of the individual specific model inside.

Results

Regional Model Predictions

The regional model produced a probability of permafrost surface with an average value of 52% for the entire study area (Figure 6.3). This prediction is for permafrost under current conditions, which are assumed to be in equilibrium. Figure 6.3 shows several geographic gradients in permafrost probabilities, which are highlighted in Table 6.1. Permafrost probability follows these patterns largely because of differences in SLRs, and this results in the interfingering of latitudinal and mountain permafrost. Thus elevation is not correlated with permafrost in the same way as it is in the Swiss Alps or portions of Scandinavia. Only the extreme southwest of the study region, where temperatures are relatively high, the snowpack is several meters thick, and treeline is

below the lower limit of permafrost exhibits a permafrost distribution similar in nature to that of the Alps.

Regional Model Comparisons

Validation of the regional model would require an independent and spatially distributed set of data for permafrost presence and absence. Such a data-set does not exist. However, it is possible to compare the regional model predictions with the more than 750 observations of permafrost presence or absence made in the individual study areas. Fully independent comparisons can be made with the distribution of rock glaciers in the region, with results from a number of ground temperature monitoring boreholes, and with the predictions from the Sa Dena Hes area.

The comparison of the presence or absence of permafrost at individual sites grouped by predicted probability from the regional model, indicates a good fit (Figure 6.4). However, all but the Sa Dena Hes results (approximately 90 points) were used to generate the model so it is not surprising that the broad patterns are represented. The comparison suggests that the regional model may slightly over-predict permafrost probabilities in areas that are classified as extensive or continuous permafrost, while slightly under-predicting probabilities in areas of sporadic discontinuous permafrost. Overall, the predicted trends in probability reflect the observed patterns within ± 10%.

A database of rock glaciers recently created for the Yukon (Page, 2009) contains the locations of all known features within the study area as well as a selection that were classified based on activity. Active and inactive rock glaciers are point indicators of permafrost, while relic rock glaciers should be indicative of permafrost absence (Haeberli et al., 2006; Janke, 2004, 2005). Almost 90% of the rock glacier locations in the complete

database (n = 1675) occur at sites where the predicted probability of permafrost is 0.8 or greater (Figure 6.5A). Only 1% of the rock glaciers are at sites with permafrost probabilities < 0.5, while 28% of the region's Yukon area falls into this category. In the sub-sample of classified rock glaciers (n = 225), more than 85% of the active features are in locations with probabilities greater than 0.8, while only ~ 70% of the inactive features are in this category (Figure 6.5B). Convective heat exchange in rock glaciers can help create colder ground conditions than on adjacent slopes (Haeberli et al., 2006; Guodong et al., 2007) and those have not been taken into account in the regional model. Therefore, the general patterns in which rock glaciers are mainly present in high probability areas appears reasonable.

Ground temperatures have been recorded at almost 20 borehole or other monitoring sites in the region (Table 6.2). Because most of these sites were instrumented with the goal of studying permafrost, the great majority exhibit perennially frozen ground. There is a relationship between predicted probability and most measured ground temperatures (Figure 6.6), with the latter being generally lower at high probabilities. However, permafrost can be present even at sites which have very low predicted probabilities, and conversely, may be absent at sites with high predicted probabilities.

The two non-permafrost sites are Northern Dancer (probability 0.95) and Carmacks (probability 0.7). At the Northern Dancer site, a potential explanation is that the model is not weighting the PISR variable as heavily as it should. Northern Dancer is located at a high elevation, highly exposed south-facing slope, which receives abundant insolation. The borehole was drilled in 1978 within a highly disturbed alpine tundra site. The organic mat had been completely stripped down to the bedrock prior to the borehole

being drilled, and the site was used as a mining road. Carmacks is also in a highly disturbed area that is used as a mining road. Thus it is possible that anthropogenic factors could have led to the loss of permafrost at these locations, which is something the model cannot accommodate. However, given the nature of probability modelling it is also true that high probabilities do not equate to permafrost presence at any given site, but indicate only that it is likely to be present.

Comparison of the Regional Model to the Sa Dena Hes Model

The regional model was created without incorporating the results from the Sa Dena Hes area because this area uses NDVI as one of its inputs. This variable could not be generated for the entire study area at the scale needed. Consequently, results from the local Sa Dena Hes model can be compared with those of the regional model (Figure 6.7). The overall percentages of areas predicted to be underlain by permafrost are within 10% of each other: 30% for the local model and 39% for the regional one. In detail, the regional model indicates a greater influence of elevation whereas the Sa Dena Hes local model is based only on slope and NDVI. Most of the lowland areas, however, display comparable low to intermediate probabilities (0.2 – 0.3) for both models. A comparison of the ground truthing sites for the area with the modeled permafrost probabilities from both the SDH and the regional models shows that the regional model is better at discriminating between permafrost and non-permafrost sites (Figure 6.8). The great majority of sites with permafrost are in locations where the probability is > 0.5, and most of the non-permafrost sites have probabilities < 0.5. The local Sa Dena Hes model produced predictions in a range of probabilities from 0.2 to 0.5. Thus it appears likely that the results of the regional model are more realistic than those of the local one.

Discussion

Comparison to Previous Maps

The regional model represents the first attempt to map permafrost in this area since the work by Heginbottom et al. (1995) and Heginbottom and Radburn (1992). It is also the first attempt internationally to model permafrost using empirical-statistical methods for an area this large and at such a fine resolution. Consequently, it is not possible to directly compare the results with previous maps at a fine resolution. However, it is possible to classify the predictions into probability classes that conform with previous maps and examine these at a small scale (i.e. large area) (Figure 6.9). The regional model is similar to the Permafrost Map of Canada but contains orders of magnitude more information. The greatest differences are present where the regional model classifies areas of high elevation in the southern part of the region as continuous permafrost. The map by Heginbottom et al. (1995) apparently did not directly take elevation sufficiently into account, and focused more on geology and coarse latitudinal and climatic gradients. It is also evident that there are areas in the northern end of the study area that are classified as sporadic in the regional model but as extensive on the map by Heginbottom et al. (1995). These are the result of the annual inversions in SLRs that are present in the Dawson and Keno areas. Another difference is the existence of an area of continuous permafrost around the Beaver Creek area. This area has a Mean Annual Air Temperature (MAAT) around -5.5°C which would place it close to the assumed temperature under which continuous permafrost can form (-6°C) (French, 2007). Although an area of continuous permafrost is not shown at this scale, Heginbottom and Radburn (1992) produced a 1:1 000 000 scale map on which higher elevation terrain in this area is categorized as continuous, while our predicted SLRs are

near zero in this area meaning that permafrost probability is independent of elevation. Finally, the zone of extensive discontinuous permafrost in the regional model is larger than in the map by Heginbottom et al. (1995), especially in the area to the south of Faro. Since there was no ground truthing undertaken there, it is possible that the regional model is over-predicting for this area where multiple local models contribute (Figure 6.2).

Inaccuracies and Uncertainties in the Regional Model

Inaccuracies in the regional model relate in part to the methods used to create it for such a large area. One source is the trend surfaces for equivalent elevation which were needed to predict values for each grid cell. Figure 6.10 shows the comparison between observed values and those predicted from the trend surface. For the treeline more than half of the 43 points were within ±20 m of the measured value and the maximum deviation was approximately ±120 m asl (Figure 6.10A). For the SLR trend surface, more than half of the 17 points were within ±0.2°C km^{-1} of the trend surface prediction and the maximum deviations were +1.2 and -1.4°C km^{-1} (Figure 6.10B).

The deviations of the trend surfaces from the measured values affect the permafrost probability results in a number of ways that depend on actual values and whether the trend surface is over- or under- predicting (Table 6.3). Spatially, the greatest potential sources of error are associated with the treeline trend surface in southwest areas around the ice fields (Figure 6.11A). The ice fields themselves were excluded from analysis because the interaction between glaciers and permafrost was not considered in the model. In the SLR surface, the largest errors are present around the Pelly Ranch and Faro areas (Figure 6.11B). SLR is too positive around Faro and too negative around Pelly Ranch. Around Faro permafrost probability is over-predicted in valley bottoms and in the

Pelly Ranch area permafrost probability is under-predicted in valley bottoms (Table 6.3). In the Pelly Ranch area, however, the relief is relatively subdued which limits the impacts.

Sources of uncertainty in the regional model are linked to assumptions made during the modelling, in particular regarding the distance decay function (Equation 6.2). Very little literature exists on the interchangeability of permafrost models among areas, an exception being Lewkowicz and Bonnaventure (2008). Figure 6.1 shows that the study area covers six different climatic zones (Wahl et al., 1987), and this was considered when choosing the decay rate, but it was not deemed the most important factor. The influence of each model had to be extended so that areas close to an individual study area were almost wholly represented by its model. But the close proximity of some of the study areas to each other (WC, JC and HS) meant that the decay had to be sharp so that other models would not play major roles. In the end the choice of the decay rate in equation (6.2) was fairly arbitrary.

Other sources of uncertainty exist in the initial BTS modelling for the individual areas themselves but these have been discussed in previous publications (Lewkowicz and Ednie, 2004; Bonnaventure and Lewkowicz, 2008; Bonnaventure and Lewkowicz, *Submitted*).

Regional Model Uses

Current permafrost distribution maps fit into one of two groups which are, for the most part, separated based on the amount of area they cover. Small-scale maps cover very large areas (e.g. Heginbottom et al., 1995, 1:7 500 000). These maps are useful for examining broad trends in permafrost but have limited use for practical purposes (e.g.

engineering projects or geohazard planning) especially in discontinuous permafrost zones. Large-scale maps cover small areas at a finer resolution (e.g. Lewkowicz and Ednie, 2004, 1:200 000), show detailed permafrost distributions and account for topographic effects, but are very limited in areal extent. Maps covering large areas are more common but, recent advances in permafrost modelling have resulted in higher levels of detail and more maps being produced, as well as the inclusion of other features such as ground ice and permafrost features. Given the areal coverage of the regional model, the most significant comparable permafrost maps include the permafrost map of Canada (Heginbottom et al., 1995), the Permafrost Characteristics of Alaska map (Jorgenson et al., 2008) and the International Permafrost Association's (IPA) Circum-Arctic Map of Permafrost and Ground Ice Conditions (Brown et al., 1997). The attributes of these maps are illustrated in Table 6.4.

The regional model represents a significant improvement on existing permafrost maps of the area (Heginbottom et al., 1995) and other comparable maps (e.g. Jorgenson et al., 2008; Brown et al., 1997). The regional model provides much more detailed spatial information on permafrost existence because the permafrost classification is given as a probability value. This feature makes the regional permafrost map very useful at multiple scales, and it should therefore be accessible at multiple scales, as an online interactive high-resolution map.

In addition, the creation of the regional model has led to a better understanding of the controlling factors on the distribution of permafrost in the Yukon. Mountain permafrost distribution in the Yukon varies greatly from that of the European Alps where permafrost is highly correlated with elevation and PISR in a linear relationship and only

above treeline. In the Yukon permafrost is observed above and below treeline, with the relationship between permafrost and elevation being non-linear. Similar relationships have been observed in Mongolia where vegetation cover and topographic wetness are the main factors governing the existence of permafrost (Etzelmüller et al., 2006). Due to this difference, permafrost in northwest North America, and likely other similar areas, cannot be modeled using the same empirical-statistical variables as the Alps (e.g. Gruber & Hoelzle, 2001). The development of the equivalent elevation variable has shown that SLRs can be greatly reduced or even inverted in these environments, which greatly impacts the distribution of permafrost. Thus the regional model takes into account the topography and individual climatic characteristics of the areas, representing a major advance over previous maps.

The regional model is expected to be of direct use as a benchmark for future permafrost studies in the Yukon and for many applications in infrastructure planning and hazards assessment. It can also be used to model the potential effects of climate change on permafrost at high resolution by altering the input variables (Bonnaventure and Lewkowicz, 2010; Janke, 2005). The regional model could be developed to examine geohazard risk as the climate changes. As an example, it would be possible to overlay the areas where permafrost probability is most sensitive to a given temperature increase, on slopes with gradients exceeding threshold values. This type of information would be of direct use to policy-makers, serving as a tool for climate change adaptation strategies throughout the region.

Conclusions

The following conclusions can be reached as a result of this research:

1) Both the variable inputs and distributions of permafrost in the Yukon are non-linear. This is evident in the spatial trends seen in treeline and SLR, which are direct input for equivalent elevation, a major variable in the regional model.

2) Trends in permafrost distribution in forested areas differ from those above treeline. Below treeline the distribution of permafrost is dependent on the sign and magnitude of the SLR. Areas with inverted SLR contain significant permafrost in valley bottoms and decrease as treeline is approached. Above treeline, permafrost distribution is highly correlated with elevation and follows a similar pattern to that seen in the Swiss Alps.

3) Uncertainties and inaccuracies are magnified in areas of high relief. Common inaccuracies that are associated with the regional model include deviations from input values in the trend surfaces used to calculate equivalent elevation. Although uncertainties are relatively small, both improper positioning of treeline or SLRs that are too positive or too negative are most problematic in high relief areas.

4) The complexities associated with the interfingering of latitudinal and mountain permafrost are incorporated into the model and appear within the spatial patterns output. The process of blending local models to interpolate between study areas allows both latitude and altitude to be taken into account in permafrost probability predictions at any location.

5) The southwest portion of the study area is “alpine”, but the rest of the region is not. The remaining portions are more closely related to permafrost distributions patterns seen in other continental areas, such as Mongolia.

Acknowledgments

This project was supported financially by the Canadian Foundation for Climate and Atmospheric Sciences, the Federal Government of Canada’s International Polar Year Program, the Natural Sciences and Engineering Research Council of Canada, the Northern Scientific Training Program (Department of Indian Affairs and Northern Development), the Yukon Geological Survey, the Geological Survey of Canada, and the Faculty of Arts, University of Ottawa. Field assistance for BTS was carried out by Julie Cossett, Paul Pearson, Katherine Henry and Chris Andrews while summer assistance with the pits and loggers was carried out by Dan Odell, Patty Bonnaventure, Jason Skucas, Andrea Sitler, Roland Bonnaventure, Megan James and Sam Darling.

References

Arctic Climate Impact Assessment. 2004: http://www.acia.uaf..edu.

Bonnaventure P.P., and Lewkowicz A.G. 2008. Mountain Permafrost Probability Mapping Using the BTS Method in two Climatically Dissimilar Locations, Northwest Canada. *Canadian Journal of Earth Sciences,* **45**: 443-455.

Bonnaventure, P.P., and Lewkowicz, A.G. 2010. Modelling climate change effects on the spatial distribution of mountain permafrost at three sites in northwest Canada. *Climatic Change*. DOI 10.1007/s10584-010-9818-5.

Bonnaventure P.P. and Lewkowicz A.G. *In Review*. Mountain Permafrost Probability Modelling in Areas Above and Below Treeline, Southern Yukon, Canada. *Canadian Journal of Earth Sciences.* Submitted November, 2010.

Brouchkov A. and Fukuda M. 2002. Preliminary Measurements on Methane Content in Permafrost, Central Yakutia, and some Experimental Data. *Permafrost and Periglacial Processes*. **13**: 187-197.

Brown, J., O.J. Ferrians Jr., J.A. Heginbottom, and E.S. Melnikov. 1997. Revised February 2001. *Circum-Arctic map of permafrost and ground-ice conditions*. Boulder, CO: National Snow and Ice Data Center/World Data Center for Glaciology. Digital Media.

Department of Energy Mines and Resources, Canada. 1974. Physiographic regions of Yukon and surrounding Canadian territory. Published in *Climate of Yukon.* Canadian Government Publishing Centre.

Dobinski, W. 1998. Permafrost occurrences in the alpine zone of the Tatra Mountains, Poland. *In* A.G. Lewkowicz and M. Allard, (eds.) *Proceedings, Seventh International Conference on Permafrost, Yellowknife, June 23-27, 1998.* Nordicana, Centre d'Etudes Nordiques, Quebec City. 231- 237.

Duk-Rodkin, A. 1996. Surficial geology, Dawson, Yukon Territory. Geological Survey of Canada, open file 3288, 1:250 000 scale.

Eyles, N. and Miall, A. 2007. Canada Rocks, The Geologic Journey. Fitzhenry and Whiteside limited. Markham Ontario.

Etzelmüller B., Heggem E.S.F., Sharkhuu N., Frauenfelder R., Kääb A., and Goulden C. 2006. Mountain permafrost distribution modelling using a multi-criteria approach in the Hövsgöl area, northern Mongolia. *Permafrost and Periglacial Processes*, **17**: 91-104.

French H.M. (2007) The Periglacial Environment, third edition. John Wiley and Sons, Ltd. Baffins Lane, Chichester, West Sussex PO19 1UD, England.

Gardaz, J.M. 1997. Distribution of Mountain Permafrost, Fontanesses Basin, Valaisian Alps, Switzerland. *Permafrost and Periglacial Processes* **8**: 101-105.

Geobase (http://www.geobase.ca/) [Acceded May 2010].

Geomatics Yukon. 2006. 30 Meter Yukon Digital Elevation Model [data file]. Whitehorse, Yukon. Available download: ftp://ftp.geomaticsyukon.ca/DEMs/30m [compiled in 2007].

Gruber, S., and Hoelzle, M. 2001. Statistical modeling of mountain permafrost distribution: Local calibration and incorporation of remotely sensed data. *Permafrost and Periglacial Processes*, **12**: 69-77.

Global Terrestrial Network for Permafrost (GTNP database) http://www.gtnp.org/ [Accessed January, 2011].

Guodong C., Yuanming L., Zhizhong S. and Fan J. 2007. 'The thermal semi-conductor' effect on crushed rocks. *Permafrost and Periglacial Processes*, **18**: 151-160.

Haeberli W., Hallet B., Arenson L., Elconin R., Humlum O., Kaab A., Kaufmann V., Ladanyi B., Matsuoka N., Springman S., Vonder Muhll D. (2006) *Permafrost and Periglacial Processes.* Permafrost Creek and Rock Glacier Dynamics. **17**: 189-214.

Heginbottom, J.A., Dubreuil, M.A., and Haker, P.T. 1995. Canada Permafrost. (1:7,500,000 scale). In *The National Atlas of Canada*, 5th Edition, sheet MCR 4177. Ottawa: National Resources Canada.

Heginbottom J.A. and Radburn L.K. 1992. Permafrost and ground ice conditions of northwestern Canada; (Scale 1:1,000,000). *Geological Survey of Canada Map* 1691A.

Hoelzle, M. 1992. Permafrost occurrence from BTS measurements and climatic parameters in the Eastern Swiss Alps. *Permafrost and Periglacial Processes*, **3**: 143-147.

Hoelzle, M., Wegmann, M., Krummenacher, B. 1999. Miniature Temperature Dataloggers for Mapping and Monitoring of Permafrost in High Mountain Areas: First Experiences from the Swiss Alps. *Permafrost and Periglacial Processes*, **10**: 113-124.

Imhof, M., Pierrehumert, G., Haeberlie, W., and Kienholz, H. 2000. Permafrost investigation in the Schilthorn Massif, Bernese Alps, Switzerland. *Permafrost and Periglacial Processes*, **11**: 189-206.

IPCC. 2007. http://www.ipcc.ch/ipccreports/assessments-reports.htm.

Isaksen K., Hauck,C., Gudevang, E., Ødegård R.S., and Sollid J.L. 2002. Mountain permafrost distribution in Dovrefjell and Jotunheimen, southern Norway, based on BTS and DC resistivity tomography data. *Norsk Geografisk Tidsskrift*. **56**: 122–136. doi:10.1080/00291950 2760056459.

Ishikawa, M., and Hirakawa, N. 2000. Mountain permafrost distribution based on BTS measurements and DC resistivity soundings in the Daisetu Moutains, Hokkaido, Japan. *Permafrost and Periglacial Processes*, **11** 109-123.

Janke, J.R. 2004. The occurrence of alpine permafrost in the Front Range of Colorado. *Geomorphology*, **67**, 375-389

Janke, J.R. 2005. Modeling past and future alpine permafrost distribution in the Colorado front range. *Earth Surface Processes and Landforms*, **30:** 1495-1508.

Jeckel, P.P. 1988. Permafrost and its altitudinal zonation in N. Lapland. In *Proceedings of the Fifth International Conference on Permafrost, Trondheim*. Tapir, Trondheim. **1** 332-337.

Jorgenson T., Yoshikawa K., Kanevskiy M., and Shur Y. 2008. Permafrost Characteristics of Alaska, *Conference proceedings from the ninth international conference on permafrost*, June 29 - July 3, 2008. Fairbanks, Alaska, USA.

King, L. 1992: Prospecting and mapping of mountain permafrost and associated phenomenon. *Permafrost and Periglacial Processes*, **3** 73-81.

Kneisel C., Rothenbühler C., Keller F. and Haeberli W. 2007: Hazard Assessment of Potential Periglacial Debris Flows Based in GIS-based Spatial Modelling and Geophysical Field Surveys: A Case Study in the Swiss Alps. *Permafrost and Periglacial Processes.* **18**: 259-268.

Lewkowicz A.G., Etzelmüller B. and Smith S.L. Characteristics of discontinuous permafrost from ground temperature measurements and electrical resistivity tomography, southern Yukon, Canada. *Permafrost and Periglacial Processes. In Press.*

Lewkowicz, A.G. and Bonnaventure, P.P. 2008. Interchangeability of Mountain Permafrost Probability Models, Northwest Canada, *Permafrost and Periglacial Processes,* **19**: 49-62.

Lewkowicz, A.G. and Bonnaventure, P.P.2011. Equivalent Elevation: a New Method to Incorporate Variable Lapse Rates Into Mountain Permafrost Modelling. *Permafrost and Periglacial Processes.* DIO 10.1002/ppp.720

Lewkowicz, A.G. and Ednie, M. 2004. Probability mapping of mountain permafrost using the BTS method, Wolf Creek, Yukon Territory, Canada. *Permafrost Periglacial. Processes.* **15** 67-80.

Lugon, R., and Delaloye, R. 2001. Modeling alpine permafrost distribution , Val de Rechy, Valais Alps (Switzerland) *Norsk geogr. Tidsskr.* **55**: 224-229.

Natural Resources Canada. 2010. Forest ecosystems of Canada http://ecosys.cfl.scf.rncan.gc.ca/classification/classif08-eng.asp [Accessed June, 2010].

Ødegard, R.S., Isaksen, K., Mastervik, M., Billdal, L., Engler, M. and Sollid, J.L. 1996. Comparison of BTS and Landsat TM data from Jotunheimen, southern Norway. *Norsk geogr. Tidsskr.* **53**: 226 – 233.

Page A. M.Sc. Thesis. 2009. A topographic and photogrammetric study of rock glaciers in the southern Yukon Territory.

Riseborough D., Shiklomanov N., Etzelmuller B., Gruber S. and Mrchenko S. (2008). Recent Advance in Permafrost Modelling. (2008). *Permafrost and Periglacial Processes* **19**: 137-156

United States Geological Survey 2010. http://data.geocomm.com/dem/ [Accesses May, 2010]

Wahl, H.E., Fraser, D.B., Harvey, R.C., Maxwell, J.B. 1987. *Climate of Yukon.* Canadian Government Publishing Centre.

Tables

Table 6.1: Permafrost probability gradient information for specific portions of the region.

Locations	South	Mid	North	Extreme SW
Valleys below treeline	Low	Moderate	High	None
Elevations close to treeline	Moderate	Moderate	Low	None
Elevations above treeline	High	High	High	High

Table 6.2: Regional model predictions for borehole sites ordered from north to south (Source GTNP database, 2011).

Location	Elevation (m asl)	Latitude / Longitude	Permafrost Present	Mean Ground Temperature (°C) / Depth (m)	Regional Model Probability
Red Creek Borehole	780	65° 9'N 138° 22'W	Yes	-2.1 / 7.0	0.72
Eagle Alaska USA Borehole	269	64° 46' N 141° 10' W	Yes	-2.4 / 20.0	0.79
Dawson Borehole	320	64° 04' N 139° 26'W	Yes	-2.0 / 3.8	0.72
Sixty Mile Borehole	1462	63° 54'N 140° 48'W	Yes	-3.6 / 23.0	0.97
Mayo Borehole	504	63° 36' N 135° 52' W	Yes	-1.1 / 16.0	0.69
Carmacks Borehole	874	62° 19'N 136° 40'W	No	+0.3 / 22.5	0.70
Ross River Borehole	659	61° 58' N 132° 27' W	Yes	-0.1 / 9.0	0.63
Alpine Burwash Borehole	1842	61° 27'N 139° 24'W	Yes	-2.0 / 30.0	0.98
Tuchitua Borehole km 161	1220	61° 19' N 129° 36' W	Yes	-0.5 / 3.2	0.66
Takhini Valley	1200	60° 54' N 135° 5' W	Yes	-0.6 / 5.0	0.21
Mount	1570	60° 37' N	Yes	-1.6 / 20.0	0.80

McIntyre Borehole		135° 8’ W			
Mount Granger	2066	60° 32’ N 135° 15’ W	Yes	-5.4 / 0.5	0.99
Wolf Creek Palsa 25 Borehole	1260	60° 29’ N 135° 13’ W	Yes	-0.3 / 5.0	0.33
Wolf Creek GSC Borehole	1195	60° 28’N 135° 11’W	Yes	-0.5 /15.3	0.27
Alaska Highway 844	677	60° 28’ N 133° 29 W	Yes	-0.1 / 1.0	0.02
Alaska Highway Borehole 825	723	60° 22’ N 133° 6’ W	Yes	-0.1 / 4.0	0.13
Northern Dancer Borehole	1623	60° 0’N 131° 36’W	No	+0.4 / 20.0	0.95

Table 6.3: Implications and results of inaccuracies in the trend surface modelling.

Error in trend surface / meaning	**Impact to the regional model**
Treeline elevation over-predicted: model has placed trees above the position of treeline.	Permafrost probability is under-predicted at higher elevations especially immediately above the true treeline. This is because the normal SLR of -6.5°C km^{-1} is used above treeline. Areas that have inverted SLRs are affected both close to treeline and in valley bottoms.
Treeline elevation under-predicted: model has placed tundra areas within a forested area.	Permafrost probability will be over-predicted in the upper-most portion of the forest. Areas that have inverted SLRs are most affected by this error
SLR over-predicted: the SLR is too positive: inverted SLRs are larger; normal SLRs are gentler.	Permafrost probability will be over-predicted in valley bottom locations but the impact is greater for inverted SLRs because permafrost probabilities are high in valley bottom locations. These impacts will be less for locations with normal SLRs where valley bottoms have low probabilities.
SLR under-predicted: The SLR is too negative: inverted SLRs are too small; normal SLRs are enhanced.	Permafrost probability will be under-predicted in valley bottom locations but the impact is greater for inverted SLRs because permafrost probabilities are high in valley bottom locations. These impacts will be less for locations with normal SLRs where valley bottoms have low probabilities.

Table 6.4: Attributes of major permafrost maps comparable in area to the regional model.

Map	**Location**	**Scale / resolution**	**Permafrost attributes**	**Methodology**	**Boundary classes**
Permafrost map of Canada (Heginbottom et al., 1995)	All of Canada	1:7 500 000	Permafrost distribution, thickness, features and ground temperatures	Rules-based approach from surficial geology and ground ice content samples	Five categories: isolated patches (<10%), sporadic discontinuous (10 – 50%), extensive discontinuous (50 – 90%), continuous (>90%) and subsea permafrost.
Permafrost Characteristics of Alaska map (Jorgenson et al., 2008)	Alaska, USA	1:7 200 000 / 2 x 2 km	Permafrost distribution, depths and features	Rule-based model from MAAT input combined with the surficial geology	Same as Heginbottom et al. (1995) except no subsea class.
IPA's Circum-Arctic Map of Permafrost and Ground Ice Conditions (Brown et al., 1997)	Northern hemisphere (25 – 90°N, 180°W – 180°E)	1:10 000 000	Permafrost distribution, ground ice.	Combination of all nationally created permafrost maps such as Heginbottom et al. (1995) for Canada.	Same as Heginbottom et al. (1995) and includes a relic permafrost class.

Figures

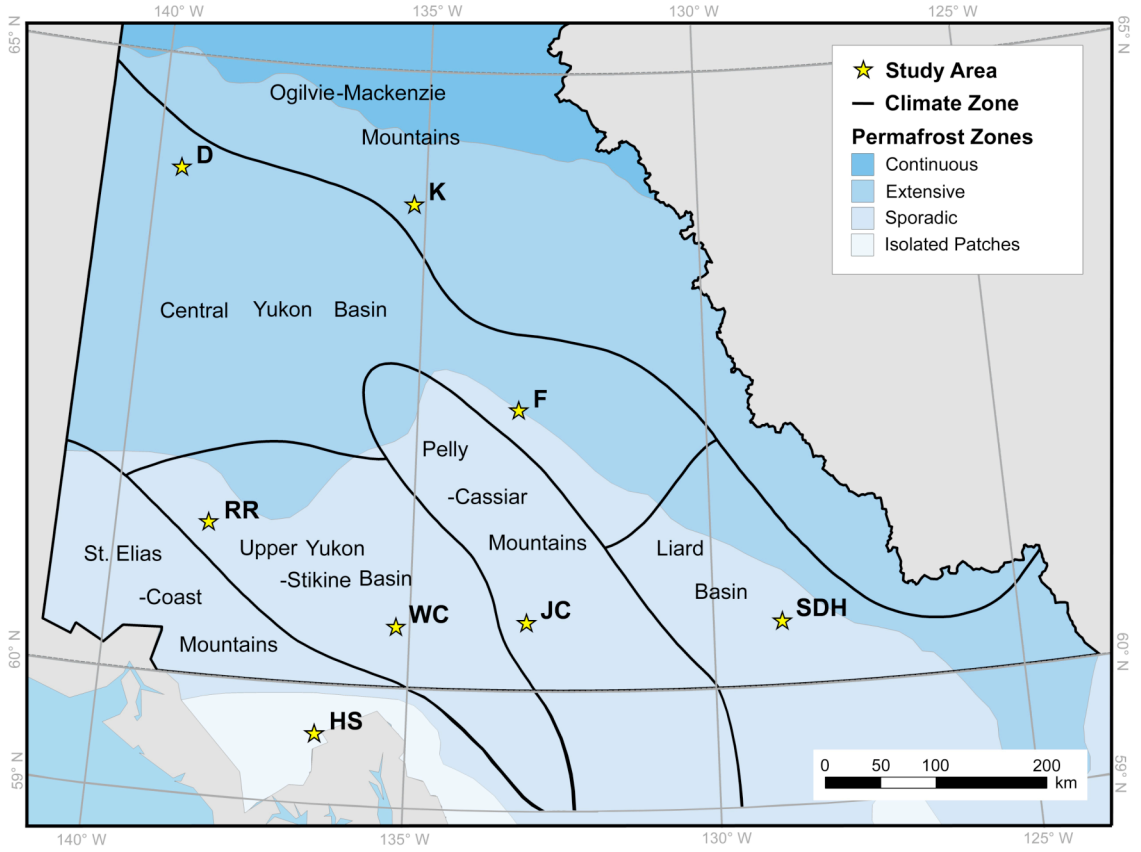

Figure 6.1: Map of the study region showing modelling locations in relation to permafrost zones (Heginbottom et al. 1995) and climatic regions (Wahl et al., 1987). JC: Johnson's Crossing, SDH: Sa Dena Hes, F: Faro, K: Keno, D: Dawson, RR: Ruby Range, HS: Haines Summit and WC: Wolf Creek.

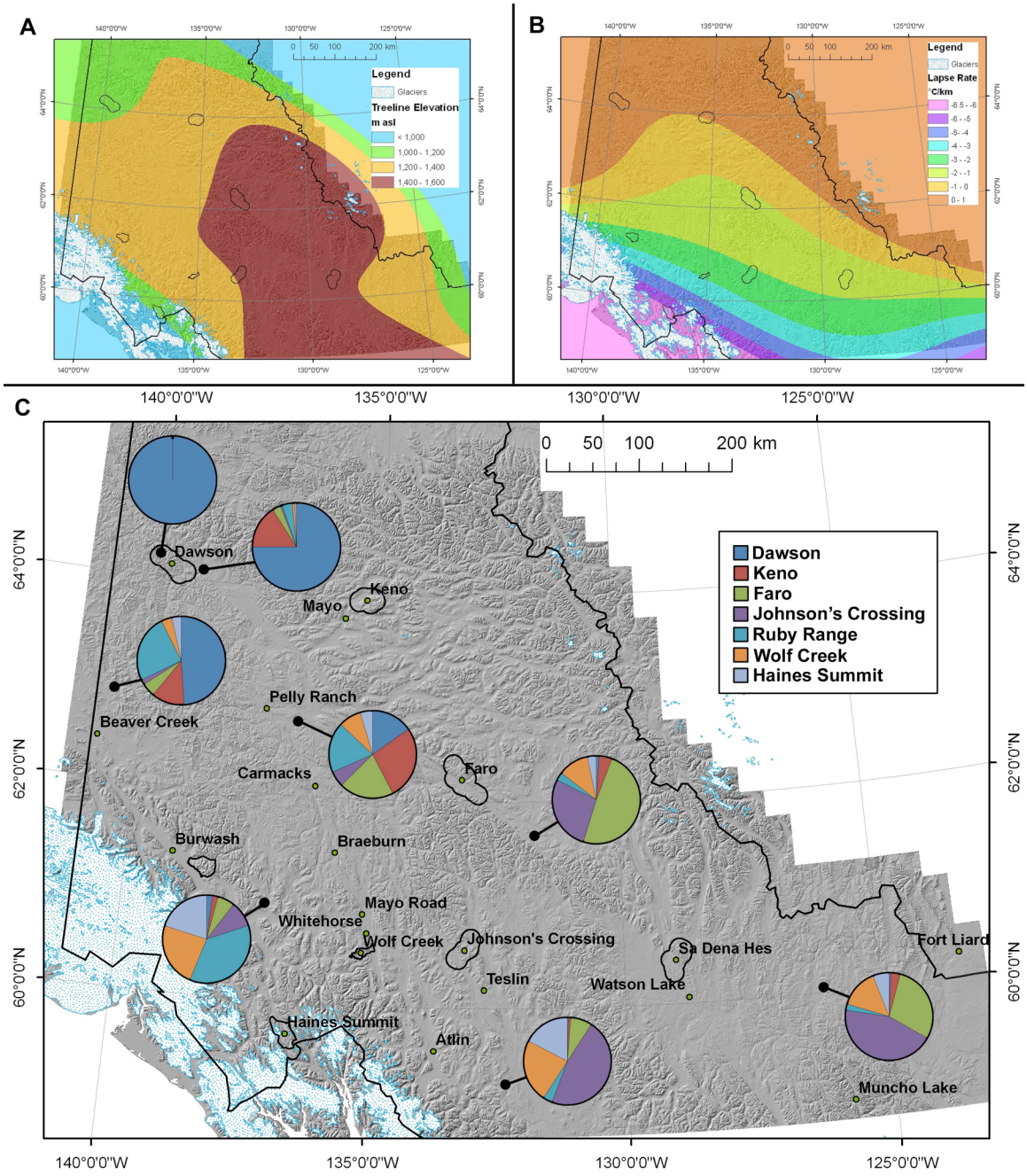

Figure 6.2: (A) 4th order polynomial trend surface representing treeline, (B) 3rd order polynomial trend surface representing surface lapse rate and (C) map displaying the percent of each individual model contributing to the regional model at eight selected locations. In (A), treeline trend surface is truncated at 800 m and 1600 m; in (B), surface lapse rate trend surface is truncated at +1°C km^{-1} and -6.5°C km^{-1}.

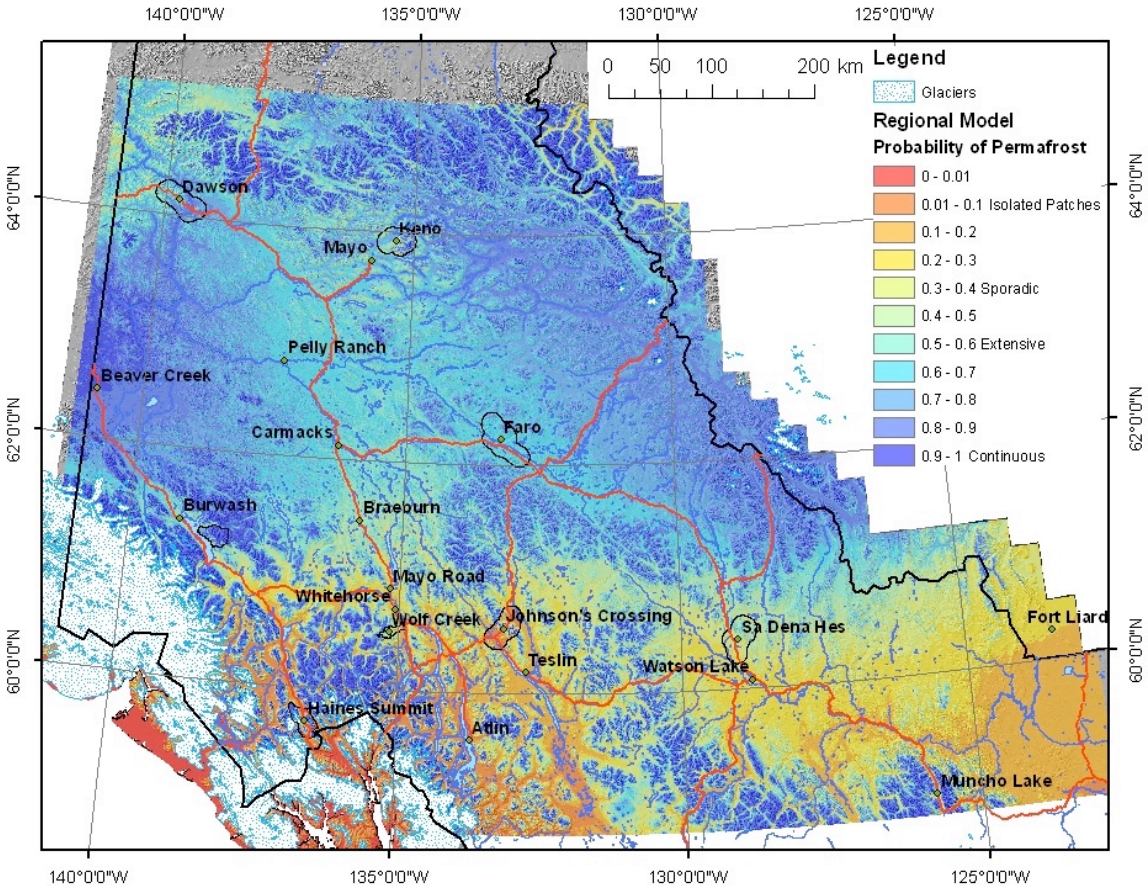

Figure 6.3: Regional model permafrost probability map with study area boundaries and locations of Environment Canada stations.

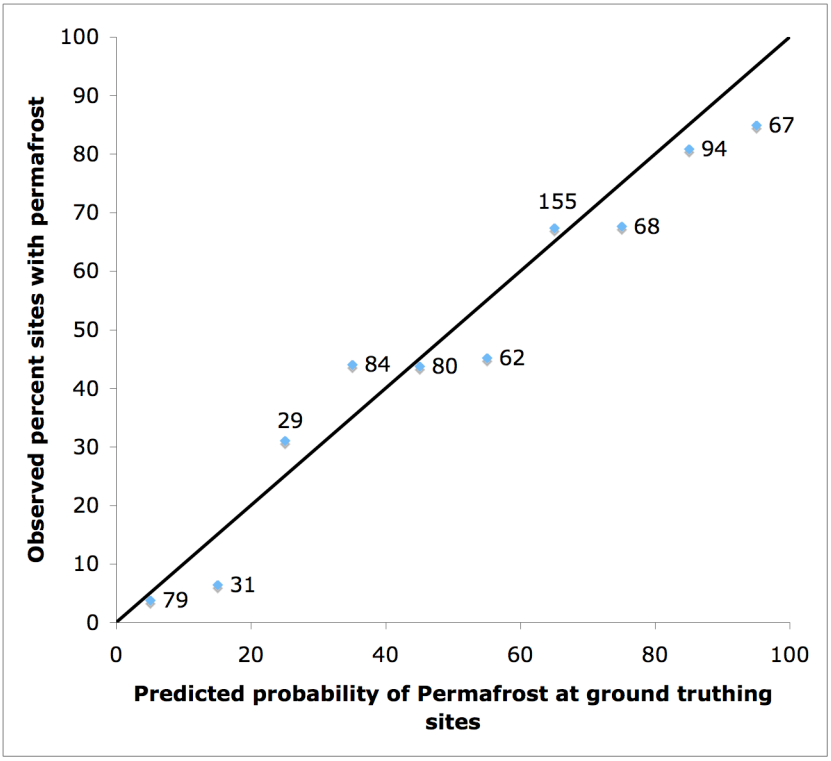

Figure 6.4: Observed presence vs. predicted probability of permafrost at ground truthing sites (n = 771). Note: points for predicted probability are plotted at the centre of each 10% division of values. Thick line is 1:1 line. Labels represent the number of field observations in each range.

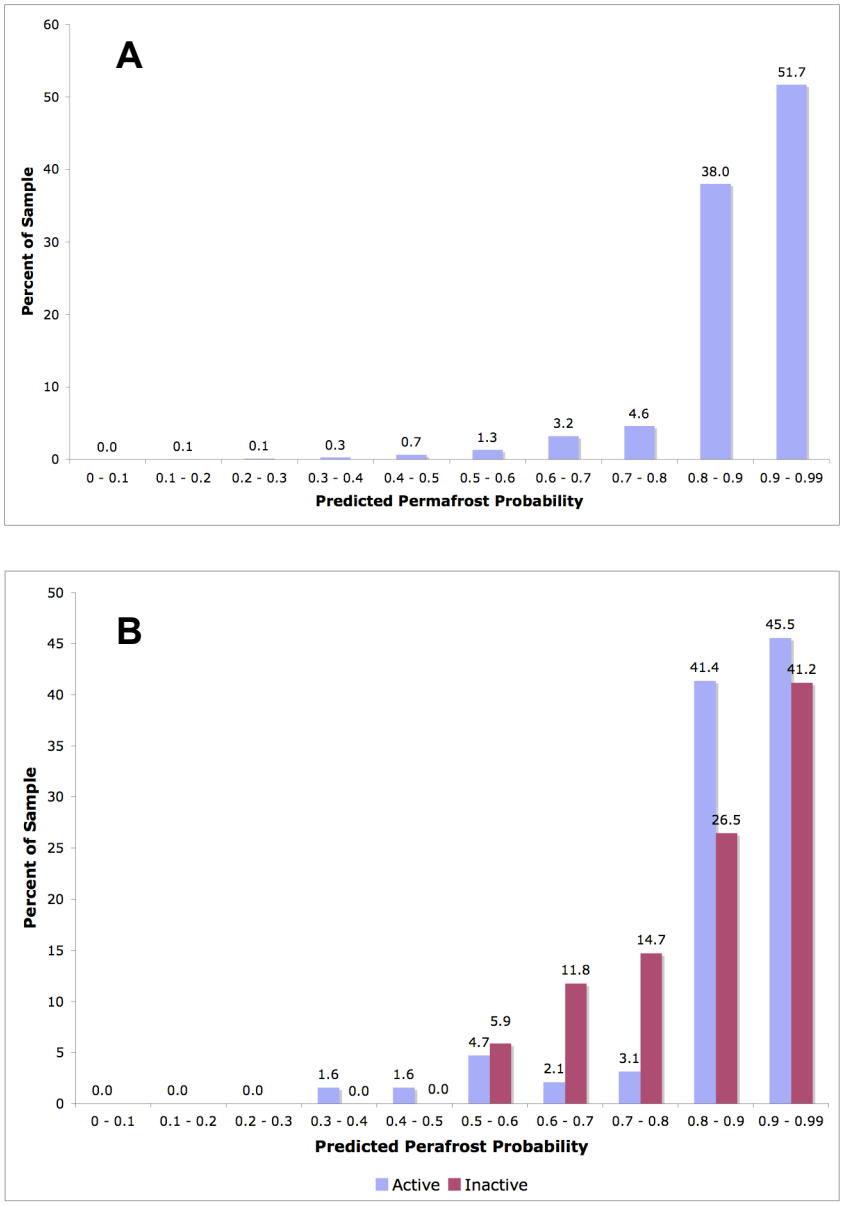

Figure 6.5: Comparison of predicted permafrost probabilities for (A) known rock glaciers sites (n = 1675) in the southern Yukon (Page, 2009), and (B) for classified rock glaciers (n = 225) (Page, 2009). Labels represent percentage of features in each probability range.

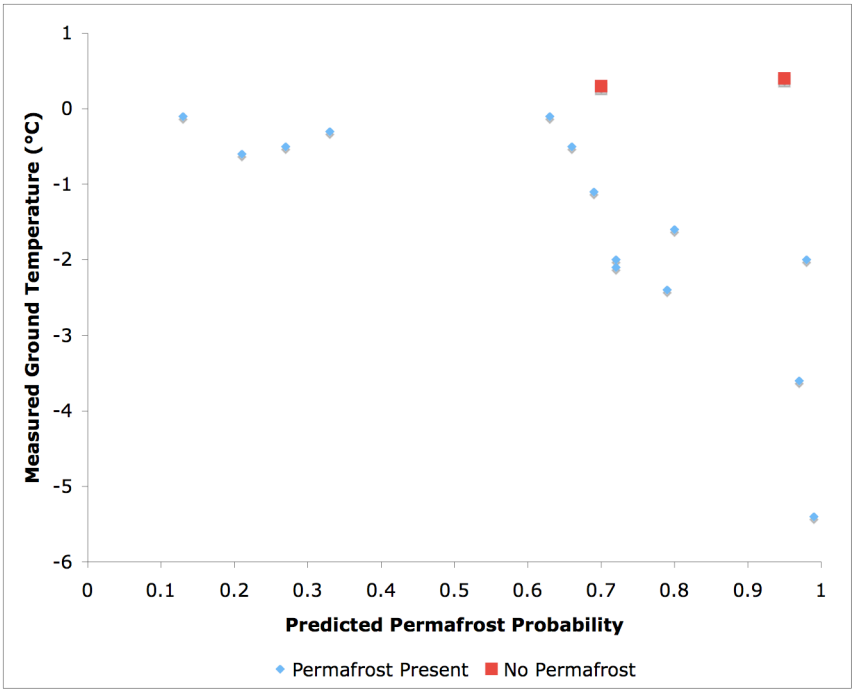

Figure 6.6: Regional permafrost model predictions for borehole sites in relation to measured ground temperatures.

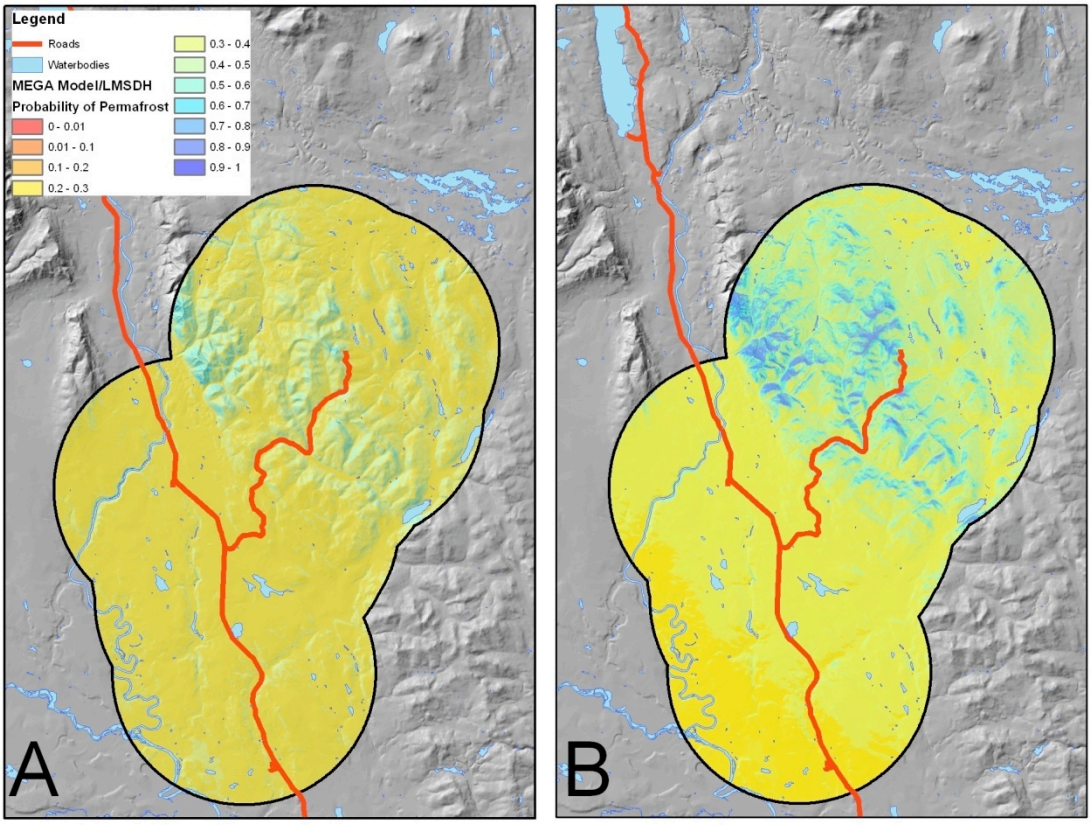

Figure 6.7: Comparison of the Sa Dena Hes local model (A), to the regional model (B) for the Sa Dena Hes area.

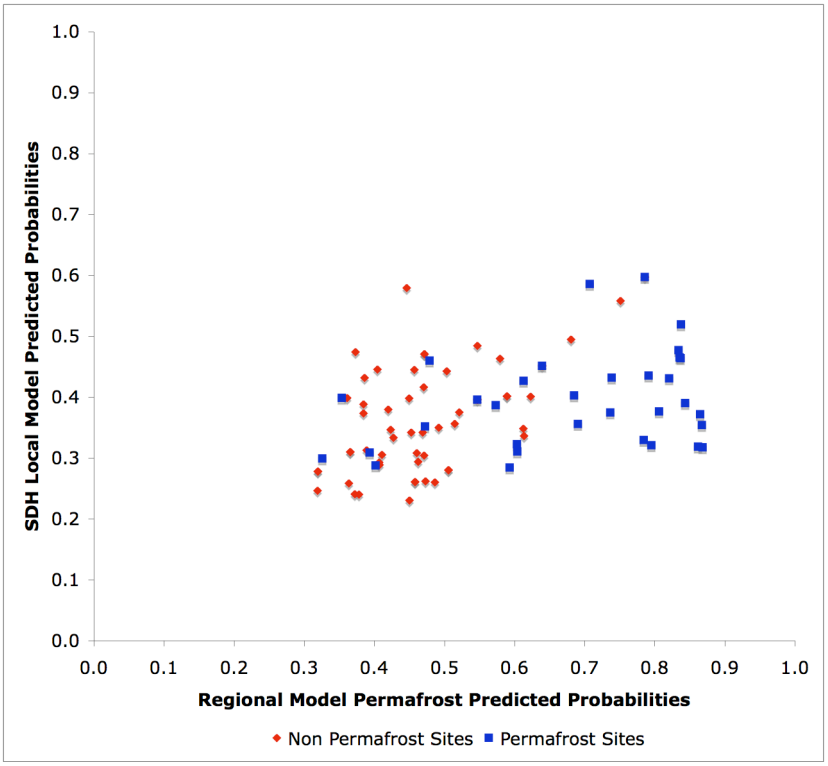

Figure 6.8: Predicted probabilities at ground truthing sites in the Sa Dena Hes area from the regional and local models.

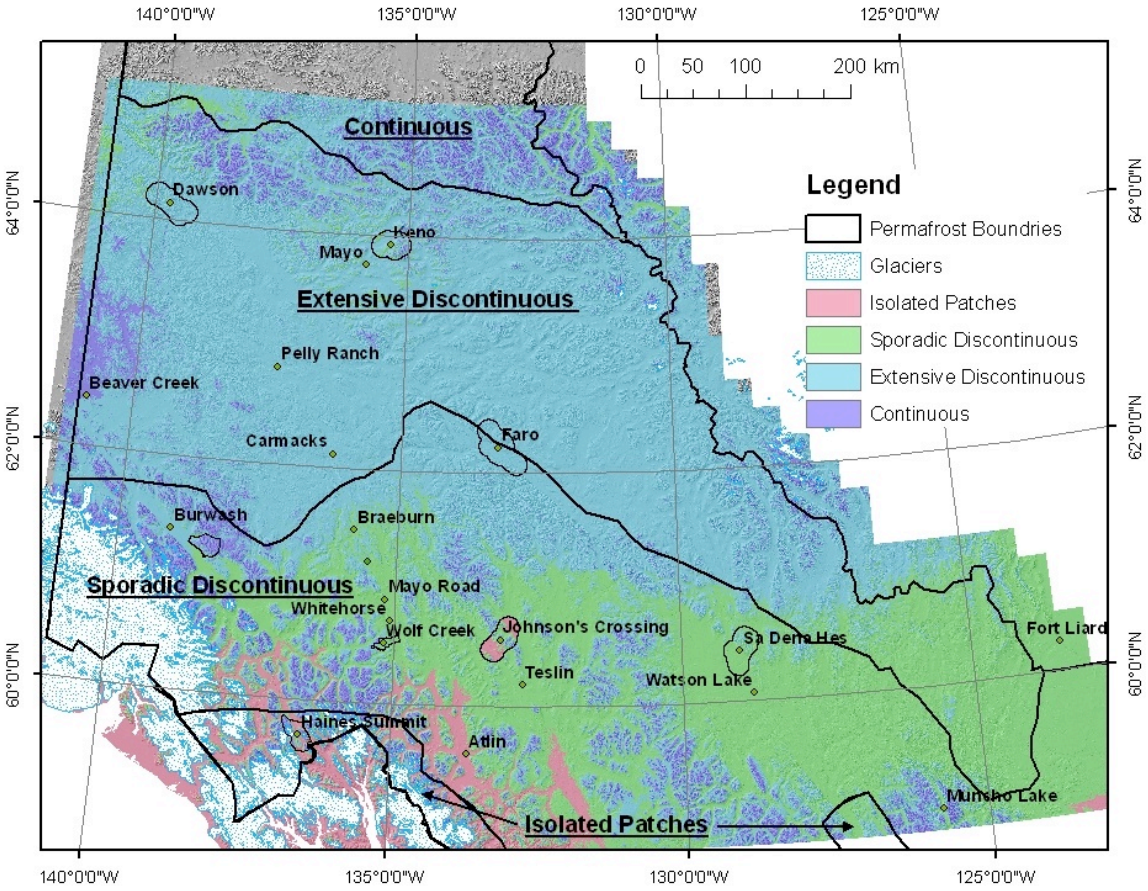

Figure 6.9: Regional model classified into traditional permafrost classes of isolated patches (<10%), sporadic discontinuous (10 – 50%), extensive discontinuous (50 – 90%) and continuous (>90%). Permafrost map of Canada boundaries after Heginbottom et al. (1995).

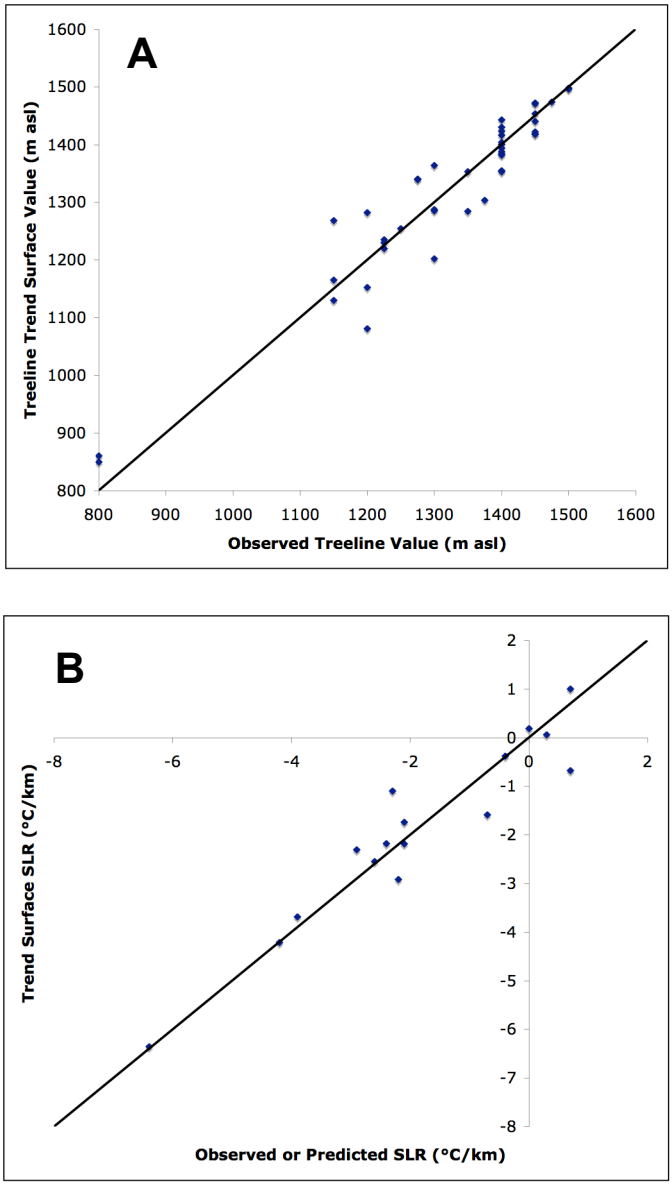

Figure 6.10: Comparison of (A) observed and predicted treeline from 4th order polynomial trend surface, and (B) observed or predicted surface lapse rates (from annual amplitude of monthly air temperatures) with values predicted from 3rd order polynomial trend surface.

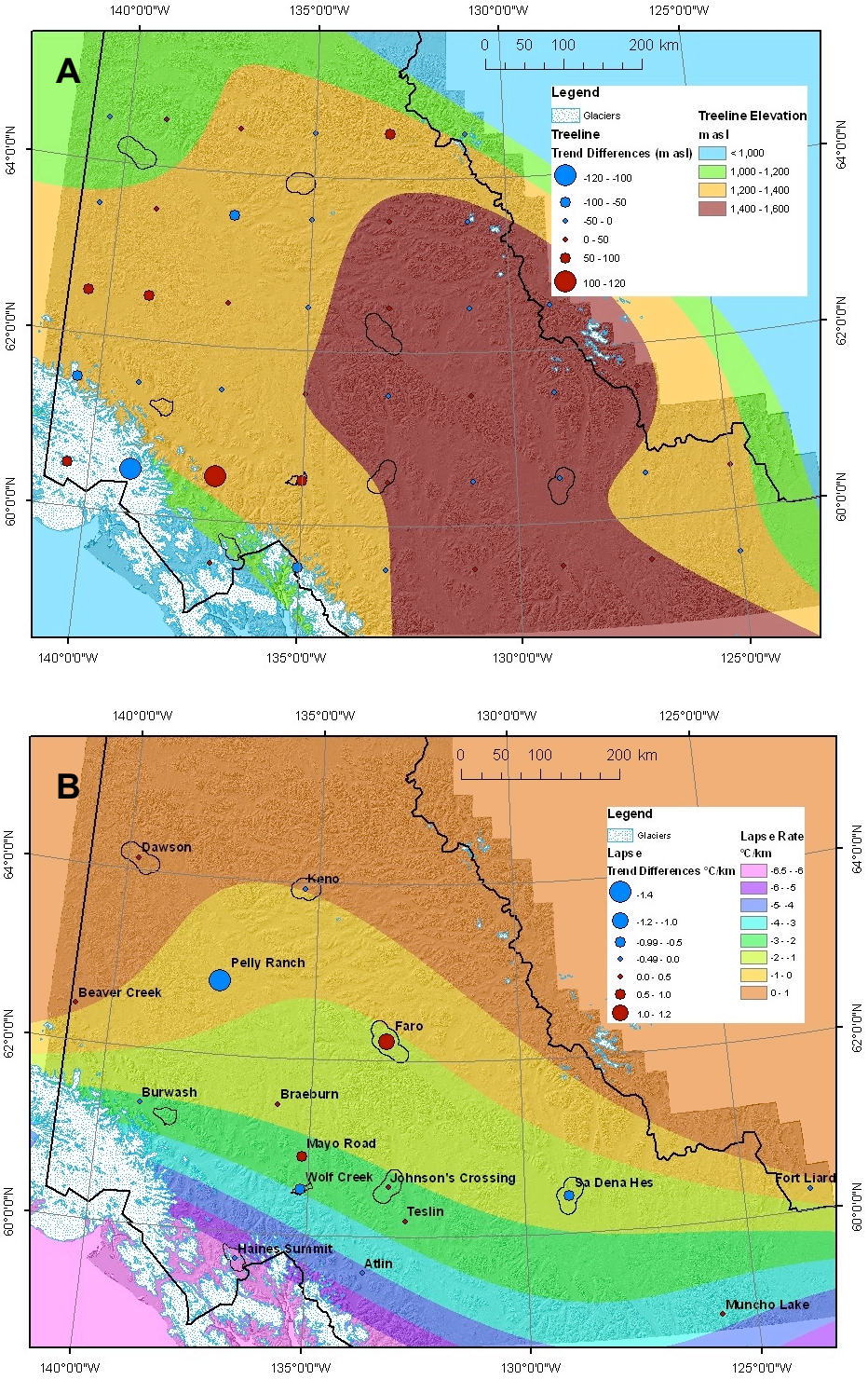

Figure 6.11: Fitted trend surface showing deviations from input values for (A) treeline elevation and (B) surface lapse rate.

Chapter Seven

Conclusions

The purpose of this study was to redress a lack of knowledge regarding the topographic and latitudinal distribution of mountain permafrost in the Yukon and extreme northern British Columbia between 59° - 65°N. BTS and ground truthing measurements were collected in eight different study areas (three prior to the Ph.D. and five for the Ph.D.) in the south and central Yukon and northwesternmost British Columbia. Local and regional permafrost probability models were generated using empirical statistical methods. Five objectives were established within this article-based thesis: 1) to examine the sensitivity of mountain permafrost to potential climatic change; 2) to explore the viability of interchangeability of permafrost models within different study areas; 3) to introduce a permafrost predictive variable capable of incorporating the effects of variable surface lapse rates; 4) to model permafrost probability above and below treeline and examine the potential use of additional explanatory variables; and 5) to model permafrost probability at high-resolution for the entire region between 59° - 65°N. This section will comment on the key contributions of each chapter, relate how the objectives tie together and comment on future research and applications.

Objective 1: Examine the sensitivity of mountain permafrost to potential climatic change

This objective was addressed in Chapter Two by changing the inputs of the elevation and potential incoming solar radiation (PISR) variables to explore the effects of

scenario-based climate warming or cooling for three study areas. The key contributions of this chapter were:

- Climate change scenarios that alter mean annual air temperature (MAAT) inputs have a more significant impact on mountain permafrost distribution than alterations to PISR. The predictions show that a change of 1 K affects the amount of permafrost from 14-24%, whereas a ±10% change in PISR only results in a 2-4% overall permafrost change.
- In the majority of areas (2 of 3) a 1-2 K increase in MAAT greatly reduces the amount of permafrost, with the areas most affected being in intermediate elevation zones. An increase of 5 K essentially eliminates permafrost in all of the study areas except where PISR has a strong ratio of standardized coefficients (Ruby Range). The strength of other explanatory variables reduces the impact of changes to MAAT.

- Mountain permafrost areas can be viewed as highly sensitive to climatic change (warming or cooling). This is because micro-sites always exist which are close to 0°C. Seasonally-frozen locations can become permafrost with a slight reduction in mean annual surface temperature. Conversely, locations with permafrost near 0°C may thaw during relatively slight warming, providing such changes persist.

Objective 2: Explore the viability of interchanging local permafrost models within a large region

This objective was addressed in Chapter Three by interchanging three locally derived BTS models and calibrating them using local validation points. This study was

the first known attempt to examine the interchangeability of permafrost probability models, and was seen as a first step toward increasing the extent of the area that could be modeled. The key contributions of this chapter were:

- Model interchangeability does not appear to be related to areas being within the same climatic zone. Rather interchangeability appears to relate to the variable ratio of standardized regression coefficients within the BTS predictive equation.
- This paper identifies three positions on the continuum specific to these study areas including: elevation-controlled (infinite ratio of the standardized coefficient of elevation to that of PISR in the BTS equation), elevation-dominated (ratio of elevation to PISR above unity) and radiation-dominated (ratio much less than unity for the same variables). Extending the continuum, the position of radiation-controlled is also theoretically possible although not present in these areas, the closest example being reported in Julián and Chueca (2007) for the Spanish Pyrenees. Interchangeability depends on where a site lies on a continuum, with similar ratios indicating good interchangeability.
- Another controlling variable on interchangeability is the hypsometry of the study areas themselves. Hypsometry impacts the actual percentage of permafrost for the study area as well as the apparent goodness of fit of the models. Models which have intermediate probability values at similar elevations, are more interchangeable. The position on the continuum as well as the hypsometry of an area appear to work in tandem to control interchangeability.

Objective 3: Develop a permafrost predictive variable capable of incorporating the effects of variable surface lapse rates

This objective was addressed in Chapter Four by introducing the concept and methodology to derive the equivalent elevation variable. Most empirical-statistical models have not included BTS data collected below treeline. As a result it was not recognized that there can be a different relationship between elevation and BTS above and below this critical boundary. Examining the air temperature data from the logger network for five study areas showed that surface lapse rates varied below treeline from one study area to another. This variability in surface lapse rates (SLRs) needed to be incorporated to allow accurate modelling at a regional scale. The key contributions of this chapter were:

- The observation that inversions in SLR occur in all of the forested portions of the study areas during winter months. This results in SLR values on an annual basis that are weak, non-existent or inverted.

- SLRs appear to be controlled by the amplitude of monthly air temperatures over the year (mean July minus mean January). This relationship generated a statistically significant correlation that showed large differences in monthly temperature resulting in SLRs close to 0°C km^{-1} or inverted; smaller amplitudes result in gentle or closer to normal SLRs. Therefore the sign and magnitude of the SLR in an area appear to be related to the local degree of continentality.

- Equivalent elevation produces a flattened or inverted physiography that adjusts low elevation areas while leaving areas above treeline unchanged. The

relationship between continentality and SLR provides a means for modelling equivalent elevation and hence, mountain permafrost probability across the entire region. As a variable it may also be useful in areas with similar terrain such as the Northwest Territories, Alaska and Mongolia.

Objective 4: Model permafrost probability above and below treeline and examine the potential use of additional explanatory variables

This objective was addressed in Chapter Five by using BTS and ground-truthing data for the five areas studied for the doctorate to locally model permafrost probability. This was the first attempt to empirically model mountain permafrost using variable relationships above and below treeline. The key contributions of this chapter were:

- In some study areas, additional explanatory variables (slope, NDVI) helped explain permafrost distribution. PISR, which has been widely used in empirical-statistical models, was significant in only one area, and this is likely the result of its reduced importance in the forest. The Topographic Position Index (TPI) variable was also tested but it was not significant in any area. It appeared that the most useful explanatory variable for predicting permafrost distribution above and below treeline is equivalent elevation.

- The spatial distribution of permafrost differed from what was expected prior to the start of the thesis, and from distributions of mountain permafrost in lower latitudes, such as in the Swiss Alps. In areas where SLRs are inverted, the highest probabilities of permafrost may be at the lowest points in terrain and within the

forest. Probabilities are also high above treeline and increase according to a normal negative SLR.

- There appears to be no relation between climatic region and permafrost explanatory variables. Thus any attempt to model permafrost outside the study areas would require the use of a blended combination of all models, potentially weighted using a distance decay function.

Objective 5/Overall Objective: Model permafrost probability at high-resolution for the Yukon between 59° - 65°N

This objective was addressed in Chapter Six with a regional permafrost model created by combining seven of the eight locally-derived empirical-statistical permafrost probability models for area between 59° - 65°N. This technique used a blended distance decay method, allowing any given area within the study region to be assigned a probability based on a portion of each model. This map, which constitutes the output of the model, can serve as a benchmark for future studies of permafrost distribution in the area and is capable of being altered to investigate the possible effects of climatic change in a scenario-based approach. This makes it of direct use as a tool in infrastructure and geohazard planning as well for climatic change adaptation strategies and northern development. The key contributions of this chapter were:

- The production of a regional high-resolution permafrost map for the Yukon and extreme northwest British Columbia. The map generated from the regional model is the largest permafrost probability map ever created at this fine a resolution. The

map shows elevational and latitudinal trends in permafrost distribution and the permafrost boundaries generally follow those of previous area maps (Heigenbottom et al., 1995) but with a much higher level of detail.

- The methodology addresses an important issue within this type of permafrost modelling with respect to interpolating between sites by developing a blended model. This also required developing a trend surface of equivalent elevation for the entire region.
- Both the variable inputs and distributions of permafrost in the Yukon are non-linear. The large area covered by the regional model and the complexities associated with the interfingering of latitudinal and mountain permafrost are incorporated in the model. The process of blending local models to interpolate between study areas allows contribution of many elements into the probability of permafrost value at any given location.

The nature of this work means that the ideas, processes and techniques constantly evolved. Each of the chapters is a significant contribution, but most importantly, they were essential to producing the regional permafrost model which was the end result of this thesis. Knowledge and methods that became important in the later chapters are the direct result of ideas generated in the earlier ones. Although certain techniques and variables would not be used in the same way now, the regional model could not have been generated without the knowledge gained earlier.

An important issue for discussion is the use of elevation as a variable in the early chapters, whereas equivalent elevation was used for Johnson's Crossing, Faro, Keno and

Dawson. Equivalent elevation addresses the presence of reduced or inverted SLRs, an issue that was raised in Chapters Two and Three but not directly addressed until Chapter Four. Because the BTS method was developed for permafrost detection in the Swiss Alps, Lewkowicz and Ednie (2004) sampled only above treeline in Wolf Creek. This was also the case for Bonnaventure and Lewkowicz (2008) in Haines Summit and Ruby Range. Thus all the BTS data obtained was collected above treeline where elevation and equivalent elevation are interchangeable. However, the regional model uses equivalent elevation in all areas, and this results in significantly higher permafrost probabilities in the lower areas of Ruby Range within the regional model. This change shows that while similar relationships between BTS and elevation exist above treeline in the Yukon and in the Swiss Alps, the use of equivalent elevation is necessary in forested area and is better suited overall for the heterogeneous mountain permafrost seen in the Yukon.

How the research would differ today

An important question that may be asked at the end of a research project of this duration, is what would be done differently if it were to be started today?

This project was challenging because we encountered factors and issues that were not anticipated, and they led us to alter portions of the methodology, and in particular, to develop the additional variable of equivalent elevation. Knowing that these differences exist would have affected the sampling and the areas selected.

The regional model was created using seven of the eight local permafrost probability models, which were distributed according to climate regions. From examining the regional model with the study areas included it is obvious that gaps exist. This is true

of any sampling network that is not continuous, but the modelling would have benefited from the inclusion of additional sampling areas including: Burwash (61° 22' N, 139° 0' W), Beaver Creek (62° 22' N, 140° 52' W), Pelly Ranch (62° 50' N, 136° 35' W), around Rancheria (60° 0' N, 131° 36' W), Tungsten, N.W.T. (61° 57' N, 128° 16' W), Atlin B.C. (59° 34' N, 133° 41' W), and Muncho Lake B.C. (58° 55' N, 125° 46' W) as there areas are close to climate stations, have adequate snow depths, a good range of topography and are accessible by road. Other areas that would be of use filling in gaps but are less accessible include: between Beaver Creek and Dawson (63° 43' N, 140° 39' W), and southeast of Atlin in B.C. (59° 08' N, 129° 51' W). The inclusion of these additional nine study areas would have allowed BTS and ground truthing but also the confirmation of the equivalent elevation surfaces.

BTS and ground truthing are the main inputs in the probability models and because of this, sampling improvements would be beneficial. One of the issues we encountered in BTS sampling was difficulty collecting points in elevations above treeline. Of the areas mentioned above, Burwash and Rancheria coincide with the locations of mining exploration camps where instrumented boreholes exist (Throop, 2010). Consequently, these areas contain roads, which would allow relatively easy access to areas above and below treeline in both summer and winter. Burwash is represented on the regional model by essentially continuous permafrost, whereas Rancheria is in the southern fringe of the discontinuous permafrost zone. Investigations into these two areas would help confirm our understanding of the pattern of permafrost probabilities.

Within each study area the BTS sampling procedure would have benefited from increased numbers of points taken above treeline. Due to the general existence of more

terrain below treeline, this might have led to lower numbers of overall measurements but overall a more homogeneous sample. It is also possible that following this suggestion may have led to the development of separate models for terrain above and below treeline which are harder to implement over very large areas.

The air temperature data from the logger network that allowed us to determine local SLRs turned out to be one of the most useful sources of data in this research. The correlation between SLRs and temperature amplitude allowed us to model SLRs for other areas with Environment Canada stations and then to develop a third order polynomial trend surface. Certain areas including Pelly Ranch, which were modeled using the trend surface, were not modeled as accurately as the majority, introducing an error. The addition of other sites would potentially help reduce these errors by having a greater number of inputs for the trend surface to be generated from. The accuracy of the equivalent elevation variable and thus the regional model would thus be enhanced as the fit of the trend surfaces improved.

Future Research Directions

The creation of the regional model of permafrost probability allows research question to be examined on a variety of topics across the landscape. The following further research directions should be examined:

- **Development of an online interactive system to view the results of the regional permafrost probability model.** One of the restrictions of the dataset is that it currently has to be viewed in paper map form, which limits the resolution. Displaying the results in a program like Google Earth or Oracle Spatial would

allow the regional model to be used more readily as a route-planning tool or at the community level.

- **The perturbation of the results of the regional model to examine potential climate change impacts.** Similar techniques to those used in Chapter Two could be employed to reflect scenario-based future changes to MAAT. This, however, would be on a much larger scale than undertaken previously, and would allow the use of the regional model to help predict the possible locations of geohazards in a changing climate. Geohazards such as active layer detachment failures, other slope instabilities, thermokarst features and hydrological changes are serious issues in the Yukon. Model perturbation would potentially identify those areas most seriously affected by a given change in MAAT over the long term. The sensitivity of permafrost in this portion of northwestern cordillera is, however, not entirely controlled by changes in MAAT, but is also affected by surface and subsurface conditions such as vegetation, thermal properties and ground ice content. These factors, in conjunction with MAAT, will determine how and when the ground responds to changes in climate. Thus any scenario-based modelling using the regional model must recognize them as potentially complicating the relationship between temperature increase and permafrost spatial response.

- **Creation of a map of gridded mean annual air temperatures using the information collected for the generation of the equivalent elevation surface.** The key to developing this map would be the trend surfaces for SLR and treeline. This information would allow other types of permafrost models to be developed for the region such as the TTOP model. This model uses seasonal n-factors to

relate ground surface temperatures to air temperatures as an empirical alternative to evaluating the energy balance directly (Lunardini, 1978; Riseborough et al., 2008). The development of a gridded air temperature surface represents an important first step towards developing a methodology to implement TTOP in the mountains of the Yukon.

- **Utilize the techniques developed to generate regional models for other areas of mountain permafrost including parts of N.W.T. and Alaska.** It is believed that the methodology is transferable into these adjacent areas and this would redress the current paucity of information.

References

Bonnaventure P.P. and Lewkowicz A.G. 2008. Mountain Permafrost Probability Mapping Using the BTS Method in two Climatically Dissimilar Locations, Northwest Canada. *Canadian Journal of Earth Sciences,* **45**: 443-455.

Julián A and Chueca J. 2007. Permafrost distribution from BTS measurements (Sierra de Telera, Central Pyrenees Spain): assessing the importance of solar radiation in a mid-elevation shaded mountainous area. *Permafrost and Periglacial Processes* **18:** 137-149.

Lewkowicz AG and Ednie M. 2004. Probability mapping of mountain permafrost using the BTS method, Wolf Creek, Yukon Territory, Canada. *Permafrost and Periglacial Processes* **15:** 67-80.

Lunardini V.J. 1978. Theory of N-factors and correlation of data. *In proceedings of the Third International Conference on Permafrost*, Vol. 1. National Council of Canada: Ottawa; 40-46.

Riseborough D., Shiklomanov N., Etzelmuller B., Gruber S. and Mrchenko S. (2008). Recent Advance in Permafrost Modelling. *Permafrost and Periglacial Processes* **19**: 137-156

Throop J., (2010) M.Sc. Thesis: Spatial and Temporal Variability in Permafrost Conditions, Northern Canada. Department of Geography, University of Ottawa.

All Thesis References

Arctic Climate Impact Assessment. 2005. http://www.acia.uaf..edu.

ACGR 1988. *Glossary of Permafrost and Related Ground-Ice Terms.* National Research of Canada, Technical Memorandum No. 142. pp.64

Anderson, L., Abbott, M.B., Finney, B.P. and Burns, S.J. 2005. Regional atmospheric circulation change in the North Pacific during the Holocene inferred from lacustrine carbonate oxygen isotopes, Yukon Territory, Canada. *Quaternary Research* **64**: 21–35.

Bonnaventure P.P. and Lewkowicz A.G. 2008. Mountain Permafrost Probability Mapping Using the BTS Method in two Climatically Dissimilar Locations, Northwest Canada. *Canadian Journal of Earth Sciences,* **45**: 443-455.

Bonnaventure P.P. and Lewkowicz A.G. 2010. Modelling climate change effects on the spatial distribution of mountain permafrost at three sites in northwest Canada. *Climatic Change*. DOI 10.1007/s10584-010-9818-5.

Bonnaventure P.P. and Lewkowicz A.G. *In Review*. Mountain Permafrost Probability Modelling in Areas Above and Below Treeline, Southern Yukon, Canada. *Canadian Journal of Earth Sciences.* Submitted November, 2010.

Brenning A., Gruber S., & Hoelzle M., 2005. Sampling and Statistical Analyses of BTS Measurements. *Permafrost and Periglacial Processes***. 16** 1 – 11.

Bring J. 1994. How to standardize regression coefficients. *The American Statistician* **48**: 209-213.

Brouchkov A. and Fukuda M. 2002. Preliminary Measurements on Methane Content in Permafrost, Central Yakutia, and some Experimental Data. *Permafrost and Periglacial Processes*. **13**: 187-197.

Brown, J., O.J. Ferrians Jr., J.A. Heginbottom, and E.S. Melnikov. 1997. Revised February 2001. *Circum-Arctic map of permafrost and ground-ice conditions*. Boulder, CO: National Snow and Ice Data Center/World Data Center for Glaciology. Digital Media.

Burn, C.R. and Smith, C.A.S. 1988. Observations of the "thermal offset" in near-surface mean annual ground temperatures at several sites near Mayo, Yukon Territory, Canada. *Arctic*, **41**(2): 99-104.

Burn, C. R. 1994. "Permafrost, tectonics, and past and future regional climate change, Yukon and adjacent Northwest Territories." *Canadian Journal of Earth Sciences* **31**: 182-191.

Burn, C. R. and F. E. Nelson 2006. "Comment on "A projection of severe near-surface permafrost degradation during the 21st century" by David M. Lawrence and Andrew G. Slater."

Geophysical Research Letters **33**(21): L21503.

Brown, R.J.E. 1966. Influence of vegetation on permafrost, Proceedings, 1st International Permafrost Conference, Purdue University, 1963. National Academy of Sciences-National Research Council Publication 1287, pp. 20-25.

Brown, R.J.E. 1970. Permafrost in Canada-its influence on northern development. University of Toronto Press, Toronto, 234 pp.

Brown, J., O.J. Ferrians, Jr., J.A. Heginbottom, and E.S. Melnikov, eds. 1997. Circum-Arctic map of permafrost and ground-ice conditions. Washington, DC: U.S. Geological Survey in Cooperation with the Circum-Pacific Council for Energy and Mineral Resources. Circum-Pacific Map Series CP-45, scale 1:10,000,000.

Croke M. S. Cess R. D. and Hameed S. 1999. Regional Cloud Cover Change Associated with Global Climate Change: Case Studies for three Regions of the United States. *Journal of Climate* **12:** 2128-2134.

Department of Energy Mines and Resources, Canada. 1974. Physiographic regions of Yukon and surrounding Canadian territory. Published in *Climate of Yukon.* Canadian Government Publishing Centre.

Dobinski, W. 1998. Permafrost occurrences in the alpine zone of the Tatra Mountains, Poland. *In* A.G. Lewkowicz and M. Allard, (eds.) *Proceedings, Seventh International Conference on Permafrost, Yellowknife, June 23-27, 1998.* Nordicana, Centre d'Etudes Nordiques, Quebec City. 231- 237.

Dorren L.K.A. 2003. A Review of Rockfall Mechanics and Modelling Approaches. *Progress in Physical Geography.* **27(1)**: 69-87.

Duchesne C., Wright J.F., and Ednie M. 2008. High Resolution numerical modelling of climate change impacts to permafrost in the vicinities of Inuvik, Norman Wells, and Fort Simpson , NWT, Canada. *Proceedings of the Ninth International Permafrost Conference, Fairbanks, Alaska.*

Duk-Rodkin, A. 1996. Surficial geology, Dawson, Yukon Territory. Geological Survey of Canada, open file 3288, 1:250 000 scale.

Ednie M., Wright J.F., and Duchesne C. 2008. Establishing initial conditions for transient ground thermal modelling in the Mackenzie Valley: a paleo-climatic reconstruction approach. *Proceedings of the Ninth International Permafrost Conference, Fairbanks, Alaska.*

Environment Canada. 2005. http://climate.weatheroffice.ec.gc.ca/climate_normals [Accessed May 17, 2005].

Environment Canada. 2007. http://www.climate.weatheroffice.ec.gc.ca/climateData/canada_e.html [Accessed June 5, 2007].

Etzelmüller, B., Berthling, I., and Ludvig Sollid, J. 1998. The distribution of permafrost in southern Norway- a GIS approach. *In* A.G. Lewkowicz and M. Allard, (eds.) *Proceedings, Seventh International Conference on Permafrost, Yellowknife, June 23-27, 1998.* Nordicana, Centre d'Etudes Nordiques, Quebec City. 251- 256.

Etzelmüller B, Ødegard RS, Berthling I, Sollid JL. 2001. Terrain parameters and remote sensing data in the analysis of permafrost distribution and periglacial processes: principles and examples from southern Norway. Permafrost and Periglacial Processes **12**: 79–92.

Etzelmüller B, Hoelzle M, Heggem ESF, Isaksen K, Mittaz C, Vonder Mühll D, Ødegård RS, Haeberli W, and Sollid JL. 2001. Mapping and modelling the occurrence and distribution of mountain permafrost. *Norwegian Journal of Geography* **55**: 186-194.

Etzelmüller, B., Heggem, E.S.F., Sharkhuu, N., Frauenfelder, R., Kääb, A. and Goulden, C. 2006. Mountain permafrost distribution modelling using a multi-criteria approach in the Hövsgöl area, northern Mongolia. *Permafrost and Periglacial Processes*, **17**: 91-104.

Etzelmüller, B., Farbrot, H., Guomundsson, A., Humlum, O., 2007. The regional distribution of mountain permafrost in Iceland. *Permafrost and Periglacial Processes*, **18**: 185-199.

Evans, S.G. and Clague, J.J. 1994. Recent climatic change and catastrophic geomorphic processes in mountain environments. *Geomorphology*, **10** 107-128.

Eyles, N. and Miall, A. 2007. Canada Rocks, The Geologic Journey. Fitzhenry and Whiteside limited. Markham Ontario.

Farnell R., Hare P. G., Blake E., Bowyer V., Schweger C., Greer S., and Gotthardt R. 2004. Multidisciplinary Investigations of Alpine Ice Patches in Southwest Yukon, Canada. *Arctic* **57:** 247-259.

Fisher D., Osterberg E., Dyke A., Dahl-Jensen D., Demuth M., Zdanowicz C., Bourgeois J., Koerner, R.M., Mayewski P., Wake C., Kreutz K., Steig E., Zheng J., Yalcin K., Goto-Azuma K., Luckman B. and Rupper S. 2008: The Mt. Logan Holocene-late Wisconsinan Isotope Record: Tropical Pacific-Yukon Connections. *Holocene*. **18(5)**: 667-677.

Francis S. 1997. *Data Integration and Ecological Stratification of Wolf Creek Watershed, South-Central Yukon.* Report prepared for Indian and Northern Affairs Canada and Agriculture Canada. Applied Ecosystem Management Ltd.: Whitehorse. 23 pp.

French, H.M. 2007. *The Periglacial Environment third edition*. John Wiley and Sons Inc., 111 River Street, Hoboken, NJ 07030, USA.

Froese, D.G., Westgate, J.A., Reyes, A.V., Enkin, R.J., Preece, S.J. 2008. "Ancient permafrost and a future, warmer arctic." *Science* **321**(5896): 1648.

Fu, P. and Rich, P.M. 1999: Design and implementation of the Solar Analyst: an Arcview extension for modeling solar radiation at landscape scales. http://www.esri.com/library/userconf/proc99/proceed/papers/pap867/p867.htm [Accessed May 21, 2005].

Fukui, K. Sone, T., Yamagata, K., Otsuki, Y., Sawada, Y., Vetrova, V. and Vyatkina, M. 2008. Relationships between permafrost distribution and surface organic layers near Esso, central Kamchatka, Russian Far East. *Permafrost and Periglacial Processes.* **19**: 85-92.

Gardaz J.M. 1997. Distribution of Mountain Permafrost, Fontanesses Basin, Valaisian Alps, Switzerland. *Permafrost and Periglacial Processes* **8** 101-105.

Geobase NTS 105D, 115G, 114P, 30 m resolution DEMs. http://www.geobase.ca [Accessed May 25, 2005].

Geobase (http://www.geobase.ca/) [Acceded May 2009].

Geomatics Yukon. 2006. 30 Meter Yukon Digital Elevation Model [data file]. Whitehorse,
Yukon. Available download: ftp://ftp.geomaticsyukon.ca/DEMs/30m [compiled in 2007].

Global Terrestrial Network for Permafrost (GTNP database) http://www.gtnp.org/ [Accessed January, 2011].

Gruber, S. and Hoelzle, M. 2001. Statistical modeling of mountain permafrost distribution: Local calibration and incorporation of remotely sensed data. *Permafrost and Periglacial Processes*, **12** 69-77.

Gruber, S. & Haeberli, W. 2009: Mountain permafrost. In: *Permafrost Soils,* edited by: Margesin, R., Biology Series Vol. 16, Springer, 33–44, doi: 10.1007/978-3-540-69371-0_3. http://www.geo.unizh.ch/~stgruber/pubs/gruber_2009_pf-soils.pdf

Haeberli W. 1973. Die Basis-Temperatur der winterlichen Schneedecke als möglicher Indikator für die Verbreitung von Permafrost in den Alpen. *Zeitschrift für Gletscherkünde und Glazialgeologie* **1-2**: 221-227.

Guodong C., Yuanming L., Zhizhong S. and Fan J. 2007. 'The thermal semi-conductor' effect on crushed rocks. *Permafrost and Periglacial Processes*, **18**: 151-160.

Haeberli W. 1973. Die basis-temperatur der winterlichen schneedecke als moglicher indikator fur die verbeitung von permafrost in den alpen. *Zeitschrift für Gletscherkünde und Glazialgeologie* **1-2**: 221-227.

Haeberli, W., Guodong, C., Gorbunov, A.P. and Harris, S.A. 1993. Mountain permafrost and climatic change. *Permafrost and Periglacial Processes*, **4** 165-174.

Haeberli W., Hallet B., Arenson L., Elconin R., Humlum O., Kaab A., Kaufmann V., Ladanyi B., Matsuoka N., Springman S., Vonder Muhll D. 2006. *Permafrost and Periglacial Processes.* Permafrost Creek and Rock Glacier Dynamics. **17**: 189-214.

Harris SA. and Brown RJE. 1982. Permafrost distribution along Rocky Mountains in Alberta. *In* French, HM (ed.) *The Roger J.E. Brown Memorial Volume, Proceedings of the Fourth Canadian Permafrost Conference, Calgary, Alberta, March 2-6, 1981*. National Research Council: Ottawa, pp. 59-67.

Harris SA. 1983. Comparison of the climatic and geomorphic methods of predicting permafrost distribution in western Yukon Territory. In *Permafrost: Fourth International Conference, Proceedings, Fairbanks, Alaska, July 17-22, 1983*. National Academy Press: Washington, DC, pp. 450-455.

Harris S.A. 1987. Altitude Trends in Permafrost Active Layer Thickness, Kluane Lake, Yukon Territory. *Arctic*, **40** 179-185.

Harris, S.A. and Corte, A.E. 1992. Interactions and relations between mountain permafrost, glaciers, snow and water. *Permafrost and Periglacial Processes*, **3** 103-110.

Harris, C., Davies, M.C.R. and Etzelmüller, B. 2001. The assessment of potential geotechnical hazards associated with mountain permafrost in a warming global climate. *Permafrost and Periglacial Processes*, **12** 145-156.

Harris, S.A. and Corte, A.E. 1992. Interactions and relations between mountain permafrost, glaciers, snow and water. *Permafrost and Periglacial Processes*, **3** 103-110.

Hauck, C., and Kneisel, C. 2006. Application of Capacitively-coupled and DC Electrical Resistivity Imaging for Mountain Permafrost Studies. *Permafrost and Periglacial Processes.* **17**: 169–177.

Hauck, C., Isaksen, K., Vonder Mühll, D., and Sollid, J.L. 2004. Geophysical Surveys Designed to Delineate the Altitudinal Limit of Mountain Permafrost: an Example from Jotunheimen, Norway. *Permafrost and Periglacial Processes.* **15**: 191–205.

Heggem ESF, Etzelmüller B, Anarmaa S, Sharkhuu N, Goulden CE, Nandinsetseg B. 2006. Spatial distribution of ground surface temperatures and active layer depths in the Hövsgöl area, northern Mongolia. *Permafrost and Periglacial Processes* **17**: 357-369.

Heginbottom JR, Dubreuil MA and Haker PT. 1995. Canada Permafrost. (1:7,500,000 scale). In *The National Atlas of Canada*, 5th Edition, sheet MCR 4177. Ottawa: National Resources Canada.

Heginbottom JA and Radburn LK. 1992. Permafrost and ground ice conditions of northwestern Canada; (Scale 1:1,000,000). *Geological Survey of Canada Map* 1691A.

Hilbich C. Hauck C. Hoelzle M. Scherler M. Schudel L. Völksch I. Vonder Mühll D. and Mäusbacher R. 2008. Monitoring mountain permafrost evolution using electrical resistivity tomography: A 7-year study of seasonal, annual, and long-term variations at Schilthorn, Swiss Alps. *Journal of Geophysical Research* 113**:** FO1S90.

Hoelzle M. 1992. Permafrost occurrence from BTS measurements and climatic parameters in the Eastern Swiss Alps. *Permafrost and Periglacial Processes* **3:** 143-147.

Hoelzle, M., Haeberli, W., Keller, F. 1993. Application of BTS measurements for modelling mountain permafrost distribution. In *Proceedings of the Sixth International Conference on Permafrost, Beijing*. South China University of Technology, Beijing. Vol.1: 272-277.

Hoelzle, M., and W. Haeberli 1995: Simulating the effects of mean annual air temperature changes on permafrost distribution and glacier size. An example from the Upper Engadin, Swiss Alps, *Ann. Glaciol*., 21, 400–405.

Hoelzle M. Wegmann M. Krummenacher B. 1999. Miniature Temperature Dataloggers for Mapping and Monitoring of Permafrost in High Mountain Areas: First Experiences from the Swiss Alps. *Permafrost and Periglacial Processes*, **10** 113-124.

Hoelzle, M., Mittaz, C., Etzelmüller, B. and Haeberli, W. 2001. Surface energy fluxes and distribution models of permafrost in European Mountain areas: an overview of current developments. *Permafrost and Periglacial Processes*, **12** 53-68.

Hosmer, D.W., and Lemeshow, S. 1989. *Applied logistic regression*. John Willey & Sons, New York, U.S.A. 16-17.

Huscroft C.A., Lipovsky P.S. and Bond J.D. 2004b. Permafrost and Landslide Activity: Case Studies from Southwestern Yukon Territory. In: Yukon Exploration and Geology 2003, D.S. Emond and L.L. Lewis (eds.) Yukon Geological Survey. p. 107-199.

Imhof, M., Pierrehumert, G., Haeberlie, W. and Kienholz, H. 2000. Permafrost investigation in the Schilthorn Massif, Bernese Alps, Switzerland. *Permafrost and Periglacial Processes*, **11** 189-206.

Inkpen, R. 2005: *Science, Philosophy and Physical Geography*. Routledge, 2 Park Square, Milton Park, Abingdon, Oxon. New York.

IPCC. 2007. http://www.ipcc.ch/ipccreports/assessments-reports.htm.

Ishikawa, M. 2003. Thermal regimes at the snow-ground interface and their implications for permafrost investigation. *Geomorphology.* **52**:105-120.

Ishikawa, M.and Hirakawa., 2002. Mountain permafrost distribution based on BTS measurements and DC resistivity soundings in the Daisetu Moutains, Hokkaido, Japan. *Permafrost and Periglacial Processes*, **11** 109-123.

Isaksen K, Hauck C, Gudevang E, Ødegård RS, Sollid JL. 2002. Mountain permafrost distribution in Dovrefjell and Jotunheimen, southern Norway, based on BTS and DC resistivity tomography data. Norsk Geografisk Tidsskrift 56: 122–136.

Janke JR. 2004. The occurrence of alpine permafrost in the Front Range of Colorado. *Geomorphology* **67**: 375-389.

Janke, J.R. 2005. Modelling past and future alpine permafrost distribution in the Colorado front range. Earth Surface Processes and Landforms, **30:** 1495-1508.

Janke, J.R. 2005b. Modeling past and future alpine permafrost distribution in the Colorado Front Range. *Earth Surface Processes and Landforms* **30**: 1495-1508. DOI: 10.1002/esp.1205.

Janowicz JR. 1999. Wolf Creek Research Basin - Overview. Wolf Creek Research Basin: Hydrology, Ecology, Environment. *In* Pomeroy, J.W., Granger, R.J (eds.) *Wolf Creek Research Basin: Hydrology, Ecology, Environment*. Saskatoon: National Water Research Institute. 125-134.

Jeckel, P.P. 1988. Permafrost and its altitudinal zonation in N. Lapland. In *Proceedings of the Fifth International Conference on Permafrost, Trondheim*. Tapir, Trondheim. Vol.**1** 332-337.

Jenness J. 2006. Topographic Position Index (TPI) v. 1.2. Online manual, Jenness Enterprises, 3020 N. Schevene Blvd. Flagstaff, AZ, 86004, USA.

Jorgenson T, Yoshikawa K, Kanevskiy M, and Shur Y. 2008. Permafrost Characteristics of Alaska, *Conference proceedings from the ninth international conference on permafrost*, June 29 - July 3, 2008. Fairbanks, Alaska, USA.

Jensen, J.R. 2005. *Introductory Digital Image Processing*. Toronto: Pearson Education Inc.

Julián A and Chueca J. 2007. Permafrost distribution from BTS measurements (Sierra de Telera, Central Pyrenees Spain): assessing the importance of solar radiation in a mid-elevation shaded mountainous area. *Permafrost and Periglacial Processes* **18:** 137-149.

Juliussen H and Humlum O. 2007. Towards a TTOP Ground Temperature Model For Mountainous Terrain in Central-Eastern Norway. *Permafrost and Periglacial Processes* **18**: 161-184.

Keller, F. and Gubler, H. 1993. Interaction between snow cover and alpine permafrost, Murtle Corvatsch. Swiss Alps. In *Proceedings of the Sixth International Conference on Permafrost, Beijing*. South China University of Technology, Beijing. Vol. 1: 332-337.

King, L. 1992. Prospecting and mapping of mountain permafrost and associated phenomenon. *Permafrost and Periglacial Processes*, **3** 73-81.

Kneisel C., Rothenbühler C., Keller F., Haeberli W. 2007. Hazard assessment of potential periglacial debris flows based on GIS-based spatial modelling and geophysical field surveys: a case study in the Swiss Alps. *Permafrost and Periglacial Processes*. **18**: 259-268.

Kneisel C., Hauck C., Fortier R., and Moorman B. 2008. Advances in Geophysical Methods for Permafrost Investigation. *Permafrost and Periglacial Processes*. **19**: 157-178.

Kremer, M., Lewkowicz, A.G., Bonnaventure, P.P. and Sawada, M.C. 2011.Utility of classification and regression tree analyses and vegetation in mountain permafrost models, Yukon Territory, Canada. *Permafrost and Periglacial Processes.* DOI 10.1002/ppp.719

Kwong, Y. T. and Gan, T.Y. 1994. Northward migration of permafrost along the Mackenzie Highway and climatic warming. *Climatic Change* **26**(4): 399-419.

Lawrence D. M. Slater A. G. Romanovsky V. E. and Nicolsky D. J. 2008. Sensitivity of a model projection of near-surface permafrost degradation to soil column and representation of soil organic matter. *Journal of Geophysical Research* **113:** F02011.

Lewkowicz, A.G. 2008. Evaluation of Miniature Temperature-loggers to Monitor Snowpack Evolution at Mountain Permafrost Sites, Northwestern Canada. *Permafrost Periglacial Processes.,* **19:** 323-331.

Lewkowicz A.G. and Bonnaventure P.P. 2008. Interchangeability of Mountain Permafrost Probability Models, Northwest Canada, *Permafrost and Periglacial Processes,* **19**: 49-62.

Lewkowicz, A.G. and Bonnaventure, P.P. 2011. Equivalent Elevation: a New Method to Incorporate Variable Lapse Rates Into Mountain Permafrost Modelling. *Permafrost and Periglacial Processes.* DOI 10.1002/ppp.720

Lewkowicz, A.G. and Ednie, M. 2004. Probability mapping of mountain permafrost using the BTS method, Wolf Creek, Yukon Territory, Canada. *Permafrost Periglacial. Processes.,* **15** 67-80.

Lewkowicz A.G. and Harris C. 2005. Frequency and Magnitude of active-layer detachment failures in discontinuous and continuous permafrost, northern Canada. *Permafrost and Periglacial Processes.* **16**: 115-130.

Lewkowicz A.G., Etzelmüller B. and Smith S.L. Characteristics of discontinuous permafrost from ground temperature measurements and electrical resistivity tomography, southern Yukon, Canada. *Permafrost and Periglacial Processes. In Press.*

Lipovsky P.S., Coates J., Lewkowicz A.G. and Trochim E. 2005. Active-layer Detachments Following the Summer 2004 Forest Fires Near Dawson City, Yukon. In: Yukon Exploration and Geology 2005, D.S. Emond, L.H. Weston, G.D. Bradshaw and L.L. Lewis (eds.), Yukon Geological Survey.

Lugon R. & Delaloye R. 2001. Modeling alpine permafrost distribution , Val de Rechy, Valais Alps (Switzerland) *Norsk geogr. Tidsskr.* **55** 224-229.

Meyer, P., Itten, K.I., Kellenberger, T., Sandmeier, S., and Sandmeier, R. 1993. Radiometric corrections of topographically induced effects on Landsat TM data in an alpine environment. *Journal of Photogrammetry and Remote Sensing* **48**: 17-28.

Natural Resources Canada. 2010. Forest ecosystems of Canada http://ecosys.cfl.scf.rncan.gc.ca/classification/classif08-eng.asp [Accessed June, 2010].

Nelson, F.E. and Outcalt, S.I. 1987. A computational method for predicting and rationalization of permafrost. *Arctic and Alpine Research,* **3** 279-288.

Ødegard R. S., Isaksen K., Mastervik M., Billdal L., Engler M., & Sollid J. L. 1996. Comparison of BTS and Landsat TM data from Jotunheimen, southern Norway. *Norsk geogr. Tidsskr.* **53** 226 – 233.

Page A. M.Sc. Thesis. 2009. A topographic and photogrammetric study of rock glaciers in the southern Yukon Territory.

Panda SK, Prakash A, Solie DN, Romanovsky VE, Jorgenson MT. 2010. Remote sensing and field-based mapping of permafrost distribution along the Alaska Highway corridor, interior Alaska. *Permafrost and Periglacial Processes*, **21**, in press.

Putkonen J. 2003. Determination of Frozen Soil Thermal Properties by Heated Needle Probe. *Permafrost and Periglacial Processes*, **14** 343-347.

Riseborough D., Shiklomanov N., Etzelmuller B., Gruber S. and Mrchenko S. 2008. Recent Advance in Permafrost Modelling. (2008). *Permafrost and Periglacial Processes* **19**: 137-156

Rouse, J.W. Jr., Hass, R.W., Schell, J.A., Deering, D.W., and Harlan, J.C. 1974. Monitoring the vernal advancement and retrogradation (Greenwave effect) of natural vegetation. NASA/GSFCT Type III Final Report, Greenbolt, MD, USA.

Salzmann, N., J. Noetzli, C. Hauck, S. Gruber, M. Hoelzle, and W. Haeberli 2007: Ground surface temperature scenarios in complex high-mountain topography based on regional climate model results, *Journal of Geophysical Research.*, 112, F02S12,

doi:10.1029/2006JF000527.

Shur Y. and Jorgenson M.T. 2007. Patterns of Permafrost Formation and Degradation in Relation to Climate and Ecosystems. *Permafrost and Periglacial Processes* **18**: 7-19

Smith, M.W. and D.W. Riseborough (1983). Permafrost sensitivity to climate change. *Permafrost, Procedeedings of the fouth International Confrence.* Washington D.C., National Acadeny Press. **1:** 1178-1183.

Smith, M.W. and Riseborough, D.W. 1996. Permafrost monitoring and detection of climate change. *Permafrost and Periglacial Processes*, **7** 301-309.

Smith, M.W. and Riseborough, D.W. 2002. Climate and limits of permafrost: A zonal analysis. *Permafrost and Periglacial Processes*, **13** 1-15.Sokal & Oden, 1978

Stocker-Mittaz, C., Hoelzle, M., Haeberli, W. 2002. Modelling alpine permafrost distribution based on energy-balance: a first step. *Permafrost and Periglacial Processes* **13**: 271–282.

Sokal, R. and Oden, N. 1978: Spatial autocorrelation in biology 1. Methodology. *Biological Journal of the Linnean Society*, **10** 199-228.

Tanarro LM, Hoelzle M, Garcia A, Ramos M, Gruber S, Gomez A, Piqueer M, and Palacios D. 2001. Permafrost distribution modelling in the mountains of the Mediterranean: Corral del Veleta, Sierra Nevada, Spain. *Norsk Geografisk Tidsskrift* **55**: 253 – 260.

Taylor A, Nixon M, Eley J, Burgess M, and Egginton P. 1998. Effects of atmospheric temperature inversions on ground surface temperatures and discontinuous permafrost,

Teillet, P.M., Guindon, B., and Goodenough, D.G. 1982. On the slope-aspect correction of
multispectral scanner data. *Canadian Journal of Remote Sensing* **8**: 84-106.

Throop J., (2010) M.Sc. Thesis: Spatial and Temporal Variability in Permafrost Conditions, Northern Canada. Department of Geography, University of Ottawa.

Norman Wells, Mackenzie Valley, Canada. *Conference Proceedings of the seventh international conference on permafrost.* June 23-27, Yellowknife, Canada. Pages 1043-1047.

United States Geological Survey 2010. http://data.geocomm.com/dem/ [Accesses May, 2010]

Vonder Mühll, D., Stucki, T. and Haeberli, W. 1998. Borehole temperatures in alpine permafrost: A ten year study. *In* A.G. Lewkowicz and M. Allard, (eds.) *Proceedings,*

Seventh International Conference on Permafrost, Yellowknife, June 23-27, 1998. Nordicana, Centre d'Etudes Nordiques, Quebec City. 1089-1095.

Wahl HE, Fraser DB, Harvey RC and Maxwell JB. 1987. *Climate of Yukon.* Canadian Government Publishing Centre.

Washburn, A.L. 1979. *Geocryology.* Edward Arnold, London. 406pp.

Ward, B.C., Bond, J.D., and Gosse, J.C. 2007. Evidence for a 55–50 ka (early Wisconsin) glaciation of the Cordilleran ice sheet, Yukon Territory, Canada. *Quaternary Research.* **68**: 141-150.

Williams, D.J., and Burn, C.R. 1996. Surficial characteristics associated with the occurrence of permafrost near Mayo, Central Yukon Territory, Canada. *Permafrost and Periglacial Processes.* **7**: pg. 193-206.

Williams P.J. and Smith M.W. 1989. The Frozen Earth: Fundamentals of Geocryology Cambridge University Press. The Edinbrugh Building, Shaftsbury Road, Cambridge CB2 2RU.

Woo M.K., Lewkowicz A.G., Rouse W.R. 1992. Response of the Canadian Permafrost Environment to Climate Change. *Physical Geography:* **13** 287 – 317.

Woo M., Kane D.L., Carey S.K., and Yang D. 2008. Progress in Permafrost Hydrology in the New Millennium. *Permafrost and Periglacial Processes*. **19**: 237-254.

Wright J.F., Duchesne C. & Cote M.M. 2003. Regional-scale permafrost mapping using the TTOP ground temperature model. *Proceedings, eighth International Conference on permafrost, Zurich, Switzerland, July 21-25, 2003* (pp. 1241-1246).

Youngblut, D.K. and Luckman, B.H. 2008: Maximum June–July temperatures in the southwest Yukon over the last 300 years reconstructed from tree-rings. *Dendrochronologia* 25, 153–66.

Appendix A

This appendix contains a larger landscape view of Figure 6.3 illustrating the Regional model permafrost probability map with study area boundaries and locations of Environment Canada stations.

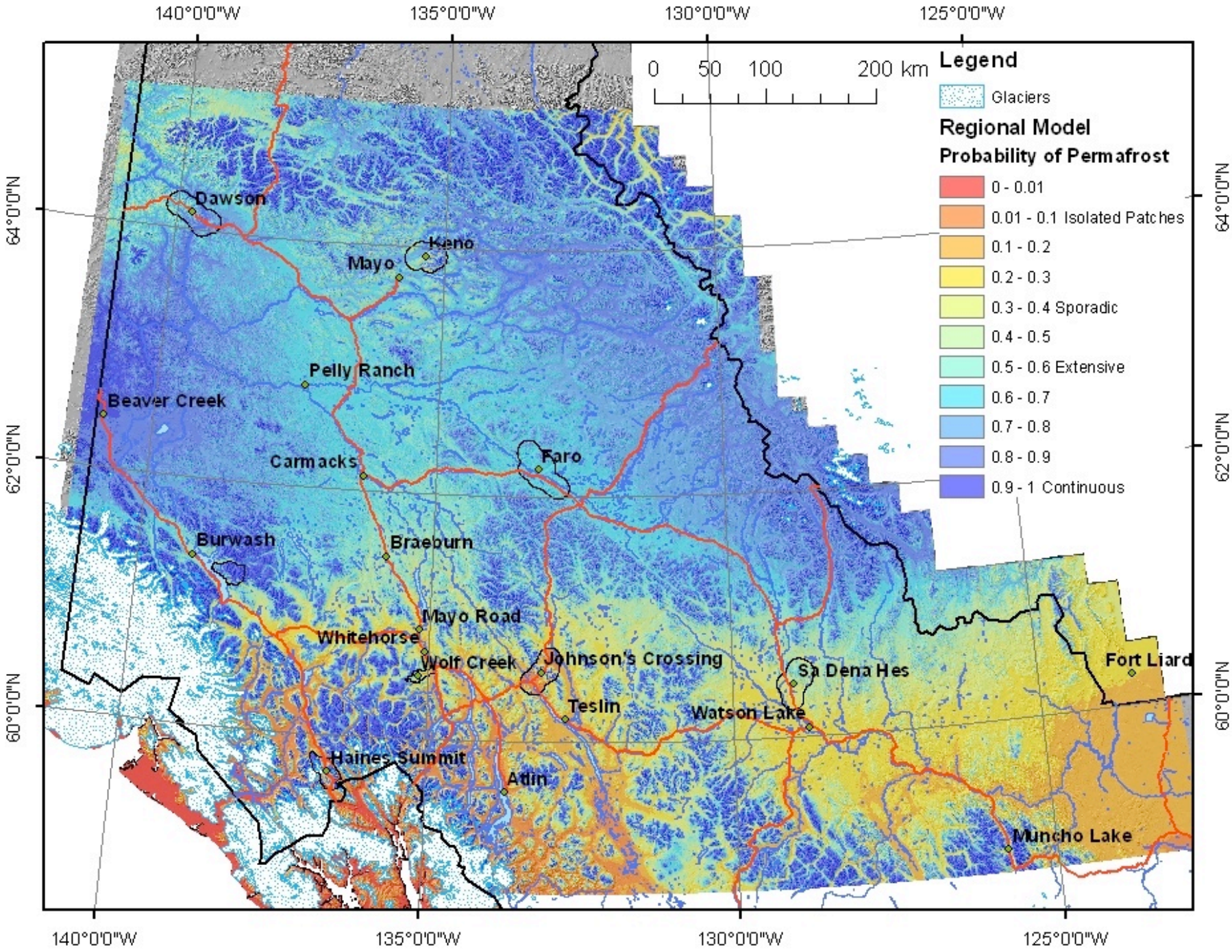
140°0'0"W
135°0'0"W
130°0'0"W
125°0'0"W
64°0'0"N
62°0'0"N
60°0'0"N
0 50 100 200 km
Legend
Glaciers
Regional Model
Probability of Permafrost
0 - 0.01
0.01 - 0.1 Isolated Patches
0.1 - 0.2
0.2 - 0.3
0.3 - 0.4 Sporadic
0.4 - 0.5
0.5 - 0.6 Extensive
0.6 - 0.7
0.7 - 0.8
0.8 - 0.9
0.9 - 1 Continuous
Dawson
Keno
Mayo
Pelly Ranch
Beaver Creek
Carmacks
Faro
Burwash
Braeburn
Mayo Road
Whitehorse
Wolf Creek
Johnson's Crossing
Teslin
Watson Lake
Sa Dena Hes
Fort Liard
Haines Summit
Atlin
Muncho Lake